

Springer Series in Statistics

Trevor Hastie
Robert Tibshirani
Jerome Friedman

The Elements of Statistical Learning

Data Mining, Inference, and Prediction

Second Edition



Springer

To our parents:

Valerie and Patrick Hastie

Vera and Sami Tibshirani

Florence and Harry Friedman

and to our families:

Samantha, Timothy, and Lynda

Charlie, Ryan, Julie, and Cheryl

Melanie, Dora, Monika, and Ildiko

Preface to the Second Edition

In God we trust, all others bring data.

—William Edwards Deming (1900-1993)¹

We have been gratified by the popularity of the first edition of *The Elements of Statistical Learning*. This, along with the fast pace of research in the statistical learning field, motivated us to update our book with a second edition.

We have added four new chapters and updated some of the existing chapters. Because many readers are familiar with the layout of the first edition, we have tried to change it as little as possible. Here is a summary of the main changes:

¹On the Web, this quote has been widely attributed to both Deming and Robert W. Hayden; however Professor Hayden told us that he can claim no credit for this quote, and ironically we could find no “data” confirming that Deming actually said this.

Chapter	What's new
1. Introduction	
2. Overview of Supervised Learning	
3. Linear Methods for Regression	LAR algorithm and generalizations of the lasso
4. Linear Methods for Classification	Lasso path for logistic regression
5. Basis Expansions and Regularization	Additional illustrations of RKHS
6. Kernel Smoothing Methods	
7. Model Assessment and Selection	Strengths and pitfalls of cross-validation
8. Model Inference and Averaging	
9. Additive Models, Trees, and Related Methods	
10. Boosting and Additive Trees	New example from ecology; some material split off to Chapter 16.
11. Neural Networks	Bayesian neural nets and the NIPS 2003 challenge
12. Support Vector Machines and Flexible Discriminants	Path algorithm for SVM classifier
13. Prototype Methods and Nearest-Neighbors	
14. Unsupervised Learning	Spectral clustering, kernel PCA, sparse PCA, non-negative matrix factorization, archetypal analysis, nonlinear dimension reduction, Google page rank algorithm, a direct approach to ICA
15. Random Forests	New
16. Ensemble Learning	New
17. Undirected Graphical Models	New
18. High-Dimensional Problems	New

Some further notes:

- Our first edition was unfriendly to colorblind readers; in particular, we tended to favor red/green contrasts which are particularly troublesome. We have changed the color palette in this edition to a large extent, replacing the above with an orange/blue contrast.
- We have changed the name of Chapter 6 from “Kernel Methods” to “Kernel Smoothing Methods”, to avoid confusion with the machine-learning kernel method that is discussed in the context of support vector machines (Chapter 11) and more generally in Chapters 5 and 14.
- In the first edition, the discussion of error-rate estimation in Chapter 7 was sloppy, as we did not clearly differentiate the notions of conditional error rates (conditional on the training set) and unconditional rates. We have fixed this in the new edition.

- Chapters 15 and 16 follow naturally from Chapter 10, and the chapters are probably best read in that order.
- In Chapter 17, we have not attempted a comprehensive treatment of graphical models, and discuss only undirected models and some new methods for their estimation. Due to a lack of space, we have specifically omitted coverage of directed graphical models.
- Chapter 18 explores the “ $p \gg N$ ” problem, which is learning in high-dimensional feature spaces. These problems arise in many areas, including genomic and proteomic studies, and document classification.

We thank the many readers who have found the (too numerous) errors in the first edition. We apologize for those and have done our best to avoid errors in this new edition. We thank Mark Segal, Bala Rajaratnam, and Larry Wasserman for comments on some of the new chapters, and many Stanford graduate and post-doctoral students who offered comments, in particular Mohammed AlQuraishi, John Boik, Holger Hoefling, Arian Maleki, Donal McMahon, Saharon Rosset, Babak Shababa, Daniela Witten, Ji Zhu and Hui Zou. We thank John Kimmel for his patience in guiding us through this new edition. RT dedicates this edition to the memory of Anna McPhee.

*Trevor Hastie
Robert Tibshirani
Jerome Friedman*
Stanford, California
August 2008

Preface to the First Edition

We are drowning in information and starving for knowledge.

—Rutherford D. Roger

The field of Statistics is constantly challenged by the problems that science and industry brings to its door. In the early days, these problems often came from agricultural and industrial experiments and were relatively small in scope. With the advent of computers and the information age, statistical problems have exploded both in size and complexity. Challenges in the areas of data storage, organization and searching have led to the new field of “data mining”; statistical and computational problems in biology and medicine have created “bioinformatics.” Vast amounts of data are being generated in many fields, and the statistician’s job is to make sense of it all: to extract important patterns and trends, and understand “what the data says.” We call this *learning from data*.

The challenges in learning from data have led to a revolution in the statistical sciences. Since computation plays such a key role, it is not surprising that much of this new development has been done by researchers in other fields such as computer science and engineering.

The learning problems that we consider can be roughly categorized as either *supervised* or *unsupervised*. In supervised learning, the goal is to predict the value of an outcome measure based on a number of input measures; in unsupervised learning, there is no outcome measure, and the goal is to describe the associations and patterns among a set of input measures.

This book is our attempt to bring together many of the important new ideas in learning, and explain them in a statistical framework. While some mathematical details are needed, we emphasize the methods and their conceptual underpinnings rather than their theoretical properties. As a result, we hope that this book will appeal not just to statisticians but also to researchers and practitioners in a wide variety of fields.

Just as we have learned a great deal from researchers outside of the field of statistics, our statistical viewpoint may help others to better understand different aspects of learning:

There is no true interpretation of anything; interpretation is a vehicle in the service of human comprehension. The value of interpretation is in enabling others to fruitfully think about an idea.

—Andreas Buja

We would like to acknowledge the contribution of many people to the conception and completion of this book. David Andrews, Leo Breiman, Andreas Buja, John Chambers, Bradley Efron, Geoffrey Hinton, Werner Stuetzle, and John Tukey have greatly influenced our careers. Balasubramanian Narasimhan gave us advice and help on many computational problems, and maintained an excellent computing environment. Shin-Ho Bang helped in the production of a number of the figures. Lee Wilkinson gave valuable tips on color production. Ilana Belitskaya, Eva Cantoni, Maya Gupta, Michael Jordan, Shanti Gopatam, Radford Neal, Jorge Picazo, Bogdan Popescu, Olivier Renaud, Saharon Rosset, John Storey, Ji Zhu, Mu Zhu, two reviewers and many students read parts of the manuscript and offered helpful suggestions. John Kimmel was supportive, patient and helpful at every phase; MaryAnn Brickner and Frank Ganz headed a superb production team at Springer. Trevor Hastie would like to thank the statistics department at the University of Cape Town for their hospitality during the final stages of this book. We gratefully acknowledge NSF and NIH for their support of this work. Finally, we would like to thank our families and our parents for their love and support.

*Trevor Hastie
Robert Tibshirani
Jerome Friedman*
Stanford, California
May 2001

The quiet statisticians have changed our world; not by discovering new facts or technical developments, but by changing the ways that we reason, experiment and form our opinions

—Ian Hacking

Contents

Preface to the Second Edition	vii
Preface to the First Edition	xi
1 Introduction	1
2 Overview of Supervised Learning	9
2.1 Introduction	9
2.2 Variable Types and Terminology	9
2.3 Two Simple Approaches to Prediction: Least Squares and Nearest Neighbors	11
2.3.1 Linear Models and Least Squares	11
2.3.2 Nearest-Neighbor Methods	14
2.3.3 From Least Squares to Nearest Neighbors	16
2.4 Statistical Decision Theory	18
2.5 Local Methods in High Dimensions	22
2.6 Statistical Models, Supervised Learning and Function Approximation	28
2.6.1 A Statistical Model for the Joint Distribution $\Pr(X, Y)$	28
2.6.2 Supervised Learning	29
2.6.3 Function Approximation	29
2.7 Structured Regression Models	32
2.7.1 Difficulty of the Problem	32

2.8	Classes of Restricted Estimators	33
2.8.1	Roughness Penalty and Bayesian Methods	34
2.8.2	Kernel Methods and Local Regression	34
2.8.3	Basis Functions and Dictionary Methods	35
2.9	Model Selection and the Bias–Variance Tradeoff	37
	Bibliographic Notes	39
	Exercises	39
3	Linear Methods for Regression	43
3.1	Introduction	43
3.2	Linear Regression Models and Least Squares	44
3.2.1	Example: Prostate Cancer	49
3.2.2	The Gauss–Markov Theorem	51
3.2.3	Multiple Regression from Simple Univariate Regression	52
3.2.4	Multiple Outputs	56
3.3	Subset Selection	57
3.3.1	Best-Subset Selection	57
3.3.2	Forward- and Backward-Stepwise Selection	58
3.3.3	Forward-Stagewise Regression	60
3.3.4	Prostate Cancer Data Example (Continued)	61
3.4	Shrinkage Methods	61
3.4.1	Ridge Regression	61
3.4.2	The Lasso	68
3.4.3	Discussion: Subset Selection, Ridge Regression and the Lasso	69
3.4.4	Least Angle Regression	73
3.5	Methods Using Derived Input Directions	79
3.5.1	Principal Components Regression	79
3.5.2	Partial Least Squares	80
3.6	Discussion: A Comparison of the Selection and Shrinkage Methods	82
3.7	Multiple Outcome Shrinkage and Selection	84
3.8	More on the Lasso and Related Path Algorithms	86
3.8.1	Incremental Forward Stagewise Regression	86
3.8.2	Piecewise-Linear Path Algorithms	89
3.8.3	The Dantzig Selector	89
3.8.4	The Grouped Lasso	90
3.8.5	Further Properties of the Lasso	91
3.8.6	Pathwise Coordinate Optimization	92
3.9	Computational Considerations	93
	Bibliographic Notes	94
	Exercises	94

4 Linear Methods for Classification	101
4.1 Introduction	101
4.2 Linear Regression of an Indicator Matrix	103
4.3 Linear Discriminant Analysis	106
4.3.1 Regularized Discriminant Analysis	112
4.3.2 Computations for LDA	113
4.3.3 Reduced-Rank Linear Discriminant Analysis . .	113
4.4 Logistic Regression	119
4.4.1 Fitting Logistic Regression Models	120
4.4.2 Example: South African Heart Disease	122
4.4.3 Quadratic Approximations and Inference . . .	124
4.4.4 L_1 Regularized Logistic Regression	125
4.4.5 Logistic Regression or LDA?	127
4.5 Separating Hyperplanes	129
4.5.1 Rosenblatt's Perceptron Learning Algorithm .	130
4.5.2 Optimal Separating Hyperplanes	132
Bibliographic Notes	135
Exercises	135
5 Basis Expansions and Regularization	139
5.1 Introduction	139
5.2 Piecewise Polynomials and Splines	141
5.2.1 Natural Cubic Splines	144
5.2.2 Example: South African Heart Disease (Continued)	146
5.2.3 Example: Phoneme Recognition	148
5.3 Filtering and Feature Extraction	150
5.4 Smoothing Splines	151
5.4.1 Degrees of Freedom and Smoother Matrices .	153
5.5 Automatic Selection of the Smoothing Parameters	156
5.5.1 Fixing the Degrees of Freedom	158
5.5.2 The Bias–Variance Tradeoff	158
5.6 Nonparametric Logistic Regression	161
5.7 Multidimensional Splines	162
5.8 Regularization and Reproducing Kernel Hilbert Spaces	167
5.8.1 Spaces of Functions Generated by Kernels .	168
5.8.2 Examples of RKHS	170
5.9 Wavelet Smoothing	174
5.9.1 Wavelet Bases and the Wavelet Transform .	176
5.9.2 Adaptive Wavelet Filtering	179
Bibliographic Notes	181
Exercises	181
Appendix: Computational Considerations for Splines	186
Appendix: B -splines	186
Appendix: Computations for Smoothing Splines . . .	189

6 Kernel Smoothing Methods	191
6.1 One-Dimensional Kernel Smoothers	192
6.1.1 Local Linear Regression	194
6.1.2 Local Polynomial Regression	197
6.2 Selecting the Width of the Kernel	198
6.3 Local Regression in \mathbb{R}^p	200
6.4 Structured Local Regression Models in \mathbb{R}^p	201
6.4.1 Structured Kernels	203
6.4.2 Structured Regression Functions	203
6.5 Local Likelihood and Other Models	205
6.6 Kernel Density Estimation and Classification	208
6.6.1 Kernel Density Estimation	208
6.6.2 Kernel Density Classification	210
6.6.3 The Naive Bayes Classifier	210
6.7 Radial Basis Functions and Kernels	212
6.8 Mixture Models for Density Estimation and Classification	214
6.9 Computational Considerations	216
Bibliographic Notes	216
Exercises	216
7 Model Assessment and Selection	219
7.1 Introduction	219
7.2 Bias, Variance and Model Complexity	219
7.3 The Bias–Variance Decomposition	223
7.3.1 Example: Bias–Variance Tradeoff	226
7.4 Optimism of the Training Error Rate	228
7.5 Estimates of In-Sample Prediction Error	230
7.6 The Effective Number of Parameters	232
7.7 The Bayesian Approach and BIC	233
7.8 Minimum Description Length	235
7.9 Vapnik–Chervonenkis Dimension	237
7.9.1 Example (Continued)	239
7.10 Cross-Validation	241
7.10.1 K -Fold Cross-Validation	241
7.10.2 The Wrong and Right Way to Do Cross-validation	245
7.10.3 Does Cross-Validation Really Work?	247
7.11 Bootstrap Methods	249
7.11.1 Example (Continued)	252
7.12 Conditional or Expected Test Error?	254
Bibliographic Notes	257
Exercises	257
8 Model Inference and Averaging	261
8.1 Introduction	261

8.2	The Bootstrap and Maximum Likelihood Methods	261
8.2.1	A Smoothing Example	261
8.2.2	Maximum Likelihood Inference	265
8.2.3	Bootstrap versus Maximum Likelihood	267
8.3	Bayesian Methods	267
8.4	Relationship Between the Bootstrap and Bayesian Inference	271
8.5	The EM Algorithm	272
8.5.1	Two-Component Mixture Model	272
8.5.2	The EM Algorithm in General	276
8.5.3	EM as a Maximization–Maximization Procedure	277
8.6	MCMC for Sampling from the Posterior	279
8.7	Bagging	282
8.7.1	Example: Trees with Simulated Data	283
8.8	Model Averaging and Stacking	288
8.9	Stochastic Search: Bumping	290
	Bibliographic Notes	292
	Exercises	293
9	Additive Models, Trees, and Related Methods	295
9.1	Generalized Additive Models	295
9.1.1	Fitting Additive Models	297
9.1.2	Example: Additive Logistic Regression	299
9.1.3	Summary	304
9.2	Tree-Based Methods	305
9.2.1	Background	305
9.2.2	Regression Trees	307
9.2.3	Classification Trees	308
9.2.4	Other Issues	310
9.2.5	Spam Example (Continued)	313
9.3	PRIM: Bump Hunting	317
9.3.1	Spam Example (Continued)	320
9.4	MARS: Multivariate Adaptive Regression Splines	321
9.4.1	Spam Example (Continued)	326
9.4.2	Example (Simulated Data)	327
9.4.3	Other Issues	328
9.5	Hierarchical Mixtures of Experts	329
9.6	Missing Data	332
9.7	Computational Considerations	334
	Bibliographic Notes	334
	Exercises	335
10	Boosting and Additive Trees	337
10.1	Boosting Methods	337
10.1.1	Outline of This Chapter	340

10.2	Boosting Fits an Additive Model	341
10.3	Forward Stagewise Additive Modeling	342
10.4	Exponential Loss and AdaBoost	343
10.5	Why Exponential Loss?	345
10.6	Loss Functions and Robustness	346
10.7	“Off-the-Shelf” Procedures for Data Mining	350
10.8	Example: Spam Data	352
10.9	Boosting Trees	353
10.10	Numerical Optimization via Gradient Boosting	358
10.10.1	Steepest Descent	358
10.10.2	Gradient Boosting	359
10.10.3	Implementations of Gradient Boosting	360
10.11	Right-Sized Trees for Boosting	361
10.12	Regularization	364
10.12.1	Shrinkage	364
10.12.2	Subsampling	365
10.13	Interpretation	367
10.13.1	Relative Importance of Predictor Variables . . .	367
10.13.2	Partial Dependence Plots	369
10.14	Illustrations	371
10.14.1	California Housing	371
10.14.2	New Zealand Fish	375
10.14.3	Demographics Data	379
	Bibliographic Notes	380
	Exercises	384
11	Neural Networks	389
11.1	Introduction	389
11.2	Projection Pursuit Regression	389
11.3	Neural Networks	392
11.4	Fitting Neural Networks	395
11.5	Some Issues in Training Neural Networks	397
11.5.1	Starting Values	397
11.5.2	Overfitting	398
11.5.3	Scaling of the Inputs	398
11.5.4	Number of Hidden Units and Layers	400
11.5.5	Multiple Minima	400
11.6	Example: Simulated Data	401
11.7	Example: ZIP Code Data	404
11.8	Discussion	408
11.9	Bayesian Neural Nets and the NIPS 2003 Challenge . . .	409
11.9.1	Bayes, Boosting and Bagging	410
11.9.2	Performance Comparisons	412
11.10	Computational Considerations	414
	Bibliographic Notes	415

Exercises	415
12 Support Vector Machines and Flexible Discriminants	417
12.1 Introduction	417
12.2 The Support Vector Classifier	417
12.2.1 Computing the Support Vector Classifier	420
12.2.2 Mixture Example (Continued)	421
12.3 Support Vector Machines and Kernels	423
12.3.1 Computing the SVM for Classification	423
12.3.2 The SVM as a Penalization Method	426
12.3.3 Function Estimation and Reproducing Kernels .	428
12.3.4 SVMs and the Curse of Dimensionality	431
12.3.5 A Path Algorithm for the SVM Classifier	432
12.3.6 Support Vector Machines for Regression	434
12.3.7 Regression and Kernels	436
12.3.8 Discussion	438
12.4 Generalizing Linear Discriminant Analysis	438
12.5 Flexible Discriminant Analysis	440
12.5.1 Computing the FDA Estimates	444
12.6 Penalized Discriminant Analysis	446
12.7 Mixture Discriminant Analysis	449
12.7.1 Example: Waveform Data	451
Bibliographic Notes	455
Exercises	455
13 Prototype Methods and Nearest-Neighbors	459
13.1 Introduction	459
13.2 Prototype Methods	459
13.2.1 K -means Clustering	460
13.2.2 Learning Vector Quantization	462
13.2.3 Gaussian Mixtures	463
13.3 k -Nearest-Neighbor Classifiers	463
13.3.1 Example: A Comparative Study	468
13.3.2 Example: k -Nearest-Neighbors and Image Scene Classification	470
13.3.3 Invariant Metrics and Tangent Distance	471
13.4 Adaptive Nearest-Neighbor Methods	475
13.4.1 Example	478
13.4.2 Global Dimension Reduction for Nearest-Neighbors	479
13.5 Computational Considerations	480
Bibliographic Notes	481
Exercises	481

14 Unsupervised Learning	485
14.1 Introduction	485
14.2 Association Rules	487
14.2.1 Market Basket Analysis	488
14.2.2 The Apriori Algorithm	489
14.2.3 Example: Market Basket Analysis	492
14.2.4 Unsupervised as Supervised Learning	495
14.2.5 Generalized Association Rules	497
14.2.6 Choice of Supervised Learning Method	499
14.2.7 Example: Market Basket Analysis (Continued) .	499
14.3 Cluster Analysis	501
14.3.1 Proximity Matrices	503
14.3.2 Dissimilarities Based on Attributes	503
14.3.3 Object Dissimilarity	505
14.3.4 Clustering Algorithms	507
14.3.5 Combinatorial Algorithms	507
14.3.6 K -means	509
14.3.7 Gaussian Mixtures as Soft K -means Clustering .	510
14.3.8 Example: Human Tumor Microarray Data	512
14.3.9 Vector Quantization	514
14.3.10 K -medoids	515
14.3.11 Practical Issues	518
14.3.12 Hierarchical Clustering	520
14.4 Self-Organizing Maps	528
14.5 Principal Components, Curves and Surfaces	534
14.5.1 Principal Components	534
14.5.2 Principal Curves and Surfaces	541
14.5.3 Spectral Clustering	544
14.5.4 Kernel Principal Components	547
14.5.5 Sparse Principal Components	550
14.6 Non-negative Matrix Factorization	553
14.6.1 Archetypal Analysis	554
14.7 Independent Component Analysis and Exploratory Projection Pursuit	557
14.7.1 Latent Variables and Factor Analysis	558
14.7.2 Independent Component Analysis	560
14.7.3 Exploratory Projection Pursuit	565
14.7.4 A Direct Approach to ICA	565
14.8 Multidimensional Scaling	570
14.9 Nonlinear Dimension Reduction and Local Multidimensional Scaling	572
14.10 The Google PageRank Algorithm	576
Bibliographic Notes	578
Exercises	579

15 Random Forests	587
15.1 Introduction	587
15.2 Definition of Random Forests	587
15.3 Details of Random Forests	592
15.3.1 Out of Bag Samples	592
15.3.2 Variable Importance	593
15.3.3 Proximity Plots	595
15.3.4 Random Forests and Overfitting	596
15.4 Analysis of Random Forests	597
15.4.1 Variance and the De-Correlation Effect	597
15.4.2 Bias	600
15.4.3 Adaptive Nearest Neighbors	601
Bibliographic Notes	602
Exercises	603
16 Ensemble Learning	605
16.1 Introduction	605
16.2 Boosting and Regularization Paths	607
16.2.1 Penalized Regression	607
16.2.2 The “Bet on Sparsity” Principle	610
16.2.3 Regularization Paths, Over-fitting and Margins .	613
16.3 Learning Ensembles	616
16.3.1 Learning a Good Ensemble	617
16.3.2 Rule Ensembles	622
Bibliographic Notes	623
Exercises	624
17 Undirected Graphical Models	625
17.1 Introduction	625
17.2 Markov Graphs and Their Properties	627
17.3 Undirected Graphical Models for Continuous Variables .	630
17.3.1 Estimation of the Parameters when the Graph Structure is Known	631
17.3.2 Estimation of the Graph Structure	635
17.4 Undirected Graphical Models for Discrete Variables . .	638
17.4.1 Estimation of the Parameters when the Graph Structure is Known	639
17.4.2 Hidden Nodes	641
17.4.3 Estimation of the Graph Structure	642
17.4.4 Restricted Boltzmann Machines	643
Exercises	645
18 High-Dimensional Problems: $p \gg N$	649
18.1 When p is Much Bigger than N	649

18.2	Diagonal Linear Discriminant Analysis and Nearest Shrunken Centroids	651
18.3	Linear Classifiers with Quadratic Regularization	654
18.3.1	Regularized Discriminant Analysis	656
18.3.2	Logistic Regression with Quadratic Regularization	657
18.3.3	The Support Vector Classifier	657
18.3.4	Feature Selection	658
18.3.5	Computational Shortcuts When $p \gg N$	659
18.4	Linear Classifiers with L_1 Regularization	661
18.4.1	Application of Lasso to Protein Mass Spectroscopy	664
18.4.2	The Fused Lasso for Functional Data	666
18.5	Classification When Features are Unavailable	668
18.5.1	Example: String Kernels and Protein Classification	668
18.5.2	Classification and Other Models Using Inner-Product Kernels and Pairwise Distances .	670
18.5.3	Example: Abstracts Classification	672
18.6	High-Dimensional Regression: Supervised Principal Components	674
18.6.1	Connection to Latent-Variable Modeling	678
18.6.2	Relationship with Partial Least Squares	680
18.6.3	Pre-Conditioning for Feature Selection	681
18.7	Feature Assessment and the Multiple-Testing Problem .	683
18.7.1	The False Discovery Rate	687
18.7.2	Asymmetric Cutpoints and the SAM Procedure	690
18.7.3	A Bayesian Interpretation of the FDR	692
18.8	Bibliographic Notes	693
	Exercises	694
	References	699
	Author Index	729
	Index	737

1

Introduction

Statistical learning plays a key role in many areas of science, finance and industry. Here are some examples of learning problems:

- Predict whether a patient, hospitalized due to a heart attack, will have a second heart attack. The prediction is to be based on demographic, diet and clinical measurements for that patient.
- Predict the price of a stock in 6 months from now, on the basis of company performance measures and economic data.
- Identify the numbers in a handwritten ZIP code, from a digitized image.
- Estimate the amount of glucose in the blood of a diabetic person, from the infrared absorption spectrum of that person's blood.
- Identify the risk factors for prostate cancer, based on clinical and demographic variables.

The science of learning plays a key role in the fields of statistics, data mining and artificial intelligence, intersecting with areas of engineering and other disciplines.

This book is about learning from data. In a typical scenario, we have an outcome measurement, usually quantitative (such as a stock price) or categorical (such as heart attack/no heart attack), that we wish to predict based on a set of *features* (such as diet and clinical measurements). We have a *training set* of data, in which we observe the outcome and feature

TABLE 1.1. Average percentage of words or characters in an email message equal to the indicated word or character. We have chosen the words and characters showing the largest difference between `spam` and `email`.

	george	you	your	hp	free	hpl	!	our	re	edu	remove
spam	0.00	2.26	1.38	0.02	0.52	0.01	0.51	0.51	0.13	0.01	0.28
email	1.27	1.27	0.44	0.90	0.07	0.43	0.11	0.18	0.42	0.29	0.01

measurements for a set of objects (such as people). Using this data we build a prediction model, or *learner*, which will enable us to predict the outcome for new unseen objects. A good learner is one that accurately predicts such an outcome.

The examples above describe what is called the *supervised learning* problem. It is called “supervised” because of the presence of the outcome variable to guide the learning process. In the *unsupervised learning problem*, we observe only the features and have no measurements of the outcome. Our task is rather to describe how the data are organized or clustered. We devote most of this book to supervised learning; the unsupervised problem is less developed in the literature, and is the focus of Chapter 14.

Here are some examples of real learning problems that are discussed in this book.

Example 1: Email Spam

The data for this example consists of information from 4601 email messages, in a study to try to predict whether the email was junk email, or “spam.” The objective was to design an automatic spam detector that could filter out spam before clogging the users’ mailboxes. For all 4601 email messages, the true outcome (email type) `email` or `spam` is available, along with the relative frequencies of 57 of the most commonly occurring words and punctuation marks in the email message. This is a supervised learning problem, with the outcome the class variable `email`/`spam`. It is also called a *classification* problem.

Table 1.1 lists the words and characters showing the largest average difference between `spam` and `email`.

Our learning method has to decide which features to use and how: for example, we might use a rule such as

```
if (%george < 0.6) & (%you > 1.5)    then spam
else email.
```

Another form of a rule might be:

```
if (0.2 · %you - 0.3 · %george) > 0    then spam
else email.
```

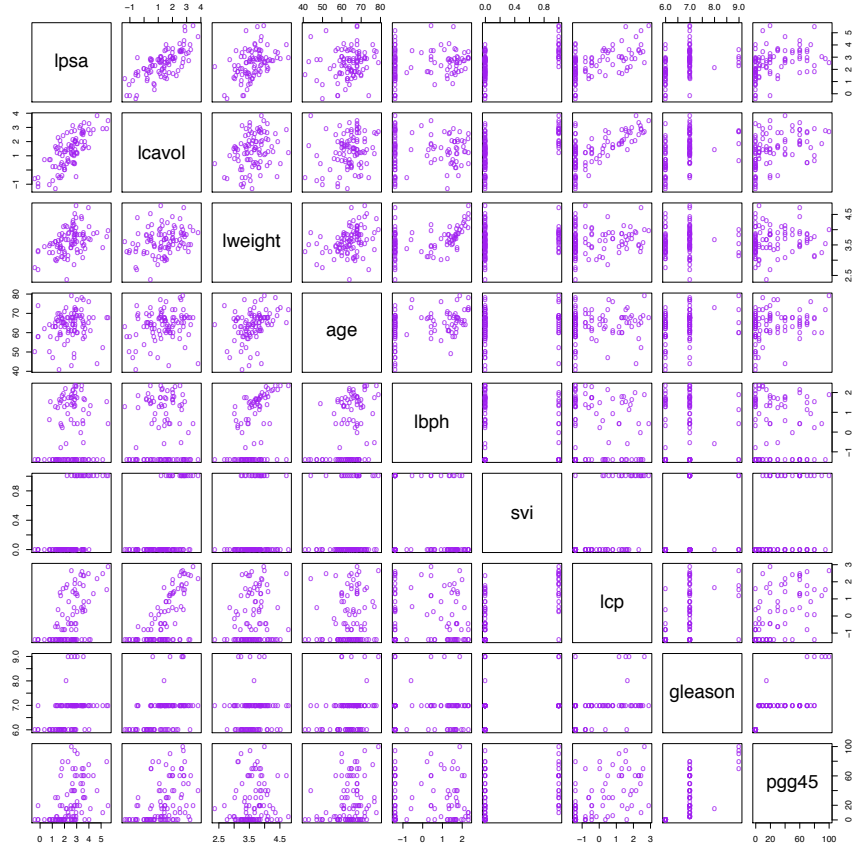


FIGURE 1.1. Scatterplot matrix of the prostate cancer data. The first row shows the response against each of the predictors in turn. Two of the predictors, `svi` and `gleason`, are categorical.

For this problem not all errors are equal; we want to avoid filtering out good email, while letting spam get through is not desirable but less serious in its consequences. We discuss a number of different methods for tackling this learning problem in the book.

Example 2: Prostate Cancer

The data for this example, displayed in Figure 1.1¹, come from a study by Stamey et al. (1989) that examined the correlation between the level of

¹There was an error in these data in the first edition of this book. Subject 32 had a value of 6.1 for `lweight`, which translates to a 449 gm prostate! The correct value is 44.9 gm. We are grateful to Prof. Stephen W. Link for alerting us to this error.

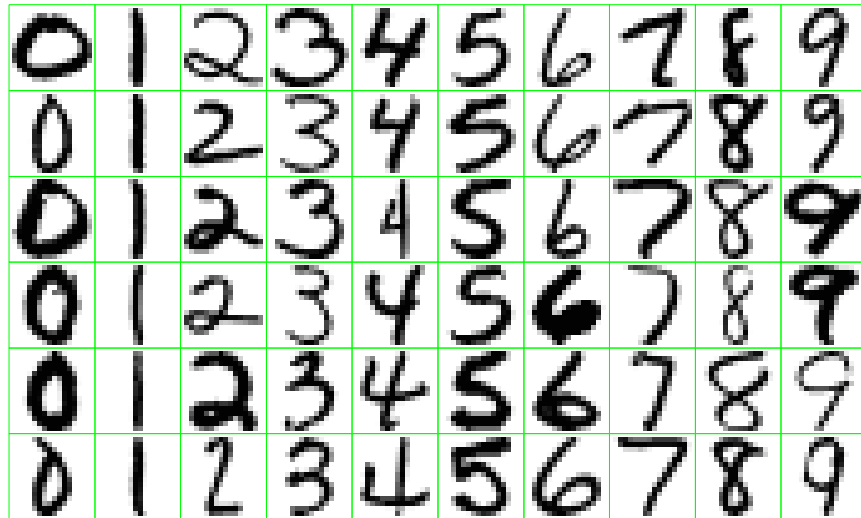


FIGURE 1.2. Examples of handwritten digits from U.S. postal envelopes.

prostate specific antigen (PSA) and a number of clinical measures, in 97 men who were about to receive a radical prostatectomy.

The goal is to predict the log of PSA (`lpsa`) from a number of measurements including log cancer volume (`lcavol`), log prostate weight `lweight`, age, log of benign prostatic hyperplasia amount `lbph`, seminal vesicle invasion `svi`, log of capsular penetration `lcp`, Gleason score `gleason`, and percent of Gleason scores 4 or 5 `pgg45`. Figure 1.1 is a scatterplot matrix of the variables. Some correlations with `lpsa` are evident, but a good predictive model is difficult to construct by eye.

This is a supervised learning problem, known as a *regression problem*, because the outcome measurement is quantitative.

Example 3: Handwritten Digit Recognition

The data from this example come from the handwritten ZIP codes on envelopes from U.S. postal mail. Each image is a segment from a five digit ZIP code, isolating a single digit. The images are 16×16 eight-bit grayscale maps, with each pixel ranging in intensity from 0 to 255. Some sample images are shown in Figure 1.2.

The images have been normalized to have approximately the same size and orientation. The task is to predict, from the 16×16 matrix of pixel intensities, the identity of each image ($0, 1, \dots, 9$) quickly and accurately. If it is accurate enough, the resulting algorithm would be used as part of an automatic sorting procedure for envelopes. This is a classification problem for which the error rate needs to be kept very low to avoid misdirection of

mail. In order to achieve this low error rate, some objects can be assigned to a “don’t know” category, and sorted instead by hand.

Example 4: DNA Expression Microarrays

DNA stands for deoxyribonucleic acid, and is the basic material that makes up human chromosomes. DNA microarrays measure the expression of a gene in a cell by measuring the amount of mRNA (messenger ribonucleic acid) present for that gene. Microarrays are considered a breakthrough technology in biology, facilitating the quantitative study of thousands of genes simultaneously from a single sample of cells.

Here is how a DNA microarray works. The nucleotide sequences for a few thousand genes are printed on a glass slide. A target sample and a reference sample are labeled with red and green dyes, and each are hybridized with the DNA on the slide. Through fluoroscopy, the log (red/green) intensities of RNA hybridizing at each site is measured. The result is a few thousand numbers, typically ranging from say -6 to 6 , measuring the expression level of each gene in the target relative to the reference sample. Positive values indicate higher expression in the target versus the reference, and vice versa for negative values.

A gene expression dataset collects together the expression values from a series of DNA microarray experiments, with each column representing an experiment. There are therefore several thousand rows representing individual genes, and tens of columns representing samples: in the particular example of Figure 1.3 there are 6830 genes (rows) and 64 samples (columns), although for clarity only a random sample of 100 rows are shown. The figure displays the data set as a heat map, ranging from green (negative) to red (positive). The samples are 64 cancer tumors from different patients.

The challenge here is to understand how the genes and samples are organized. Typical questions include the following:

- (a) which samples are most similar to each other, in terms of their expression profiles across genes?
- (b) which genes are most similar to each other, in terms of their expression profiles across samples?
- (c) do certain genes show very high (or low) expression for certain cancer samples?

We could view this task as a regression problem, with two categorical predictor variables—genes and samples—with the response variable being the level of expression. However, it is probably more useful to view it as *unsupervised learning* problem. For example, for question (a) above, we think of the samples as points in 6830-dimensional space, which we want to *cluster* together in some way.

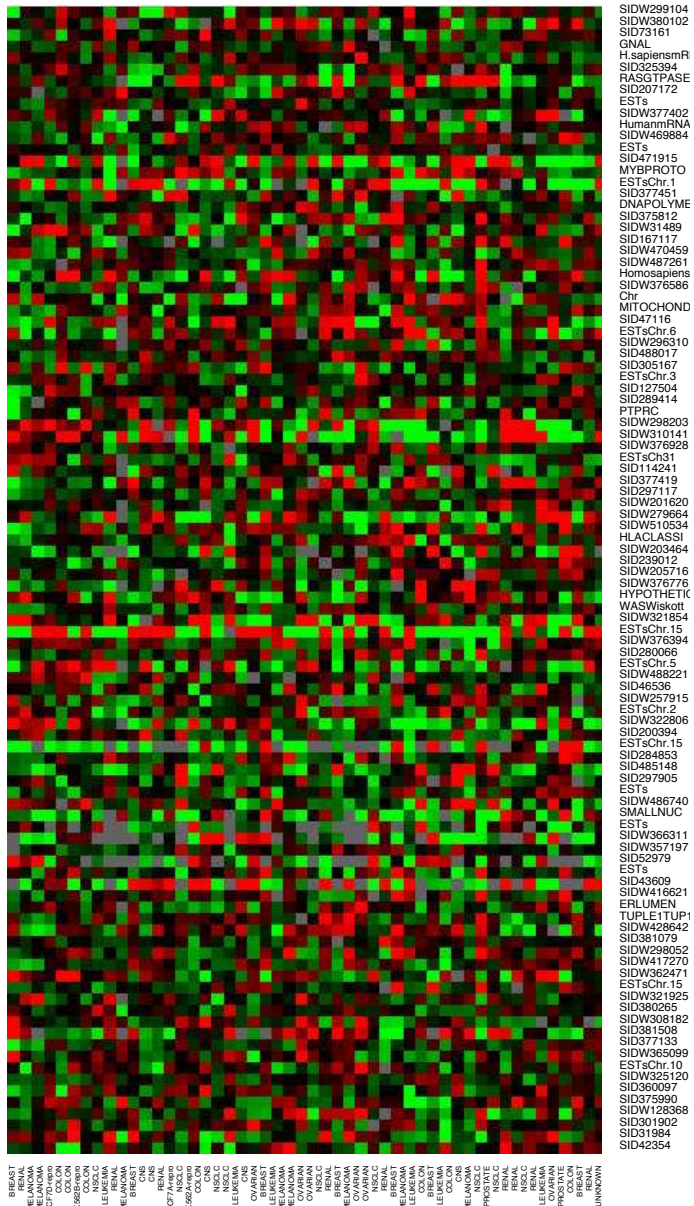


FIGURE 1.3. DNA microarray data: expression matrix of 6830 genes (rows) and 64 samples (columns), for the human tumor data. Only a random sample of 100 rows are shown. The display is a heat map, ranging from bright green (negative, under expressed) to bright red (positive, over expressed). Missing values are gray. The rows and columns are displayed in a randomly chosen order.

Who Should Read this Book

This book is designed for researchers and students in a broad variety of fields: statistics, artificial intelligence, engineering, finance and others. We expect that the reader will have had at least one elementary course in statistics, covering basic topics including linear regression.

We have not attempted to write a comprehensive catalog of learning methods, but rather to describe some of the most important techniques. Equally notable, we describe the underlying concepts and considerations by which a researcher can judge a learning method. We have tried to write this book in an intuitive fashion, emphasizing concepts rather than mathematical details.

As statisticians, our exposition will naturally reflect our backgrounds and areas of expertise. However in the past eight years we have been attending conferences in neural networks, data mining and machine learning, and our thinking has been heavily influenced by these exciting fields. This influence is evident in our current research, and in this book.

How This Book is Organized

Our view is that one must understand simple methods before trying to grasp more complex ones. Hence, after giving an overview of the supervising learning problem in [Chapter 2](#), we discuss linear methods for regression and classification in [Chapters 3 and 4](#). In [Chapter 5](#) we describe splines, wavelets and regularization/penalization methods for a single predictor, while [Chapter 6](#) covers kernel methods and local regression. Both of these sets of methods are important building blocks for high-dimensional learning techniques. Model assessment and selection is the topic of [Chapter 7](#), covering the concepts of bias and variance, overfitting and methods such as cross-validation for choosing models. [Chapter 8](#) discusses model inference and averaging, including an overview of maximum likelihood, Bayesian inference and the bootstrap, the EM algorithm, Gibbs sampling and bagging. A related procedure called boosting is the focus of [Chapter 10](#).

In [Chapters 9–13](#) we describe a series of structured methods for supervised learning, with [Chapters 9 and 11](#) covering regression and [Chapters 12 and 13](#) focusing on classification. [Chapter 14](#) describes methods for unsupervised learning. Two recently proposed techniques, random forests and ensemble learning, are discussed in [Chapters 15 and 16](#). We describe undirected graphical models in [Chapter 17](#) and finally we study high-dimensional problems in [Chapter 18](#).

At the end of each chapter we discuss [computational considerations](#) important for data mining applications, including how the computations scale with the number of observations and predictors. Each chapter ends with [Bibliographic Notes](#) giving background references for the material.

We recommend that Chapters 1–4 be first read in sequence. Chapter 7 should also be considered mandatory, as it covers central concepts that pertain to all learning methods. With this in mind, the rest of the book can be read sequentially, or sampled, depending on the reader’s interest.



The symbol indicates a technically difficult section, one that can be skipped without interrupting the flow of the discussion.

Book Website

The website for this book is located at

<http://www-stat.stanford.edu/ElemStatLearn>

It contains a number of resources, including many of the datasets used in this book.

Note for Instructors

We have successively used the first edition of this book as the basis for a two-quarter course, and with the additional materials in this second edition, it could even be used for a three-quarter sequence. Exercises are provided at the end of each chapter. It is important for students to have access to good software tools for these topics. We used the R and S-PLUS programming languages in our courses.

2

Overview of Supervised Learning

2.1 Introduction

The first three examples described in Chapter 1 have several components in common. For each there is a set of variables that might be denoted as *inputs*, which are measured or preset. These have some influence on one or more *outputs*. For each example the goal is to use the inputs to predict the values of the outputs. This exercise is called *supervised learning*.

We have used the more modern language of machine learning. In the statistical literature the inputs are often called the *predictors*, a term we will use interchangeably with inputs, and more classically the *independent variables*. In the pattern recognition literature the term *features* is preferred, which we use as well. The outputs are called the *responses*, or classically the *dependent variables*.

2.2 Variable Types and Terminology

The outputs vary in nature among the examples. In the glucose prediction example, the output is a *quantitative* measurement, where some measurements are bigger than others, and measurements close in value are close in nature. In the famous Iris discrimination example due to R. A. Fisher, the output is *qualitative* (species of Iris) and assumes values in a finite set $\mathcal{G} = \{\text{Virginica, Setosa and Versicolor}\}$. In the handwritten digit example the output is one of 10 different digit *classes*: $\mathcal{G} = \{0, 1, \dots, 9\}$. In both of

these there is no explicit ordering in the classes, and in fact often descriptive labels rather than numbers are used to denote the classes. Qualitative variables are also referred to as *categorical* or *discrete* variables as well as *factors*.

For both types of outputs it makes sense to think of using the inputs to predict the output. Given some specific atmospheric measurements today and yesterday, we want to predict the ozone level tomorrow. Given the grayscale values for the pixels of the digitized image of the handwritten digit, we want to predict its class label.

This distinction in output type has led to a naming convention for the prediction tasks: *regression* when we predict quantitative outputs, and *classification* when we predict qualitative outputs. We will see that these two tasks have a lot in common, and in particular both can be viewed as a task in function approximation.

Inputs also vary in measurement type; we can have some of each of qualitative and quantitative input variables. These have also led to distinctions in the types of methods that are used for prediction: some methods are defined most naturally for quantitative inputs, some most naturally for qualitative and some for both.

A third variable type is *ordered categorical*, such as *small*, *medium* and *large*, where there is an ordering between the values, but no metric notion is appropriate (the difference between medium and small need not be the same as that between large and medium). These are discussed further in Chapter 4.

Qualitative variables are typically represented numerically by codes. The easiest case is when there are only two classes or categories, such as “success” or “failure,” “survived” or “died.” These are often represented by a single binary digit or bit as 0 or 1, or else by -1 and 1. For reasons that will become apparent, such numeric codes are sometimes referred to as *targets*. When there are more than two categories, several alternatives are available. The most useful and commonly used coding is via *dummy variables*. Here a K -level qualitative variable is represented by a vector of K binary variables or bits, only one of which is “on” at a time. Although more compact coding schemes are possible, dummy variables are symmetric in the levels of the factor.

We will typically denote an input variable by the symbol X . If X is a vector, its components can be accessed by subscripts X_j . Quantitative outputs will be denoted by Y , and qualitative outputs by G (for group). We use uppercase letters such as X , Y or G when referring to the generic aspects of a variable. Observed values are written in lowercase; hence the i th observed value of X is written as x_i (where x_i is again a scalar or vector). Matrices are represented by bold uppercase letters; for example, a set of N input p -vectors x_i , $i = 1, \dots, N$ would be represented by the $N \times p$ matrix \mathbf{X} . In general, vectors will not be bold, except when they have N components; this convention distinguishes a p -vector of inputs x_i for the

i th observation from the N -vector \mathbf{x}_j consisting of all the observations on variable X_j . Since all vectors are assumed to be column vectors, the i th row of \mathbf{X} is x_i^T , the vector transpose of x_i .

For the moment we can loosely state the learning task as follows: given the value of an input vector X , make a good prediction of the output Y , denoted by \hat{Y} (pronounced “y-hat”). If Y takes values in \mathbb{R} then so should \hat{Y} ; likewise for categorical outputs, \hat{G} should take values in the same set \mathcal{G} associated with G .

For a two-class G , one approach is to denote the binary coded target as Y , and then treat it as a quantitative output. The predictions \hat{Y} will typically lie in $[0, 1]$, and we can assign to \hat{G} the class label according to whether $\hat{y} > 0.5$. This approach generalizes to K -level qualitative outputs as well.

We need data to construct prediction rules, often a lot of it. We thus suppose we have available a set of measurements (x_i, y_i) or (x_i, g_i) , $i = 1, \dots, N$, known as the *training data*, with which to construct our prediction rule.

2.3 Two Simple Approaches to Prediction: Least Squares and Nearest Neighbors

In this section we develop two simple but powerful prediction methods: the linear model fit by least squares and the k -nearest-neighbor prediction rule. The linear model makes huge assumptions about structure and yields stable but possibly inaccurate predictions. The method of k -nearest neighbors makes very mild structural assumptions: its predictions are often accurate but can be unstable.

2.3.1 Linear Models and Least Squares

The linear model has been a mainstay of statistics for the past 30 years and remains one of our most important tools. Given a vector of inputs $X^T = (X_1, X_2, \dots, X_p)$, we predict the output Y via the model

$$\hat{Y} = \hat{\beta}_0 + \sum_{j=1}^p X_j \hat{\beta}_j. \quad (2.1)$$

The term $\hat{\beta}_0$ is the intercept, also known as the *bias* in machine learning. Often it is convenient to include the constant variable 1 in X , include $\hat{\beta}_0$ in the vector of coefficients $\hat{\beta}$, and then write the linear model in vector form as an inner product

$$\hat{Y} = X^T \hat{\beta}, \quad (2.2)$$

where X^T denotes vector or matrix transpose (X being a column vector). Here we are modeling a single output, so \hat{Y} is a scalar; in general \hat{Y} can be a K -vector, in which case β would be a $p \times K$ matrix of coefficients. In the $(p + 1)$ -dimensional input–output space, (X, \hat{Y}) represents a hyperplane. If the constant is included in X , then the hyperplane includes the origin and is a subspace; if not, it is an affine set cutting the Y -axis at the point $(0, \hat{\beta}_0)$. From now on we assume that the intercept is included in $\hat{\beta}$.

Viewed as a function over the p -dimensional input space, $f(X) = X^T \beta$ is linear, and the gradient $f'(X) = \beta$ is a vector in input space that points in the steepest uphill direction.

How do we fit the linear model to a set of training data? There are many different methods, but by far the most popular is the method of *least squares*. In this approach, we pick the coefficients β to minimize the residual sum of squares

$$\text{RSS}(\beta) = \sum_{i=1}^N (y_i - x_i^T \beta)^2. \quad (2.3)$$

$\text{RSS}(\beta)$ is a quadratic function of the parameters, and hence its minimum always exists, but may not be unique. The solution is easiest to characterize in matrix notation. We can write

$$\text{RSS}(\beta) = (\mathbf{y} - \mathbf{X}\beta)^T (\mathbf{y} - \mathbf{X}\beta), \quad (2.4)$$

where \mathbf{X} is an $N \times p$ matrix with each row an input vector, and \mathbf{y} is an N -vector of the outputs in the training set. Differentiating w.r.t. β we get the *normal equations*

$$\mathbf{X}^T (\mathbf{y} - \mathbf{X}\beta) = 0. \quad (2.5)$$

If $\mathbf{X}^T \mathbf{X}$ is nonsingular, then the unique solution is given by

$$\hat{\beta} = (\mathbf{X}^T \mathbf{X})^{-1} \mathbf{X}^T \mathbf{y}, \quad (2.6)$$

and the fitted value at the i th input x_i is $\hat{y}_i = \hat{y}(x_i) = x_i^T \hat{\beta}$. At an arbitrary input x_0 the prediction is $\hat{y}(x_0) = x_0^T \hat{\beta}$. The entire fitted surface is characterized by the p parameters $\hat{\beta}$. Intuitively, it seems that we do not need a very large data set to fit such a model.

Let's look at an example of the linear model in a classification context. Figure 2.1 shows a scatterplot of training data on a pair of inputs X_1 and X_2 . The data are simulated, and for the present the simulation model is not important. The output class variable G has the values **BLUE** or **ORANGE**, and is represented as such in the scatterplot. There are 100 points in each of the two classes. The linear regression model was fit to these data, with the response Y coded as 0 for **BLUE** and 1 for **ORANGE**. The fitted values \hat{Y} are converted to a fitted class variable \hat{G} according to the rule

$$\hat{G} = \begin{cases} \text{ORANGE} & \text{if } \hat{Y} > 0.5, \\ \text{BLUE} & \text{if } \hat{Y} \leq 0.5. \end{cases} \quad (2.7)$$

Linear Regression of 0/1 Response

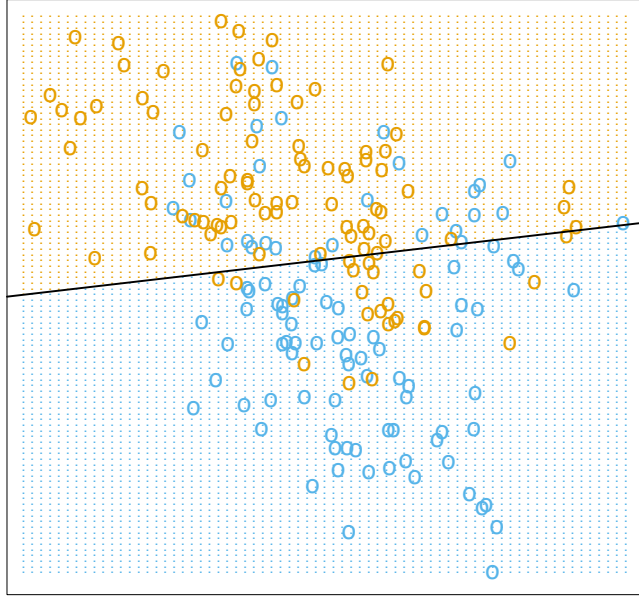


FIGURE 2.1. A classification example in two dimensions. The classes are coded as a binary variable (**BLUE** = 0, **ORANGE** = 1), and then fit by linear regression. The line is the decision boundary defined by $x^T \hat{\beta} = 0.5$. The orange shaded region denotes that part of input space classified as **ORANGE**, while the blue region is classified as **BLUE**.

The set of points in \mathbb{R}^2 classified as **ORANGE** corresponds to $\{x : x^T \hat{\beta} > 0.5\}$, indicated in Figure 2.1, and the two predicted classes are separated by the *decision boundary* $\{x : x^T \hat{\beta} = 0.5\}$, which is linear in this case. We see that for these data there are several misclassifications on both sides of the decision boundary. Perhaps our linear model is too rigid—or are such errors unavoidable? Remember that these are errors on the training data itself, and we have not said where the constructed data came from. Consider the two possible scenarios:

Scenario 1: The training data in each class were generated from bivariate Gaussian distributions with uncorrelated components and different means.

Scenario 2: The training data in each class came from a mixture of 10 low-variance Gaussian distributions, with individual means themselves distributed as Gaussian.

A mixture of Gaussians is best described in terms of the generative model. One first generates a discrete variable that determines which of

the component Gaussians to use, and then generates an observation from the chosen density. In the case of one Gaussian per class, we will see in Chapter 4 that a linear decision boundary is the best one can do, and that our estimate is almost optimal. The region of overlap is inevitable, and future data to be predicted will be plagued by this overlap as well.

In the case of mixtures of tightly clustered Gaussians the story is different. A linear decision boundary is unlikely to be optimal, and in fact is not. The optimal decision boundary is nonlinear and disjoint, and as such will be much more difficult to obtain.

We now look at another classification and regression procedure that is in some sense at the opposite end of the spectrum to the linear model, and far better suited to the second scenario.

2.3.2 Nearest-Neighbor Methods

Nearest-neighbor methods use those observations in the training set \mathcal{T} closest in input space to x to form \hat{Y} . Specifically, the k -nearest neighbor fit for \hat{Y} is defined as follows:

$$\hat{Y}(x) = \frac{1}{k} \sum_{x_i \in N_k(x)} y_i, \quad (2.8)$$

where $N_k(x)$ is the neighborhood of x defined by the k closest points x_i in the training sample. Closeness implies a metric, which for the moment we assume is Euclidean distance. So, in words, we find the k observations with x_i closest to x in input space, and average their responses.

In Figure 2.2 we use the same training data as in Figure 2.1, and use 15-nearest-neighbor averaging of the binary coded response as the method of fitting. Thus \hat{Y} is the proportion of **ORANGE**'s in the neighborhood, and so assigning class **ORANGE** to \hat{G} if $\hat{Y} > 0.5$ amounts to a majority vote in the neighborhood. The colored regions indicate all those points in input space classified as **BLUE** or **ORANGE** by such a rule, in this case found by evaluating the procedure on a fine grid in input space. We see that the decision boundaries that separate the **BLUE** from the **ORANGE** regions are far more irregular, and respond to local clusters where one class dominates.

Figure 2.3 shows the results for 1-nearest-neighbor classification: \hat{Y} is assigned the value y_ℓ of the closest point x_ℓ to x in the training data. In this case the regions of classification can be computed relatively easily, and correspond to a *Voronoi tessellation* of the training data. Each point x_i has an associated tile bounding the region for which it is the closest input point. For all points x in the tile, $\hat{G}(x) = g_i$. The decision boundary is even more irregular than before.

The method of k -nearest-neighbor averaging is defined in exactly the same way for regression of a quantitative output Y , although $k = 1$ would be an unlikely choice.

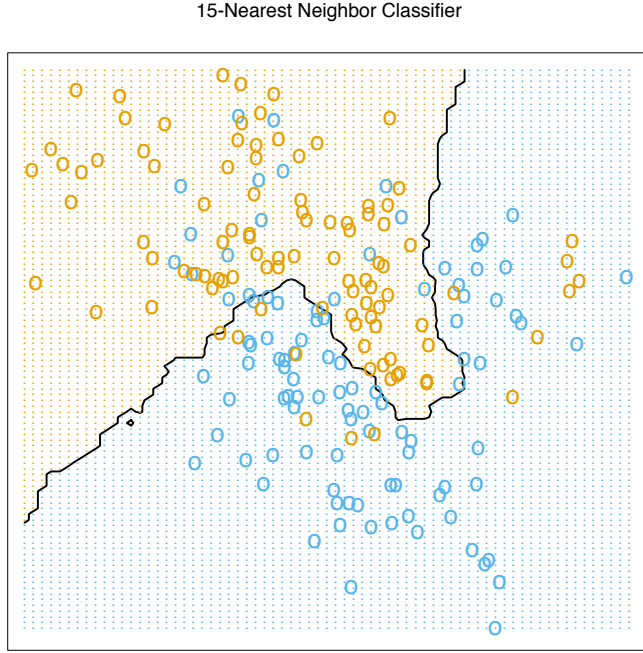


FIGURE 2.2. The same classification example in two dimensions as in Figure 2.1. The classes are coded as a binary variable (BLUE = 0, ORANGE = 1) and then fit by 15-nearest-neighbor averaging as in (2.8). The predicted class is hence chosen by majority vote amongst the 15-nearest neighbors.

In Figure 2.2 we see that far fewer training observations are misclassified than in Figure 2.1. This should not give us too much comfort, though, since in Figure 2.3 *none* of the training data are misclassified. A little thought suggests that for k -nearest-neighbor fits, the error on the training data should be approximately an increasing function of k , and will always be 0 for $k = 1$. An independent test set would give us a more satisfactory means for comparing the different methods.

It appears that k -nearest-neighbor fits have a single parameter, the number of neighbors k , compared to the p parameters in least-squares fits. Although this is the case, we will see that the *effective* number of parameters of k -nearest neighbors is N/k and is generally bigger than p , and decreases with increasing k . To get an idea of why, note that if the neighborhoods were nonoverlapping, there would be N/k neighborhoods and we would fit one parameter (a mean) in each neighborhood.

It is also clear that we cannot use sum-of-squared errors on the training set as a criterion for picking k , since we would always pick $k = 1$! It would seem that k -nearest-neighbor methods would be more appropriate for the mixture Scenario 2 described above, while for Gaussian data the decision boundaries of k -nearest neighbors would be unnecessarily noisy.

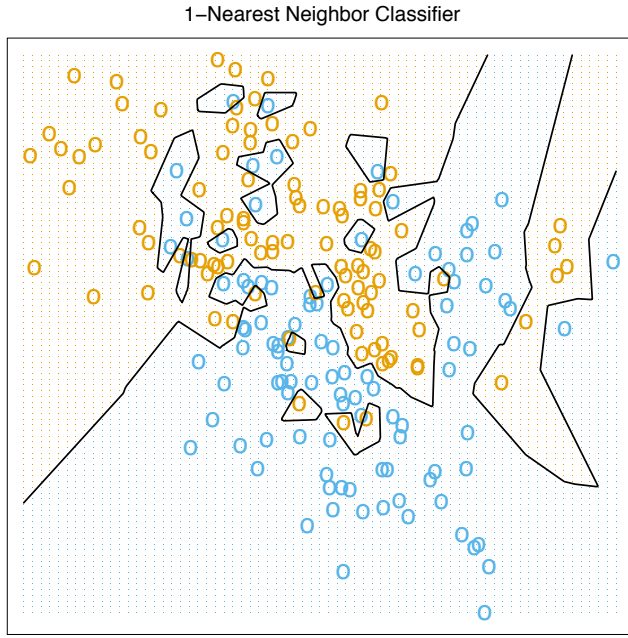


FIGURE 2.3. The same classification example in two dimensions as in Figure 2.1. The classes are coded as a binary variable (**BLUE** = 0, **ORANGE** = 1), and then predicted by 1-nearest-neighbor classification.

2.3.3 From Least Squares to Nearest Neighbors

The linear decision boundary from least squares is very smooth, and apparently stable to fit. It does appear to rely heavily on the assumption that a linear decision boundary is appropriate. In language we will develop shortly, it has low variance and potentially high bias.

On the other hand, the k -nearest-neighbor procedures do not appear to rely on any stringent assumptions about the underlying data, and can adapt to any situation. However, any particular subregion of the decision boundary depends on a handful of input points and their particular positions, and is thus wiggly and unstable—high variance and low bias.

Each method has its own situations for which it works best; in particular linear regression is more appropriate for Scenario 1 above, while nearest neighbors are more suitable for Scenario 2. The time has come to expose the oracle! The data in fact were simulated from a model somewhere between the two, but closer to Scenario 2. First we generated 10 means m_k from a bivariate Gaussian distribution $N((1, 0)^T, \mathbf{I})$ and labeled this class **BLUE**. Similarly, 10 more were drawn from $N((0, 1)^T, \mathbf{I})$ and labeled class **ORANGE**. Then for each class we generated 100 observations as follows: for each observation, we picked an m_k at random with probability $1/10$, and

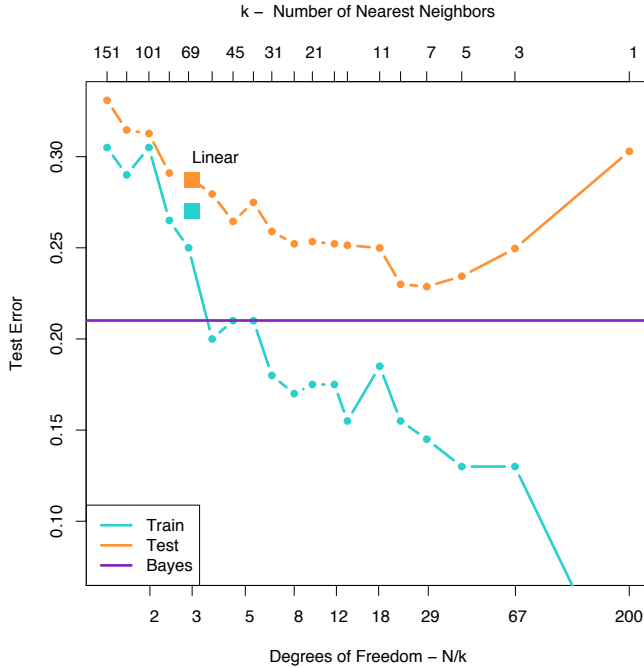


FIGURE 2.4. Misclassification curves for the simulation example used in Figures 2.1, 2.2 and 2.3. A single training sample of size 200 was used, and a test sample of size 10,000. The orange curves are test and the blue are training error for k -nearest-neighbor classification. The results for linear regression are the bigger orange and blue squares at three degrees of freedom. The purple line is the optimal Bayes error rate.

then generated a $N(m_k, \mathbf{I}/5)$, thus leading to a mixture of Gaussian clusters for each class. Figure 2.4 shows the results of classifying 10,000 new observations generated from the model. We compare the results for least squares and those for k -nearest neighbors for a range of values of k .

A large subset of the most popular techniques in use today are variants of these two simple procedures. In fact 1-nearest-neighbor, the simplest of all, captures a large percentage of the market for low-dimensional problems. The following list describes some ways in which these simple procedures have been enhanced:

- Kernel methods use weights that decrease smoothly to zero with distance from the target point, rather than the effective 0/1 weights used by k -nearest neighbors.
- In high-dimensional spaces the distance kernels are modified to emphasize some variable more than others.

- Local regression fits linear models by locally weighted least squares, rather than fitting constants locally.
- Linear models fit to a basis expansion of the original inputs allow arbitrarily complex models.
- Projection pursuit and neural network models consist of sums of non-linearly transformed linear models.

2.4 Statistical Decision Theory

In this section we develop a small amount of theory that provides a framework for developing models such as those discussed informally so far. We first consider the case of a quantitative output, and place ourselves in the world of random variables and probability spaces. Let $X \in \mathbb{R}^p$ denote a real valued random input vector, and $Y \in \mathbb{R}$ a real valued random output variable, with joint distribution $\Pr(X, Y)$. We seek a function $f(X)$ for predicting Y given values of the input X . This theory requires a *loss function* $L(Y, f(X))$ for penalizing errors in prediction, and by far the most common and convenient is *squared error loss*: $L(Y, f(X)) = (Y - f(X))^2$. This leads us to a criterion for choosing f ,

$$\text{EPE}(f) = \mathbb{E}(Y - f(X))^2 \quad (2.9)$$

$$= \int [y - f(x)]^2 \Pr(dx, dy), \quad (2.10)$$

the expected (squared) prediction error . By conditioning¹ on X , we can write EPE as

$$\text{EPE}(f) = \mathbb{E}_X \mathbb{E}_{Y|X} ([Y - f(X)]^2 | X) \quad (2.11)$$

and we see that it suffices to minimize EPE pointwise:

$$f(x) = \operatorname{argmin}_c \mathbb{E}_{Y|X} ([Y - c]^2 | X = x). \quad (2.12)$$

The solution is

$$f(x) = \mathbb{E}(Y | X = x), \quad (2.13)$$

the conditional expectation, also known as the *regression* function. Thus the best prediction of Y at any point $X = x$ is the conditional mean, when best is measured by average squared error.

The nearest-neighbor methods attempt to directly implement this recipe using the training data. At each point x , we might ask for the average of all

¹Conditioning here amounts to factoring the joint density $\Pr(X, Y) = \Pr(Y|X)\Pr(X)$ where $\Pr(Y|X) = \Pr(Y, X)/\Pr(X)$, and splitting up the bivariate integral accordingly.

those y_i s with input $x_i = x$. Since there is typically at most one observation at any point x , we settle for

$$\hat{f}(x) = \text{Ave}(y_i | x_i \in N_k(x)), \quad (2.14)$$

where “Ave” denotes average, and $N_k(x)$ is the neighborhood containing the k points in \mathcal{T} closest to x . Two approximations are happening here:

- expectation is approximated by averaging over sample data;
- conditioning at a point is relaxed to conditioning on some region “close” to the target point.

For large training sample size N , the points in the neighborhood are likely to be close to x , and as k gets large the average will get more stable. In fact, under mild regularity conditions on the joint probability distribution $\Pr(X, Y)$, one can show that as $N, k \rightarrow \infty$ such that $k/N \rightarrow 0$, $\hat{f}(x) \rightarrow E(Y|X = x)$. In light of this, why look further, since it seems we have a universal approximator? We often do not have very large samples. If the linear or some more structured model is appropriate, then we can usually get a more stable estimate than k -nearest neighbors, although such knowledge has to be learned from the data as well. There are other problems though, sometimes disastrous. In Section 2.5 we see that as the dimension p gets large, so does the metric size of the k -nearest neighborhood. So settling for nearest neighborhood as a surrogate for conditioning will fail us miserably. The convergence above still holds, but the *rate* of convergence decreases as the dimension increases.

How does linear regression fit into this framework? The simplest explanation is that one assumes that the regression function $f(x)$ is approximately linear in its arguments:

$$f(x) \approx x^T \beta. \quad (2.15)$$

This is a model-based approach—we specify a model for the regression function. Plugging this linear model for $f(x)$ into EPE (2.9) and differentiating we can solve for β theoretically:

$$\beta = [E(XX^T)]^{-1}E(XY). \quad (2.16)$$

Note we have *not* conditioned on X ; rather we have used our knowledge of the functional relationship to *pool* over values of X . The least squares solution (2.6) amounts to replacing the expectation in (2.16) by averages over the training data.

So both k -nearest neighbors and least squares end up approximating conditional expectations by averages. But they differ dramatically in terms of model assumptions:

- Least squares assumes $f(x)$ is well approximated by a globally linear function.

- k -nearest neighbors assumes $f(x)$ is well approximated by a locally constant function.

Although the latter seems more palatable, we have already seen that we may pay a price for this flexibility.

Many of the more modern techniques described in this book are model based, although far more flexible than the rigid linear model. For example, additive models assume that

$$f(X) = \sum_{j=1}^p f_j(X_j). \quad (2.17)$$

This retains the additivity of the linear model, but each coordinate function f_j is arbitrary. It turns out that the optimal estimate for the additive model uses techniques such as k -nearest neighbors to approximate *univariate* conditional expectations *simultaneously* for each of the coordinate functions. Thus the problems of estimating a conditional expectation in high dimensions are swept away in this case by imposing some (often unrealistic) model assumptions, in this case additivity.

Are we happy with the criterion (2.11)? What happens if we replace the L_2 loss function with the L_1 : $E|Y - f(X)|$? The solution in this case is the conditional median,

$$\hat{f}(x) = \text{median}(Y|X = x), \quad (2.18)$$

which is a different measure of location, and its estimates are more robust than those for the conditional mean. L_1 criteria have discontinuities in their derivatives, which have hindered their widespread use. Other more resistant loss functions will be mentioned in later chapters, but squared error is analytically convenient and the most popular.

What do we do when the output is a categorical variable G ? The same paradigm works here, except we need a different loss function for penalizing prediction errors. An estimate \hat{G} will assume values in \mathcal{G} , the set of possible classes. Our loss function can be represented by a $K \times K$ matrix \mathbf{L} , where $K = \text{card}(\mathcal{G})$. \mathbf{L} will be zero on the diagonal and nonnegative elsewhere, where $L(k, \ell)$ is the price paid for classifying an observation belonging to class \mathcal{G}_k as \mathcal{G}_ℓ . Most often we use the *zero-one* loss function, where all misclassifications are charged a single unit. The expected prediction error is

$$\text{EPE} = E[L(G, \hat{G}(X))], \quad (2.19)$$

where again the expectation is taken with respect to the joint distribution $\Pr(G, X)$. Again we condition, and can write EPE as

$$\text{EPE} = E_X \sum_{k=1}^K L[\mathcal{G}_k, \hat{G}(X)] \Pr(\mathcal{G}_k | X) \quad (2.20)$$

Bayes Optimal Classifier

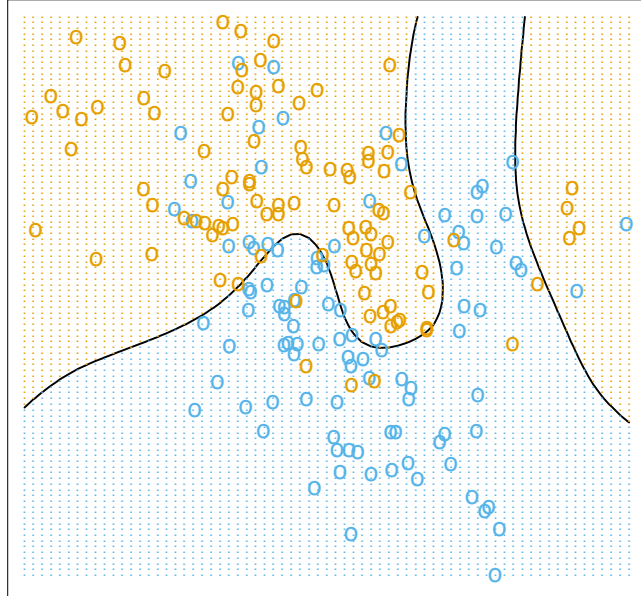


FIGURE 2.5. The optimal Bayes decision boundary for the simulation example of Figures 2.1, 2.2 and 2.3. Since the generating density is known for each class, this boundary can be calculated exactly (Exercise 2.2).

and again it suffices to minimize EPE pointwise:

$$\hat{G}(x) = \operatorname{argmin}_{g \in \mathcal{G}} \sum_{k=1}^K L(\mathcal{G}_k, g) \Pr(\mathcal{G}_k | X = x). \quad (2.21)$$

With the 0–1 loss function this simplifies to

$$\hat{G}(x) = \operatorname{argmin}_{g \in \mathcal{G}} [1 - \Pr(g | X = x)] \quad (2.22)$$

or simply

$$\hat{G}(x) = \mathcal{G}_k \text{ if } \Pr(\mathcal{G}_k | X = x) = \max_{g \in \mathcal{G}} \Pr(g | X = x). \quad (2.23)$$

This reasonable solution is known as the *Bayes classifier*, and says that we classify to the most probable class, using the conditional (discrete) distribution $\Pr(G|X)$. Figure 2.5 shows the Bayes-optimal decision boundary for our simulation example. The error rate of the Bayes classifier is called the *Bayes rate*.

Again we see that the k -nearest neighbor classifier directly approximates this solution—a majority vote in a nearest neighborhood amounts to exactly this, except that conditional probability at a point is relaxed to conditional probability within a neighborhood of a point, and probabilities are estimated by training-sample proportions.

Suppose for a two-class problem we had taken the dummy-variable approach and coded G via a binary Y , followed by squared error loss estimation. Then $\hat{f}(X) = E(Y|X) = \Pr(G = G_1|X)$ if G_1 corresponded to $Y = 1$. Likewise for a K -class problem, $E(Y_k|X) = \Pr(G = G_k|X)$. This shows that our dummy-variable regression procedure, followed by classification to the largest fitted value, is another way of representing the Bayes classifier. Although this theory is exact, in practice problems can occur, depending on the regression model used. For example, when linear regression is used, $\hat{f}(X)$ need not be positive, and we might be suspicious about using it as an estimate of a probability. We will discuss a variety of approaches to modeling $\Pr(G|X)$ in Chapter 4.

2.5 Local Methods in High Dimensions

We have examined two learning techniques for prediction so far: the stable but biased linear model and the less stable but apparently less biased class of k -nearest-neighbor estimates. It would seem that with a reasonably large set of training data, we could always approximate the theoretically optimal conditional expectation by k -nearest-neighbor averaging, since we should be able to find a fairly large neighborhood of observations close to any x and average them. This approach and our intuition breaks down in high dimensions, and the phenomenon is commonly referred to as the *curse of dimensionality* (Bellman, 1961). There are many manifestations of this problem, and we will examine a few here.

Consider the nearest-neighbor procedure for inputs uniformly distributed in a p -dimensional unit hypercube, as in Figure 2.6. Suppose we send out a hypercubical neighborhood about a target point to capture a fraction r of the observations. Since this corresponds to a fraction r of the unit volume, the expected edge length will be $e_p(r) = r^{1/p}$. In ten dimensions $e_{10}(0.01) = 0.63$ and $e_{10}(0.1) = 0.80$, while the entire range for each input is only 1.0. So to capture 1% or 10% of the data to form a local average, we must cover 63% or 80% of the range of each input variable. Such neighborhoods are no longer “local.” Reducing r dramatically does not help much either, since the fewer observations we average, the higher is the variance of our fit.

Another consequence of the sparse sampling in high dimensions is that all sample points are close to an edge of the sample. Consider N data points uniformly distributed in a p -dimensional unit ball centered at the origin. Suppose we consider a nearest-neighbor estimate at the origin. The median

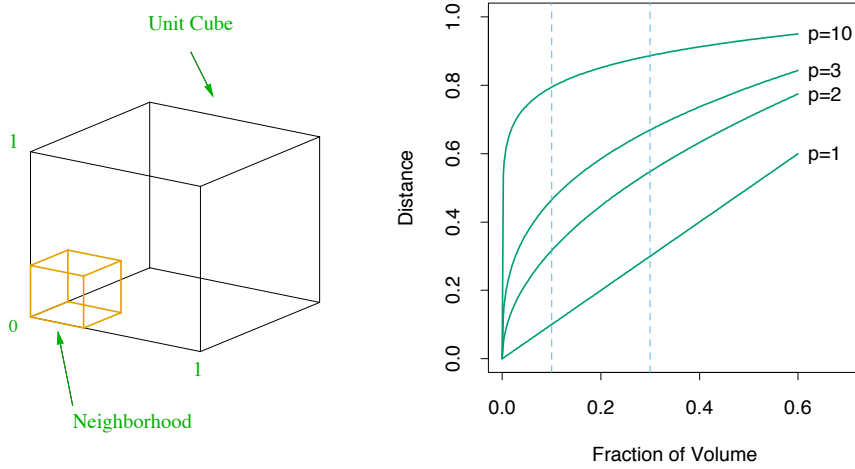


FIGURE 2.6. The curse of dimensionality is well illustrated by a subcubical neighborhood for uniform data in a unit cube. The figure on the right shows the side-length of the subcube needed to capture a fraction r of the volume of the data, for different dimensions p . In ten dimensions we need to cover 80% of the range of each coordinate to capture 10% of the data.

distance from the origin to the closest data point is given by the expression

$$d(p, N) = \left(1 - \frac{1}{2}^{1/N}\right)^{1/p} \quad (2.24)$$

(Exercise 2.3). A more complicated expression exists for the mean distance to the closest point. For $N = 500$, $p = 10$, $d(p, N) \approx 0.52$, more than halfway to the boundary. Hence most data points are closer to the boundary of the sample space than to any other data point. The reason that this presents a problem is that prediction is much more difficult near the edges of the training sample. One must extrapolate from neighboring sample points rather than interpolate between them.

Another manifestation of the curse is that the sampling density is proportional to $N^{1/p}$, where p is the dimension of the input space and N is the sample size. Thus, if $N_1 = 100$ represents a dense sample for a single input problem, then $N_{10} = 100^{10}$ is the sample size required for the same sampling density with 10 inputs. Thus in high dimensions all feasible training samples sparsely populate the input space.

Let us construct another uniform example. Suppose we have 1000 training examples x_i generated uniformly on $[-1, 1]^p$. Assume that the true relationship between X and Y is

$$Y = f(X) = e^{-8\|X\|^2},$$

without any measurement error. We use the 1-nearest-neighbor rule to predict y_0 at the test-point $x_0 = 0$. Denote the training set by \mathcal{T} . We can

compute the expected prediction error at x_0 for our procedure, averaging over all such samples of size 1000. Since the problem is deterministic, this is the mean squared error (MSE) for estimating $f(0)$:

$$\begin{aligned} \text{MSE}(x_0) &= \mathbb{E}_{\mathcal{T}}[f(x_0) - \hat{y}_0]^2 \\ &= \mathbb{E}_{\mathcal{T}}[\hat{y}_0 - \mathbb{E}_{\mathcal{T}}(\hat{y}_0)]^2 + [\mathbb{E}_{\mathcal{T}}(\hat{y}_0) - f(x_0)]^2 \\ &= \text{Var}_{\mathcal{T}}(\hat{y}_0) + \text{Bias}^2(\hat{y}_0). \end{aligned} \quad (2.25)$$

Figure 2.7 illustrates the setup. We have broken down the MSE into two components that will become familiar as we proceed: variance and squared bias. Such a decomposition is always possible and often useful, and is known as the *bias-variance decomposition*. Unless the nearest neighbor is at 0, \hat{y}_0 will be smaller than $f(0)$ in this example, and so the average estimate will be biased downward. The variance is due to the sampling variance of the 1-nearest neighbor. In low dimensions and with $N = 1000$, the nearest neighbor is very close to 0, and so both the bias and variance are small. As the dimension increases, the nearest neighbor tends to stray further from the target point, and both bias and variance are incurred. By $p = 10$, for more than 99% of the samples the nearest neighbor is a distance greater than 0.5 from the origin. Thus as p increases, the estimate tends to be 0 more often than not, and hence the MSE levels off at 1.0, as does the bias, and the variance starts dropping (an artifact of this example).

Although this is a highly contrived example, similar phenomena occur more generally. The complexity of functions of many variables can grow exponentially with the dimension, and if we wish to be able to estimate such functions with the same accuracy as function in low dimensions, then we need the size of our training set to grow exponentially as well. In this example, the function is a complex interaction of all p variables involved.

The dependence of the bias term on distance depends on the truth, and it need not always dominate with 1-nearest neighbor. For example, if the function always involves only a few dimensions as in Figure 2.8, then the variance can dominate instead.

Suppose, on the other hand, that we know that the relationship between Y and X is linear,

$$Y = X^T \beta + \varepsilon, \quad (2.26)$$

where $\varepsilon \sim N(0, \sigma^2)$ and we fit the model by least squares to the training data. For an arbitrary test point x_0 , we have $\hat{y}_0 = x_0^T \hat{\beta}$, which can be written as $\hat{y}_0 = x_0^T \beta + \sum_{i=1}^N \ell_i(x_0) \varepsilon_i$, where $\ell_i(x_0)$ is the i th element of $\mathbf{X}(\mathbf{X}^T \mathbf{X})^{-1} x_0$. Since under this model the least squares estimates are

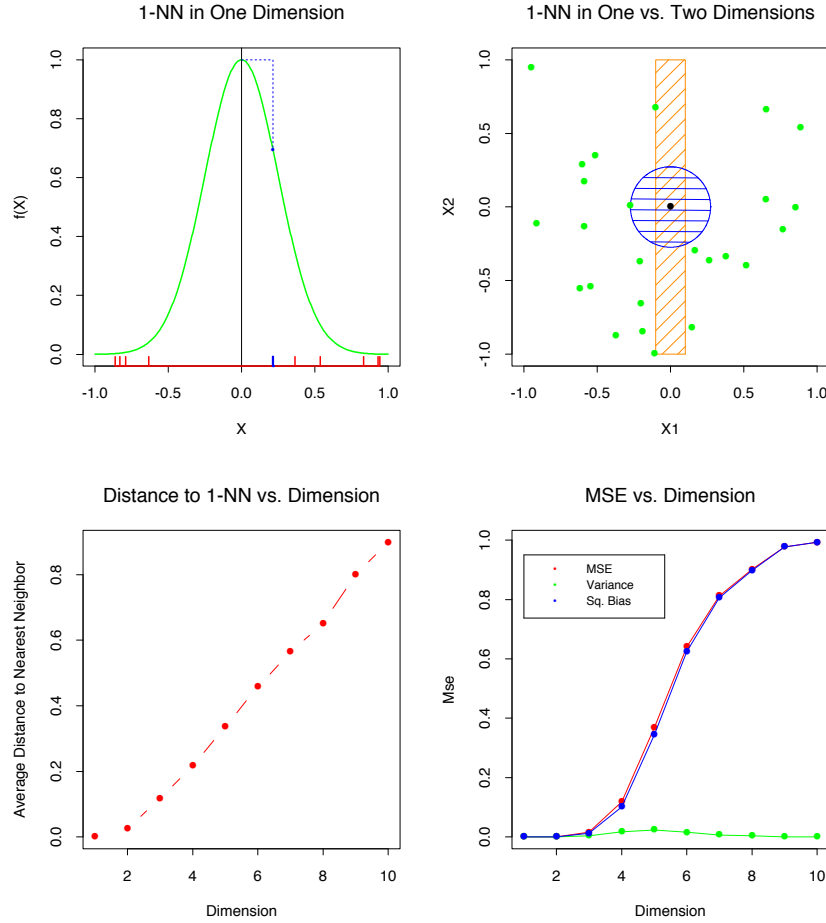


FIGURE 2.7. A simulation example, demonstrating the curse of dimensionality and its effect on MSE, bias and variance. The input features are uniformly distributed in $[-1, 1]^p$ for $p = 1, \dots, 10$. The top left panel shows the target function (no noise) in \mathbb{R}^p : $f(X) = e^{-8||X||^2}$, and demonstrates the error that 1-nearest neighbor makes in estimating $f(0)$. The training point is indicated by the blue tick mark. The top right panel illustrates why the radius of the 1-nearest neighborhood increases with dimension p . The lower left panel shows the average radius of the 1-nearest neighborhoods. The lower-right panel shows the MSE, squared bias and variance curves as a function of dimension p .

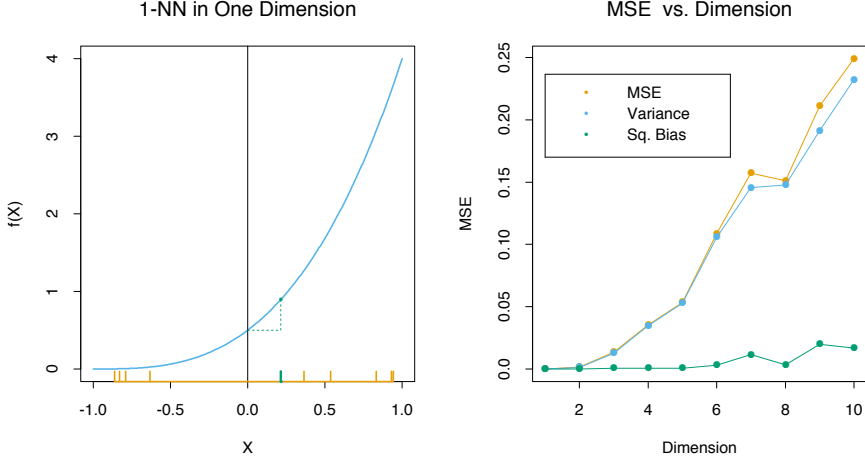


FIGURE 2.8. A simulation example with the same setup as in Figure 2.7. Here the function is constant in all but one dimension: $F(X) = \frac{1}{2}(X_1 + 1)^3$. The variance dominates.

unbiased, we find that

$$\begin{aligned}
\text{EPE}(x_0) &= \mathbb{E}_{y_0|x_0} \mathbb{E}_{\mathcal{T}}(y_0 - \hat{y}_0)^2 \\
&= \text{Var}(y_0|x_0) + \mathbb{E}_{\mathcal{T}}[\hat{y}_0 - \mathbb{E}_{\mathcal{T}}\hat{y}_0]^2 + [\mathbb{E}_{\mathcal{T}}\hat{y}_0 - x_0^T \beta]^2 \\
&= \text{Var}(y_0|x_0) + \text{Var}_{\mathcal{T}}(\hat{y}_0) + \text{Bias}^2(\hat{y}_0) \\
&= \sigma^2 + \mathbb{E}_{\mathcal{T}} x_0^T (\mathbf{X}^T \mathbf{X})^{-1} x_0 \sigma^2 + 0^2.
\end{aligned} \tag{2.27}$$

Here we have incurred an additional variance σ^2 in the prediction error, since our target is not deterministic. There is no bias, and the variance depends on x_0 . If N is large and \mathcal{T} were selected at random, and assuming $\mathbb{E}(X) = 0$, then $\mathbf{X}^T \mathbf{X} \rightarrow N \text{Cov}(X)$ and

$$\begin{aligned}
\mathbb{E}_{x_0} \text{EPE}(x_0) &\sim \mathbb{E}_{x_0} x_0^T \text{Cov}(X)^{-1} x_0 \sigma^2 / N + \sigma^2 \\
&= \text{trace}[\text{Cov}(X)^{-1} \text{Cov}(x_0)] \sigma^2 / N + \sigma^2 \\
&= \sigma^2 (p/N) + \sigma^2.
\end{aligned} \tag{2.28}$$

Here we see that the expected EPE increases linearly as a function of p , with slope σ^2/N . If N is large and/or σ^2 is small, this growth in variance is negligible (0 in the deterministic case). By imposing some heavy restrictions on the class of models being fitted, we have avoided the curse of dimensionality. Some of the technical details in (2.27) and (2.28) are derived in Exercise 2.5.

Figure 2.9 compares 1-nearest neighbor vs. least squares in two situations, both of which have the form $Y = f(X) + \varepsilon$, X uniform as before, and $\varepsilon \sim N(0, 1)$. The sample size is $N = 500$. For the orange curve, $f(x)$

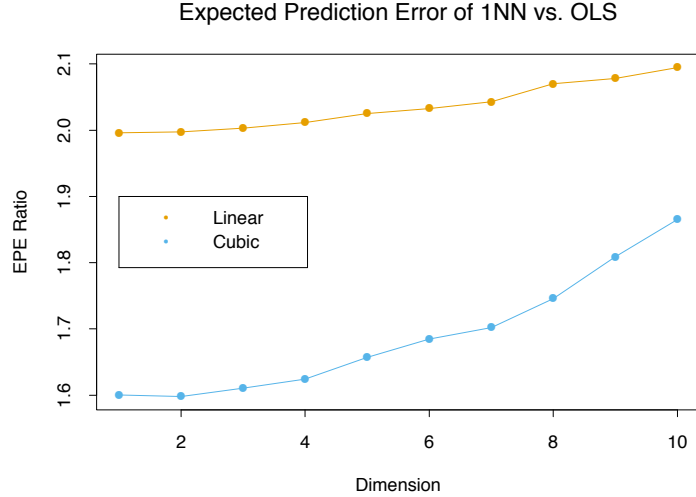


FIGURE 2.9. The curves show the expected prediction error (at $x_0 = 0$) for 1-nearest neighbor relative to least squares for the model $Y = f(X) + \varepsilon$. For the orange curve, $f(x) = x_1$, while for the blue curve $f(x) = \frac{1}{2}(x_1 + 1)^3$.

is linear in the first coordinate, for the blue curve, cubic as in Figure 2.8. Shown is the relative EPE of 1-nearest neighbor to least squares, which appears to start at around 2 for the linear case. Least squares is unbiased in this case, and as discussed above the EPE is slightly above $\sigma^2 = 1$. The EPE for 1-nearest neighbor is always above 2, since the variance of $\hat{f}(x_0)$ in this case is at least σ^2 , and the ratio increases with dimension as the nearest neighbor strays from the target point. For the cubic case, least squares is biased, which moderates the ratio. Clearly we could manufacture examples where the bias of least squares would dominate the variance, and the 1-nearest neighbor would come out the winner.

By relying on rigid assumptions, the linear model has no bias at all and negligible variance, while the error in 1-nearest neighbor is substantially larger. However, if the assumptions are wrong, all bets are off and the 1-nearest neighbor may dominate. We will see that there is a whole spectrum of models between the rigid linear models and the extremely flexible 1-nearest-neighbor models, each with their own assumptions and biases, which have been proposed specifically to avoid the exponential growth in complexity of functions in high dimensions by drawing heavily on these assumptions.

Before we delve more deeply, let us elaborate a bit on the concept of *statistical models* and see how they fit into the prediction framework.

2.6 Statistical Models, Supervised Learning and Function Approximation

Our goal is to find a useful approximation $\hat{f}(x)$ to the function $f(x)$ that underlies the predictive relationship between the inputs and outputs. In the theoretical setting of Section 2.4, we saw that squared error loss lead us to the regression function $f(x) = \text{E}(Y|X = x)$ for a quantitative response. The class of nearest-neighbor methods can be viewed as direct estimates of this conditional expectation, but we have seen that they can fail in at least two ways:

- if the dimension of the input space is high, the nearest neighbors need not be close to the target point, and can result in large errors;
- if special structure is known to exist, this can be used to reduce both the bias and the variance of the estimates.

We anticipate using other classes of models for $f(x)$, in many cases specifically designed to overcome the dimensionality problems, and here we discuss a framework for incorporating them into the prediction problem.

2.6.1 A Statistical Model for the Joint Distribution $\text{Pr}(X, Y)$

Suppose in fact that our data arose from a statistical model

$$Y = f(X) + \varepsilon, \quad (2.29)$$

where the random error ε has $\text{E}(\varepsilon) = 0$ and is independent of X . Note that for this model, $f(x) = \text{E}(Y|X = x)$, and in fact the conditional distribution $\text{Pr}(Y|X)$ depends on X *only* through the conditional mean $f(x)$.

The additive error model is a useful approximation to the truth. For most systems the input–output pairs (X, Y) will not have a deterministic relationship $Y = f(X)$. Generally there will be other unmeasured variables that also contribute to Y , including measurement error. The additive model assumes that we can capture all these departures from a deterministic relationship via the error ε .

For some problems a deterministic relationship does hold. Many of the classification problems studied in machine learning are of this form, where the response surface can be thought of as a colored map defined in \mathbb{R}^p . The training data consist of colored examples from the map $\{x_i, g_i\}$, and the goal is to be able to color any point. Here the function is deterministic, and the randomness enters through the x location of the training points. For the moment we will not pursue such problems, but will see that they can be handled by techniques appropriate for the error-based models.

The assumption in (2.29) that the errors are independent and identically distributed is not strictly necessary, but seems to be at the back of our mind

when we average squared errors uniformly in our EPE criterion. With such a model it becomes natural to use least squares as a data criterion for model estimation as in (2.1). Simple modifications can be made to avoid the independence assumption; for example, we can have $\text{Var}(Y|X = x) = \sigma(x)$, and now both the mean and variance depend on X . In general the conditional distribution $\Pr(Y|X)$ can depend on X in complicated ways, but the additive error model precludes these.

So far we have concentrated on the quantitative response. Additive error models are typically not used for qualitative outputs G ; in this case the target function $p(X)$ is the conditional density $\Pr(G|X)$, and this is modeled directly. For example, for two-class data, it is often reasonable to assume that the data arise from independent binary trials, with the probability of one particular outcome being $p(X)$, and the other $1 - p(X)$. Thus if Y is the 0–1 coded version of G , then $E(Y|X = x) = p(x)$, but the variance depends on x as well: $\text{Var}(Y|X = x) = p(x)[1 - p(x)]$.

2.6.2 Supervised Learning

Before we launch into more statistically oriented jargon, we present the function-fitting paradigm from a machine learning point of view. Suppose for simplicity that the errors are additive and that the model $Y = f(X) + \varepsilon$ is a reasonable assumption. Supervised learning attempts to learn f by example through a *teacher*. One observes the system under study, both the inputs and outputs, and assembles a *training* set of observations $\mathcal{T} = (x_i, y_i)$, $i = 1, \dots, N$. The observed input values to the system x_i are also fed into an artificial system, known as a learning algorithm (usually a computer program), which also produces outputs $\hat{f}(x_i)$ in response to the inputs. The learning algorithm has the property that it can modify its input/output relationship \hat{f} in response to differences $y_i - \hat{f}(x_i)$ between the original and generated outputs. This process is known as *learning by example*. Upon completion of the learning process the hope is that the artificial and real outputs will be close enough to be useful for all sets of inputs likely to be encountered in practice.

2.6.3 Function Approximation

The learning paradigm of the previous section has been the motivation for research into the supervised learning problem in the fields of machine learning (with analogies to human reasoning) and neural networks (with biological analogies to the brain). The approach taken in applied mathematics and statistics has been from the perspective of function approximation and estimation. Here the data pairs $\{x_i, y_i\}$ are viewed as points in a $(p + 1)$ -dimensional Euclidean space. The function $f(x)$ has domain equal to the p -dimensional input subspace, and is related to the data via a model

such as $y_i = f(x_i) + \varepsilon_i$. For convenience in this chapter we will assume the domain is \mathbb{R}^p , a p -dimensional Euclidean space, although in general the inputs can be of mixed type. The goal is to obtain a useful approximation to $f(x)$ for all x in some region of \mathbb{R}^p , given the representations in \mathcal{T} . Although somewhat less glamorous than the learning paradigm, treating supervised learning as a problem in function approximation encourages the geometrical concepts of Euclidean spaces and mathematical concepts of probabilistic inference to be applied to the problem. This is the approach taken in this book.

Many of the approximations we will encounter have associated a set of parameters θ that can be modified to suit the data at hand. For example, the linear model $f(x) = x^T \beta$ has $\theta = \beta$. Another class of useful approximators can be expressed as *linear basis expansions*

$$f_\theta(x) = \sum_{k=1}^K h_k(x)\theta_k, \quad (2.30)$$

where the h_k are a suitable set of functions or transformations of the input vector x . Traditional examples are polynomial and trigonometric expansions, where for example h_k might be x_1^2 , $x_1x_2^2$, $\cos(x_1)$ and so on. We also encounter nonlinear expansions, such as the sigmoid transformation common to neural network models,

$$h_k(x) = \frac{1}{1 + \exp(-x^T \beta_k)}. \quad (2.31)$$

We can use least squares to estimate the parameters θ in f_θ as we did for the linear model, by minimizing the residual sum-of-squares

$$\text{RSS}(\theta) = \sum_{i=1}^N (y_i - f_\theta(x_i))^2 \quad (2.32)$$

as a function of θ . This seems a reasonable criterion for an additive error model. In terms of function approximation, we imagine our parameterized function as a surface in $p + 1$ space, and what we observe are noisy realizations from it. This is easy to visualize when $p = 2$ and the vertical coordinate is the output y , as in Figure 2.10. The noise is in the output coordinate, so we find the set of parameters such that the fitted surface gets as close to the observed points as possible, where close is measured by the sum of squared vertical errors in $\text{RSS}(\theta)$.

For the linear model we get a simple closed form solution to the minimization problem. This is also true for the basis function methods, if the basis functions themselves do not have any hidden parameters. Otherwise the solution requires either iterative methods or numerical optimization.

While least squares is generally very convenient, it is not the only criterion used and in some cases would not make much sense. A more general

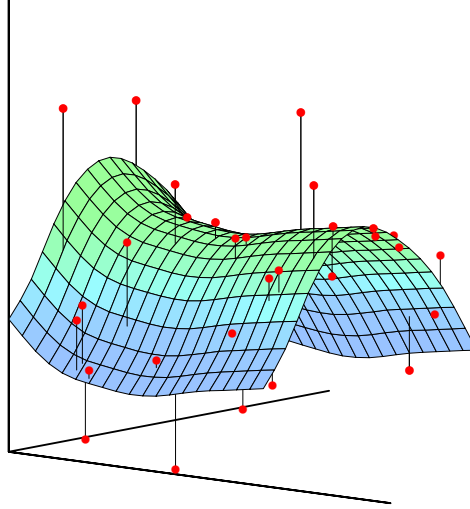


FIGURE 2.10. Least squares fitting of a function of two inputs. The parameters of $f_\theta(x)$ are chosen so as to minimize the sum-of-squared vertical errors.

principle for estimation is *maximum likelihood estimation*. Suppose we have a random sample $y_i, i = 1, \dots, N$ from a density $\Pr_\theta(y)$ indexed by some parameters θ . The log-probability of the observed sample is

$$L(\theta) = \sum_{i=1}^N \log \Pr_\theta(y_i). \quad (2.33)$$

The principle of maximum likelihood assumes that the most reasonable values for θ are those for which the probability of the observed sample is largest. Least squares for the additive error model $Y = f_\theta(X) + \varepsilon$, with $\varepsilon \sim N(0, \sigma^2)$, is equivalent to maximum likelihood using the conditional likelihood

$$\Pr(Y|X, \theta) = N(f_\theta(X), \sigma^2). \quad (2.34)$$

So although the additional assumption of normality seems more restrictive, the results are the same. The log-likelihood of the data is

$$L(\theta) = -\frac{N}{2} \log(2\pi) - N \log \sigma - \frac{1}{2\sigma^2} \sum_{i=1}^N (y_i - f_\theta(x_i))^2, \quad (2.35)$$

and the only term involving θ is the last, which is $\text{RSS}(\theta)$ up to a scalar negative multiplier.

A more interesting example is the multinomial likelihood for the regression function $\Pr(G|X)$ for a qualitative output G . Suppose we have a model $\Pr(G = G_k|X = x) = p_{k,\theta}(x)$, $k = 1, \dots, K$ for the conditional probability of each class given X , indexed by the parameter vector θ . Then the

log-likelihood (also referred to as the cross-entropy) is

$$L(\theta) = \sum_{i=1}^N \log p_{g_i, \theta}(x_i), \quad (2.36)$$

and when maximized it delivers values of θ that best conform with the data in this likelihood sense.

2.7 Structured Regression Models

We have seen that although nearest-neighbor and other local methods focus directly on estimating the function at a point, they face problems in high dimensions. They may also be inappropriate even in low dimensions in cases where more structured approaches can make more efficient use of the data. This section introduces classes of such structured approaches. Before we proceed, though, we discuss further the need for such classes.

2.7.1 Difficulty of the Problem

Consider the RSS criterion for an arbitrary function f ,

$$\text{RSS}(f) = \sum_{i=1}^N (y_i - f(x_i))^2. \quad (2.37)$$

Minimizing (2.37) leads to infinitely many solutions: any function \hat{f} passing through the training points (x_i, y_i) is a solution. Any particular solution chosen might be a poor predictor at test points different from the training points. If there are multiple observation pairs $x_i, y_{i\ell}$, $\ell = 1, \dots, N_i$ at each value of x_i , the risk is limited. In this case, the solutions pass through the average values of the $y_{i\ell}$ at each x_i ; see Exercise 2.6. The situation is similar to the one we have already visited in Section 2.4; indeed, (2.37) is the finite sample version of (2.11) on page 18. If the sample size N were sufficiently large such that repeats were guaranteed and densely arranged, it would seem that these solutions might all tend to the limiting conditional expectation.

In order to obtain useful results for finite N , we must restrict the eligible solutions to (2.37) to a smaller set of functions. How to decide on the nature of the restrictions is based on considerations outside of the data. These restrictions are sometimes encoded via the parametric representation of f_θ , or may be built into the learning method itself, either implicitly or explicitly. These restricted classes of solutions are the major topic of this book. One thing should be clear, though. Any restrictions imposed on f that lead to a unique solution to (2.37) do not really remove the ambiguity

caused by the multiplicity of solutions. There are infinitely many possible restrictions, each leading to a unique solution, so the ambiguity has simply been transferred to the choice of constraint.

In general the constraints imposed by most learning methods can be described as *complexity* restrictions of one kind or another. This usually means some kind of regular behavior in small neighborhoods of the input space. That is, for all input points x sufficiently close to each other in some metric, \hat{f} exhibits some special structure such as nearly constant, linear or low-order polynomial behavior. The estimator is then obtained by averaging or polynomial fitting in that neighborhood.

The strength of the constraint is dictated by the neighborhood size. The larger the size of the neighborhood, the stronger the constraint, and the more sensitive the solution is to the particular choice of constraint. For example, local constant fits in infinitesimally small neighborhoods is no constraint at all; local linear fits in very large neighborhoods is almost a globally linear model, and is very restrictive.

The nature of the constraint depends on the metric used. Some methods, such as kernel and local regression and tree-based methods, directly specify the metric and size of the neighborhood. The nearest-neighbor methods discussed so far are based on the assumption that locally the function is constant; close to a target input x_0 , the function does not change much, and so close outputs can be averaged to produce $\hat{f}(x_0)$. Other methods such as splines, neural networks and basis-function methods implicitly define neighborhoods of local behavior. In Section 5.4.1 we discuss the concept of an *equivalent kernel* (see Figure 5.8 on page 157), which describes this local dependence for any method linear in the outputs. These equivalent kernels in many cases look just like the explicitly defined weighting kernels discussed above—peaked at the target point and falling away smoothly away from it.

One fact should be clear by now. Any method that attempts to produce locally varying functions in small isotropic neighborhoods will run into problems in high dimensions—again the curse of dimensionality. And conversely, all methods that overcome the dimensionality problems have an associated—and often implicit or adaptive—metric for measuring neighborhoods, which basically does not allow the neighborhood to be simultaneously small in all directions.

2.8 Classes of Restricted Estimators

The variety of nonparametric regression techniques or learning methods fall into a number of different classes depending on the nature of the restrictions imposed. These classes are not distinct, and indeed some methods fall in several classes. Here we give a brief summary, since detailed descriptions

are given in later chapters. Each of the classes has associated with it one or more parameters, sometimes appropriately called *smoothing* parameters, that control the effective size of the local neighborhood. Here we describe three broad classes.

2.8.1 Roughness Penalty and Bayesian Methods

Here the class of functions is controlled by explicitly penalizing $\text{RSS}(f)$ with a roughness penalty

$$\text{PRSS}(f; \lambda) = \text{RSS}(f) + \lambda J(f). \quad (2.38)$$

The user-selected functional $J(f)$ will be large for functions f that vary too rapidly over small regions of input space. For example, the popular *cubic smoothing spline* for one-dimensional inputs is the solution to the penalized least-squares criterion

$$\text{PRSS}(f; \lambda) = \sum_{i=1}^N (y_i - f(x_i))^2 + \lambda \int [f''(x)]^2 dx. \quad (2.39)$$

The roughness penalty here controls large values of the second derivative of f , and the amount of penalty is dictated by $\lambda \geq 0$. For $\lambda = 0$ no penalty is imposed, and any interpolating function will do, while for $\lambda = \infty$ only functions linear in x are permitted.

Penalty functionals J can be constructed for functions in any dimension, and special versions can be created to impose special structure. For example, additive penalties $J(f) = \sum_{j=1}^p J(f_j)$ are used in conjunction with additive functions $f(X) = \sum_{j=1}^p f_j(X_j)$ to create additive models with smooth coordinate functions. Similarly, *projection pursuit regression* models have $f(X) = \sum_{m=1}^M g_m(\alpha_m^T X)$ for adaptively chosen directions α_m , and the functions g_m can each have an associated roughness penalty.

Penalty function, or *regularization* methods, express our prior belief that the type of functions we seek exhibit a certain type of smooth behavior, and indeed can usually be cast in a Bayesian framework. The penalty J corresponds to a log-prior, and $\text{PRSS}(f; \lambda)$ the log-posterior distribution, and minimizing $\text{PRSS}(f; \lambda)$ amounts to finding the posterior mode. We discuss roughness-penalty approaches in Chapter 5 and the Bayesian paradigm in Chapter 8.

2.8.2 Kernel Methods and Local Regression

These methods can be thought of as explicitly providing estimates of the regression function or conditional expectation by specifying the nature of the local neighborhood, and of the class of regular functions fitted locally. The local neighborhood is specified by a *kernel function* $K_\lambda(x_0, x)$ which assigns

weights to points x in a region around x_0 (see Figure 6.1 on page 192). For example, the Gaussian kernel has a weight function based on the Gaussian density function

$$K_\lambda(x_0, x) = \frac{1}{\lambda} \exp \left[-\frac{\|x - x_0\|^2}{2\lambda} \right] \quad (2.40)$$

and assigns weights to points that die exponentially with their squared Euclidean distance from x_0 . The parameter λ corresponds to the variance of the Gaussian density, and controls the width of the neighborhood. The simplest form of kernel estimate is the Nadaraya–Watson weighted average

$$\hat{f}(x_0) = \frac{\sum_{i=1}^N K_\lambda(x_0, x_i) y_i}{\sum_{i=1}^N K_\lambda(x_0, x_i)}. \quad (2.41)$$

In general we can define a local regression estimate of $f(x_0)$ as $f_{\hat{\theta}}(x_0)$, where $\hat{\theta}$ minimizes

$$\text{RSS}(f_\theta, x_0) = \sum_{i=1}^N K_\lambda(x_0, x_i) (y_i - f_\theta(x_i))^2, \quad (2.42)$$

and f_θ is some parameterized function, such as a low-order polynomial. Some examples are:

- $f_\theta(x) = \theta_0$, the constant function; this results in the Nadaraya–Watson estimate in (2.41) above.
- $f_\theta(x) = \theta_0 + \theta_1 x$ gives the popular local linear regression model.

Nearest-neighbor methods can be thought of as kernel methods having a more data-dependent metric. Indeed, the metric for k -nearest neighbors is

$$K_k(x, x_0) = I(\|x - x_0\| \leq \|x_{(k)} - x_0\|),$$

where $x_{(k)}$ is the training observation ranked k th in distance from x_0 , and $I(S)$ is the indicator of the set S .

These methods of course need to be modified in high dimensions, to avoid the curse of dimensionality. Various adaptations are discussed in Chapter 6.

2.8.3 Basis Functions and Dictionary Methods

This class of methods includes the familiar linear and polynomial expansions, but more importantly a wide variety of more flexible models. The model for f is a linear expansion of basis functions

$$f_\theta(x) = \sum_{m=1}^M \theta_m h_m(x), \quad (2.43)$$

where each of the h_m is a function of the input x , and the term linear here refers to the action of the parameters θ . This class covers a wide variety of methods. In some cases the sequence of basis functions is prescribed, such as a basis for polynomials in x of total degree M .

For one-dimensional x , polynomial splines of degree K can be represented by an appropriate sequence of M spline basis functions, determined in turn by $M - K$ knots. These produce functions that are piecewise polynomials of degree K between the knots, and joined up with continuity of degree $K - 1$ at the knots. As an example consider linear splines, or piecewise linear functions. One intuitively satisfying basis consists of the functions $b_1(x) = 1$, $b_2(x) = x$, and $b_{m+2}(x) = (x - t_m)_+$, $m = 1, \dots, M - 2$, where t_m is the m th knot, and z_+ denotes positive part. Tensor products of spline bases can be used for inputs with dimensions larger than one (see Section 5.2, and the CART and MARS models in Chapter 9.) The parameter θ can be the total degree of the polynomial or the number of knots in the case of splines.

Radial basis functions are symmetric p -dimensional kernels located at particular centroids,

$$f_\theta(x) = \sum_{m=1}^M K_{\lambda_m}(\mu_m, x)\theta_m; \quad (2.44)$$

for example, the Gaussian kernel $K_\lambda(\mu, x) = e^{-||x-\mu||^2/2\lambda}$ is popular.

Radial basis functions have centroids μ_m and scales λ_m that have to be determined. The spline basis functions have knots. In general we would like the data to dictate them as well. Including these as parameters changes the regression problem from a straightforward linear problem to a combinatorially hard nonlinear problem. In practice, shortcuts such as greedy algorithms or two stage processes are used. Section 6.7 describes some such approaches.

A single-layer feed-forward neural network model with linear output weights can be thought of as an adaptive basis function method. The model has the form

$$f_\theta(x) = \sum_{m=1}^M \beta_m \sigma(\alpha_m^T x + b_m), \quad (2.45)$$

where $\sigma(x) = 1/(1 + e^{-x})$ is known as the *activation* function. Here, as in the projection pursuit model, the directions α_m and the *bias* terms b_m have to be determined, and their estimation is the meat of the computation. Details are give in Chapter 11.

These adaptively chosen basis function methods are also known as *dictionary* methods, where one has available a possibly infinite set or dictionary \mathcal{D} of candidate basis functions from which to choose, and models are built up by employing some kind of search mechanism.

2.9 Model Selection and the Bias–Variance Tradeoff

All the models described above and many others discussed in later chapters have a *smoothing* or *complexity* parameter that has to be determined:

- the multiplier of the penalty term;
- the width of the kernel;
- or the number of basis functions.

In the case of the smoothing spline, the parameter λ indexes models ranging from a straight line fit to the interpolating model. Similarly a local degree- m polynomial model ranges between a degree- m global polynomial when the window size is infinitely large, to an interpolating fit when the window size shrinks to zero. This means that we cannot use residual sum-of-squares on the training data to determine these parameters as well, since we would always pick those that gave interpolating fits and hence zero residuals. Such a model is unlikely to predict future data well at all.

The k -nearest-neighbor regression fit $\hat{f}_k(x_0)$ usefully illustrates the competing forces that affect the predictive ability of such approximations. Suppose the data arise from a model $Y = f(X) + \varepsilon$, with $E(\varepsilon) = 0$ and $\text{Var}(\varepsilon) = \sigma^2$. For simplicity here we assume that the values of x_i in the sample are fixed in advance (nonrandom). The expected prediction error at x_0 , also known as *test* or *generalization* error, can be decomposed:

$$\begin{aligned} \text{EPE}_k(x_0) &= E[(Y - \hat{f}_k(x_0))^2 | X = x_0] \\ &= \sigma^2 + [\text{Bias}^2(\hat{f}_k(x_0)) + \text{Var}_{\mathcal{T}}(\hat{f}_k(x_0))] \end{aligned} \quad (2.46)$$

$$= \sigma^2 + \left[f(x_0) - \frac{1}{k} \sum_{\ell=1}^k f(x_{(\ell)}) \right]^2 + \frac{\sigma^2}{k}. \quad (2.47)$$

The subscripts in parentheses (ℓ) indicate the sequence of nearest neighbors to x_0 .

There are three terms in this expression. The first term σ^2 is the *irreducible* error—the variance of the new test target—and is beyond our control, even if we know the true $f(x_0)$.

The second and third terms are under our control, and make up the *mean squared error* of $\hat{f}_k(x_0)$ in estimating $f(x_0)$, which is broken down into a bias component and a variance component. The bias term is the squared difference between the true mean $f(x_0)$ and the expected value of the estimate— $[E_{\mathcal{T}}(\hat{f}_k(x_0)) - f(x_0)]^2$ —where the expectation averages the randomness in the training data. This term will most likely increase with k , if the true function is reasonably smooth. For small k the few closest neighbors will have values $f(x_{(\ell)})$ close to $f(x_0)$, so their average should

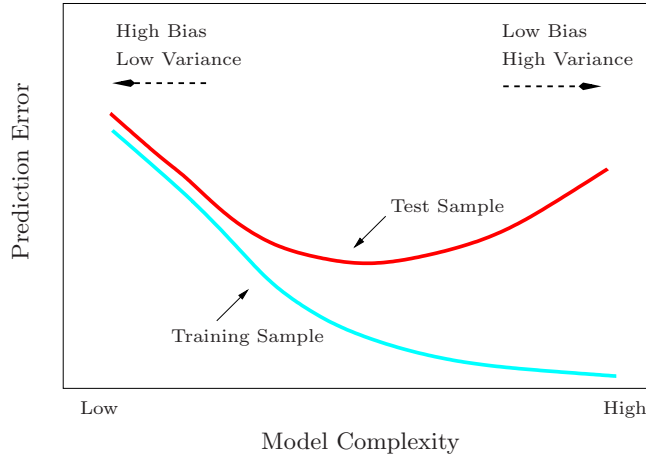


FIGURE 2.11. Test and training error as a function of model complexity.

be close to $f(x_0)$. As k grows, the neighbors are further away, and then anything can happen.

The variance term is simply the variance of an average here, and decreases as the inverse of k . So as k varies, there is a *bias-variance tradeoff*.

More generally, as the *model complexity* of our procedure is increased, the variance tends to increase and the squared bias tends to decrease. The opposite behavior occurs as the model complexity is decreased. For k -nearest neighbors, the model complexity is controlled by k .

Typically we would like to choose our model complexity to trade bias off with variance in such a way as to minimize the test error. An obvious estimate of test error is the *training error* $\frac{1}{N} \sum_i (y_i - \hat{y}_i)^2$. Unfortunately training error is not a good estimate of test error, as it does not properly account for model complexity.

Figure 2.11 shows the typical behavior of the test and training error, as model complexity is varied. The training error tends to decrease whenever we increase the model complexity, that is, whenever we fit the data harder. However with too much fitting, the model adapts itself too closely to the training data, and will not generalize well (i.e., have large test error). In that case the predictions $\hat{f}(x_0)$ will have large variance, as reflected in the last term of expression (2.46). In contrast, if the model is not complex enough, it will *underfit* and may have large bias, again resulting in poor generalization. In Chapter 7 we discuss methods for estimating the test error of a prediction method, and hence estimating the optimal amount of model complexity for a given prediction method and training set.

Bibliographic Notes

Some good general books on the learning problem are Duda et al. (2000), Bishop (1995),(Bishop, 2006), Ripley (1996), Cherkassky and Mulier (2007) and Vapnik (1996). Parts of this chapter are based on Friedman (1994b).

Exercises

Ex. 2.1 Suppose each of K -classes has an associated target t_k , which is a vector of all zeros, except a one in the k th position. Show that classifying to the largest element of \hat{y} amounts to choosing the closest target, $\min_k \|t_k - \hat{y}\|$, if the elements of \hat{y} sum to one.

Ex. 2.2 Show how to compute the Bayes decision boundary for the simulation example in Figure 2.5.

Ex. 2.3 Derive equation (2.24).

Ex. 2.4 The edge effect problem discussed on page 23 is not peculiar to uniform sampling from bounded domains. Consider inputs drawn from a spherical multinormal distribution $X \sim N(0, \mathbf{I}_p)$. The squared distance from any sample point to the origin has a χ_p^2 distribution with mean p . Consider a prediction point x_0 drawn from this distribution, and let $a = x_0/\|x_0\|$ be an associated unit vector. Let $z_i = a^T x_i$ be the projection of each of the training points on this direction.

Show that the z_i are distributed $N(0, 1)$ with expected squared distance from the origin 1, while the target point has expected squared distance p from the origin.

Hence for $p = 10$, a randomly drawn test point is about 3.1 standard deviations from the origin, while all the training points are on average one standard deviation along direction a . So most prediction points see themselves as lying on the edge of the training set.

Ex. 2.5

- (a) Derive equation (2.27). The last line makes use of (3.8) through a conditioning argument.
- (b) Derive equation (2.28), making use of the *cyclic* property of the trace operator [$\text{trace}(AB) = \text{trace}(BA)$], and its linearity (which allows us to interchange the order of trace and expectation).

Ex. 2.6 Consider a regression problem with inputs x_i and outputs y_i , and a parameterized model $f_\theta(x)$ to be fit by least squares. Show that if there are observations with *tied* or *identical* values of x , then the fit can be obtained from a reduced weighted least squares problem.

Ex. 2.7 Suppose we have a sample of N pairs x_i, y_i drawn i.i.d. from the distribution characterized as follows:

$$\begin{aligned}x_i &\sim h(x), \text{ the design density} \\y_i &= f(x_i) + \varepsilon_i, \text{ } f \text{ is the regression function} \\\varepsilon_i &\sim (0, \sigma^2) \text{ (mean zero, variance } \sigma^2)\end{aligned}$$

We construct an estimator for f linear in the y_i ,

$$\hat{f}(x_0) = \sum_{i=1}^N \ell_i(x_0; \mathcal{X}) y_i,$$

where the weights $\ell_i(x_0; \mathcal{X})$ do not depend on the y_i , but do depend on the entire training sequence of x_i , denoted here by \mathcal{X} .

- (a) Show that linear regression and k -nearest-neighbor regression are members of this class of estimators. Describe explicitly the weights $\ell_i(x_0; \mathcal{X})$ in each of these cases.
- (b) Decompose the conditional mean-squared error

$$E_{\mathcal{Y}|\mathcal{X}}(f(x_0) - \hat{f}(x_0))^2$$

into a conditional squared bias and a conditional variance component.
Like \mathcal{X} , \mathcal{Y} represents the entire training sequence of y_i .

- (c) Decompose the (unconditional) mean-squared error

$$E_{\mathcal{Y}, \mathcal{X}}(f(x_0) - \hat{f}(x_0))^2$$

into a squared bias and a variance component.

- (d) Establish a relationship between the squared biases and variances in the above two cases.

Ex. 2.8 Compare the classification performance of linear regression and k -nearest neighbor classification on the `zipcode` data. In particular, consider only the 2's and 3's, and $k = 1, 3, 5, 7$ and 15. Show both the training and test error for each choice. The `zipcode` data are available from the book website www-stat.stanford.edu/ElemStatLearn.

Ex. 2.9 Consider a linear regression model with p parameters, fit by least squares to a set of training data $(x_1, y_1), \dots, (x_N, y_N)$ drawn at random from a population. Let $\hat{\beta}$ be the least squares estimate. Suppose we have some test data $(\tilde{x}_1, \tilde{y}_1), \dots, (\tilde{x}_M, \tilde{y}_M)$ drawn at random from the same population as the training data. If $R_{tr}(\beta) = \frac{1}{N} \sum_1^N (y_i - \beta^T x_i)^2$ and $R_{te}(\beta) = \frac{1}{M} \sum_1^M (\tilde{y}_i - \beta^T \tilde{x}_i)^2$, prove that

$$E[R_{tr}(\hat{\beta})] \leq E[R_{te}(\hat{\beta})],$$

where the expectations are over all that is random in each expression. [This exercise was brought to our attention by Ryan Tibshirani, from a homework assignment given by Andrew Ng.]

3

Linear Methods for Regression

3.1 Introduction

A linear regression model assumes that the regression function $E(Y|X)$ is linear in the inputs X_1, \dots, X_p . Linear models were largely developed in the precomputer age of statistics, but even in today's computer era there are still good reasons to study and use them. They are simple and often provide an adequate and interpretable description of how the inputs affect the output. For prediction purposes they can sometimes outperform fancier nonlinear models, especially in situations with small numbers of training cases, low signal-to-noise ratio or sparse data. Finally, linear methods can be applied to transformations of the inputs and this considerably expands their scope. These generalizations are sometimes called basis-function methods, and are discussed in Chapter 5.

In this chapter we describe linear methods for regression, while in the next chapter we discuss linear methods for classification. On some topics we go into considerable detail, as it is our firm belief that an understanding of linear methods is essential for understanding nonlinear ones. In fact, many nonlinear techniques are direct generalizations of the linear methods discussed here.

3.2 Linear Regression Models and Least Squares

As introduced in Chapter 2, we have an input vector $X^T = (X_1, X_2, \dots, X_p)$, and want to predict a real-valued output Y . The linear regression model has the form

$$f(X) = \beta_0 + \sum_{j=1}^p X_j \beta_j. \quad (3.1)$$

The linear model either assumes that the regression function $E(Y|X)$ is linear, or that the linear model is a reasonable approximation. Here the β_j 's are unknown parameters or coefficients, and the variables X_j can come from different sources:

- quantitative inputs;
- transformations of quantitative inputs, such as log, square-root or square;
- basis expansions, such as $X_2 = X_1^2$, $X_3 = X_1^3$, leading to a polynomial representation;
- numeric or “dummy” coding of the levels of qualitative inputs. For example, if G is a five-level factor input, we might create X_j , $j = 1, \dots, 5$, such that $X_j = I(G = j)$. Together this group of X_j represents the effect of G by a set of level-dependent constants, since in $\sum_{j=1}^5 X_j \beta_j$, one of the X_j 's is one, and the others are zero.
- interactions between variables, for example, $X_3 = X_1 \cdot X_2$.

No matter the source of the X_j , the model is linear in the parameters.

Typically we have a set of training data $(x_1, y_1) \dots (x_N, y_N)$ from which to estimate the parameters β . Each $x_i = (x_{i1}, x_{i2}, \dots, x_{ip})^T$ is a vector of feature measurements for the i th case. The most popular estimation method is *least squares*, in which we pick the coefficients $\beta = (\beta_0, \beta_1, \dots, \beta_p)^T$ to minimize the residual sum of squares

$$\begin{aligned} \text{RSS}(\beta) &= \sum_{i=1}^N (y_i - f(x_i))^2 \\ &= \sum_{i=1}^N \left(y_i - \beta_0 - \sum_{j=1}^p x_{ij} \beta_j \right)^2. \end{aligned} \quad (3.2)$$

From a statistical point of view, this criterion is reasonable if the training observations (x_i, y_i) represent independent random draws from their population. Even if the x_i 's were not drawn randomly, the criterion is still valid if the y_i 's are conditionally independent given the inputs x_i . Figure 3.1 illustrates the geometry of least-squares fitting in the \mathbb{R}^{p+1} -dimensional

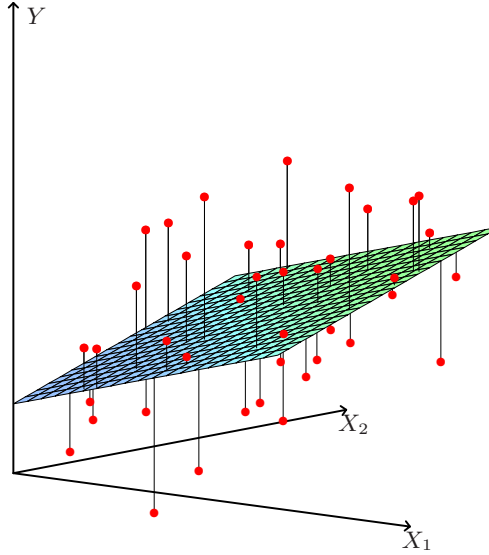


FIGURE 3.1. Linear least squares fitting with $X \in \mathbb{R}^2$. We seek the linear function of X that minimizes the sum of squared residuals from Y .

space occupied by the pairs (X, Y) . Note that (3.2) makes no assumptions about the validity of model (3.1); it simply finds the best linear fit to the data. Least squares fitting is intuitively satisfying no matter how the data arise; the criterion measures the average lack of fit.

How do we minimize (3.2)? Denote by \mathbf{X} the $N \times (p + 1)$ matrix with each row an input vector (with a 1 in the first position), and similarly let \mathbf{y} be the N -vector of outputs in the training set. Then we can write the residual sum-of-squares as

$$\text{RSS}(\beta) = (\mathbf{y} - \mathbf{X}\beta)^T(\mathbf{y} - \mathbf{X}\beta). \quad (3.3)$$

This is a quadratic function in the $p + 1$ parameters. Differentiating with respect to β we obtain

$$\begin{aligned} \frac{\partial \text{RSS}}{\partial \beta} &= -2\mathbf{X}^T(\mathbf{y} - \mathbf{X}\beta) \\ \frac{\partial^2 \text{RSS}}{\partial \beta \partial \beta^T} &= 2\mathbf{X}^T \mathbf{X}. \end{aligned} \quad (3.4)$$

Assuming (for the moment) that \mathbf{X} has full column rank, and hence $\mathbf{X}^T \mathbf{X}$ is positive definite, we set the first derivative to zero

$$\mathbf{X}^T(\mathbf{y} - \mathbf{X}\beta) = 0 \quad (3.5)$$

to obtain the unique solution

$$\hat{\beta} = (\mathbf{X}^T \mathbf{X})^{-1} \mathbf{X}^T \mathbf{y}. \quad (3.6)$$

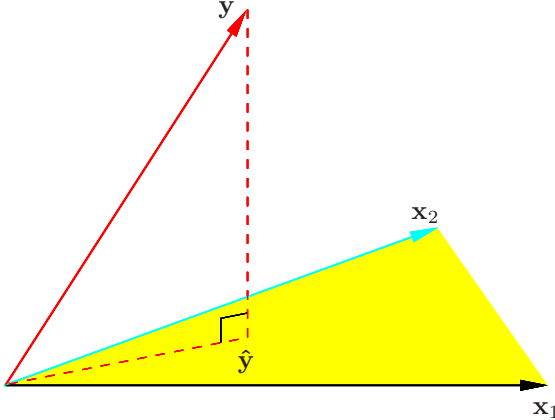


FIGURE 3.2. The N -dimensional geometry of least squares regression with two predictors. The outcome vector \mathbf{y} is orthogonally projected onto the hyperplane spanned by the input vectors \mathbf{x}_1 and \mathbf{x}_2 . The projection $\hat{\mathbf{y}}$ represents the vector of the least squares predictions

The predicted values at an input vector x_0 are given by $\hat{f}(x_0) = (1 : x_0)^T \hat{\beta}$; the fitted values at the training inputs are

$$\hat{\mathbf{y}} = \mathbf{X}\hat{\beta} = \mathbf{X}(\mathbf{X}^T\mathbf{X})^{-1}\mathbf{X}^T\mathbf{y}, \quad (3.7)$$

where $\hat{y}_i = \hat{f}(x_i)$. The matrix $\mathbf{H} = \mathbf{X}(\mathbf{X}^T\mathbf{X})^{-1}\mathbf{X}^T$ appearing in equation (3.7) is sometimes called the “hat” matrix because it puts the hat on \mathbf{y} .

Figure 3.2 shows a different geometrical representation of the least squares estimate, this time in \mathbb{R}^N . We denote the column vectors of \mathbf{X} by $\mathbf{x}_0, \mathbf{x}_1, \dots, \mathbf{x}_p$, with $\mathbf{x}_0 \equiv 1$. For much of what follows, this first column is treated like any other. These vectors span a subspace of \mathbb{R}^N , also referred to as the column space of \mathbf{X} . We minimize $\text{RSS}(\beta) = \|\mathbf{y} - \mathbf{X}\beta\|^2$ by choosing $\hat{\beta}$ so that the residual vector $\mathbf{y} - \hat{\mathbf{y}}$ is orthogonal to this subspace. This orthogonality is expressed in (3.5), and the resulting estimate $\hat{\mathbf{y}}$ is hence the *orthogonal projection* of \mathbf{y} onto this subspace. The hat matrix \mathbf{H} computes the orthogonal projection, and hence it is also known as a projection matrix.

It might happen that the columns of \mathbf{X} are not linearly independent, so that \mathbf{X} is not of full rank. This would occur, for example, if two of the inputs were perfectly correlated, (e.g., $\mathbf{x}_2 = 3\mathbf{x}_1$). Then $\mathbf{X}^T\mathbf{X}$ is singular and the least squares coefficients $\hat{\beta}$ are not uniquely defined. However, the fitted values $\hat{\mathbf{y}} = \mathbf{X}\hat{\beta}$ are still the projection of \mathbf{y} onto the column space of \mathbf{X} ; there is just more than one way to express that projection in terms of the column vectors of \mathbf{X} . The non-full-rank case occurs most often when one or more qualitative inputs are coded in a redundant fashion. There is usually a natural way to resolve the non-unique representation, by recoding and/or dropping redundant columns in \mathbf{X} . Most regression software packages detect these redundancies and automatically implement

some strategy for removing them. Rank deficiencies can also occur in signal and image analysis, where the number of inputs p can exceed the number of training cases N . In this case, the features are typically reduced by filtering or else the fitting is controlled by regularization (Section 5.2.3 and Chapter 18).

Up to now we have made minimal assumptions about the true distribution of the data. In order to pin down the sampling properties of $\hat{\beta}$, we now assume that the observations y_i are uncorrelated and have constant variance σ^2 , and that the x_i are fixed (non random). The variance–covariance matrix of the least squares parameter estimates is easily derived from (3.6) and is given by

$$\text{Var}(\hat{\beta}) = (\mathbf{X}^T \mathbf{X})^{-1} \sigma^2. \quad (3.8)$$

Typically one estimates the variance σ^2 by

$$\hat{\sigma}^2 = \frac{1}{N-p-1} \sum_{i=1}^N (y_i - \hat{y}_i)^2.$$

The $N-p-1$ rather than N in the denominator makes $\hat{\sigma}^2$ an unbiased estimate of σ^2 : $E(\hat{\sigma}^2) = \sigma^2$.

To draw inferences about the parameters and the model, additional assumptions are needed. We now assume that (3.1) is the correct model for the mean; that is, the conditional expectation of Y is linear in X_1, \dots, X_p . We also assume that the deviations of Y around its expectation are additive and Gaussian. Hence

$$\begin{aligned} Y &= E(Y|X_1, \dots, X_p) + \varepsilon \\ &= \beta_0 + \sum_{j=1}^p X_j \beta_j + \varepsilon, \end{aligned} \quad (3.9)$$

where the error ε is a Gaussian random variable with expectation zero and variance σ^2 , written $\varepsilon \sim N(0, \sigma^2)$.

Under (3.9), it is easy to show that

$$\hat{\beta} \sim N(\beta, (\mathbf{X}^T \mathbf{X})^{-1} \sigma^2). \quad (3.10)$$

This is a multivariate normal distribution with mean vector and variance–covariance matrix as shown. Also

$$(N-p-1)\hat{\sigma}^2 \sim \sigma^2 \chi_{N-p-1}^2, \quad (3.11)$$

a chi-squared distribution with $N-p-1$ degrees of freedom. In addition $\hat{\beta}$ and $\hat{\sigma}^2$ are statistically independent. We use these distributional properties to form tests of hypothesis and confidence intervals for the parameters β_j .

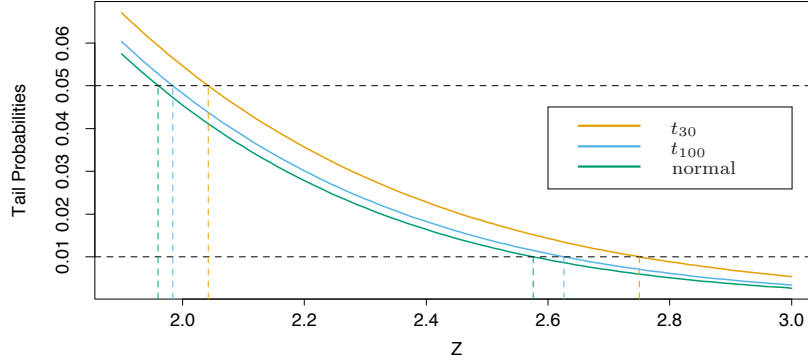


FIGURE 3.3. The tail probabilities $\Pr(|Z| > z)$ for three distributions, t_{30} , t_{100} and standard normal. Shown are the appropriate quantiles for testing significance at the $p = 0.05$ and 0.01 levels. The difference between t and the standard normal becomes negligible for N bigger than about 100.

To test the hypothesis that a particular coefficient $\beta_j = 0$, we form the standardized coefficient or *Z-score*

$$z_j = \frac{\hat{\beta}_j}{\hat{\sigma} \sqrt{v_j}}, \quad (3.12)$$

where v_j is the j th diagonal element of $(\mathbf{X}^T \mathbf{X})^{-1}$. Under the null hypothesis that $\beta_j = 0$, z_j is distributed as t_{N-p-1} (a t distribution with $N - p - 1$ degrees of freedom), and hence a large (absolute) value of z_j will lead to rejection of this null hypothesis. If $\hat{\sigma}$ is replaced by a known value σ , then z_j would have a standard normal distribution. The difference between the tail quantiles of a t -distribution and a standard normal become negligible as the sample size increases, and so we typically use the normal quantiles (see Figure 3.3).

Often we need to test for the significance of groups of coefficients simultaneously. For example, to test if a categorical variable with k levels can be excluded from a model, we need to test whether the coefficients of the dummy variables used to represent the levels can all be set to zero. Here we use the F statistic,

$$F = \frac{(\text{RSS}_0 - \text{RSS}_1)/(p_1 - p_0)}{\text{RSS}_1/(N - p_1 - 1)}, \quad (3.13)$$

where RSS_1 is the residual sum-of-squares for the least squares fit of the bigger model with $p_1 + 1$ parameters, and RSS_0 the same for the nested smaller model with $p_0 + 1$ parameters, having $p_1 - p_0$ parameters constrained to be

zero. The F statistic measures the change in residual sum-of-squares per additional parameter in the bigger model, and it is normalized by an estimate of σ^2 . Under the Gaussian assumptions, and the null hypothesis that the smaller model is correct, the F statistic will have a $F_{p_1-p_0, N-p_1-1}$ distribution. It can be shown (Exercise 3.1) that the z_j in (3.12) are equivalent to the F statistic for dropping the single coefficient β_j from the model. For large N , the quantiles of $F_{p_1-p_0, N-p_1-1}$ approach those of $\chi^2_{p_1-p_0}/(p_1-p_0)$.

Similarly, we can isolate β_j in (3.10) to obtain a $1-2\alpha$ confidence interval for β_j :

$$(\hat{\beta}_j - z^{(1-\alpha)} v_j^{\frac{1}{2}} \hat{\sigma}, \quad \hat{\beta}_j + z^{(1-\alpha)} v_j^{\frac{1}{2}} \hat{\sigma}). \quad (3.14)$$

Here $z^{(1-\alpha)}$ is the $1-\alpha$ percentile of the normal distribution:

$$\begin{aligned} z^{(1-0.025)} &= 1.96, \\ z^{(1-0.05)} &= 1.645, \text{ etc.} \end{aligned}$$

Hence the standard practice of reporting $\hat{\beta} \pm 2 \cdot \text{se}(\hat{\beta})$ amounts to an approximate 95% confidence interval. Even if the Gaussian error assumption does not hold, this interval will be approximately correct, with its coverage approaching $1-2\alpha$ as the sample size $N \rightarrow \infty$.

In a similar fashion we can obtain an approximate confidence set for the entire parameter vector β , namely

$$C_\beta = \{\beta | (\hat{\beta} - \beta)^T \mathbf{X}^T \mathbf{X} (\hat{\beta} - \beta) \leq \hat{\sigma}^2 \chi^2_{p+1}^{(1-\alpha)}\}, \quad (3.15)$$

where $\chi^2_\ell^{(1-\alpha)}$ is the $1-\alpha$ percentile of the chi-squared distribution on ℓ degrees of freedom: for example, $\chi^2_5^{(1-0.05)} = 11.1$, $\chi^2_5^{(1-0.1)} = 9.2$. This confidence set for β generates a corresponding confidence set for the true function $f(x) = x^T \beta$, namely $\{x^T \beta | \beta \in C_\beta\}$ (Exercise 3.2; see also Figure 5.4 in Section 5.2.2 for examples of confidence bands for functions).

3.2.1 Example: Prostate Cancer

The data for this example come from a study by Stamey et al. (1989). They examined the correlation between the level of prostate-specific antigen and a number of clinical measures in men who were about to receive a radical prostatectomy. The variables are log cancer volume (`1cavol`), log prostate weight (`1weight`), `age`, log of the amount of benign prostatic hyperplasia (`1bph`), seminal vesicle invasion (`svi`), log of capsular penetration (`1cp`), Gleason score (`gleason`), and percent of Gleason scores 4 or 5 (`pgg45`). The correlation matrix of the predictors given in Table 3.1 shows many strong correlations. Figure 1.1 (page 3) of Chapter 1 is a scatterplot matrix showing every pairwise plot between the variables. We see that `svi` is a binary variable, and `gleason` is an ordered categorical variable. We see, for

TABLE 3.1. Correlations of predictors in the prostate cancer data.

	lcavol	lweight	age	lbph	svi	lcp	gleason
lweight	0.300						
age	0.286	0.317					
lbph	0.063	0.437	0.287				
svi	0.593	0.181	0.129	-0.139			
lcp	0.692	0.157	0.173	-0.089	0.671		
gleason	0.426	0.024	0.366	0.033	0.307	0.476	
pgg45	0.483	0.074	0.276	-0.030	0.481	0.663	0.757

TABLE 3.2. Linear model fit to the prostate cancer data. The Z score is the coefficient divided by its standard error (3.12). Roughly a Z score larger than two in absolute value is significantly nonzero at the $p = 0.05$ level.

Term	Coefficient	Std. Error	Z Score
Intercept	2.46	0.09	27.60
lcavol	0.68	0.13	5.37
lweight	0.26	0.10	2.75
age	-0.14	0.10	-1.40
lbph	0.21	0.10	2.06
svi	0.31	0.12	2.47
lcp	-0.29	0.15	-1.87
gleason	-0.02	0.15	-0.15
pgg45	0.27	0.15	1.74

example, that both `lcavol` and `lcp` show a strong relationship with the response `lpsa`, and with each other. We need to fit the effects jointly to untangle the relationships between the predictors and the response.

We fit a linear model to the log of prostate-specific antigen, `lpsa`, after first standardizing the predictors to have unit variance. We randomly split the dataset into a training set of size 67 and a test set of size 30. We applied least squares estimation to the training set, producing the estimates, standard errors and Z -scores shown in Table 3.2. The Z -scores are defined in (3.12), and measure the effect of dropping that variable from the model. A Z -score greater than 2 in absolute value is approximately significant at the 5% level. (For our example, we have nine parameters, and the 0.025 tail quantiles of the t_{67-9} distribution are $\pm 2.002!$) The predictor `lcavol` shows the strongest effect, with `lweight` and `svi` also strong. Notice that `lcp` is not significant, once `lcavol` is in the model (when used in a model without `lcavol`, `lcp` is strongly significant). We can also test for the exclusion of a number of terms at once, using the F -statistic (3.13). For example, we consider dropping all the non-significant terms in Table 3.2, namely `age`,

`lcp`, `gleason`, and `pgg45`. We get

$$F = \frac{(32.81 - 29.43)/(9 - 5)}{29.43/(67 - 9)} = 1.67, \quad (3.16)$$

which has a *p*-value of 0.17 ($\Pr(F_{4,58} > 1.67) = 0.17$), and hence is not significant.

The mean prediction error on the test data is 0.521 . In contrast, prediction using the mean training value of `1psa` has a test error of 1.057 , which is called the “base error rate.” Hence the linear model reduces the base error rate by about 50% . We will return to this example later to compare various selection and shrinkage methods.

3.2.2 The Gauss–Markov Theorem

One of the most famous results in statistics asserts that the least squares estimates of the parameters β have the smallest variance among all linear unbiased estimates. We will make this precise here, and also make clear that the restriction to unbiased estimates is not necessarily a wise one. This observation will lead us to consider biased estimates such as ridge regression later in the chapter. We focus on estimation of any linear combination of the parameters $\theta = a^T \beta$; for example, predictions $f(x_0) = x_0^T \beta$ are of this form. The least squares estimate of $a^T \beta$ is

$$\hat{\theta} = a^T \hat{\beta} = a^T (\mathbf{X}^T \mathbf{X})^{-1} \mathbf{X}^T \mathbf{y}. \quad (3.17)$$

Considering \mathbf{X} to be fixed, this is a linear function $\mathbf{c}_0^T \mathbf{y}$ of the response vector \mathbf{y} . If we assume that the linear model is correct, $a^T \hat{\beta}$ is unbiased since

$$\begin{aligned} E(a^T \hat{\beta}) &= E(a^T (\mathbf{X}^T \mathbf{X})^{-1} \mathbf{X}^T \mathbf{y}) \\ &= a^T (\mathbf{X}^T \mathbf{X})^{-1} \mathbf{X}^T \mathbf{X} \beta \\ &= a^T \beta. \end{aligned} \quad (3.18)$$

The Gauss–Markov theorem states that if we have any other linear estimator $\tilde{\theta} = \mathbf{c}^T \mathbf{y}$ that is unbiased for $a^T \beta$, that is, $E(\mathbf{c}^T \mathbf{y}) = a^T \beta$, then

$$\text{Var}(a^T \hat{\beta}) \leq \text{Var}(\mathbf{c}^T \mathbf{y}). \quad (3.19)$$

The proof (Exercise 3.3) uses the triangle inequality. For simplicity we have stated the result in terms of estimation of a single parameter $a^T \beta$, but with a few more definitions one can state it in terms of the entire parameter vector β (Exercise 3.3).

Consider the mean squared error of an estimator $\tilde{\theta}$ in estimating θ :

$$\begin{aligned} \text{MSE}(\tilde{\theta}) &= E(\tilde{\theta} - \theta)^2 \\ &= \text{Var}(\tilde{\theta}) + [E(\tilde{\theta}) - \theta]^2. \end{aligned} \quad (3.20)$$

The first term is the variance, while the second term is the squared bias. The Gauss-Markov theorem implies that the least squares estimator has the smallest mean squared error of all linear estimators with no bias. However, there may well exist a biased estimator with smaller mean squared error. Such an estimator would trade a little bias for a larger reduction in variance. Biased estimates are commonly used. Any method that shrinks or sets to zero some of the least squares coefficients may result in a biased estimate. We discuss many examples, including variable subset selection and ridge regression, later in this chapter. From a more pragmatic point of view, most models are distortions of the truth, and hence are biased; picking the right model amounts to creating the right balance between bias and variance. We go into these issues in more detail in Chapter 7.

Mean squared error is intimately related to prediction accuracy, as discussed in Chapter 2. Consider the prediction of the new response at input x_0 ,

$$Y_0 = f(x_0) + \varepsilon_0. \quad (3.21)$$

Then the expected prediction error of an estimate $\tilde{f}(x_0) = x_0^T \tilde{\beta}$ is

$$\begin{aligned} E(Y_0 - \tilde{f}(x_0))^2 &= \sigma^2 + E(x_0^T \tilde{\beta} - f(x_0))^2 \\ &= \sigma^2 + \text{MSE}(\tilde{f}(x_0)). \end{aligned} \quad (3.22)$$

Therefore, expected prediction error and mean squared error differ only by the constant σ^2 , representing the variance of the new observation y_0 .

3.2.3 Multiple Regression from Simple Univariate Regression

The linear model (3.1) with $p > 1$ inputs is called the *multiple linear regression model*. The least squares estimates (3.6) for this model are best understood in terms of the estimates for the *univariate* ($p = 1$) linear model, as we indicate in this section.

Suppose first that we have a univariate model with no intercept, that is,

$$Y = X\beta + \varepsilon. \quad (3.23)$$

The least squares estimate and residuals are

$$\begin{aligned} \hat{\beta} &= \frac{\sum_1^N x_i y_i}{\sum_1^N x_i^2}, \\ r_i &= y_i - x_i \hat{\beta}. \end{aligned} \quad (3.24)$$

In convenient vector notation, we let $\mathbf{y} = (y_1, \dots, y_N)^T$, $\mathbf{x} = (x_1, \dots, x_N)^T$ and define

$$\begin{aligned} \langle \mathbf{x}, \mathbf{y} \rangle &= \sum_{i=1}^N x_i y_i, \\ &= \mathbf{x}^T \mathbf{y}, \end{aligned} \quad (3.25)$$

the *inner product* between \mathbf{x} and \mathbf{y} ¹. Then we can write

$$\begin{aligned}\hat{\beta} &= \frac{\langle \mathbf{x}, \mathbf{y} \rangle}{\langle \mathbf{x}, \mathbf{x} \rangle}, \\ \mathbf{r} &= \mathbf{y} - \mathbf{x}\hat{\beta}.\end{aligned}\tag{3.26}$$

As we will see, this simple univariate regression provides the building block for multiple linear regression. Suppose next that the inputs $\mathbf{x}_1, \mathbf{x}_2, \dots, \mathbf{x}_p$ (the columns of the data matrix \mathbf{X}) are orthogonal; that is $\langle \mathbf{x}_j, \mathbf{x}_k \rangle = 0$ for all $j \neq k$. Then it is easy to check that the multiple least squares estimates $\hat{\beta}_j$ are equal to $\langle \mathbf{x}_j, \mathbf{y} \rangle / \langle \mathbf{x}_j, \mathbf{x}_j \rangle$ —the univariate estimates. In other words, when the inputs are orthogonal, they have no effect on each other's parameter estimates in the model.

Orthogonal inputs occur most often with balanced, designed experiments (where orthogonality is enforced), but almost never with observational data. Hence we will have to orthogonalize them in order to carry this idea further. Suppose next that we have an intercept and a single input \mathbf{x} . Then the least squares coefficient of \mathbf{x} has the form

$$\hat{\beta}_1 = \frac{\langle \mathbf{x} - \bar{x}\mathbf{1}, \mathbf{y} \rangle}{\langle \mathbf{x} - \bar{x}\mathbf{1}, \mathbf{x} - \bar{x}\mathbf{1} \rangle},\tag{3.27}$$

where $\bar{x} = \sum_i x_i / N$, and $\mathbf{1} = \mathbf{x}_0$, the vector of N ones. We can view the estimate (3.27) as the result of two applications of the simple regression (3.26). The steps are:

1. regress \mathbf{x} on $\mathbf{1}$ to produce the residual $\mathbf{z} = \mathbf{x} - \bar{x}\mathbf{1}$;
2. regress \mathbf{y} on the residual \mathbf{z} to give the coefficient $\hat{\beta}_1$.

In this procedure, “regress \mathbf{b} on \mathbf{a} ” means a simple univariate regression of \mathbf{b} on \mathbf{a} with no intercept, producing coefficient $\hat{\gamma} = \langle \mathbf{a}, \mathbf{b} \rangle / \langle \mathbf{a}, \mathbf{a} \rangle$ and residual vector $\mathbf{b} - \hat{\gamma}\mathbf{a}$. We say that \mathbf{b} is adjusted for \mathbf{a} , or is “orthogonalized” with respect to \mathbf{a} .

Step 1 orthogonalizes \mathbf{x} with respect to $\mathbf{x}_0 = \mathbf{1}$. Step 2 is just a simple univariate regression, using the orthogonal predictors $\mathbf{1}$ and \mathbf{z} . Figure 3.4 shows this process for two general inputs \mathbf{x}_1 and \mathbf{x}_2 . The orthogonalization does not change the subspace spanned by \mathbf{x}_1 and \mathbf{x}_2 , it simply produces an orthogonal basis for representing it.

This recipe generalizes to the case of p inputs, as shown in Algorithm 3.1. Note that the inputs $\mathbf{z}_0, \dots, \mathbf{z}_{j-1}$ in step 2 are orthogonal, hence the simple regression coefficients computed there are in fact also the multiple regression coefficients.

¹The inner-product notation is suggestive of generalizations of linear regression to different metric spaces, as well as to probability spaces.

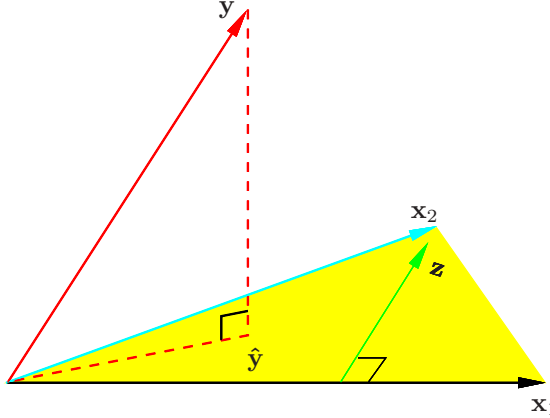


FIGURE 3.4. Least squares regression by orthogonalization of the inputs. The vector \mathbf{x}_2 is regressed on the vector \mathbf{x}_1 , leaving the residual vector \mathbf{z} . The regression of \mathbf{y} on \mathbf{z} gives the multiple regression coefficient of \mathbf{x}_2 . Adding together the projections of \mathbf{y} on each of \mathbf{x}_1 and \mathbf{z} gives the least squares fit $\hat{\mathbf{y}}$.

Algorithm 3.1 Regression by Successive Orthogonalization.

1. Initialize $\mathbf{z}_0 = \mathbf{x}_0 = \mathbf{1}$.
2. For $j = 1, 2, \dots, p$

Regress \mathbf{x}_j on $\mathbf{z}_0, \mathbf{z}_1, \dots, \mathbf{z}_{j-1}$ to produce coefficients $\hat{\gamma}_{\ell j} = \langle \mathbf{z}_\ell, \mathbf{x}_j \rangle / \langle \mathbf{z}_\ell, \mathbf{z}_\ell \rangle$, $\ell = 0, \dots, j-1$ and residual vector $\mathbf{z}_j = \mathbf{x}_j - \sum_{k=0}^{j-1} \hat{\gamma}_{kj} \mathbf{z}_k$.

3. Regress \mathbf{y} on the residual \mathbf{z}_p to give the estimate $\hat{\beta}_p$.
-

The result of this algorithm is

$$\hat{\beta}_p = \frac{\langle \mathbf{z}_p, \mathbf{y} \rangle}{\langle \mathbf{z}_p, \mathbf{z}_p \rangle}. \quad (3.28)$$

Re-arranging the residual in step 2, we can see that each of the \mathbf{x}_j is a linear combination of the \mathbf{z}_k , $k \leq j$. Since the \mathbf{z}_j are all orthogonal, they form a basis for the column space of \mathbf{X} , and hence the least squares projection onto this subspace is $\hat{\mathbf{y}}$. Since \mathbf{z}_p alone involves \mathbf{x}_p (with coefficient 1), we see that the coefficient (3.28) is indeed the multiple regression coefficient of \mathbf{y} on \mathbf{x}_p . This key result exposes the effect of correlated inputs in multiple regression. Note also that by rearranging the \mathbf{x}_j , any one of them could be in the last position, and a similar results holds. Hence stated more generally, we have shown that the j th multiple regression coefficient is the univariate regression coefficient of \mathbf{y} on $\mathbf{x}_{j+1}, \dots, \mathbf{x}_p$, the residual after regressing \mathbf{x}_j on $\mathbf{x}_0, \mathbf{x}_1, \dots, \mathbf{x}_{j-1}, \mathbf{x}_{j+1}, \dots, \mathbf{x}_p$:

The multiple regression coefficient $\hat{\beta}_j$ represents the additional contribution of \mathbf{x}_j on \mathbf{y} , after \mathbf{x}_j has been adjusted for $\mathbf{x}_0, \mathbf{x}_1, \dots, \mathbf{x}_{j-1}, \mathbf{x}_{j+1}, \dots, \mathbf{x}_p$.

If \mathbf{x}_p is highly correlated with some of the other \mathbf{x}_k 's, the residual vector \mathbf{z}_p will be close to zero, and from (3.28) the coefficient $\hat{\beta}_p$ will be very unstable. This will be true for all the variables in the correlated set. In such situations, we might have all the Z-scores (as in Table 3.2) be small—any one of the set can be deleted—yet we cannot delete them all. From (3.28) we also obtain an alternate formula for the variance estimates (3.8),

$$\text{Var}(\hat{\beta}_p) = \frac{\sigma^2}{\langle \mathbf{z}_p, \mathbf{z}_p \rangle} = \frac{\sigma^2}{\|\mathbf{z}_p\|^2}. \quad (3.29)$$

In other words, the precision with which we can estimate $\hat{\beta}_p$ depends on the length of the residual vector \mathbf{z}_p ; this represents how much of \mathbf{x}_p is unexplained by the other \mathbf{x}_k 's.

Algorithm 3.1 is known as the *Gram–Schmidt* procedure for multiple regression, and is also a useful numerical strategy for computing the estimates. We can obtain from it not just $\hat{\beta}_p$, but also the entire multiple least squares fit, as shown in Exercise 3.4.

We can represent step 2 of Algorithm 3.1 in matrix form:

$$\mathbf{X} = \mathbf{Z}\boldsymbol{\Gamma}, \quad (3.30)$$

where \mathbf{Z} has as columns the \mathbf{z}_j (in order), and $\boldsymbol{\Gamma}$ is the upper triangular matrix with entries $\hat{\gamma}_{kj}$. Introducing the diagonal matrix \mathbf{D} with j th diagonal entry $D_{jj} = \|\mathbf{z}_j\|$, we get

$$\begin{aligned} \mathbf{X} &= \mathbf{Z}\mathbf{D}^{-1}\mathbf{D}\boldsymbol{\Gamma} \\ &= \mathbf{Q}\mathbf{R}, \end{aligned} \quad (3.31)$$

the so-called *QR* decomposition of \mathbf{X} . Here \mathbf{Q} is an $N \times (p+1)$ orthogonal matrix, $\mathbf{Q}^T\mathbf{Q} = \mathbf{I}$, and \mathbf{R} is a $(p+1) \times (p+1)$ upper triangular matrix.

The **QR** decomposition represents a convenient orthogonal basis for the column space of \mathbf{X} . It is easy to see, for example, that the least squares solution is given by

$$\hat{\beta} = \mathbf{R}^{-1}\mathbf{Q}^T\mathbf{y}, \quad (3.32)$$

$$\hat{\mathbf{y}} = \mathbf{Q}\mathbf{Q}^T\mathbf{y}. \quad (3.33)$$

Equation (3.32) is easy to solve because \mathbf{R} is upper triangular (Exercise 3.4).

3.2.4 Multiple Outputs

Suppose we have multiple outputs Y_1, Y_2, \dots, Y_K that we wish to predict from our inputs $X_0, X_1, X_2, \dots, X_p$. We assume a linear model for each output

$$Y_k = \beta_{0k} + \sum_{j=1}^p X_j \beta_{jk} + \varepsilon_k \quad (3.34)$$

$$= f_k(X) + \varepsilon_k. \quad (3.35)$$

With N training cases we can write the model in matrix notation

$$\mathbf{Y} = \mathbf{XB} + \mathbf{E}. \quad (3.36)$$

Here \mathbf{Y} is the $N \times K$ response matrix, with ik entry y_{ik} , \mathbf{X} is the $N \times (p+1)$ input matrix, \mathbf{B} is the $(p+1) \times K$ matrix of parameters and \mathbf{E} is the $N \times K$ matrix of errors. A straightforward generalization of the univariate loss function (3.2) is

$$\text{RSS}(\mathbf{B}) = \sum_{k=1}^K \sum_{i=1}^N (y_{ik} - f_k(x_i))^2 \quad (3.37)$$

$$= \text{tr}[(\mathbf{Y} - \mathbf{XB})^T (\mathbf{Y} - \mathbf{XB})]. \quad (3.38)$$

The least squares estimates have exactly the same form as before

$$\hat{\mathbf{B}} = (\mathbf{X}^T \mathbf{X})^{-1} \mathbf{X}^T \mathbf{Y}. \quad (3.39)$$

Hence the coefficients for the k th outcome are just the least squares estimates in the regression of \mathbf{y}_k on $\mathbf{x}_0, \mathbf{x}_1, \dots, \mathbf{x}_p$. Multiple outputs do not affect one another's least squares estimates.

If the errors $\varepsilon = (\varepsilon_1, \dots, \varepsilon_K)$ in (3.34) are correlated, then it might seem appropriate to modify (3.37) in favor of a multivariate version. Specifically, suppose $\text{Cov}(\varepsilon) = \boldsymbol{\Sigma}$, then the multivariate weighted criterion

$$\text{RSS}(\mathbf{B}; \boldsymbol{\Sigma}) = \sum_{i=1}^N (y_i - f(x_i))^T \boldsymbol{\Sigma}^{-1} (y_i - f(x_i)) \quad (3.40)$$

arises naturally from multivariate Gaussian theory. Here $f(x)$ is the vector function $(f_1(x), \dots, f_K(x))^T$, and y_i the vector of K responses for observation i . However, it can be shown that again the solution is given by (3.39); K separate regressions that ignore the correlations (Exercise 3.11). If the $\boldsymbol{\Sigma}_i$ vary among observations, then this is no longer the case, and the solution for \mathbf{B} no longer decouples.

In Section 3.7 we pursue the multiple outcome problem, and consider situations where it does pay to combine the regressions.

3.3 Subset Selection

There are two reasons why we are often not satisfied with the least squares estimates (3.6).

- The first is *prediction accuracy*: the least squares estimates often have low bias but large variance. Prediction accuracy can sometimes be improved by shrinking or setting some coefficients to zero. By doing so we sacrifice a little bit of bias to reduce the variance of the predicted values, and hence may improve the overall prediction accuracy.
- The second reason is *interpretation*. With a large number of predictors, we often would like to determine a smaller subset that exhibit the strongest effects. In order to get the “big picture,” we are willing to sacrifice some of the small details.

In this section we describe a number of approaches to variable subset selection with linear regression. In later sections we discuss shrinkage and hybrid approaches for controlling variance, as well as other dimension-reduction strategies. These all fall under the general heading *model selection*. Model selection is not restricted to linear models; Chapter 7 covers this topic in some detail.

With subset selection we retain only a subset of the variables, and eliminate the rest from the model. Least squares regression is used to estimate the coefficients of the inputs that are retained. There are a number of different strategies for choosing the subset.

3.3.1 Best-Subset Selection

Best subset regression finds for each $k \in \{0, 1, 2, \dots, p\}$ the subset of size k that gives smallest residual sum of squares (3.2). An efficient algorithm—the *leaps and bounds* procedure (Furnival and Wilson, 1974)—makes this feasible for p as large as 30 or 40. Figure 3.5 shows all the subset models for the prostate cancer example. The lower boundary represents the models that are eligible for selection by the best-subsets approach. Note that the best subset of size 2, for example, need not include the variable that was in the best subset of size 1 (for this example all the subsets are nested). The best-subset curve (red lower boundary in Figure 3.5) is necessarily decreasing, so cannot be used to select the subset size k . The question of how to choose k involves the tradeoff between bias and variance, along with the more subjective desire for parsimony. There are a number of criteria that one may use; typically we choose the smallest model that minimizes an estimate of the expected prediction error.

Many of the other approaches that we discuss in this chapter are similar, in that they use the training data to produce a sequence of models varying in complexity and indexed by a single parameter. In the next section we use

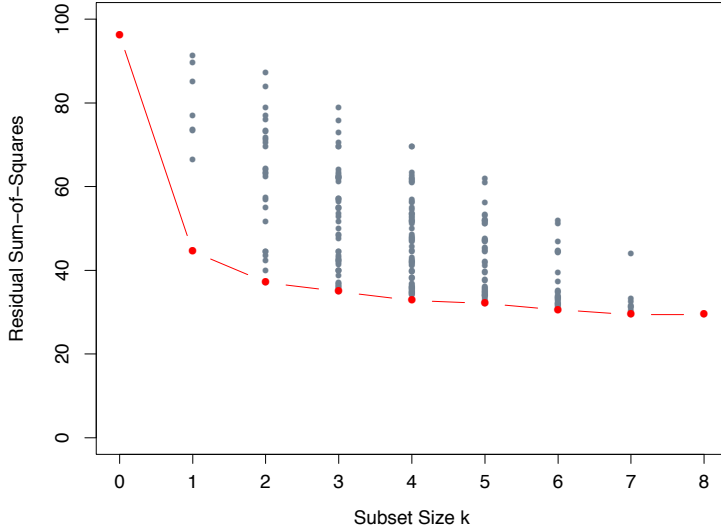


FIGURE 3.5. All possible subset models for the prostate cancer example. At each subset size is shown the residual sum-of-squares for each model of that size.

cross-validation to estimate prediction error and select k ; the AIC criterion is a popular alternative. We defer more detailed discussion of these and other approaches to Chapter 7.

3.3.2 Forward- and Backward-Stepwise Selection

Rather than search through all possible subsets (which becomes infeasible for p much larger than 40), we can seek a good path through them. *Forward-stepwise selection* starts with the intercept, and then sequentially adds into the model the predictor that most improves the fit. With many candidate predictors, this might seem like a lot of computation; however, clever updating algorithms can exploit the QR decomposition for the current fit to rapidly establish the next candidate (Exercise 3.9). Like best-subset regression, forward stepwise produces a sequence of models indexed by k , the subset size, which must be determined.

Forward-stepwise selection is a *greedy algorithm*, producing a nested sequence of models. In this sense it might seem sub-optimal compared to best-subset selection. However, there are several reasons why it might be preferred:

- *Computational*; for large p we cannot compute the best subset sequence, but we can always compute the forward stepwise sequence (even when $p \gg N$).
- *Statistical*; a price is paid in variance for selecting the best subset of each size; forward stepwise is a more constrained search, and will have lower variance, but perhaps more bias.

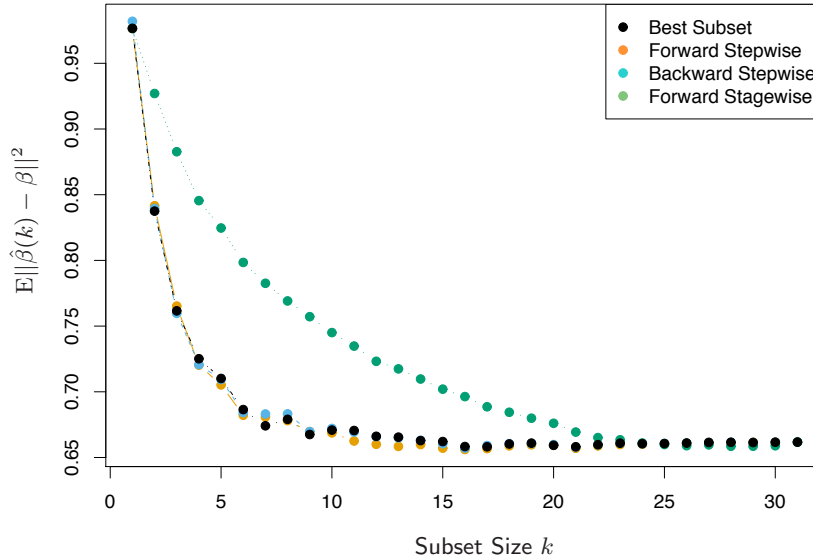


FIGURE 3.6. Comparison of four subset-selection techniques on a simulated linear regression problem $Y = X^T \beta + \varepsilon$. There are $N = 300$ observations on $p = 31$ standard Gaussian variables, with pairwise correlations all equal to 0.85. For 10 of the variables, the coefficients are drawn at random from a $N(0, 0.4)$ distribution; the rest are zero. The noise $\varepsilon \sim N(0, 6.25)$, resulting in a signal-to-noise ratio of 0.64. Results are averaged over 50 simulations. Shown is the mean-squared error of the estimated coefficient $\hat{\beta}(k)$ at each step from the true β .

Backward-stepwise selection starts with the full model, and sequentially deletes the predictor that has the least impact on the fit. The candidate for dropping is the variable with the smallest Z-score (Exercise 3.10). Backward selection can only be used when $N > p$, while forward stepwise can always be used.

Figure 3.6 shows the results of a small simulation study to compare best-subset regression with the simpler alternatives forward and backward selection. Their performance is very similar, as is often the case. Included in the figure is forward stagewise regression (next section), which takes longer to reach minimum error.

On the prostate cancer example, best-subset, forward and backward selection all gave exactly the same sequence of terms.

Some software packages implement hybrid stepwise-selection strategies that consider both forward and backward moves at each step, and select the “best” of the two. For example in the R package the `step` function uses the AIC criterion for weighing the choices, which takes proper account of the number of parameters fit; at each step an add or drop will be performed that minimizes the AIC score.

Other more traditional packages base the selection on F -statistics, adding “significant” terms, and dropping “non-significant” terms. These are out of fashion, since they do not take proper account of the multiple testing issues. It is also tempting after a model search to print out a summary of the chosen model, such as in Table 3.2; however, the standard errors are not valid, since they do not account for the search process. The bootstrap (Section 8.2) can be useful in such settings.

Finally, we note that often variables come in groups (such as the dummy variables that code a multi-level categorical predictor). Smart stepwise procedures (such as `step` in R) will add or drop whole groups at a time, taking proper account of their degrees-of-freedom.

3.3.3 Forward-Stagewise Regression

Forward-stagewise regression (FS) is even more constrained than forward-stepwise regression. It starts like forward-stepwise regression, with an intercept equal to \bar{y} , and centered predictors with coefficients initially all 0. At each step the algorithm identifies the variable most correlated with the current residual. It then computes the simple linear regression coefficient of the residual on this chosen variable, and then adds it to the current coefficient for that variable. This is continued till none of the variables have correlation with the residuals—i.e. the least-squares fit when $N > p$.

Unlike forward-stepwise regression, none of the other variables are adjusted when a term is added to the model. As a consequence, forward stagewise can take many more than p steps to reach the least squares fit, and historically has been dismissed as being inefficient. It turns out that this “slow fitting” can pay dividends in high-dimensional problems. We see in Section 3.8.1 that both forward stagewise and a variant which is slowed down even further are quite competitive, especially in very high-dimensional problems.

Forward-stagewise regression is included in Figure 3.6. In this example it takes over 1000 steps to get all the correlations below 10^{-4} . For subset size k , we plotted the error for the last step for which there were k nonzero coefficients. Although it catches up with the best fit, it takes longer to do so.

3.3.4 Prostate Cancer Data Example (Continued)

Table 3.3 shows the coefficients from a number of different selection and shrinkage methods. They are *best-subset selection* using an all-subsets search, *ridge regression*, the *lasso*, *principal components regression* and *partial least squares*. Each method has a complexity parameter, and this was chosen to minimize an estimate of prediction error based on tenfold cross-validation; full details are given in Section 7.10. Briefly, cross-validation works by dividing the training data randomly into ten equal parts. The learning method is fit—for a range of values of the complexity parameter—to nine-tenths of the data, and the prediction error is computed on the remaining one-tenth. This is done in turn for each one-tenth of the data, and the ten prediction error estimates are averaged. From this we obtain an estimated prediction error curve as a function of the complexity parameter.

Note that we have already divided these data into a training set of size 67 and a test set of size 30. Cross-validation is applied to the training set, since selecting the shrinkage parameter is part of the training process. The test set is there to judge the performance of the selected model.

The estimated prediction error curves are shown in Figure 3.7. Many of the curves are very flat over large ranges near their minimum. Included are estimated standard error bands for each estimated error rate, based on the ten error estimates computed by cross-validation. We have used the “one-standard-error” rule—we pick the most parsimonious model within one standard error of the minimum (Section 7.10, page 244). Such a rule acknowledges the fact that the tradeoff curve is estimated with error, and hence takes a conservative approach.

Best-subset selection chose to use the two predictors `lcvol` and `lweight`. The last two lines of the table give the average prediction error (and its estimated standard error) over the test set.

3.4 Shrinkage Methods

By retaining a subset of the predictors and discarding the rest, subset selection produces a model that is interpretable and has possibly lower prediction error than the full model. However, because it is a discrete process—variables are either retained or discarded—it often exhibits high variance, and so doesn’t reduce the prediction error of the full model. Shrinkage methods are more continuous, and don’t suffer as much from high variability.

3.4.1 Ridge Regression

Ridge regression shrinks the regression coefficients by imposing a penalty on their size. The ridge coefficients minimize a penalized residual sum of

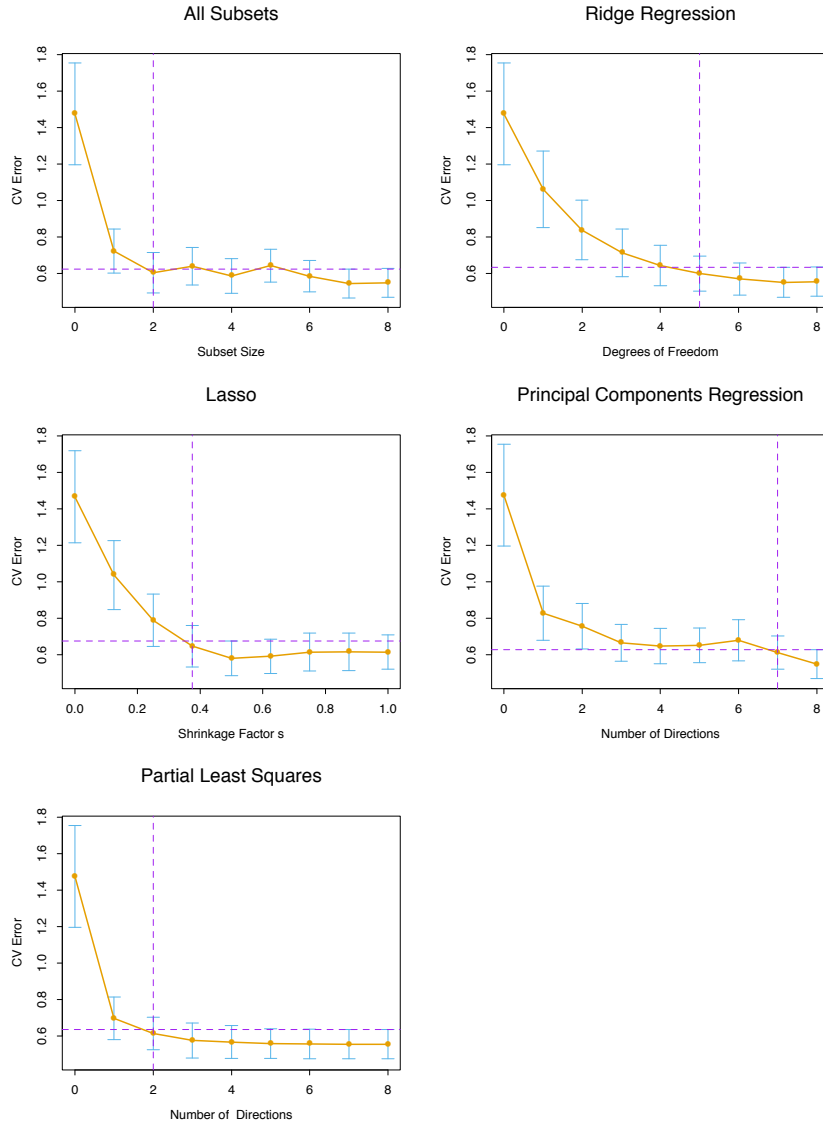


FIGURE 3.7. Estimated prediction error curves and their standard errors for the various selection and shrinkage methods. Each curve is plotted as a function of the corresponding complexity parameter for that method. The horizontal axis has been chosen so that the model complexity increases as we move from left to right. The estimates of prediction error and their standard errors were obtained by tenfold cross-validation; full details are given in Section 7.10. The least complex model within one standard error of the best is chosen, indicated by the purple vertical broken lines.

TABLE 3.3. Estimated coefficients and test error results, for different subset and shrinkage methods applied to the prostate data. The blank entries correspond to variables omitted.

Term	LS	Best Subset	Ridge	Lasso	PCR	PLS
Intercept	2.465	2.477	2.452	2.468	2.497	2.452
lcavol	0.680	0.740	0.420	0.533	0.543	0.419
lweight	0.263	0.316	0.238	0.169	0.289	0.344
age	-0.141		-0.046		-0.152	-0.026
lbph	0.210		0.162	0.002	0.214	0.220
svi	0.305		0.227	0.094	0.315	0.243
lcp	-0.288		0.000		-0.051	0.079
gleason	-0.021		0.040		0.232	0.011
pgg45	0.267		0.133		-0.056	0.084
Test Error	0.521	0.492	0.492	0.479	0.449	0.528
Std Error	0.179	0.143	0.165	0.164	0.105	0.152

squares,

$$\hat{\beta}^{\text{ridge}} = \underset{\beta}{\operatorname{argmin}} \left\{ \sum_{i=1}^N \left(y_i - \beta_0 - \sum_{j=1}^p x_{ij} \beta_j \right)^2 + \lambda \sum_{j=1}^p \beta_j^2 \right\}. \quad (3.41)$$

Here $\lambda \geq 0$ is a complexity parameter that controls the amount of shrinkage: the larger the value of λ , the greater the amount of shrinkage. The coefficients are shrunk toward zero (and each other). The idea of penalizing by the sum-of-squares of the parameters is also used in neural networks, where it is known as *weight decay* (Chapter 11).

An equivalent way to write the ridge problem is

$$\begin{aligned} \hat{\beta}^{\text{ridge}} &= \underset{\beta}{\operatorname{argmin}} \sum_{i=1}^N \left(y_i - \beta_0 - \sum_{j=1}^p x_{ij} \beta_j \right)^2, \\ &\text{subject to } \sum_{j=1}^p \beta_j^2 \leq t, \end{aligned} \quad (3.42)$$

which makes explicit the size constraint on the parameters. There is a one-to-one correspondence between the parameters λ in (3.41) and t in (3.42). When there are many correlated variables in a linear regression model, their coefficients can become poorly determined and exhibit high variance. A wildly large positive coefficient on one variable can be canceled by a similarly large negative coefficient on its correlated cousin. By imposing a size constraint on the coefficients, as in (3.42), this problem is alleviated.

The ridge solutions are not equivariant under scaling of the inputs, and so one normally standardizes the inputs before solving (3.41). In addition,

notice that the intercept β_0 has been left out of the penalty term. Penalization of the intercept would make the procedure depend on the origin chosen for Y ; that is, adding a constant c to each of the targets y_i would not simply result in a shift of the predictions by the same amount c . It can be shown (Exercise 3.5) that the solution to (3.41) can be separated into two parts, after reparametrization using *centered* inputs: each x_{ij} gets replaced by $x_{ij} - \bar{x}_j$. We estimate β_0 by $\bar{y} = \frac{1}{N} \sum_1^N y_i$. The remaining coefficients get estimated by a ridge regression without intercept, using the centered x_{ij} . Henceforth we assume that this centering has been done, so that the input matrix \mathbf{X} has p (rather than $p + 1$) columns.

Writing the criterion in (3.41) in matrix form,

$$\text{RSS}(\lambda) = (\mathbf{y} - \mathbf{X}\beta)^T(\mathbf{y} - \mathbf{X}\beta) + \lambda\beta^T\beta, \quad (3.43)$$

the ridge regression solutions are easily seen to be

$$\hat{\beta}^{\text{ridge}} = (\mathbf{X}^T\mathbf{X} + \lambda\mathbf{I})^{-1}\mathbf{X}^T\mathbf{y}, \quad (3.44)$$

where \mathbf{I} is the $p \times p$ identity matrix. Notice that with the choice of quadratic penalty $\beta^T\beta$, the ridge regression solution is again a linear function of \mathbf{y} . The solution adds a positive constant to the diagonal of $\mathbf{X}^T\mathbf{X}$ before inversion. This makes the problem nonsingular, even if $\mathbf{X}^T\mathbf{X}$ is not of full rank, and was the main motivation for ridge regression when it was first introduced in statistics (Hoerl and Kennard, 1970). Traditional descriptions of ridge regression start with definition (3.44). We choose to motivate it via (3.41) and (3.42), as these provide insight into how it works.

Figure 3.8 shows the ridge coefficient estimates for the prostate cancer example, plotted as functions of $\text{df}(\lambda)$, the *effective degrees of freedom* implied by the penalty λ (defined in (3.50) on page 68). In the case of orthonormal inputs, the ridge estimates are just a scaled version of the least squares estimates, that is, $\hat{\beta}^{\text{ridge}} = \hat{\beta}/(1 + \lambda)$.

Ridge regression can also be derived as the mean or mode of a posterior distribution, with a suitably chosen prior distribution. In detail, suppose $y_i \sim N(\beta_0 + x_i^T\beta, \sigma^2)$, and the parameters β_j are each distributed as $N(0, \tau^2)$, independently of one another. Then the (negative) log-posterior density of β , with τ^2 and σ^2 assumed known, is equal to the expression in curly braces in (3.41), with $\lambda = \sigma^2/\tau^2$ (Exercise 3.6). Thus the ridge estimate is the mode of the posterior distribution; since the distribution is Gaussian, it is also the posterior mean.

The *singular value decomposition* (SVD) of the centered input matrix \mathbf{X} gives us some additional insight into the nature of ridge regression. This decomposition is extremely useful in the analysis of many statistical methods. The SVD of the $N \times p$ matrix \mathbf{X} has the form

$$\mathbf{X} = \mathbf{UDV}^T. \quad (3.45)$$

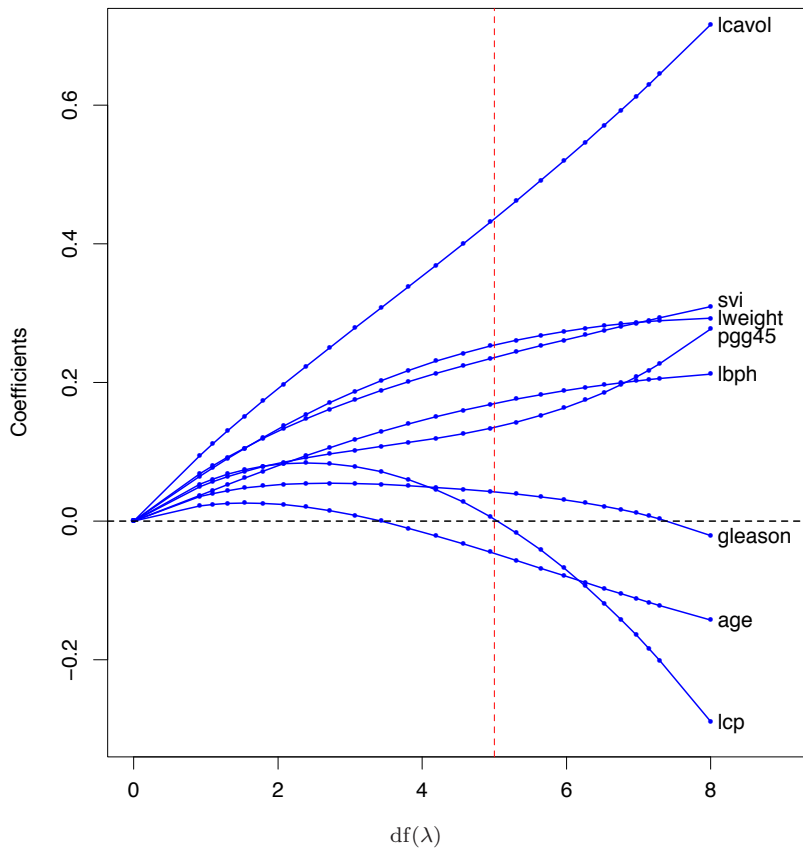


FIGURE 3.8. Profiles of ridge coefficients for the prostate cancer example, as the tuning parameter λ is varied. Coefficients are plotted versus $df(\lambda)$, the effective degrees of freedom. A vertical line is drawn at $df = 5.0$, the value chosen by cross-validation.

Here \mathbf{U} and \mathbf{V} are $N \times p$ and $p \times p$ orthogonal matrices, with the columns of \mathbf{U} spanning the column space of \mathbf{X} , and the columns of \mathbf{V} spanning the row space. \mathbf{D} is a $p \times p$ diagonal matrix, with diagonal entries $d_1 \geq d_2 \geq \dots \geq d_p \geq 0$ called the singular values of \mathbf{X} . If one or more values $d_j = 0$, \mathbf{X} is singular.

Using the singular value decomposition we can write the least squares fitted vector as

$$\begin{aligned}\hat{\mathbf{X}}\hat{\beta}^{\text{ls}} &= \mathbf{X}(\mathbf{X}^T\mathbf{X})^{-1}\mathbf{X}^T\mathbf{y} \\ &= \mathbf{U}\mathbf{U}^T\mathbf{y},\end{aligned}\quad (3.46)$$

after some simplification. Note that $\mathbf{U}^T\mathbf{y}$ are the coordinates of \mathbf{y} with respect to the orthonormal basis \mathbf{U} . Note also the similarity with (3.33); \mathbf{Q} and \mathbf{U} are generally different orthogonal bases for the column space of \mathbf{X} (Exercise 3.8).

Now the ridge solutions are

$$\begin{aligned}\hat{\mathbf{X}}\hat{\beta}^{\text{ridge}} &= \mathbf{X}(\mathbf{X}^T\mathbf{X} + \lambda\mathbf{I})^{-1}\mathbf{X}^T\mathbf{y} \\ &= \mathbf{U}\mathbf{D}(\mathbf{D}^2 + \lambda\mathbf{I})^{-1}\mathbf{D}\mathbf{U}^T\mathbf{y} \\ &= \sum_{j=1}^p \mathbf{u}_j \frac{d_j^2}{d_j^2 + \lambda} \mathbf{u}_j^T \mathbf{y},\end{aligned}\quad (3.47)$$

where the \mathbf{u}_j are the columns of \mathbf{U} . Note that since $\lambda \geq 0$, we have $d_j^2/(d_j^2 + \lambda) \leq 1$. Like linear regression, ridge regression computes the coordinates of \mathbf{y} with respect to the orthonormal basis \mathbf{U} . It then shrinks these coordinates by the factors $d_j^2/(d_j^2 + \lambda)$. This means that a greater amount of shrinkage is applied to the coordinates of basis vectors with smaller d_j^2 .

What does a small value of d_j^2 mean? The SVD of the centered matrix \mathbf{X} is another way of expressing the *principal components* of the variables in \mathbf{X} . The sample covariance matrix is given by $\mathbf{S} = \mathbf{X}^T\mathbf{X}/N$, and from (3.45) we have

$$\mathbf{X}^T\mathbf{X} = \mathbf{V}\mathbf{D}^2\mathbf{V}^T,\quad (3.48)$$

which is the *eigen decomposition* of $\mathbf{X}^T\mathbf{X}$ (and of \mathbf{S} , up to a factor N). The eigenvectors v_j (columns of \mathbf{V}) are also called the *principal components* (or Karhunen–Loeve) directions of \mathbf{X} . The first principal component direction v_1 has the property that $\mathbf{z}_1 = \mathbf{X}v_1$ has the largest sample variance amongst all normalized linear combinations of the columns of \mathbf{X} . This sample variance is easily seen to be

$$\text{Var}(\mathbf{z}_1) = \text{Var}(\mathbf{X}v_1) = \frac{d_1^2}{N},\quad (3.49)$$

and in fact $\mathbf{z}_1 = \mathbf{X}v_1 = \mathbf{u}_1 d_1$. The derived variable \mathbf{z}_1 is called the first principal component of \mathbf{X} , and hence \mathbf{u}_1 is the normalized first principal

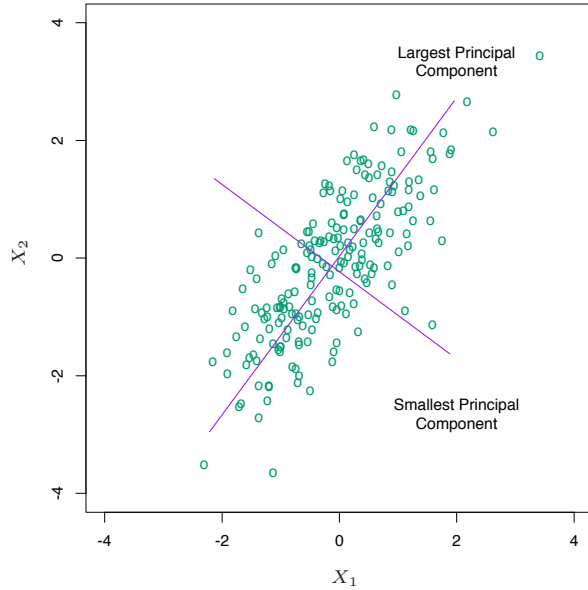


FIGURE 3.9. Principal components of some input data points. The largest principal component is the direction that maximizes the variance of the projected data, and the smallest principal component minimizes that variance. Ridge regression projects \mathbf{y} onto these components, and then shrinks the coefficients of the low-variance components more than the high-variance components.

component. Subsequent principal components \mathbf{z}_j have maximum variance d_j^2/N , subject to being orthogonal to the earlier ones. Conversely the last principal component has *minimum* variance. Hence the small singular values d_j correspond to directions in the column space of \mathbf{X} having small variance, and ridge regression shrinks these directions the most.

Figure 3.9 illustrates the principal components of some data points in two dimensions. If we consider fitting a linear surface over this domain (the Y -axis is sticking out of the page), the configuration of the data allow us to determine its gradient more accurately in the long direction than the short. Ridge regression protects against the potentially high variance of gradients estimated in the short directions. The implicit assumption is that the response will tend to vary most in the directions of high variance of the inputs. This is often a reasonable assumption, since predictors are often chosen for study because they vary with the response variable, but need not hold in general.

In Figure 3.7 we have plotted the estimated prediction error versus the quantity

$$\begin{aligned} \text{df}(\lambda) &= \text{tr}[\mathbf{X}(\mathbf{X}^T \mathbf{X} + \lambda \mathbf{I})^{-1} \mathbf{X}^T], \\ &= \text{tr}(\mathbf{H}_\lambda) \\ &= \sum_{j=1}^p \frac{d_j^2}{d_j^2 + \lambda}. \end{aligned} \quad (3.50)$$

This monotone decreasing function of λ is the *effective degrees of freedom* of the ridge regression fit. Usually in a linear-regression fit with p variables, the degrees-of-freedom of the fit is p , the number of free parameters. The idea is that although all p coefficients in a ridge fit will be non-zero, they are fit in a restricted fashion controlled by λ . Note that $\text{df}(\lambda) = p$ when $\lambda = 0$ (no regularization) and $\text{df}(\lambda) \rightarrow 0$ as $\lambda \rightarrow \infty$. Of course there is always an additional one degree of freedom for the intercept, which was removed *a priori*. This definition is motivated in more detail in Section 3.4.4 and Sections 7.4–7.6. In Figure 3.7 the minimum occurs at $\text{df}(\lambda) = 5.0$. Table 3.3 shows that ridge regression reduces the test error of the full least squares estimates by a small amount.

3.4.2 The Lasso

The lasso is a shrinkage method like ridge, with subtle but important differences. The lasso estimate is defined by

$$\begin{aligned} \hat{\beta}^{\text{lasso}} &= \underset{\beta}{\operatorname{argmin}} \sum_{i=1}^N \left(y_i - \beta_0 - \sum_{j=1}^p x_{ij} \beta_j \right)^2 \\ &\text{subject to } \sum_{j=1}^p |\beta_j| \leq t. \end{aligned} \quad (3.51)$$

Just as in ridge regression, we can re-parametrize the constant β_0 by standardizing the predictors; the solution for $\hat{\beta}_0$ is \bar{y} , and thereafter we fit a model without an intercept (Exercise 3.5). In the signal processing literature, the lasso is also known as *basis pursuit* (Chen et al., 1998).

We can also write the lasso problem in the equivalent *Lagrangian form*

$$\hat{\beta}^{\text{lasso}} = \underset{\beta}{\operatorname{argmin}} \left\{ \frac{1}{2} \sum_{i=1}^N \left(y_i - \beta_0 - \sum_{j=1}^p x_{ij} \beta_j \right)^2 + \lambda \sum_{j=1}^p |\beta_j| \right\}. \quad (3.52)$$

Notice the similarity to the ridge regression problem (3.42) or (3.41): the L_2 ridge penalty $\sum_1^p \beta_j^2$ is replaced by the L_1 lasso penalty $\sum_1^p |\beta_j|$. This latter constraint makes the solutions nonlinear in the y_i , and there is no closed form expression as in ridge regression. Computing the lasso solution

is a quadratic programming problem, although we see in Section 3.4.4 that efficient algorithms are available for computing the entire path of solutions as λ is varied, with the same computational cost as for ridge regression. Because of the nature of the constraint, making t sufficiently small will cause some of the coefficients to be exactly zero. Thus the lasso does a kind of continuous subset selection. If t is chosen larger than $t_0 = \sum_1^p |\hat{\beta}_j|$ (where $\hat{\beta}_j = \hat{\beta}_j^{\text{ls}}$, the least squares estimates), then the lasso estimates are the $\hat{\beta}_j$'s. On the other hand, for $t = t_0/2$ say, then the least squares coefficients are shrunk by about 50% on average. However, the nature of the shrinkage is not obvious, and we investigate it further in Section 3.4.4 below. Like the subset size in variable subset selection, or the penalty parameter in ridge regression, t should be adaptively chosen to minimize an estimate of expected prediction error.

In Figure 3.7, for ease of interpretation, we have plotted the lasso prediction error estimates versus the standardized parameter $s = t / \sum_1^p |\hat{\beta}_j|$. A value $\hat{s} \approx 0.36$ was chosen by 10-fold cross-validation; this caused four coefficients to be set to zero (fifth column of Table 3.3). The resulting model has the second lowest test error, slightly lower than the full least squares model, but the standard errors of the test error estimates (last line of Table 3.3) are fairly large.

Figure 3.10 shows the lasso coefficients as the standardized tuning parameter $s = t / \sum_1^p |\hat{\beta}_j|$ is varied. At $s = 1.0$ these are the least squares estimates; they decrease to 0 as $s \rightarrow 0$. This decrease is not always strictly monotonic, although it is in this example. A vertical line is drawn at $s = 0.36$, the value chosen by cross-validation.

3.4.3 Discussion: Subset Selection, Ridge Regression and the Lasso

In this section we discuss and compare the three approaches discussed so far for restricting the linear regression model: subset selection, ridge regression and the lasso.

In the case of an orthonormal input matrix \mathbf{X} the three procedures have explicit solutions. Each method applies a simple transformation to the least squares estimate $\hat{\beta}_j$, as detailed in Table 3.4.

Ridge regression does a proportional shrinkage. Lasso translates each coefficient by a constant factor λ , truncating at zero. This is called “soft thresholding,” and is used in the context of wavelet-based smoothing in Section 5.9. Best-subset selection drops all variables with coefficients smaller than the M th largest; this is a form of “hard-thresholding.”

Back to the nonorthogonal case; some pictures help understand their relationship. Figure 3.11 depicts the lasso (left) and ridge regression (right) when there are only two parameters. The residual sum of squares has elliptical contours, centered at the full least squares estimate. The constraint

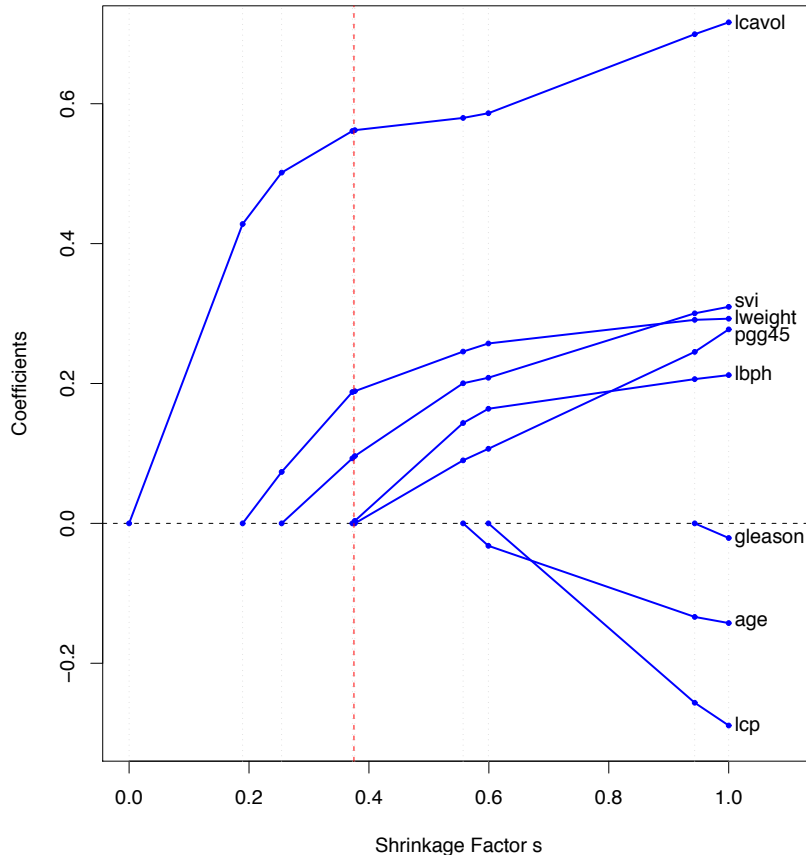


FIGURE 3.10. Profiles of lasso coefficients, as the tuning parameter t is varied. Coefficients are plotted versus $s = t / \sum_1^p |\hat{\beta}_j|$. A vertical line is drawn at $s = 0.36$, the value chosen by cross-validation. Compare Figure 3.8 on page 65; the lasso profiles hit zero, while those for ridge do not. The profiles are piece-wise linear, and so are computed only at the points displayed; see Section 3.4.4 for details.

TABLE 3.4. Estimators of β_j in the case of orthonormal columns of \mathbf{X} . M and λ are constants chosen by the corresponding techniques; sign denotes the sign of its argument (± 1), and x_+ denotes “positive part” of x . Below the table, estimators are shown by broken red lines. The 45° line in gray shows the unrestricted estimate for reference.

Estimator	Formula
Best subset (size M)	$\hat{\beta}_j \cdot I(\hat{\beta}_j \geq \hat{\beta}_{(M)})$
Ridge	$\hat{\beta}_j / (1 + \lambda)$
Lasso	$\text{sign}(\hat{\beta}_j)(\hat{\beta}_j - \lambda)_+$

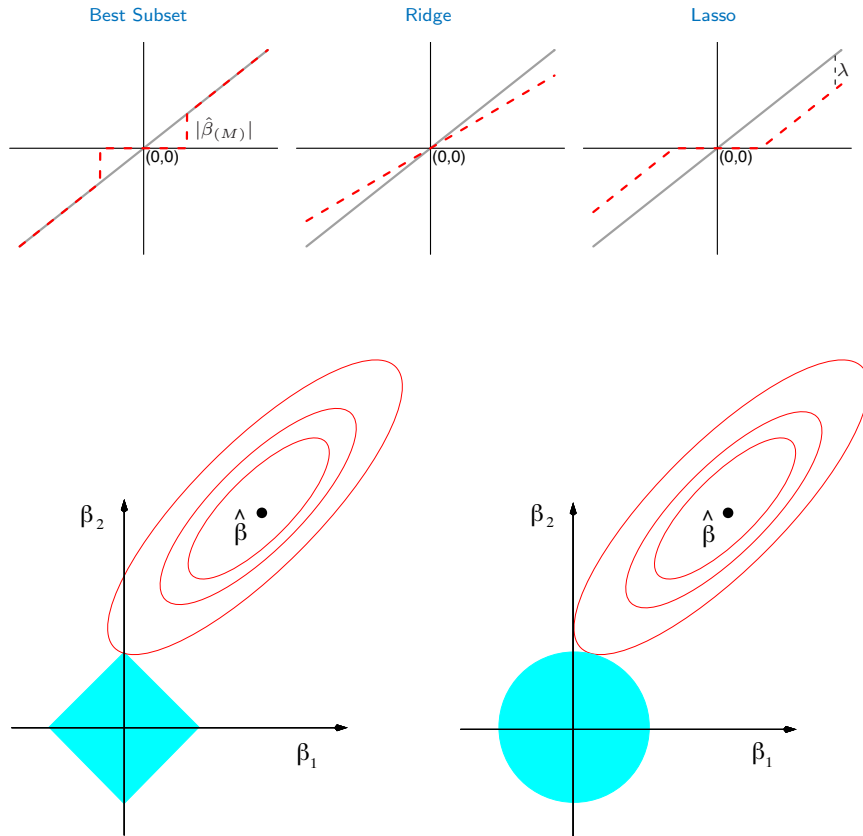


FIGURE 3.11. Estimation picture for the lasso (left) and ridge regression (right). Shown are contours of the error and constraint functions. The solid blue areas are the constraint regions $|\beta_1| + |\beta_2| \leq t$ and $\beta_1^2 + \beta_2^2 \leq t^2$, respectively, while the red ellipses are the contours of the least squares error function.

region for ridge regression is the disk $\beta_1^2 + \beta_2^2 \leq t$, while that for lasso is the diamond $|\beta_1| + |\beta_2| \leq t$. Both methods find the first point where the elliptical contours hit the constraint region. Unlike the disk, the diamond has corners; if the solution occurs at a corner, then it has one parameter β_j equal to zero. When $p > 2$, the diamond becomes a rhomboid, and has many corners, flat edges and faces; there are many more opportunities for the estimated parameters to be zero.

We can generalize ridge regression and the lasso, and view them as Bayes estimates. Consider the criterion

$$\tilde{\beta} = \underset{\beta}{\operatorname{argmin}} \left\{ \sum_{i=1}^N (y_i - \beta_0 - \sum_{j=1}^p x_{ij}\beta_j)^2 + \lambda \sum_{j=1}^p |\beta_j|^q \right\} \quad (3.53)$$

for $q \geq 0$. The contours of constant value of $\sum_j |\beta_j|^q$ are shown in Figure 3.12, for the case of two inputs.

Thinking of $|\beta_j|^q$ as the log-prior density for β_j , these are also the equi-contours of the prior distribution of the parameters. The value $q = 0$ corresponds to variable subset selection, as the penalty simply counts the number of nonzero parameters; $q = 1$ corresponds to the lasso, while $q = 2$ to ridge regression. Notice that for $q \leq 1$, the prior is not uniform in direction, but concentrates more mass in the coordinate directions. The prior corresponding to the $q = 1$ case is an independent double exponential (or Laplace) distribution for each input, with density $(1/2\tau) \exp(-|\beta|/\tau)$ and $\tau = 1/\lambda$. The case $q = 1$ (lasso) is the smallest q such that the constraint region is convex; non-convex constraint regions make the optimization problem more difficult.

In this view, the lasso, ridge regression and best subset selection are Bayes estimates with different priors. Note, however, that they are derived as posterior modes, that is, maximizers of the posterior. It is more common to use the mean of the posterior as the Bayes estimate. Ridge regression is also the posterior mean, but the lasso and best subset selection are not.

Looking again at the criterion (3.53), we might try using other values of q besides 0, 1, or 2. Although one might consider estimating q from the data, our experience is that it is not worth the effort for the extra variance incurred. Values of $q \in (1, 2)$ suggest a compromise between the lasso and ridge regression. Although this is the case, with $q > 1$, $|\beta_j|^q$ is differentiable at 0, and so does not share the ability of lasso ($q = 1$) for

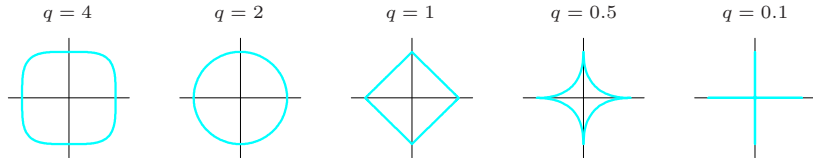


FIGURE 3.12. Contours of constant value of $\sum_j |\beta_j|^q$ for given values of q .

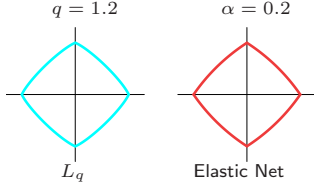


FIGURE 3.13. Contours of constant value of $\sum_j |\beta_j|^q$ for $q = 1.2$ (left plot), and the elastic-net penalty $\sum_j (\alpha\beta_j^2 + (1-\alpha)|\beta_j|)$ for $\alpha = 0.2$ (right plot). Although visually very similar, the elastic-net has sharp (non-differentiable) corners, while the $q = 1.2$ penalty does not.

setting coefficients exactly to zero. Partly for this reason as well as for computational tractability, Zou and Hastie (2005) introduced the *elastic-net* penalty

$$\lambda \sum_{j=1}^p (\alpha\beta_j^2 + (1-\alpha)|\beta_j|), \quad (3.54)$$

a different compromise between ridge and lasso. Figure 3.13 compares the L_q penalty with $q = 1.2$ and the elastic-net penalty with $\alpha = 0.2$; it is hard to detect the difference by eye. The elastic-net selects variables like the lasso, and shrinks together the coefficients of correlated predictors like ridge. It also has considerable computational advantages over the L_q penalties. We discuss the elastic-net further in Section 18.4.

3.4.4 Least Angle Regression

Least angle regression (LAR) is a relative newcomer (Efron et al., 2004), and can be viewed as a kind of “democratic” version of forward stepwise regression (Section 3.3.2). As we will see, LAR is intimately connected with the lasso, and in fact provides an extremely efficient algorithm for computing the entire lasso path as in Figure 3.10.

Forward stepwise regression builds a model sequentially, adding one variable at a time. At each step, it identifies the best variable to include in the *active set*, and then updates the least squares fit to include all the active variables.

Least angle regression uses a similar strategy, but only enters “as much” of a predictor as it deserves. At the first step it identifies the variable most correlated with the response. Rather than fit this variable completely, LAR moves the coefficient of this variable continuously toward its least-squares value (causing its correlation with the evolving residual to decrease in absolute value). As soon as another variable “catches up” in terms of correlation with the residual, the process is paused. The second variable then joins the active set, and their coefficients are moved together in a way that keeps their correlations tied and decreasing. This process is continued

until all the variables are in the model, and ends at the full least-squares fit. Algorithm 3.2 provides the details. The termination condition in step 5 requires some explanation. If $p > N - 1$, the LAR algorithm reaches a zero residual solution after $N - 1$ steps (the -1 is because we have centered the data).

Algorithm 3.2 Least Angle Regression.

1. Standardize the predictors to have mean zero and unit norm. Start with the residual $\mathbf{r} = \mathbf{y} - \bar{\mathbf{y}}$, $\beta_1, \beta_2, \dots, \beta_p = 0$.
 2. Find the predictor \mathbf{x}_j most correlated with \mathbf{r} .
 3. Move β_j from 0 towards its least-squares coefficient $\langle \mathbf{x}_j, \mathbf{r} \rangle$, until some other competitor \mathbf{x}_k has as much correlation with the current residual as does \mathbf{x}_j .
 4. Move β_j and β_k in the direction defined by their joint least squares coefficient of the current residual on $(\mathbf{x}_j, \mathbf{x}_k)$, until some other competitor \mathbf{x}_l has as much correlation with the current residual.
 5. Continue in this way until all p predictors have been entered. After $\min(N - 1, p)$ steps, we arrive at the full least-squares solution.
-

Suppose \mathcal{A}_k is the active set of variables at the beginning of the k th step, and let $\beta_{\mathcal{A}_k}$ be the coefficient vector for these variables at this step; there will be $k - 1$ nonzero values, and the one just entered will be zero. If $\mathbf{r}_k = \mathbf{y} - \mathbf{X}_{\mathcal{A}_k} \beta_{\mathcal{A}_k}$ is the current residual, then the direction for this step is

$$\delta_k = (\mathbf{X}_{\mathcal{A}_k}^T \mathbf{X}_{\mathcal{A}_k})^{-1} \mathbf{X}_{\mathcal{A}_k}^T \mathbf{r}_k. \quad (3.55)$$

The coefficient profile then evolves as $\beta_{\mathcal{A}_k}(\alpha) = \beta_{\mathcal{A}_k} + \alpha \cdot \delta_k$. Exercise 3.23 verifies that the directions chosen in this fashion do what is claimed: keep the correlations tied and decreasing. If the fit vector at the beginning of this step is $\hat{\mathbf{f}}_k$, then it evolves as $\hat{\mathbf{f}}_k(\alpha) = \hat{\mathbf{f}}_k + \alpha \cdot \mathbf{u}_k$, where $\mathbf{u}_k = \mathbf{X}_{\mathcal{A}_k} \delta_k$ is the new fit direction. The name “least angle” arises from a geometrical interpretation of this process; \mathbf{u}_k makes the smallest (and equal) angle with each of the predictors in \mathcal{A}_k (Exercise 3.24). Figure 3.14 shows the absolute correlations decreasing and joining ranks with each step of the LAR algorithm, using simulated data.

By construction the coefficients in LAR change in a piecewise linear fashion. Figure 3.15 [left panel] shows the LAR coefficient profile evolving as a function of their L_1 arc length ². Note that we do not need to take small

²The L_1 arc-length of a differentiable curve $\beta(s)$ for $s \in [0, S]$ is given by $\text{TV}(\beta, S) = \int_0^S \|\dot{\beta}(s)\|_1 ds$, where $\dot{\beta}(s) = \partial \beta(s) / \partial s$. For the piecewise-linear LAR coefficient profile, this amounts to summing the L_1 norms of the changes in coefficients from step to step.

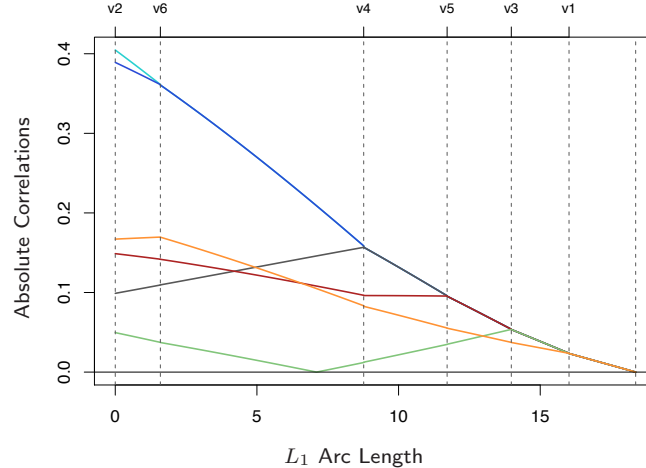


FIGURE 3.14. Progression of the absolute correlations during each step of the LAR procedure, using a simulated data set with six predictors. The labels at the top of the plot indicate which variables enter the active set at each step. The step length are measured in units of L_1 arc length.

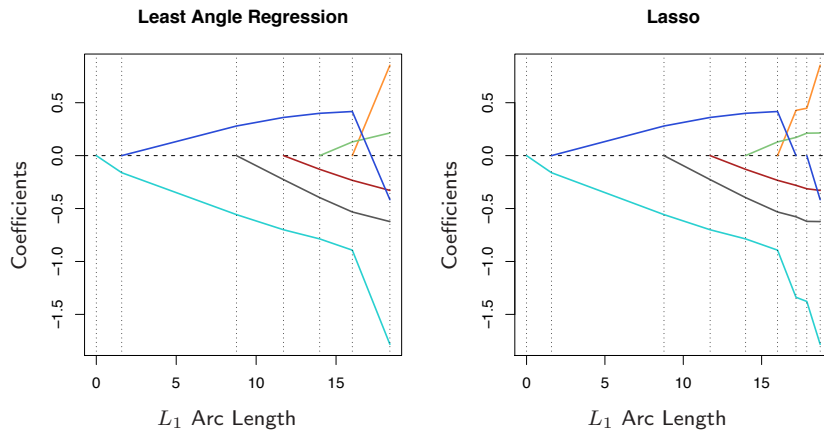


FIGURE 3.15. Left panel shows the LAR coefficient profiles on the simulated data, as a function of the L_1 arc length. The right panel shows the Lasso profile. They are identical until the dark-blue coefficient crosses zero at an arc length of about 18.

steps and recheck the correlations in step 3; using knowledge of the covariance of the predictors and the piecewise linearity of the algorithm, we can work out the exact step length at the beginning of each step (Exercise 3.25).

The right panel of Figure 3.15 shows the lasso coefficient profiles on the same data. They are almost identical to those in the left panel, and differ for the first time when the blue coefficient passes back through zero. For the prostate data, the LAR coefficient profile turns out to be identical to the lasso profile in Figure 3.10, which never crosses zero. These observations lead to a simple modification of the LAR algorithm that gives the entire lasso path, which is also piecewise-linear.

Algorithm 3.2a *Least Angle Regression: Lasso Modification.*

- 4a. If a non-zero coefficient hits zero, drop its variable from the active set of variables and recompute the current joint least squares direction.
-

The LAR(lasso) algorithm is extremely efficient, requiring the same order of computation as that of a single least squares fit using the p predictors. Least angle regression always takes p steps to get to the full least squares estimates. The lasso path can have more than p steps, although the two are often quite similar. Algorithm 3.2 with the lasso modification 3.2a is an efficient way of computing the solution to any lasso problem, especially when $p \gg N$. Osborne et al. (2000a) also discovered a piecewise-linear path for computing the lasso, which they called a *homotopy* algorithm.

We now give a heuristic argument for why these procedures are so similar. Although the LAR algorithm is stated in terms of correlations, if the input features are standardized, it is equivalent and easier to work with inner-products. Suppose \mathcal{A} is the active set of variables at some stage in the algorithm, tied in their absolute inner-product with the current residuals $\mathbf{y} - \mathbf{X}\beta$. We can express this as

$$\mathbf{x}_j^T(\mathbf{y} - \mathbf{X}\beta) = \gamma \cdot s_j, \quad \forall j \in \mathcal{A} \quad (3.56)$$

where $s_j \in \{-1, 1\}$ indicates the sign of the inner-product, and γ is the common value. Also $|\mathbf{x}_k^T(\mathbf{y} - \mathbf{X}\beta)| \leq \gamma \quad \forall k \notin \mathcal{A}$. Now consider the lasso criterion (3.52), which we write in vector form

$$R(\beta) = \frac{1}{2} \|\mathbf{y} - \mathbf{X}\beta\|_2^2 + \lambda \|\beta\|_1. \quad (3.57)$$

Let \mathcal{B} be the active set of variables in the solution for a given value of λ . For these variables $R(\beta)$ is differentiable, and the stationarity conditions give

$$\mathbf{x}_j^T(\mathbf{y} - \mathbf{X}\beta) = \lambda \cdot \text{sign}(\beta_j), \quad \forall j \in \mathcal{B} \quad (3.58)$$

Comparing (3.58) with (3.56), we see that they are identical only if the sign of β_j matches the sign of the inner product. That is why the LAR

algorithm and lasso start to differ when an active coefficient passes through zero; condition (3.58) is violated for that variable, and it is kicked out of the active set \mathcal{B} . Exercise 3.23 shows that these equations imply a piecewise-linear coefficient profile as λ decreases. The stationarity conditions for the non-active variables require that

$$|\mathbf{x}_k^T(\mathbf{y} - \mathbf{X}\beta)| \leq \lambda, \quad \forall k \notin \mathcal{B}, \quad (3.59)$$

which again agrees with the LAR algorithm.

Figure 3.16 compares LAR and lasso to forward stepwise and stagewise regression. The setup is the same as in Figure 3.6 on page 59, except here $N = 100$ here rather than 300, so the problem is more difficult. We see that the more aggressive forward stepwise starts to overfit quite early (well before the 10 true variables can enter the model), and ultimately performs worse than the slower forward stagewise regression. The behavior of LAR and lasso is similar to that of forward stagewise regression. Incremental forward stagewise is similar to LAR and lasso, and is described in Section 3.8.1.

Degrees-of-Freedom Formula for LAR and Lasso

Suppose that we fit a linear model via the least angle regression procedure, stopping at some number of steps $k < p$, or equivalently using a lasso bound t that produces a constrained version of the full least squares fit. How many parameters, or “degrees of freedom” have we used?

Consider first a linear regression using a subset of k features. If this subset is prespecified in advance without reference to the training data, then the degrees of freedom used in the fitted model is defined to be k . Indeed, in classical statistics, the number of linearly independent parameters is what is meant by “degrees of freedom.” Alternatively, suppose that we carry out a best subset selection to determine the “optimal” set of k predictors. Then the resulting model has k parameters, but in some sense we have used up more than k degrees of freedom.

We need a more general definition for the effective degrees of freedom of an adaptively fitted model. We define the degrees of freedom of the fitted vector $\hat{\mathbf{y}} = (\hat{y}_1, \hat{y}_2, \dots, \hat{y}_N)$ as

$$\text{df}(\hat{\mathbf{y}}) = \frac{1}{\sigma^2} \sum_{i=1}^N \text{Cov}(\hat{y}_i, y_i). \quad (3.60)$$

Here $\text{Cov}(\hat{y}_i, y_i)$ refers to the sampling covariance between the predicted value \hat{y}_i and its corresponding outcome value y_i . This makes intuitive sense: the harder that we fit to the data, the larger this covariance and hence $\text{df}(\hat{\mathbf{y}})$. Expression (3.60) is a useful notion of degrees of freedom, one that can be applied to any model prediction $\hat{\mathbf{y}}$. This includes models that are

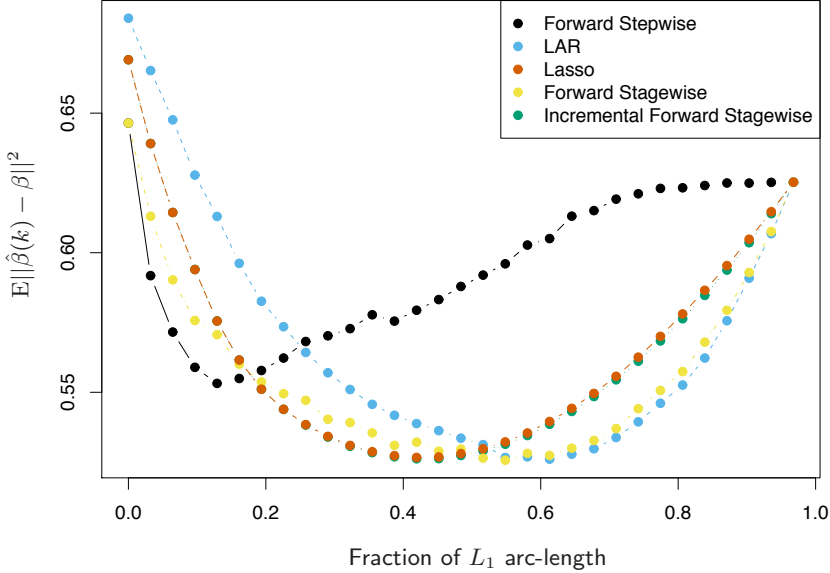


FIGURE 3.16. Comparison of LAR and lasso with forward stepwise, forward stagewise (FS) and incremental forward stagewise (FS_0) regression. The setup is the same as in Figure 3.6, except $N = 100$ here rather than 300. Here the slower FS regression ultimately outperforms forward stepwise. LAR and lasso show similar behavior to FS and FS_0 . Since the procedures take different numbers of steps (across simulation replicates and methods), we plot the MSE as a function of the fraction of total L_1 arc-length toward the least-squares fit.

adaptively fitted to the training data. This definition is motivated and discussed further in Sections 7.4–7.6.

Now for a linear regression with k fixed predictors, it is easy to show that $df(\hat{y}) = k$. Likewise for ridge regression, this definition leads to the closed-form expression (3.50) on page 68: $df(\hat{y}) = \text{tr}(\mathbf{S}_\lambda)$. In both these cases, (3.60) is simple to evaluate because the fit $\hat{y} = \mathbf{H}_\lambda \mathbf{y}$ is linear in \mathbf{y} . If we think about definition (3.60) in the context of a best subset selection of size k , it seems clear that $df(\hat{y})$ will be larger than k , and this can be verified by estimating $\text{Cov}(\hat{y}_i, y_i)/\sigma^2$ directly by simulation. However there is no closed form method for estimating $df(\hat{y})$ for best subset selection.

For LAR and lasso, something magical happens. These techniques are adaptive in a smoother way than best subset selection, and hence estimation of degrees of freedom is more tractable. Specifically it can be shown that after the k th step of the LAR procedure, the effective degrees of freedom of the fit vector is exactly k . Now for the lasso, the (modified) LAR procedure

often takes more than p steps, since predictors can drop out. Hence the definition is a little different; for the lasso, at any stage $\text{df}(\hat{\mathbf{y}})$ approximately equals the number of predictors in the model. While this approximation works reasonably well anywhere in the lasso path, for each k it works best at the *last* model in the sequence that contains k predictors. A detailed study of the degrees of freedom for the lasso may be found in Zou et al. (2007).

3.5 Methods Using Derived Input Directions

In many situations we have a large number of inputs, often very correlated. The methods in this section produce a small number of linear combinations Z_m , $m = 1, \dots, M$ of the original inputs X_j , and the Z_m are then used in place of the X_j as inputs in the regression. The methods differ in how the linear combinations are constructed.

3.5.1 Principal Components Regression

In this approach the linear combinations Z_m used are the principal components as defined in Section 3.4.1 above.

Principal component regression forms the derived input columns $\mathbf{z}_m = \mathbf{X}\mathbf{v}_m$, and then regresses \mathbf{y} on $\mathbf{z}_1, \mathbf{z}_2, \dots, \mathbf{z}_M$ for some $M \leq p$. Since the \mathbf{z}_m are orthogonal, this regression is just a sum of univariate regressions:

$$\hat{\mathbf{y}}_{(M)}^{\text{PCR}} = \bar{y}\mathbf{1} + \sum_{m=1}^M \hat{\theta}_m \mathbf{z}_m, \quad (3.61)$$

where $\hat{\theta}_m = \langle \mathbf{z}_m, \mathbf{y} \rangle / \langle \mathbf{z}_m, \mathbf{z}_m \rangle$. Since the \mathbf{z}_m are each linear combinations of the original \mathbf{x}_j , we can express the solution (3.61) in terms of coefficients of the \mathbf{x}_j (Exercise 3.13):

$$\hat{\beta}^{\text{PCR}}(M) = \sum_{m=1}^M \hat{\theta}_m v_m. \quad (3.62)$$

As with ridge regression, principal components depend on the scaling of the inputs, so typically we first standardize them. Note that if $M = p$, we would just get back the usual least squares estimates, since the columns of $\mathbf{Z} = \mathbf{UD}$ span the column space of \mathbf{X} . For $M < p$ we get a reduced regression. We see that principal components regression is very similar to ridge regression: both operate via the principal components of the input matrix. Ridge regression shrinks the coefficients of the principal components (Figure 3.17), shrinking more depending on the size of the corresponding eigenvalue; principal components regression discards the $p - M$ smallest eigenvalue components. Figure 3.17 illustrates this.

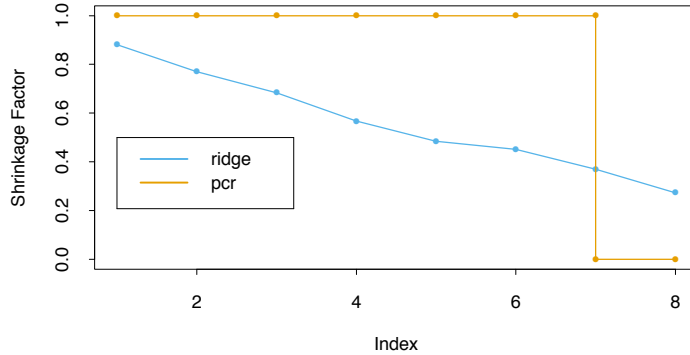


FIGURE 3.17. Ridge regression shrinks the regression coefficients of the principal components, using shrinkage factors $d_j^2/(d_j^2 + \lambda)$ as in (3.47). Principal component regression truncates them. Shown are the shrinkage and truncation patterns corresponding to Figure 3.7, as a function of the principal component index.

In Figure 3.7 we see that cross-validation suggests seven terms; the resulting model has the lowest test error in Table 3.3.

3.5.2 Partial Least Squares

This technique also constructs a set of linear combinations of the inputs for regression, but unlike principal components regression it uses \mathbf{y} (in addition to \mathbf{X}) for this construction. Like principal component regression, partial least squares (PLS) is not scale invariant, so we assume that each \mathbf{x}_j is standardized to have mean 0 and variance 1. PLS begins by computing $\hat{\varphi}_{1j} = \langle \mathbf{x}_j, \mathbf{y} \rangle$ for each j . From this we construct the derived input $\mathbf{z}_1 = \sum_j \hat{\varphi}_{1j} \mathbf{x}_j$, which is the first partial least squares direction. Hence in the construction of each \mathbf{z}_m , the inputs are weighted by the strength of their univariate effect on \mathbf{y} ³. The outcome \mathbf{y} is regressed on \mathbf{z}_1 giving coefficient $\hat{\theta}_1$, and then we orthogonalize $\mathbf{x}_1, \dots, \mathbf{x}_p$ with respect to \mathbf{z}_1 . We continue this process, until $M \leq p$ directions have been obtained. In this manner, partial least squares produces a sequence of derived, orthogonal inputs or directions $\mathbf{z}_1, \mathbf{z}_2, \dots, \mathbf{z}_M$. As with principal-component regression, if we were to construct all $M = p$ directions, we would get back a solution equivalent to the usual least squares estimates; using $M < p$ directions produces a reduced regression. The procedure is described fully in Algorithm 3.3.

³Since the \mathbf{x}_j are standardized, the first directions $\hat{\varphi}_{1j}$ are the univariate regression coefficients (up to an irrelevant constant); this is not the case for subsequent directions.

Algorithm 3.3 Partial Least Squares.

1. Standardize each \mathbf{x}_j to have mean zero and variance one. Set $\hat{\mathbf{y}}^{(0)} = \bar{y}\mathbf{1}$, and $\mathbf{x}_j^{(0)} = \mathbf{x}_j$, $j = 1, \dots, p$.
2. For $m = 1, 2, \dots, p$
 - (a) $\mathbf{z}_m = \sum_{j=1}^p \hat{\varphi}_{mj} \mathbf{x}_j^{(m-1)}$, where $\hat{\varphi}_{mj} = \langle \mathbf{x}_j^{(m-1)}, \mathbf{y} \rangle$.
 - (b) $\hat{\theta}_m = \langle \mathbf{z}_m, \mathbf{y} \rangle / \langle \mathbf{z}_m, \mathbf{z}_m \rangle$.
 - (c) $\hat{\mathbf{y}}^{(m)} = \hat{\mathbf{y}}^{(m-1)} + \hat{\theta}_m \mathbf{z}_m$.
 - (d) Orthogonalize each $\mathbf{x}_j^{(m-1)}$ with respect to \mathbf{z}_m : $\mathbf{x}_j^{(m)} = \mathbf{x}_j^{(m-1)} - [\langle \mathbf{z}_m, \mathbf{x}_j^{(m-1)} \rangle / \langle \mathbf{z}_m, \mathbf{z}_m \rangle] \mathbf{z}_m$, $j = 1, 2, \dots, p$.
3. Output the sequence of fitted vectors $\{\hat{\mathbf{y}}^{(m)}\}_1^p$. Since the $\{\mathbf{z}_\ell\}_1^m$ are linear in the original \mathbf{x}_j , so is $\hat{\mathbf{y}}^{(m)} = \mathbf{X}\hat{\beta}^{pls}(m)$. These linear coefficients can be recovered from the sequence of PLS transformations.

In the prostate cancer example, cross-validation chose $M = 2$ PLS directions in Figure 3.7. This produced the model given in the rightmost column of Table 3.3.

What optimization problem is partial least squares solving? Since it uses the response \mathbf{y} to construct its directions, its solution path is a nonlinear function of \mathbf{y} . It can be shown (Exercise 3.15) that partial least squares seeks directions that have high variance *and* have high correlation with the response, in contrast to principal components regression which keys only on high variance (Stone and Brooks, 1990; Frank and Friedman, 1993). In particular, the m th principal component direction v_m solves:

$$\begin{aligned} & \max_{\alpha} \text{Var}(\mathbf{X}\alpha) \\ & \text{subject to } \|\alpha\| = 1, \alpha^T \mathbf{S}v_\ell = 0, \ell = 1, \dots, m-1, \end{aligned} \tag{3.63}$$

where \mathbf{S} is the sample covariance matrix of the \mathbf{x}_j . The conditions $\alpha^T \mathbf{S}v_\ell = 0$ ensures that $\mathbf{z}_m = \mathbf{X}\alpha$ is uncorrelated with all the previous linear combinations $\mathbf{z}_\ell = \mathbf{X}v_\ell$. The m th PLS direction $\hat{\varphi}_m$ solves:

$$\begin{aligned} & \max_{\alpha} \text{Corr}^2(\mathbf{y}, \mathbf{X}\alpha) \text{Var}(\mathbf{X}\alpha) \\ & \text{subject to } \|\alpha\| = 1, \alpha^T \mathbf{S}\hat{\varphi}_\ell = 0, \ell = 1, \dots, m-1. \end{aligned} \tag{3.64}$$

Further analysis reveals that the variance aspect tends to dominate, and so partial least squares behaves much like ridge regression and principal components regression. We discuss this further in the next section.

If the input matrix \mathbf{X} is orthogonal, then partial least squares finds the least squares estimates after $m = 1$ steps. Subsequent steps have no effect

since the $\hat{\varphi}_{mj}$ are zero for $m > 1$ (Exercise 3.14). It can also be shown that the sequence of PLS coefficients for $m = 1, 2, \dots, p$ represents the conjugate gradient sequence for computing the least squares solutions (Exercise 3.18).

3.6 Discussion: A Comparison of the Selection and Shrinkage Methods

There are some simple settings where we can understand better the relationship between the different methods described above. Consider an example with two correlated inputs X_1 and X_2 , with correlation ρ . We assume that the true regression coefficients are $\beta_1 = 4$ and $\beta_2 = 2$. Figure 3.18 shows the coefficient profiles for the different methods, as their tuning parameters are varied. The top panel has $\rho = 0.5$, the bottom panel $\rho = -0.5$. The tuning parameters for ridge and lasso vary over a continuous range, while best subset, PLS and PCR take just two discrete steps to the least squares solution. In the top panel, starting at the origin, ridge regression shrinks the coefficients together until it finally converges to least squares. PLS and PCR show similar behavior to ridge, although are discrete and more extreme. Best subset overshoots the solution and then backtracks. The behavior of the lasso is intermediate to the other methods. When the correlation is negative (lower panel), again PLS and PCR roughly track the ridge path, while all of the methods are more similar to one another.

It is interesting to compare the shrinkage behavior of these different methods. Recall that ridge regression shrinks all directions, but shrinks low-variance directions more. Principal components regression leaves M high-variance directions alone, and discards the rest. Interestingly, it can be shown that partial least squares also tends to shrink the low-variance directions, but can actually inflate some of the higher variance directions. This can make PLS a little unstable, and cause it to have slightly higher prediction error compared to ridge regression. A full study is given in Frank and Friedman (1993). These authors conclude that for minimizing prediction error, ridge regression is generally preferable to variable subset selection, principal components regression and partial least squares. However the improvement over the latter two methods was only slight.

To summarize, PLS, PCR and ridge regression tend to behave similarly. Ridge regression may be preferred because it shrinks smoothly, rather than in discrete steps. Lasso falls somewhere between ridge regression and best subset regression, and enjoys some of the properties of each.

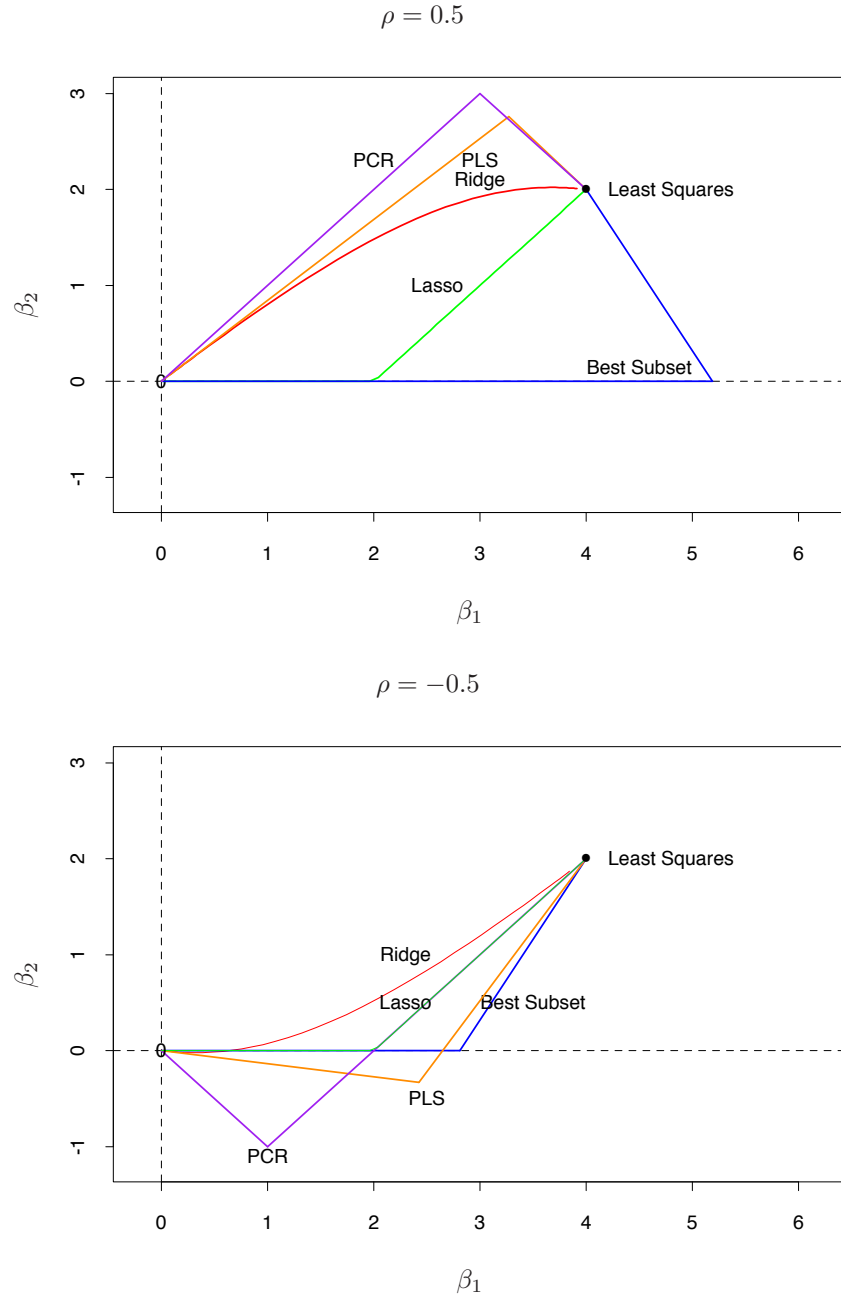


FIGURE 3.18. Coefficient profiles from different methods for a simple problem: two inputs with correlation ± 0.5 , and the true regression coefficients $\beta = (4, 2)$.

3.7 Multiple Outcome Shrinkage and Selection



As noted in Section 3.2.4, the least squares estimates in a multiple-output linear model are simply the individual least squares estimates for each of the outputs.

To apply selection and shrinkage methods in the multiple output case, one could apply a univariate technique individually to each outcome or simultaneously to all outcomes. With ridge regression, for example, we could apply formula (3.44) to each of the K columns of the outcome matrix \mathbf{Y} , using possibly different parameters λ , or apply it to all columns using the same value of λ . The former strategy would allow different amounts of regularization to be applied to different outcomes but require estimation of k separate regularization parameters $\lambda_1, \dots, \lambda_k$, while the latter would permit all k outputs to be used in estimating the sole regularization parameter λ .

Other more sophisticated shrinkage and selection strategies that exploit correlations in the different responses can be helpful in the multiple output case. Suppose for example that among the outputs we have

$$Y_k = f(X) + \varepsilon_k \quad (3.65)$$

$$Y_\ell = f(X) + \varepsilon_\ell; \quad (3.66)$$

i.e., (3.65) and (3.66) share the same structural part $f(X)$ in their models. It is clear in this case that we should pool our observations on Y_k and Y_ℓ to estimate the common f .

Combining responses is at the heart of *canonical correlation analysis* (CCA), a data reduction technique developed for the multiple output case. Similar to PCA, CCA finds a sequence of uncorrelated linear combinations $\mathbf{X}v_m$, $m = 1, \dots, M$ of the \mathbf{x}_j , and a corresponding sequence of uncorrelated linear combinations $\mathbf{Y}u_m$ of the responses \mathbf{y}_k , such that the correlations

$$\text{Corr}^2(\mathbf{Y}u_m, \mathbf{X}v_m) \quad (3.67)$$

are successively maximized. Note that at most $M = \min(K, p)$ directions can be found. The leading canonical response variates are those linear combinations (derived responses) best predicted by the \mathbf{x}_j ; in contrast, the trailing canonical variates can be poorly predicted by the \mathbf{x}_j , and are candidates for being dropped. The CCA solution is computed using a generalized SVD of the sample cross-covariance matrix $\mathbf{Y}^T\mathbf{X}/N$ (assuming \mathbf{Y} and \mathbf{X} are centered; Exercise 3.20).

Reduced-rank regression (Izenman, 1975; van der Merwe and Zidek, 1980) formalizes this approach in terms of a regression model that explicitly pools information. Given an error covariance $\text{Cov}(\varepsilon) = \boldsymbol{\Sigma}$, we solve the following

restricted multivariate regression problem:

$$\hat{\mathbf{B}}^{\text{rr}}(m) = \underset{\text{rank}(\mathbf{B})=m}{\operatorname{argmin}} \sum_{i=1}^N (y_i - \mathbf{B}^T x_i)^T \boldsymbol{\Sigma}^{-1} (y_i - \mathbf{B}^T x_i). \quad (3.68)$$

With $\boldsymbol{\Sigma}$ replaced by the estimate $\mathbf{Y}^T \mathbf{Y}/N$, one can show (Exercise 3.21) that the solution is given by a CCA of \mathbf{Y} and \mathbf{X} :

$$\hat{\mathbf{B}}^{\text{rr}}(m) = \hat{\mathbf{B}} \mathbf{U}_m \mathbf{U}_m^-, \quad (3.69)$$

where \mathbf{U}_m is the $K \times m$ sub-matrix of \mathbf{U} consisting of the first m columns, and \mathbf{U} is the $K \times M$ matrix of *left* canonical vectors u_1, u_2, \dots, u_M . \mathbf{U}_m^- is its generalized inverse. Writing the solution as

$$\hat{\mathbf{B}}^{\text{rr}}(M) = (\mathbf{X}^T \mathbf{X})^{-1} \mathbf{X}^T (\mathbf{Y} \mathbf{U}_m) \mathbf{U}_m^-, \quad (3.70)$$

we see that reduced-rank regression performs a linear regression on the pooled response matrix $\mathbf{Y} \mathbf{U}_m$, and then maps the coefficients (and hence the fits as well) back to the original response space. The reduced-rank fits are given by

$$\begin{aligned} \hat{\mathbf{Y}}^{\text{rr}}(m) &= \mathbf{X} (\mathbf{X}^T \mathbf{X})^{-1} \mathbf{X}^T \mathbf{Y} \mathbf{U}_m \mathbf{U}_m^- \\ &= \mathbf{H} \mathbf{Y} \mathbf{P}_m, \end{aligned} \quad (3.71)$$

where \mathbf{H} is the usual linear regression projection operator, and \mathbf{P}_m is the rank- m CCA response projection operator. Although a better estimate of $\boldsymbol{\Sigma}$ would be $(\mathbf{Y} - \mathbf{X} \hat{\mathbf{B}})^T (\mathbf{Y} - \mathbf{X} \hat{\mathbf{B}})/(N-pK)$, one can show that the solution remains the same (Exercise 3.22).

Reduced-rank regression borrows strength among responses by truncating the CCA. Breiman and Friedman (1997) explored with some success shrinkage of the canonical variates between \mathbf{X} and \mathbf{Y} , a smooth version of *reduced rank* regression. Their proposal has the form (compare (3.69))

$$\hat{\mathbf{B}}^{\text{c+w}} = \hat{\mathbf{B}} \mathbf{U} \boldsymbol{\Lambda} \mathbf{U}^{-1}, \quad (3.72)$$

where $\boldsymbol{\Lambda}$ is a diagonal shrinkage matrix (the “c+w” stands for “Curds and Whey,” the name they gave to their procedure). Based on optimal prediction in the population setting, they show that $\boldsymbol{\Lambda}$ has diagonal entries

$$\lambda_m = \frac{c_m^2}{c_m^2 + \frac{p}{N}(1-c_m^2)}, \quad m = 1, \dots, M, \quad (3.73)$$

where c_m is the m th canonical correlation coefficient. Note that as the ratio of the number of input variables to sample size p/N gets small, the shrinkage factors approach 1. Breiman and Friedman (1997) proposed modified versions of $\boldsymbol{\Lambda}$ based on training data and cross-validation, but the general form is the same. Here the fitted response has the form

$$\hat{\mathbf{Y}}^{\text{c+w}} = \mathbf{H} \mathbf{Y} \mathbf{S}^{\text{c+w}}, \quad (3.74)$$

where $\mathbf{S}^{c+w} = \mathbf{U}\Lambda\mathbf{U}^{-1}$ is the response shrinkage operator.

Breiman and Friedman (1997) also suggested shrinking in both the Y space and X space. This leads to hybrid shrinkage models of the form

$$\hat{\mathbf{Y}}^{\text{ridge},c+w} = \mathbf{A}_\lambda \mathbf{Y} \mathbf{S}^{c+w}, \quad (3.75)$$

where $\mathbf{A}_\lambda = \mathbf{X}(\mathbf{X}^T \mathbf{X} + \lambda \mathbf{I})^{-1} \mathbf{X}^T$ is the ridge regression shrinkage operator, as in (3.46) on page 66. Their paper and the discussions thereof contain many more details.

3.8 More on the Lasso and Related Path Algorithms

Since the publication of the LAR algorithm (Efron et al., 2004) there has been a lot of activity in developing algorithms for fitting regularization paths for a variety of different problems. In addition, L_1 regularization has taken on a life of its own, leading to the development of the field *compressed sensing* in the signal-processing literature. (Donoho, 2006a; Candes, 2006). In this section we discuss some related proposals and other path algorithms, starting off with a precursor to the LAR algorithm.

3.8.1 Incremental Forward Stagewise Regression

Here we present another LAR-like algorithm, this time focused on forward stagewise regression. Interestingly, efforts to understand a flexible nonlinear regression procedure (boosting) led to a new algorithm for linear models (LAR). In reading the first edition of this book and the forward stagewise

Algorithm 3.4 Incremental Forward Stagewise Regression— FS_ϵ .

1. Start with the residual \mathbf{r} equal to \mathbf{y} and $\beta_1, \beta_2, \dots, \beta_p = 0$. All the predictors are standardized to have mean zero and unit norm.
 2. Find the predictor \mathbf{x}_j most correlated with \mathbf{r}
 3. Update $\beta_j \leftarrow \beta_j + \delta_j$, where $\delta_j = \epsilon \cdot \text{sign}[\langle \mathbf{x}_j, \mathbf{r} \rangle]$ and $\epsilon > 0$ is a small step size, and set $\mathbf{r} \leftarrow \mathbf{r} - \delta_j \mathbf{x}_j$.
 4. Repeat steps 2 and 3 many times, until the residuals are uncorrelated with all the predictors.
-

Algorithm 16.1 of Chapter 16⁴, our colleague Brad Efron realized that with

⁴In the first edition, this was Algorithm 10.4 in Chapter 10.

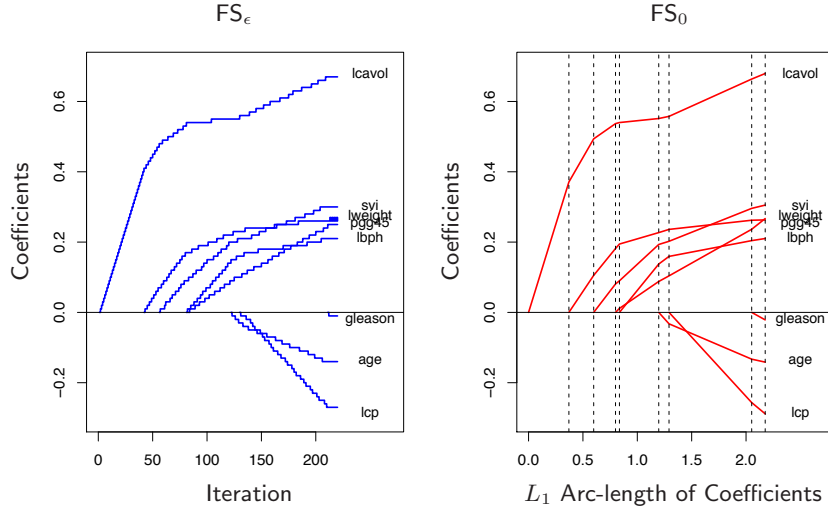


FIGURE 3.19. Coefficient profiles for the prostate data. The left panel shows incremental forward stagewise regression with step size $\epsilon = 0.01$. The right panel shows the infinitesimal version FS_0 obtained letting $\epsilon \rightarrow 0$. This profile was fit by the modification 3.2b to the LAR Algorithm 3.2. In this example the FS_0 profiles are monotone, and hence identical to those of lasso and LAR.

linear models, one could explicitly construct the piecewise-linear lasso paths of Figure 3.10. This led him to propose the LAR procedure of Section 3.4.4, as well as the incremental version of forward-stagewise regression presented here.

Consider the linear-regression version of the forward-stagewise boosting algorithm 16.1 proposed in Section 16.1 (page 608). It generates a coefficient profile by repeatedly updating (by a small amount ϵ) the coefficient of the variable most correlated with the current residuals. Algorithm 3.4 gives the details. Figure 3.19 (left panel) shows the progress of the algorithm on the prostate data with step size $\epsilon = 0.01$. If $\delta_j = \langle \mathbf{x}_j, \mathbf{r} \rangle$ (the least-squares coefficient of the residual on j th predictor), then this is exactly the usual forward stagewise procedure (FS) outlined in Section 3.3.3.

Here we are mainly interested in small values of ϵ . Letting $\epsilon \rightarrow 0$ gives the right panel of Figure 3.19, which in this case is identical to the lasso path in Figure 3.10. We call this limiting procedure *infinitesimal forward stagewise regression* or FS_0 . This procedure plays an important role in non-linear, adaptive methods like boosting (Chapters 10 and 16) and is the version of incremental forward stagewise regression that is most amenable to theoretical analysis. Bühlmann and Hothorn (2007) refer to the same procedure as “L2boost”, because of its connections to boosting.

Efron originally thought that the LAR Algorithm 3.2 was an implementation of FS_0 , allowing each tied predictor a chance to update their coefficients in a balanced way, while remaining tied in correlation. However, he then realized that the LAR least-squares fit amongst the tied predictors can result in coefficients moving in the *opposite* direction to their correlation, which cannot happen in Algorithm 3.4. The following modification of the LAR algorithm implements FS_0 :

Algorithm 3.2b Least Angle Regression: FS_0 Modification.

4. Find the new direction by solving the constrained least squares problem

$$\min_b \|\mathbf{r} - \mathbf{X}_{\mathcal{A}} b\|_2^2 \text{ subject to } b_j s_j \geq 0, j \in \mathcal{A},$$

where s_j is the sign of $\langle \mathbf{x}_j, \mathbf{r} \rangle$.

The modification amounts to a non-negative least squares fit, keeping the signs of the coefficients the same as those of the correlations. One can show that this achieves the optimal balancing of infinitesimal “update turns” for the variables tied for maximal correlation (Hastie et al., 2007). Like lasso, the entire FS_0 path can be computed very efficiently via the LAR algorithm.

As a consequence of these results, if the LAR profiles are monotone non-increasing or non-decreasing, as they are in Figure 3.19, then all three methods—LAR, lasso, and FS_0 —give identical profiles. If the profiles are not monotone but do not cross the zero axis, then LAR and lasso are identical.

Since FS_0 is different from the lasso, it is natural to ask if it optimizes a criterion. The answer is more complex than for lasso; the FS_0 coefficient profile is the solution to a differential equation. While the lasso makes optimal progress in terms of reducing the residual sum-of-squares per unit increase in L_1 -norm of the coefficient vector β , FS_0 is optimal per unit increase in L_1 arc-length traveled along the coefficient path. Hence its coefficient path is discouraged from changing directions too often.

FS_0 is more constrained than lasso, and in fact can be viewed as a monotone version of the lasso; see Figure 16.3 on page 614 for a dramatic example. FS_0 may be useful in $p \gg N$ situations, where its coefficient profiles are much smoother and hence have less variance than those of lasso. More details on FS_0 are given in Section 16.2.3 and Hastie et al. (2007). Figure 3.16 includes FS_0 where its performance is very similar to that of the lasso.

3.8.2 Piecewise-Linear Path Algorithms

The least angle regression procedure exploits the piecewise linear nature of the lasso solution paths. It has led to similar “path algorithms” for other regularized problems. Suppose we solve

$$\hat{\beta}(\lambda) = \operatorname{argmin}_{\beta} [R(\beta) + \lambda J(\beta)], \quad (3.76)$$

with

$$R(\beta) = \sum_{i=1}^N L(y_i, \beta_0 + \sum_{j=1}^p x_{ij}\beta_j), \quad (3.77)$$

where both the loss function L and the penalty function J are convex. Then the following are sufficient conditions for the solution path $\hat{\beta}(\lambda)$ to be piecewise linear (Rosset and Zhu, 2007):

1. R is quadratic or piecewise-quadratic as a function of β , and
2. J is piecewise linear in β .

This also implies (in principle) that the solution path can be efficiently computed. Examples include squared- and absolute-error loss, “Huberized” losses, and the L_1, L_∞ penalties on β . Another example is the “hinge loss” function used in the support vector machine. There the loss is piecewise linear, and the penalty is quadratic. Interestingly, this leads to a piecewise-linear path algorithm in the *dual space*; more details are given in Section 12.3.5.

3.8.3 The Dantzig Selector

Candes and Tao (2007) proposed the following criterion:

$$\min_{\beta} \|\beta\|_1 \text{ subject to } \|\mathbf{X}^T(\mathbf{y} - \mathbf{X}\beta)\|_\infty \leq s. \quad (3.78)$$

They call the solution the *Dantzig selector* (DS). It can be written equivalently as

$$\min_{\beta} \|\mathbf{X}^T(\mathbf{y} - \mathbf{X}\beta)\|_\infty \text{ subject to } \|\beta\|_1 \leq t. \quad (3.79)$$

Here $\|\cdot\|_\infty$ denotes the L_∞ norm, the maximum absolute value of the components of the vector. In this form it resembles the lasso, replacing squared error loss by the maximum absolute value of its gradient. Note that as t gets large, both procedures yield the least squares solution if $N < p$. If $p \geq N$, they both yield the least squares solution with minimum L_1 norm. However for smaller values of t , the DS procedure produces a different path of solutions than the lasso.

Candes and Tao (2007) show that the solution to DS is a linear programming problem; hence the name Dantzig selector, in honor of the late

George Dantzig, the inventor of the simplex method for linear programming. They also prove a number of interesting mathematical properties for the method, related to its ability to recover an underlying sparse coefficient vector. These same properties also hold for the lasso, as shown later by Bickel et al. (2008).

Unfortunately the operating properties of the DS method are somewhat unsatisfactory. The method seems similar in spirit to the lasso, especially when we look at the lasso's stationary conditions (3.58). Like the LAR algorithm, the lasso maintains the same inner product (and correlation) with the current residual for all variables in the active set, and moves their coefficients to optimally decrease the residual sum of squares. In the process, this common correlation is decreased monotonically (Exercise 3.23), and at all times this correlation is larger than that for non-active variables. The Dantzig selector instead tries to minimize the maximum inner product of the current residual with all the predictors. Hence it can achieve a smaller maximum than the lasso, but in the process a curious phenomenon can occur. If the size of the active set is m , there will be m variables tied with maximum correlation. However, these need not coincide with the active set! Hence it can include a variable in the model that has smaller correlation with the current residual than some of the excluded variables (Efron et al., 2007). This seems unreasonable and may be responsible for its sometimes inferior prediction accuracy. Efron et al. (2007) also show that DS can yield extremely erratic coefficient paths as the regularization parameter s is varied.

3.8.4 The Grouped Lasso

In some problems, the predictors belong to pre-defined groups; for example genes that belong to the same biological pathway, or collections of indicator (dummy) variables for representing the levels of a categorical predictor. In this situation it may be desirable to shrink and select the members of a group together. The *grouped lasso* is one way to achieve this. Suppose that the p predictors are divided into L groups, with p_ℓ the number in group ℓ . For ease of notation, we use a matrix \mathbf{X}_ℓ to represent the predictors corresponding to the ℓ th group, with corresponding coefficient vector β_ℓ . The grouped-lasso minimizes the convex criterion

$$\min_{\beta \in \mathbb{R}^p} \left(\|\mathbf{y} - \beta_0 \mathbf{1} - \sum_{\ell=1}^L \mathbf{X}_\ell \beta_\ell\|_2^2 + \lambda \sum_{\ell=1}^L \sqrt{p_\ell} \|\beta_\ell\|_2 \right), \quad (3.80)$$

where the $\sqrt{p_\ell}$ terms accounts for the varying group sizes, and $\|\cdot\|_2$ is the Euclidean norm (not squared). Since the Euclidean norm of a vector β_ℓ is zero only if all of its components are zero, this procedure encourages sparsity at both the group and individual levels. That is, for some values of λ , an entire group of predictors may drop out of the model. This procedure

was proposed by Bakin (1999) and Lin and Zhang (2006), and studied and generalized by Yuan and Lin (2007). Generalizations include more general L_2 norms $\|\eta\|_K = (\eta^T K \eta)^{1/2}$, as well as allowing overlapping groups of predictors (Zhao et al., 2008). There are also connections to methods for fitting sparse additive models (Lin and Zhang, 2006; Ravikumar et al., 2008).

3.8.5 Further Properties of the Lasso

A number of authors have studied the ability of the lasso and related procedures to recover the correct model, as N and p grow. Examples of this work include Knight and Fu (2000), Greenshtein and Ritov (2004), Tropp (2004), Donoho (2006b), Meinshausen (2007), Meinshausen and Bühlmann (2006), Tropp (2006), Zhao and Yu (2006), Wainwright (2006), and Bunea et al. (2007). For example Donoho (2006b) focuses on the $p > N$ case and considers the lasso solution as the bound t gets large. In the limit this gives the solution with minimum L_1 norm among all models with zero training error. He shows that under certain assumptions on the model matrix \mathbf{X} , if the true model is sparse, this solution identifies the correct predictors with high probability.

Many of the results in this area assume a condition on the model matrix of the form

$$\max_{j \in \mathcal{S}^c} \|\mathbf{x}_j^T \mathbf{X}_{\mathcal{S}} (\mathbf{X}_{\mathcal{S}}^T \mathbf{X}_{\mathcal{S}})^{-1}\|_1 \leq (1 - \epsilon) \text{ for some } \epsilon \in (0, 1]. \quad (3.81)$$

Here \mathcal{S} indexes the subset of features with non-zero coefficients in the true underlying model, and $\mathbf{X}_{\mathcal{S}}$ are the columns of \mathbf{X} corresponding to those features. Similarly \mathcal{S}^c are the features with true coefficients equal to zero, and $\mathbf{X}_{\mathcal{S}^c}$ the corresponding columns. This says that the least squares coefficients for the columns of $\mathbf{X}_{\mathcal{S}^c}$ on $\mathbf{X}_{\mathcal{S}}$ are not too large, that is, the “good” variables \mathcal{S} are not too highly correlated with the nuisance variables \mathcal{S}^c .

Regarding the coefficients themselves, the lasso shrinkage causes the estimates of the non-zero coefficients to be biased towards zero, and in general they are not consistent⁵. One approach for reducing this bias is to run the lasso to identify the set of non-zero coefficients, and then fit an unrestricted linear model to the selected set of features. This is not always feasible, if the selected set is large. Alternatively, one can use the lasso to select the set of non-zero predictors, and then apply the lasso again, but using only the selected predictors from the first step. This is known as the *relaxed lasso* (Meinshausen, 2007). The idea is to use cross-validation to estimate the initial penalty parameter for the lasso, and then again for a second penalty parameter applied to the selected set of predictors. Since

⁵Statistical consistency means as the sample size grows, the estimates converge to the true values.

the variables in the second step have less ‘‘competition’’ from noise variables, cross-validation will tend to pick a smaller value for λ , and hence their coefficients will be shrunk less than those in the initial estimate.

Alternatively, one can modify the lasso penalty function so that larger coefficients are shrunk less severely; the *smoothly clipped absolute deviation* (SCAD) penalty of Fan and Li (2005) replaces $\lambda|\beta|$ by $J_a(\beta, \lambda)$, where

$$\frac{dJ_a(\beta, \lambda)}{d\beta} = \lambda \cdot \text{sign}(\beta) \left[I(|\beta| \leq \lambda) + \frac{(a\lambda - |\beta|)_+}{(a-1)\lambda} I(|\beta| > \lambda) \right] \quad (3.82)$$

for some $a \geq 2$. The second term in square-braces reduces the amount of shrinkage in the lasso for larger values of β , with ultimately no shrinkage as $a \rightarrow \infty$. Figure 3.20 shows the SCAD penalty, along with the lasso and

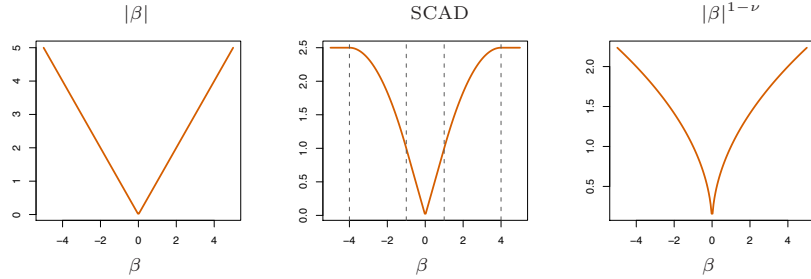


FIGURE 3.20. The lasso and two alternative non-convex penalties designed to penalize large coefficients less. For SCAD we use $\lambda = 1$ and $a = 4$, and $\nu = \frac{1}{2}$ in the last panel.

$|\beta|^{1-\nu}$. However this criterion is non-convex, which is a drawback since it makes the computation much more difficult. The *adaptive lasso* (Zou, 2006) uses a weighted penalty of the form $\sum_{j=1}^p w_j |\beta_j|$ where $w_j = 1/|\hat{\beta}_j|^\nu$, $\hat{\beta}_j$ is the ordinary least squares estimate and $\nu > 0$. This is a practical approximation to the $|\beta|^q$ penalties ($q = 1 - \nu$ here) discussed in Section 3.4.3. The adaptive lasso yields consistent estimates of the parameters while retaining the attractive convexity property of the lasso.

3.8.6 Pathwise Coordinate Optimization

An alternate approach to the LARS algorithm for computing the lasso solution is simple coordinate descent. This idea was proposed by Fu (1998) and Daubechies et al. (2004), and later studied and generalized by Friedman et al. (2007), Wu and Lange (2008) and others. The idea is to fix the penalty parameter λ in the Lagrangian form (3.52) and optimize successively over each parameter, holding the other parameters fixed at their current values.

Suppose the predictors are all standardized to have mean zero and unit norm. Denote by $\hat{\beta}_k(\lambda)$ the current estimate for β_k at penalty parameter

λ . We can rearrange (3.52) to isolate β_j ,

$$R(\tilde{\beta}(\lambda), \beta_j) = \frac{1}{2} \sum_{i=1}^N \left(y_i - \sum_{k \neq j} x_{ik} \tilde{\beta}_k(\lambda) - x_{ij} \beta_j \right)^2 + \lambda \sum_{k \neq j} |\tilde{\beta}_k(\lambda)| + \lambda |\beta_j|, \quad (3.83)$$

where we have suppressed the intercept and introduced a factor $\frac{1}{2}$ for convenience. This can be viewed as a univariate lasso problem with response variable the partial residual $y_i - \tilde{y}_i^{(j)} = y_i - \sum_{k \neq j} x_{ik} \tilde{\beta}_k(\lambda)$. This has an explicit solution, resulting in the update

$$\tilde{\beta}_j(\lambda) \leftarrow S \left(\sum_{i=1}^N x_{ij} (y_i - \tilde{y}_i^{(j)}), \lambda \right). \quad (3.84)$$

Here $S(t, \lambda) = \text{sign}(t)(|t| - \lambda)_+$ is the soft-thresholding operator in Table 3.4 on page 71. The first argument to $S(\cdot)$ is the simple least-squares coefficient of the partial residual on the standardized variable x_{ij} . Repeated iteration of (3.84)—cycling through each variable in turn until convergence—yields the lasso estimate $\hat{\beta}(\lambda)$.

We can also use this simple algorithm to efficiently compute the lasso solutions at a grid of values of λ . We start with the smallest value λ_{\max} for which $\hat{\beta}(\lambda_{\max}) = 0$, decrease it a little and cycle through the variables until convergence. Then λ is decreased again and the process is repeated, using the previous solution as a “warm start” for the new value of λ . This can be faster than the LARS algorithm, especially in large problems. A key to its speed is the fact that the quantities in (3.84) can be updated quickly as j varies, and often the update is to leave $\tilde{\beta}_j = 0$. On the other hand, it delivers solutions over a grid of λ values, rather than the entire solution path. The same kind of algorithm can be applied to the elastic net, the grouped lasso and many other models in which the penalty is a sum of functions of the individual parameters (Friedman et al., 2010). It can also be applied, with some substantial modifications, to the fused lasso (Section 18.4.2); details are in Friedman et al. (2007).

3.9 Computational Considerations

Least squares fitting is usually done via the Cholesky decomposition of the matrix $\mathbf{X}^T \mathbf{X}$ or a QR decomposition of \mathbf{X} . With N observations and p features, the Cholesky decomposition requires $p^3 + Np^2/2$ operations, while the QR decomposition requires Np^2 operations. Depending on the relative size of N and p , the Cholesky can sometimes be faster; on the other hand, it can be less numerically stable (Lawson and Hansen, 1974). Computation of the lasso via the LAR algorithm has the same order of computation as a least squares fit.

Bibliographic Notes

Linear regression is discussed in many statistics books, for example, Seber (1984), Weisberg (1980) and Mardia et al. (1979). Ridge regression was introduced by Hoerl and Kennard (1970), while the lasso was proposed by Tibshirani (1996). Around the same time, lasso-type penalties were proposed in the *basis pursuit* method for signal processing (Chen et al., 1998). The least angle regression procedure was proposed in Efron et al. (2004); related to this is the earlier homotopy procedure of Osborne et al. (2000a) and Osborne et al. (2000b). Their algorithm also exploits the piecewise linearity used in the LAR/lasso algorithm, but lacks its transparency. The criterion for the forward stagewise criterion is discussed in Hastie et al. (2007). Park and Hastie (2007) develop a path algorithm similar to least angle regression for generalized regression models. Partial least squares was introduced by Wold (1975). Comparisons of shrinkage methods may be found in Copas (1983) and Frank and Friedman (1993).

Exercises

Ex. 3.1 Show that the F statistic (3.13) for dropping a single coefficient from a model is equal to the square of the corresponding z -score (3.12).

Ex. 3.2 Given data on two variables X and Y , consider fitting a cubic polynomial regression model $f(X) = \sum_{j=0}^3 \beta_j X^j$. In addition to plotting the fitted curve, you would like a 95% confidence band about the curve. Consider the following two approaches:

1. At each point x_0 , form a 95% confidence interval for the linear function $a^T \beta = \sum_{j=0}^3 \beta_j x_0^j$.
2. Form a 95% confidence set for β as in (3.15), which in turn generates confidence intervals for $f(x_0)$.

How do these approaches differ? Which band is likely to be wider? Conduct a small simulation experiment to compare the two methods.

Ex. 3.3 Gauss–Markov theorem:

- (a) Prove the Gauss–Markov theorem: the least squares estimate of a parameter $a^T \beta$ has variance no bigger than that of any other linear unbiased estimate of $a^T \beta$ (Section 3.2.2).
- (b) The matrix inequality $\mathbf{B} \preceq \mathbf{A}$ holds if $\mathbf{A} - \mathbf{B}$ is positive semidefinite. Show that if $\hat{\mathbf{V}}$ is the variance-covariance matrix of the least squares estimate of β and $\tilde{\mathbf{V}}$ is the variance-covariance matrix of any other linear unbiased estimate, then $\hat{\mathbf{V}} \preceq \tilde{\mathbf{V}}$.

Ex. 3.4 Show how the vector of least squares coefficients can be obtained from a single pass of the Gram–Schmidt procedure (Algorithm 3.1). Represent your solution in terms of the QR decomposition of \mathbf{X} .

Ex. 3.5 Consider the ridge regression problem (3.41). Show that this problem is equivalent to the problem

$$\hat{\beta}^c = \underset{\beta^c}{\operatorname{argmin}} \left\{ \sum_{i=1}^N [y_i - \beta_0^c - \sum_{j=1}^p (x_{ij} - \bar{x}_j) \beta_j^c]^2 + \lambda \sum_{j=1}^p \beta_j^{c2} \right\}. \quad (3.85)$$

Give the correspondence between β^c and the original β in (3.41). Characterize the solution to this modified criterion. Show that a similar result holds for the lasso.

Ex. 3.6 Show that the ridge regression estimate is the mean (and mode) of the posterior distribution, under a Gaussian prior $\beta \sim N(0, \tau \mathbf{I})$, and Gaussian sampling model $\mathbf{y} \sim N(\mathbf{X}\beta, \sigma^2 \mathbf{I})$. Find the relationship between the regularization parameter λ in the ridge formula, and the variances τ and σ^2 .

Ex. 3.7 Assume $y_i \sim N(\beta_0 + x_i^T \beta, \sigma^2)$, $i = 1, 2, \dots, N$, and the parameters β_j , $j = 1, \dots, p$ are each distributed as $N(0, \tau^2)$, independently of one another. Assuming σ^2 and τ^2 are known, and β_0 is not governed by a prior (or has a flat improper prior), show that the (minus) log-posterior density of β is proportional to $\sum_{i=1}^N (y_i - \beta_0 - \sum_j x_{ij} \beta_j)^2 + \lambda \sum_{j=1}^p \beta_j^2$ where $\lambda = \sigma^2 / \tau^2$.

Ex. 3.8 Consider the QR decomposition of the uncentered $N \times (p+1)$ matrix \mathbf{X} (whose first column is all ones), and the SVD of the $N \times p$ centered matrix $\tilde{\mathbf{X}}$. Show that \mathbf{Q}_2 and \mathbf{U} span the same subspace, where \mathbf{Q}_2 is the sub-matrix of \mathbf{Q} with the first column removed. Under what circumstances will they be the same, up to sign flips?

Ex. 3.9 *Forward stepwise regression.* Suppose we have the QR decomposition for the $N \times q$ matrix \mathbf{X}_1 in a multiple regression problem with response \mathbf{y} , and we have an additional $p-q$ predictors in the matrix \mathbf{X}_2 . Denote the current residual by \mathbf{r} . We wish to establish which one of these additional variables will reduce the residual-sum-of-squares the most when included with those in \mathbf{X}_1 . Describe an efficient procedure for doing this.

Ex. 3.10 *Backward stepwise regression.* Suppose we have the multiple regression fit of \mathbf{y} on \mathbf{X} , along with the standard errors and Z-scores as in Table 3.2. We wish to establish which variable, when dropped, will increase the residual sum-of-squares the least. How would you do this?

Ex. 3.11 Show that the solution to the multivariate linear regression problem (3.40) is given by (3.39). What happens if the covariance matrices Σ_i are different for each observation?

Ex. 3.12 Show that the ridge regression estimates can be obtained by ordinary least squares regression on an augmented data set. We augment the centered matrix \mathbf{X} with p additional rows $\sqrt{\lambda}\mathbf{I}$, and augment \mathbf{y} with p zeros. By introducing artificial data having response value zero, the fitting procedure is forced to shrink the coefficients toward zero. This is related to the idea of *hints* due to Abu-Mostafa (1995), where model constraints are implemented by adding artificial data examples that satisfy them.

Ex. 3.13 Derive the expression (3.62), and show that $\hat{\beta}^{\text{pcr}}(p) = \hat{\beta}^{\text{ls}}$.

Ex. 3.14 Show that in the orthogonal case, PLS stops after $m = 1$ steps, because subsequent $\hat{\varphi}_{mj}$ in step 2 in Algorithm 3.3 are zero.

Ex. 3.15 Verify expression (3.64), and hence show that the partial least squares directions are a compromise between the ordinary regression coefficient and the principal component directions.

Ex. 3.16 Derive the entries in Table 3.4, the explicit forms for estimators in the orthogonal case.

Ex. 3.17 Repeat the analysis of Table 3.3 on the spam data discussed in Chapter 1.

Ex. 3.18 Read about conjugate gradient algorithms (Murray et al., 1981, for example), and establish a connection between these algorithms and partial least squares.

Ex. 3.19 Show that $\|\hat{\beta}^{\text{ridge}}\|$ increases as its tuning parameter $\lambda \rightarrow 0$. Does the same property hold for the lasso and partial least squares estimates? For the latter, consider the “tuning parameter” to be the successive steps in the algorithm.

Ex. 3.20 Consider the canonical-correlation problem (3.67). Show that the leading pair of canonical variates u_1 and v_1 solve the problem

$$\max_{\substack{u^T(\mathbf{Y}^T\mathbf{Y})u=1 \\ v^T(\mathbf{X}^T\mathbf{X})v=1}} u^T(\mathbf{Y}^T\mathbf{X})v, \quad (3.86)$$

a generalized SVD problem. Show that the solution is given by $u_1 = (\mathbf{Y}^T\mathbf{Y})^{-\frac{1}{2}}u_1^*$, and $v_1 = (\mathbf{X}^T\mathbf{X})^{-\frac{1}{2}}v_1^*$, where u_1^* and v_1^* are the leading left and right singular vectors in

$$(\mathbf{Y}^T\mathbf{Y})^{-\frac{1}{2}}(\mathbf{Y}^T\mathbf{X})(\mathbf{X}^T\mathbf{X})^{-\frac{1}{2}} = \mathbf{U}^*\mathbf{D}^*\mathbf{V}^{*T}. \quad (3.87)$$

Show that the entire sequence $u_m, v_m, m = 1, \dots, \min(K, p)$ is also given by (3.87).

Ex. 3.21 Show that the solution to the reduced-rank regression problem (3.68), with Σ estimated by $\mathbf{Y}^T\mathbf{Y}/N$, is given by (3.69). *Hint:* Transform

\mathbf{Y} to $\mathbf{Y}^* = \mathbf{Y}\Sigma^{-\frac{1}{2}}$, and solved in terms of the canonical vectors u_m^* . Show that $\mathbf{U}_m = \Sigma^{-\frac{1}{2}}\mathbf{U}_m^*$, and a generalized inverse is $\mathbf{U}_m^- = \mathbf{U}_m^{*T}\Sigma^{\frac{1}{2}}$.

Ex. 3.22 Show that the solution in Exercise 3.21 does not change if Σ is estimated by the more natural quantity $(\mathbf{Y} - \mathbf{X}\hat{\mathbf{B}})^T(\mathbf{Y} - \mathbf{X}\hat{\mathbf{B}})/(N - pK)$.

Ex. 3.23 Consider a regression problem with all variables and response having mean zero and standard deviation one. Suppose also that each variable has identical absolute correlation with the response:

$$\frac{1}{N}|\langle \mathbf{x}_j, \mathbf{y} \rangle| = \lambda, \quad j = 1, \dots, p.$$

Let $\hat{\beta}$ be the least-squares coefficient of \mathbf{y} on \mathbf{X} , and let $\mathbf{u}(\alpha) = \alpha\mathbf{X}\hat{\beta}$ for $\alpha \in [0, 1]$ be the vector that moves a fraction α toward the least squares fit \mathbf{u} . Let RSS be the residual sum-of-squares from the full least squares fit.

(a) Show that

$$\frac{1}{N}|\langle \mathbf{x}_j, \mathbf{y} - \mathbf{u}(\alpha) \rangle| = (1 - \alpha)\lambda, \quad j = 1, \dots, p,$$

and hence the correlations of each \mathbf{x}_j with the residuals remain equal in magnitude as we progress toward \mathbf{u} .

(b) Show that these correlations are all equal to

$$\lambda(\alpha) = \frac{(1 - \alpha)}{\sqrt{(1 - \alpha)^2 + \frac{\alpha(2 - \alpha)}{N} \cdot RSS}} \cdot \lambda,$$

and hence they decrease monotonically to zero.

(c) Use these results to show that the LAR algorithm in Section 3.4.4 keeps the correlations tied and monotonically decreasing, as claimed in (3.55).

Ex. 3.24 LAR directions. Using the notation around equation (3.55) on page 74, show that the LAR direction makes an equal angle with each of the predictors in \mathcal{A}_k .

Ex. 3.25 LAR look-ahead (Efron et al., 2004, Sec. 2). Starting at the beginning of the k th step of the LAR algorithm, derive expressions to identify the next variable to enter the active set at step $k + 1$, and the value of α at which this occurs (using the notation around equation (3.55) on page 74).

Ex. 3.26 Forward stepwise regression enters the variable at each step that most reduces the residual sum-of-squares. LAR adjusts variables that have the most (absolute) correlation with the current residuals. Show that these two entry criteria are not necessarily the same. [Hint: let $\mathbf{x}_{j,\mathcal{A}}$ be the j th

variable, linearly adjusted for all the variables currently in the model. Show that the first criterion amounts to identifying the j for which $\text{Cor}(\mathbf{x}_{j,\mathcal{A}}, \mathbf{r})$ is largest in magnitude.

Ex. 3.27 Lasso and LAR: Consider the lasso problem in Lagrange multiplier form: with $L(\beta) = \frac{1}{2} \sum_i (y_i - \sum_j x_{ij} \beta_j)^2$, we minimize

$$L(\beta) + \lambda \sum_j |\beta_j| \quad (3.88)$$

for fixed $\lambda > 0$.

- (a) Setting $\beta_j = \beta_j^+ - \beta_j^-$ with $\beta_j^+, \beta_j^- \geq 0$, expression (3.88) becomes $L(\beta) + \lambda \sum_j (\beta_j^+ + \beta_j^-)$. Show that the Lagrange dual function is

$$L(\beta) + \lambda \sum_j (\beta_j^+ + \beta_j^-) - \sum_j \lambda_j^+ \beta_j^+ - \sum_j \lambda_j^- \beta_j^- \quad (3.89)$$

and the Karush–Kuhn–Tucker optimality conditions are

$$\begin{aligned} \nabla L(\beta)_j + \lambda - \lambda_j^+ &= 0 \\ -\nabla L(\beta)_j + \lambda - \lambda_j^- &= 0 \\ \lambda_j^+ \beta_j^+ &= 0 \\ \lambda_j^- \beta_j^- &= 0, \end{aligned}$$

along with the non-negativity constraints on the parameters and all the Lagrange multipliers.

- (b) Show that $|\nabla L(\beta)_j| \leq \lambda \forall j$, and that the KKT conditions imply one of the following three scenarios:

$$\begin{aligned} \lambda = 0 &\Rightarrow \nabla L(\beta)_j = 0 \forall j \\ \beta_j^+ > 0, \lambda > 0 &\Rightarrow \lambda_j^+ = 0, \nabla L(\beta)_j = -\lambda < 0, \beta_j^- = 0 \\ \beta_j^- > 0, \lambda > 0 &\Rightarrow \lambda_j^- = 0, \nabla L(\beta)_j = \lambda > 0, \beta_j^+ = 0. \end{aligned}$$

Hence show that for any “active” predictor having $\beta_j \neq 0$, we must have $\nabla L(\beta)_j = -\lambda$ if $\beta_j > 0$, and $\nabla L(\beta)_j = \lambda$ if $\beta_j < 0$. Assuming the predictors are standardized, relate λ to the correlation between the j th predictor and the current residuals.

- (c) Suppose that the set of active predictors is unchanged for $\lambda_0 \geq \lambda \geq \lambda_1$. Show that there is a vector γ_0 such that

$$\hat{\beta}(\lambda) = \hat{\beta}(\lambda_0) - (\lambda - \lambda_0)\gamma_0 \quad (3.90)$$

Thus the lasso solution path is linear as λ ranges from λ_0 to λ_1 (Efron et al., 2004; Rosset and Zhu, 2007).

Ex. 3.28 Suppose for a given t in (3.51), the fitted lasso coefficient for variable X_j is $\hat{\beta}_j = a$. Suppose we augment our set of variables with an identical copy $X_j^* = X_j$. Characterize the effect of this exact collinearity by describing the set of solutions for $\hat{\beta}_j$ and $\hat{\beta}_j^*$, using the same value of t .

Ex. 3.29 Suppose we run a ridge regression with parameter λ on a single variable X , and get coefficient a . We now include an exact copy $X^* = X$, and refit our ridge regression. Show that both coefficients are identical, and derive their value. Show in general that if m copies of a variable X_j are included in a ridge regression, their coefficients are all the same.

Ex. 3.30 Consider the elastic-net optimization problem:

$$\min_{\beta} \|\mathbf{y} - \mathbf{X}\beta\|^2 + \lambda[\alpha\|\beta\|_2^2 + (1-\alpha)\|\beta\|_1]. \quad (3.91)$$

Show how one can turn this into a lasso problem, using an augmented version of \mathbf{X} and \mathbf{y} .

4

Linear Methods for Classification

4.1 Introduction

In this chapter we revisit the classification problem and focus on linear methods for classification. Since our predictor $G(x)$ takes values in a discrete set \mathcal{G} , we can always divide the input space into a collection of regions labeled according to the classification. We saw in Chapter 2 that the boundaries of these regions can be rough or smooth, depending on the prediction function. For an important class of procedures, these *decision boundaries* are linear; this is what we will mean by linear methods for classification.

There are several different ways in which linear decision boundaries can be found. In Chapter 2 we fit linear regression models to the class indicator variables, and classify to the largest fit. Suppose there are K classes, for convenience labeled $1, 2, \dots, K$, and the fitted linear model for the k th indicator response variable is $\hat{f}_k(x) = \hat{\beta}_{k0} + \hat{\beta}_k^T x$. The decision boundary between class k and ℓ is that set of points for which $\hat{f}_k(x) = \hat{f}_\ell(x)$, that is, the set $\{x : (\hat{\beta}_{k0} - \hat{\beta}_{\ell0}) + (\hat{\beta}_k - \hat{\beta}_\ell)^T x = 0\}$, an affine set or hyperplane.¹ Since the same is true for any pair of classes, the input space is divided into regions of constant classification, with piecewise hyperplanar decision boundaries. This regression approach is a member of a class of methods that model *discriminant functions* $\delta_k(x)$ for each class, and then classify x to the class with the largest value for its discriminant function. Methods

¹Strictly speaking, a hyperplane passes through the origin, while an affine set need not. We sometimes ignore the distinction and refer in general to hyperplanes.

that model the posterior probabilities $\Pr(G = k|X = x)$ are also in this class. Clearly, if either the $\delta_k(x)$ or $\Pr(G = k|X = x)$ are linear in x , then the decision boundaries will be linear.

Actually, all we require is that some monotone transformation of δ_k or $\Pr(G = k|X = x)$ be linear for the decision boundaries to be linear. For example, if there are two classes, a popular model for the posterior probabilities is

$$\begin{aligned}\Pr(G = 1|X = x) &= \frac{\exp(\beta_0 + \beta^T x)}{1 + \exp(\beta_0 + \beta^T x)}, \\ \Pr(G = 2|X = x) &= \frac{1}{1 + \exp(\beta_0 + \beta^T x)}.\end{aligned}\tag{4.1}$$

Here the monotone transformation is the *logit* transformation: $\log[p/(1-p)]$, and in fact we see that

$$\log \frac{\Pr(G = 1|X = x)}{\Pr(G = 2|X = x)} = \beta_0 + \beta^T x.\tag{4.2}$$

The decision boundary is the set of points for which the *log-odds* are zero, and this is a hyperplane defined by $\{\mathbf{x}|\beta_0 + \beta^T \mathbf{x} = 0\}$. We discuss two very popular but different methods that result in linear log-odds or logits: linear discriminant analysis and linear logistic regression. Although they differ in their derivation, the essential difference between them is in the way the linear function is fit to the training data.

A more direct approach is to explicitly model the boundaries between the classes as linear. For a two-class problem in a p -dimensional input space, this amounts to modeling the decision boundary as a hyperplane—in other words, a normal vector and a cut-point. We will look at two methods that explicitly look for “separating hyperplanes.” The first is the well-known *perceptron* model of Rosenblatt (1958), with an algorithm that finds a separating hyperplane in the training data, if one exists. The second method, due to Vapnik (1996), finds an *optimally separating hyperplane* if one exists, else finds a hyperplane that minimizes some measure of overlap in the training data. We treat the separable case here, and defer treatment of the nonseparable case to Chapter 12.

While this entire chapter is devoted to linear decision boundaries, there is considerable scope for generalization. For example, we can expand our variable set X_1, \dots, X_p by including their squares and cross-products $X_1^2, X_2^2, \dots, X_1 X_2, \dots$, thereby adding $p(p+1)/2$ additional variables. Linear functions in the augmented space map down to quadratic functions in the original space—hence linear decision boundaries to quadratic decision boundaries. Figure 4.1 illustrates the idea. The data are the same: the left plot uses linear decision boundaries in the two-dimensional space shown, while the right plot uses linear decision boundaries in the augmented five-dimensional space described above. This approach can be used with any basis transfor-

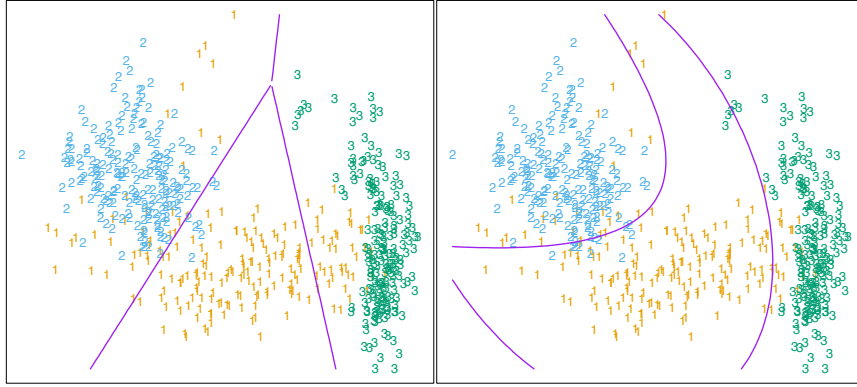


FIGURE 4.1. The left plot shows some data from three classes, with linear decision boundaries found by linear discriminant analysis. The right plot shows quadratic decision boundaries. These were obtained by finding linear boundaries in the five-dimensional space $X_1, X_2, X_1X_2, X_1^2, X_2^2$. Linear inequalities in this space are quadratic inequalities in the original space.

mation $h(X)$ where $h : \mathbb{R}^p \mapsto \mathbb{R}^q$ with $q > p$, and will be explored in later chapters.

4.2 Linear Regression of an Indicator Matrix

Here each of the response categories are coded via an indicator variable. Thus if \mathcal{G} has K classes, there will be K such indicators Y_k , $k = 1, \dots, K$, with $Y_k = 1$ if $G = k$ else 0. These are collected together in a vector $Y = (Y_1, \dots, Y_K)$, and the N training instances of these form an $N \times K$ *indicator response matrix* \mathbf{Y} . \mathbf{Y} is a matrix of 0's and 1's, with each row having a single 1. We fit a linear regression model to each of the columns of \mathbf{Y} simultaneously, and the fit is given by

$$\hat{\mathbf{Y}} = \mathbf{X}(\mathbf{X}^T \mathbf{X})^{-1} \mathbf{X}^T \mathbf{Y}. \quad (4.3)$$

Chapter 3 has more details on linear regression. Note that we have a coefficient vector for each response column \mathbf{y}_k , and hence a $(p+1) \times K$ coefficient matrix $\hat{\mathbf{B}} = (\mathbf{X}^T \mathbf{X})^{-1} \mathbf{X}^T \mathbf{Y}$. Here \mathbf{X} is the model matrix with $p+1$ columns corresponding to the p inputs, and a leading column of 1's for the intercept.

A new observation with input x is classified as follows:

- compute the fitted output $\hat{f}(x)^T = (1, x^T) \hat{\mathbf{B}}$, a K vector;
- identify the largest component and classify accordingly:

$$\hat{G}(x) = \operatorname{argmax}_{k \in \mathcal{G}} \hat{f}_k(x). \quad (4.4)$$

What is the rationale for this approach? One rather formal justification is to view the regression as an estimate of conditional expectation. For the random variable Y_k , $E(Y_k|X = x) = \Pr(G = k|X = x)$, so conditional expectation of each of the Y_k seems a sensible goal. The real issue is: how good an approximation to conditional expectation is the rather rigid linear regression model? Alternatively, are the $\hat{f}_k(x)$ reasonable estimates of the posterior probabilities $\Pr(G = k|X = x)$, and more importantly, does this matter?

It is quite straightforward to verify that $\sum_{k \in \mathcal{G}} \hat{f}_k(x) = 1$ for any x , as long as there is an intercept in the model (column of 1's in \mathbf{X}). However, the $\hat{f}_k(x)$ can be negative or greater than 1, and typically some are. This is a consequence of the rigid nature of linear regression, especially if we make predictions outside the hull of the training data. These violations in themselves do not guarantee that this approach will not work, and in fact on many problems it gives similar results to more standard linear methods for classification. If we allow linear regression onto basis expansions $h(X)$ of the inputs, this approach can lead to consistent estimates of the probabilities. As the size of the training set N grows bigger, we adaptively include more basis elements so that linear regression onto these basis functions approaches conditional expectation. We discuss such approaches in Chapter 5.

A more simplistic viewpoint is to construct *targets* t_k for each class, where t_k is the k th column of the $K \times K$ identity matrix. Our prediction problem is to try and reproduce the appropriate target for an observation. With the same coding as before, the response vector y_i (i th row of \mathbf{Y}) for observation i has the value $y_i = t_k$ if $g_i = k$. We might then fit the linear model by least squares:

$$\min_{\mathbf{B}} \sum_{i=1}^N \|y_i - [(1, x_i^T) \mathbf{B}]^T\|^2. \quad (4.5)$$

The criterion is a sum-of-squared Euclidean distances of the fitted vectors from their targets. A new observation is classified by computing its fitted vector $\hat{f}(x)$ and classifying to the closest target:

$$\hat{G}(x) = \operatorname{argmin}_k \|\hat{f}(x) - t_k\|^2. \quad (4.6)$$

This is exactly the same as the previous approach:

- The sum-of-squared-norm criterion is exactly the criterion for multiple response linear regression, just viewed slightly differently. Since a squared norm is itself a sum of squares, the components decouple and can be rearranged as a separate linear model for each element. Note that this is only possible because there is nothing in the model that binds the different responses together.

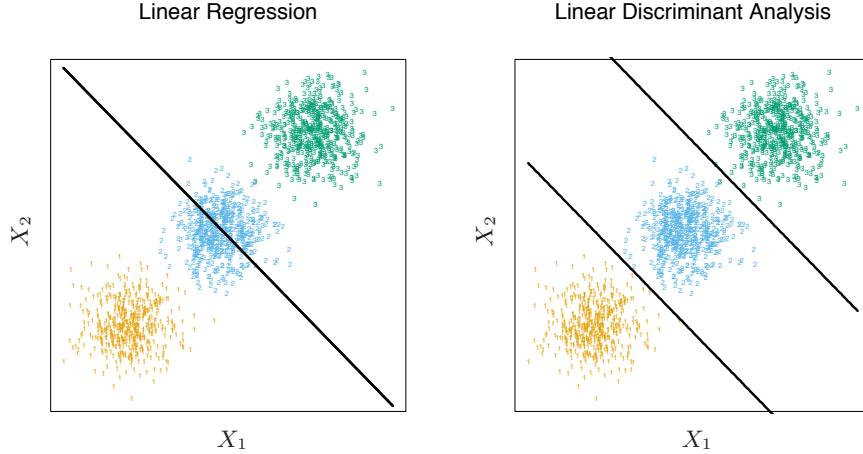


FIGURE 4.2. The data come from three classes in \mathbb{R}^2 and are easily separated by linear decision boundaries. The right plot shows the boundaries found by linear discriminant analysis. The left plot shows the boundaries found by linear regression of the indicator response variables. The middle class is completely masked (never dominates).

- The closest target classification rule (4.6) is easily seen to be exactly the same as the maximum fitted component criterion (4.4).

There is a serious problem with the regression approach when the number of classes $K \geq 3$, especially prevalent when K is large. Because of the rigid nature of the regression model, classes can be *masked* by others. Figure 4.2 illustrates an extreme situation when $K = 3$. The three classes are perfectly separated by linear decision boundaries, yet linear regression misses the middle class completely.

In Figure 4.3 we have projected the data onto the line joining the three centroids (there is no information in the orthogonal direction in this case), and we have included and coded the three response variables Y_1 , Y_2 and Y_3 . The three regression lines (left panel) are included, and we see that the line corresponding to the middle class is horizontal and its fitted values are never dominant! Thus, observations from class 2 are classified either as class 1 or class 3. The right panel uses quadratic regression rather than linear regression. For this simple example a quadratic rather than linear fit (for the middle class at least) would solve the problem. However, it can be seen that if there were four rather than three classes lined up like this, a quadratic would not come down fast enough, and a cubic would be needed as well. A loose but general rule is that if $K \geq 3$ classes are lined up, polynomial terms up to degree $K - 1$ might be needed to resolve them. Note also that these are polynomials along the derived direction passing through the centroids, which can have arbitrary orientation. So in

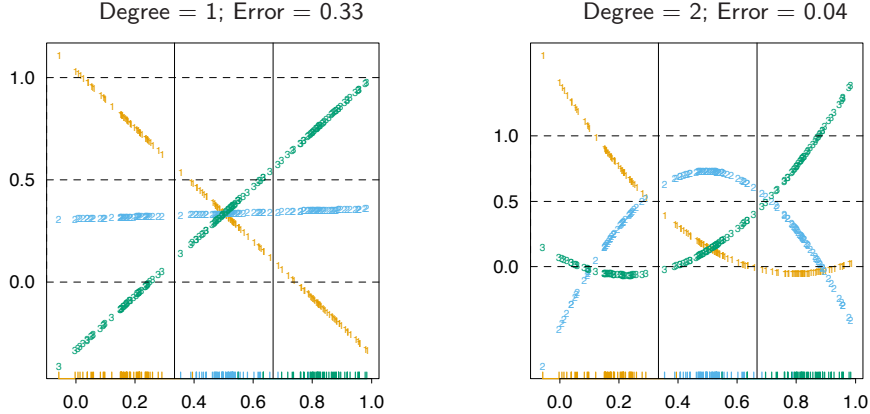


FIGURE 4.3. The effects of masking on linear regression in \mathbb{R}^p for a three-class problem. The rug plot at the base indicates the positions and class membership of each observation. The three curves in each panel are the fitted regressions to the three-class indicator variables; for example, for the blue class, y_{blue} is 1 for the blue observations, and 0 for the green and orange. The fits are linear and quadratic polynomials. Above each plot is the training error rate. The Bayes error rate is 0.025 for this problem, as is the LDA error rate.

p -dimensional input space, one would need general polynomial terms and cross-products of total degree $K - 1$, $O(p^{K-1})$ terms in all, to resolve such worst-case scenarios.

The example is extreme, but for large K and small p such maskings naturally occur. As a more realistic illustration, Figure 4.4 is a projection of the training data for a vowel recognition problem onto an informative two-dimensional subspace. There are $K = 11$ classes in $p = 10$ dimensions. This is a difficult classification problem, and the best methods achieve around 40% errors on the test data. The main point here is summarized in Table 4.1; linear regression has an error rate of 67%, while a close relative, linear discriminant analysis, has an error rate of 56%. It seems that masking has hurt in this case. While all the other methods in this chapter are based on linear functions of x as well, they use them in such a way that avoids this masking problem.

4.3 Linear Discriminant Analysis

Decision theory for classification (Section 2.4) tells us that we need to know the class posteriors $\Pr(G|X)$ for optimal classification. Suppose $f_k(x)$ is the class-conditional density of X in class $G = k$, and let π_k be the prior probability of class k , with $\sum_{k=1}^K \pi_k = 1$. A simple application of Bayes

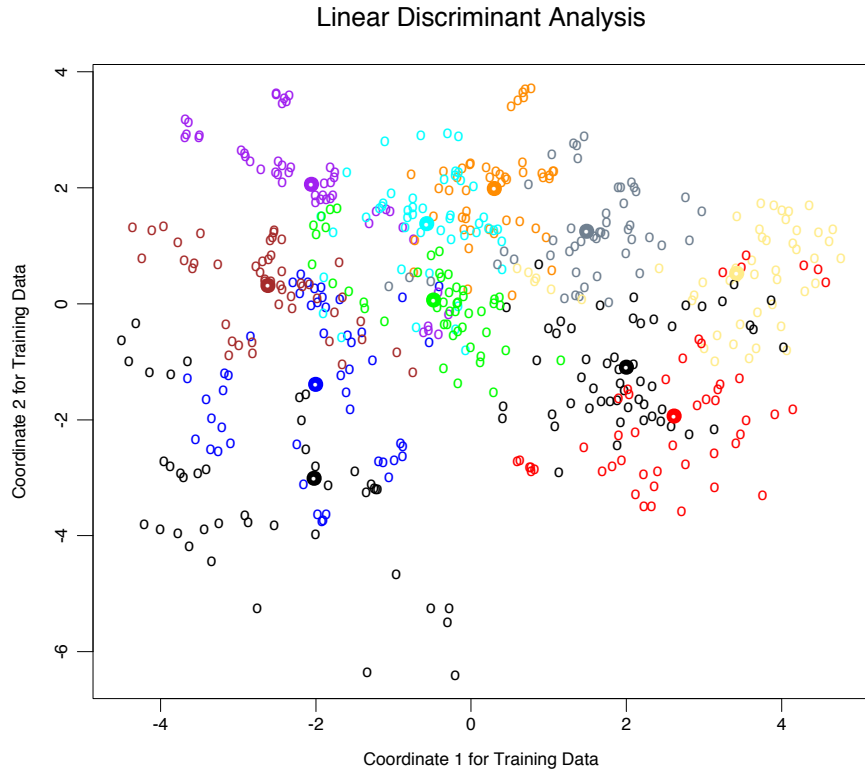


FIGURE 4.4. A two-dimensional plot of the vowel training data. There are eleven classes with $X \in \mathbb{R}^{10}$, and this is the best view in terms of a LDA model (Section 4.3.3). The heavy circles are the projected mean vectors for each class. The class overlap is considerable.

TABLE 4.1. Training and test error rates using a variety of linear techniques on the vowel data. There are eleven classes in ten dimensions, of which three account for 90% of the variance (via a principal components analysis). We see that linear regression is hurt by masking, increasing the test and training error by over 10%.

Technique	Error Rates	
	Training	Test
Linear regression	0.48	0.67
Linear discriminant analysis	0.32	0.56
Quadratic discriminant analysis	0.01	0.53
Logistic regression	0.22	0.51

theorem gives us

$$\Pr(G = k|X = x) = \frac{f_k(x)\pi_k}{\sum_{\ell=1}^K f_\ell(x)\pi_\ell}. \quad (4.7)$$

We see that in terms of ability to classify, having the $f_k(x)$ is almost equivalent to having the quantity $\Pr(G = k|X = x)$.

Many techniques are based on models for the class densities:

- linear and quadratic discriminant analysis use Gaussian densities;
- more flexible mixtures of Gaussians allow for nonlinear decision boundaries (Section 6.8);
- general nonparametric density estimates for each class density allow the most flexibility (Section 6.6.2);
- *Naive Bayes* models are a variant of the previous case, and assume that each of the class densities are products of marginal densities; that is, they assume that the inputs are conditionally independent in each class (Section 6.6.3).

Suppose that we model each class density as multivariate Gaussian

$$f_k(x) = \frac{1}{(2\pi)^{p/2}|\Sigma_k|^{1/2}} e^{-\frac{1}{2}(x-\mu_k)^T \Sigma_k^{-1}(x-\mu_k)}. \quad (4.8)$$

Linear discriminant analysis (LDA) arises in the special case when we assume that the classes have a common covariance matrix $\Sigma_k = \Sigma \forall k$. In comparing two classes k and ℓ , it is sufficient to look at the log-ratio, and we see that

$$\begin{aligned} \log \frac{\Pr(G = k|X = x)}{\Pr(G = \ell|X = x)} &= \log \frac{f_k(x)}{f_\ell(x)} + \log \frac{\pi_k}{\pi_\ell} \\ &= \log \frac{\pi_k}{\pi_\ell} - \frac{1}{2}(\mu_k + \mu_\ell)^T \Sigma^{-1}(\mu_k - \mu_\ell) \\ &\quad + x^T \Sigma^{-1}(\mu_k - \mu_\ell), \end{aligned} \quad (4.9)$$

an equation linear in x . The equal covariance matrices cause the normalization factors to cancel, as well as the quadratic part in the exponents. This linear log-odds function implies that the decision boundary between classes k and ℓ —the set where $\Pr(G = k|X = x) = \Pr(G = \ell|X = x)$ —is linear in x ; in p dimensions a hyperplane. This is of course true for any pair of classes, so all the decision boundaries are linear. If we divide \mathbb{R}^p into regions that are classified as class 1, class 2, etc., these regions will be separated by hyperplanes. Figure 4.5 (left panel) shows an idealized example with three classes and $p = 2$. Here the data do arise from three Gaussian distributions with a common covariance matrix. We have included in

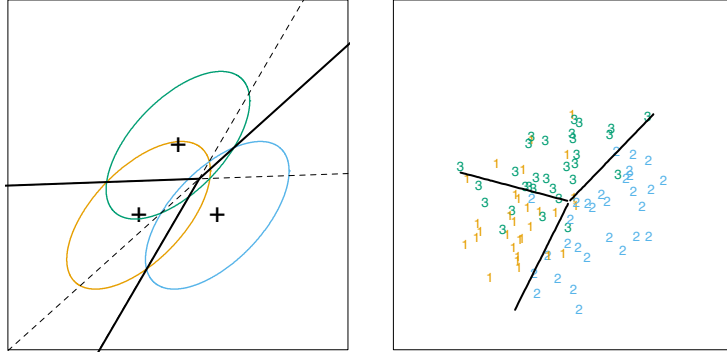


FIGURE 4.5. The left panel shows three Gaussian distributions, with the same covariance and different means. Included are the contours of constant density enclosing 95% of the probability in each case. The Bayes decision boundaries between each pair of classes are shown (broken straight lines), and the Bayes decision boundaries separating all three classes are the thicker solid lines (a subset of the former). On the right we see a sample of 30 drawn from each Gaussian distribution, and the fitted LDA decision boundaries.

in the figure the contours corresponding to 95% highest probability density, as well as the class centroids. Notice that the decision boundaries are not the perpendicular bisectors of the line segments joining the centroids. This would be the case if the covariance Σ were spherical $\sigma^2\mathbf{I}$, and the class priors were equal. From (4.9) we see that the *linear discriminant functions*

$$\delta_k(x) = x^T \Sigma^{-1} \mu_k - \frac{1}{2} \mu_k^T \Sigma^{-1} \mu_k + \log \pi_k \quad (4.10)$$

are an equivalent description of the decision rule, with $G(x) = \text{argmax}_k \delta_k(x)$.

In practice we do not know the parameters of the Gaussian distributions, and will need to estimate them using our training data:

- $\hat{\pi}_k = N_k/N$, where N_k is the number of class- k observations;
- $\hat{\mu}_k = \sum_{g_i=k} x_i / N_k$;
- $\hat{\Sigma} = \sum_{k=1}^K \sum_{g_i=k} (x_i - \hat{\mu}_k)(x_i - \hat{\mu}_k)^T / (N - K)$.

Figure 4.5 (right panel) shows the estimated decision boundaries based on a sample of size 30 each from three Gaussian distributions. Figure 4.1 on page 103 is another example, but here the classes are not Gaussian.

With two classes there is a simple correspondence between linear discriminant analysis and classification by linear regression, as in (4.5). The LDA rule classifies to class 2 if

$$x^T \hat{\Sigma}^{-1} (\hat{\mu}_2 - \hat{\mu}_1) > \frac{1}{2} (\hat{\mu}_2 + \hat{\mu}_1)^T \hat{\Sigma}^{-1} (\hat{\mu}_2 - \hat{\mu}_1) - \log(N_2/N_1), \quad (4.11)$$

and class 1 otherwise. Suppose we code the targets in the two classes as +1 and -1, respectively. It is easy to show that the coefficient vector from least squares is proportional to the LDA direction given in (4.11) (Exercise 4.2). [In fact, this correspondence occurs for any (distinct) coding of the targets; see Exercise 4.2]. However unless $N_1 = N_2$ the intercepts are different and hence the resulting decision rules are different.

Since this derivation of the LDA direction via least squares does not use a Gaussian assumption for the features, its applicability extends beyond the realm of Gaussian data. However the derivation of the particular intercept or cut-point given in (4.11) *does* require Gaussian data. Thus it makes sense to instead choose the cut-point that empirically minimizes training error for a given dataset. This is something we have found to work well in practice, but have not seen it mentioned in the literature.

With more than two classes, LDA is not the same as linear regression of the class indicator matrix, and it avoids the masking problems associated with that approach (Hastie et al., 1994). A correspondence between regression and LDA can be established through the notion of *optimal scoring*, discussed in Section 12.5.

Getting back to the general discriminant problem (4.8), if the Σ_k are not assumed to be equal, then the convenient cancellations in (4.9) do not occur; in particular the pieces quadratic in x remain. We then get *quadratic discriminant functions* (QDA),

$$\delta_k(x) = -\frac{1}{2} \log |\Sigma_k| - \frac{1}{2}(x - \mu_k)^T \Sigma_k^{-1} (x - \mu_k) + \log \pi_k. \quad (4.12)$$

The decision boundary between each pair of classes k and ℓ is described by a quadratic equation $\{x : \delta_k(x) = \delta_\ell(x)\}$.

Figure 4.6 shows an example (from Figure 4.1 on page 103) where the three classes are Gaussian mixtures (Section 6.8) and the decision boundaries are approximated by quadratic equations in x . Here we illustrate two popular ways of fitting these quadratic boundaries. The right plot uses QDA as described here, while the left plot uses LDA in the enlarged five-dimensional quadratic polynomial space. The differences are generally small; QDA is the preferred approach, with the LDA method a convenient substitute ².

The estimates for QDA are similar to those for LDA, except that separate covariance matrices must be estimated for each class. When p is large this can mean a dramatic increase in parameters. Since the decision boundaries are functions of the parameters of the densities, counting the number of parameters must be done with care. For LDA, it seems there are $(K - 1) \times (p + 1)$ parameters, since we only need the differences $\delta_k(x) - \delta_K(x)$

²For this figure and many similar figures in the book we compute the decision boundaries by an exhaustive contouring method. We compute the decision rule on a fine lattice of points, and then use contouring algorithms to compute the boundaries.

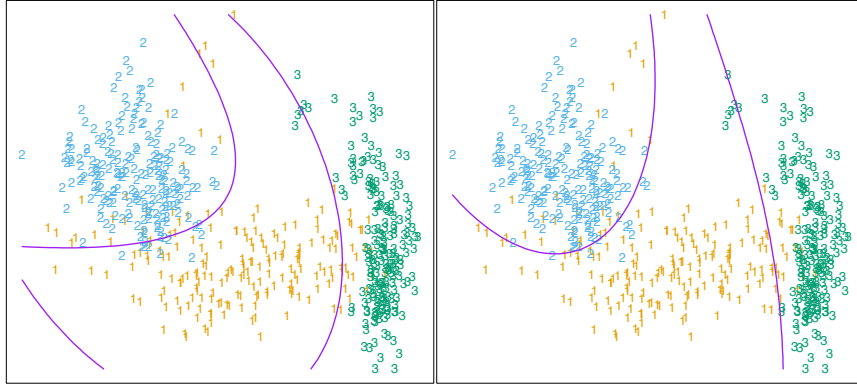


FIGURE 4.6. Two methods for fitting quadratic boundaries. The left plot shows the quadratic decision boundaries for the data in Figure 4.1 (obtained using LDA in the five-dimensional space $X_1, X_2, X_1X_2, X_1^2, X_2^2$). The right plot shows the quadratic decision boundaries found by QDA. The differences are small, as is usually the case.

between the discriminant functions where K is some pre-chosen class (here we have chosen the last), and each difference requires $p + 1$ parameters³. Likewise for QDA there will be $(K - 1) \times \{p(p + 3)/2 + 1\}$ parameters. Both LDA and QDA perform well on an amazingly large and diverse set of classification tasks. For example, in the STATLOG project (Michie et al., 1994) LDA was among the top three classifiers for 7 of the 22 datasets, QDA among the top three for four datasets, and one of the pair were in the top three for 10 datasets. Both techniques are widely used, and entire books are devoted to LDA. It seems that whatever exotic tools are the rage of the day, we should always have available these two simple tools. The question arises why LDA and QDA have such a good track record. The reason is not likely to be that the data are approximately Gaussian, and in addition for LDA that the covariances are approximately equal. More likely a reason is that the data can only support simple decision boundaries such as linear or quadratic, and the estimates provided via the Gaussian models are stable. This is a bias variance tradeoff—we can put up with the bias of a linear decision boundary because it can be estimated with much lower variance than more exotic alternatives. This argument is less believable for QDA, since it can have many parameters itself, although perhaps fewer than the non-parametric alternatives.

³Although we fit the covariance matrix $\hat{\Sigma}$ to compute the LDA discriminant functions, a much reduced function of it is all that is required to estimate the $O(p)$ parameters needed to compute the decision boundaries.

Regularized Discriminant Analysis on the Vowel Data

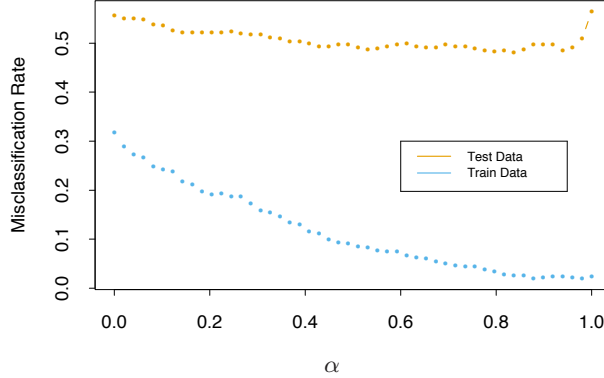


FIGURE 4.7. Test and training errors for the vowel data, using regularized discriminant analysis with a series of values of $\alpha \in [0, 1]$. The optimum for the test data occurs around $\alpha = 0.9$, close to quadratic discriminant analysis.

4.3.1 Regularized Discriminant Analysis

Friedman (1989) proposed a compromise between LDA and QDA, which allows one to shrink the separate covariances of QDA toward a common covariance as in LDA. These methods are very similar in flavor to ridge regression. The regularized covariance matrices have the form

$$\hat{\Sigma}_k(\alpha) = \alpha \hat{\Sigma}_k + (1 - \alpha) \hat{\Sigma}, \quad (4.13)$$

where $\hat{\Sigma}$ is the pooled covariance matrix as used in LDA. Here $\alpha \in [0, 1]$ allows a continuum of models between LDA and QDA, and needs to be specified. In practice α can be chosen based on the performance of the model on validation data, or by cross-validation.

Figure 4.7 shows the results of RDA applied to the vowel data. Both the training and test error improve with increasing α , although the test error increases sharply after $\alpha = 0.9$. The large discrepancy between the training and test error is partly due to the fact that there are many repeat measurements on a small number of individuals, different in the training and test set.

Similar modifications allow $\hat{\Sigma}$ itself to be shrunk toward the scalar covariance,

$$\hat{\Sigma}(\gamma) = \gamma \hat{\Sigma} + (1 - \gamma) \hat{\sigma}^2 \mathbf{I} \quad (4.14)$$

for $\gamma \in [0, 1]$. Replacing $\hat{\Sigma}$ in (4.13) by $\hat{\Sigma}(\gamma)$ leads to a more general family of covariances $\hat{\Sigma}(\alpha, \gamma)$ indexed by a pair of parameters.

In Chapter 12, we discuss other regularized versions of LDA, which are more suitable when the data arise from digitized analog signals and images.

In these situations the features are high-dimensional and correlated, and the LDA coefficients can be regularized to be smooth or sparse in the original domain of the signal. This leads to better generalization and allows for easier interpretation of the coefficients. In Chapter 18 we also deal with very high-dimensional problems, where for example the features are gene-expression measurements in microarray studies. There the methods focus on the case $\gamma = 0$ in (4.14), and other severely regularized versions of LDA.

4.3.2 Computations for LDA

As a lead-in to the next topic, we briefly digress on the computations required for LDA and especially QDA. Their computations are simplified by diagonalizing $\hat{\Sigma}$ or $\hat{\Sigma}_k$. For the latter, suppose we compute the eigen-decomposition for each $\hat{\Sigma}_k = \mathbf{U}_k \mathbf{D}_k \mathbf{U}_k^T$, where \mathbf{U}_k is $p \times p$ orthonormal, and \mathbf{D}_k a diagonal matrix of positive eigenvalues $d_{k\ell}$. Then the ingredients for $\delta_k(x)$ (4.12) are

- $(x - \hat{\mu}_k)^T \hat{\Sigma}_k^{-1} (x - \hat{\mu}_k) = [\mathbf{U}_k^T (x - \hat{\mu}_k)]^T \mathbf{D}_k^{-1} [\mathbf{U}_k^T (x - \hat{\mu}_k)];$
- $\log |\hat{\Sigma}_k| = \sum_\ell \log d_{k\ell}.$

In light of the computational steps outlined above, the LDA classifier can be implemented by the following pair of steps:

- *Sphere* the data with respect to the common covariance estimate $\hat{\Sigma}$: $X^* \leftarrow \mathbf{D}^{-\frac{1}{2}} \mathbf{U}^T X$, where $\hat{\Sigma} = \mathbf{U} \mathbf{D} \mathbf{U}^T$. The common covariance estimate of X^* will now be the identity.
- Classify to the closest class centroid in the transformed space, modulo the effect of the class prior probabilities π_k .

4.3.3 Reduced-Rank Linear Discriminant Analysis

So far we have discussed LDA as a restricted Gaussian classifier. Part of its popularity is due to an additional restriction that allows us to view informative low-dimensional projections of the data.

The K centroids in p -dimensional input space lie in an affine subspace of dimension $\leq K - 1$, and if p is much larger than K , this will be a considerable drop in dimension. Moreover, in locating the closest centroid, we can ignore distances orthogonal to this subspace, since they will contribute equally to each class. Thus we might just as well project the X^* onto this centroid-spanning subspace H_{K-1} , and make distance comparisons there. Thus there is a fundamental dimension reduction in LDA, namely, that we need only consider the data in a subspace of dimension at most $K - 1$.

If $K = 3$, for instance, this could allow us to view the data in a two-dimensional plot, color-coding the classes. In doing so we would not have relinquished any of the information needed for LDA classification.

What if $K > 3$? We might then ask for a $L < K - 1$ dimensional subspace $H_L \subseteq H_{K-1}$ optimal for LDA in some sense. Fisher defined optimal to mean that the projected centroids were spread out as much as possible in terms of variance. This amounts to finding principal component subspaces of the centroids themselves (principal components are described briefly in Section 3.5.1, and in more detail in Section 14.5.1). Figure 4.4 shows such an optimal two-dimensional subspace for the vowel data. Here there are eleven classes, each a different vowel sound, in a ten-dimensional input space. The centroids require the full space in this case, since $K - 1 = p$, but we have shown an optimal two-dimensional subspace. The dimensions are ordered, so we can compute additional dimensions in sequence. Figure 4.8 shows four additional pairs of coordinates, also known as *canonical* or *discriminant* variables. In summary then, finding the sequences of optimal subspaces for LDA involves the following steps:

- compute the $K \times p$ matrix of class centroids \mathbf{M} and the common covariance matrix \mathbf{W} (for *within-class* covariance);
- compute $\mathbf{M}^* = \mathbf{MW}^{-\frac{1}{2}}$ using the eigen-decomposition of \mathbf{W} ;
- compute \mathbf{B}^* , the covariance matrix of \mathbf{M}^* (\mathbf{B} for *between-class* covariance), and its eigen-decomposition $\mathbf{B}^* = \mathbf{V}^* \mathbf{D}_B \mathbf{V}^{*T}$. The columns v_ℓ^* of \mathbf{V}^* in sequence from first to last define the coordinates of the optimal subspaces.

Combining all these operations the ℓ th *discriminant variable* is given by $Z_\ell = v_\ell^T X$ with $v_\ell = \mathbf{W}^{-\frac{1}{2}} v_\ell^*$.

Fisher arrived at this decomposition via a different route, without referring to Gaussian distributions at all. He posed the problem:

Find the linear combination $Z = a^T X$ such that the between-class variance is maximized relative to the within-class variance.

Again, the between class variance is the variance of the class means of Z , and the within class variance is the pooled variance about the means. Figure 4.9 shows why this criterion makes sense. Although the direction joining the centroids separates the means as much as possible (i.e., maximizes the between-class variance), there is considerable overlap between the projected classes due to the nature of the covariances. By taking the covariance into account as well, a direction with minimum overlap can be found.

The between-class variance of Z is $a^T \mathbf{B} a$ and the within-class variance $a^T \mathbf{W} a$, where \mathbf{W} is defined earlier, and \mathbf{B} is the covariance matrix of the class centroid matrix \mathbf{M} . Note that $\mathbf{B} + \mathbf{W} = \mathbf{T}$, where \mathbf{T} is the *total* covariance matrix of X , ignoring class information.

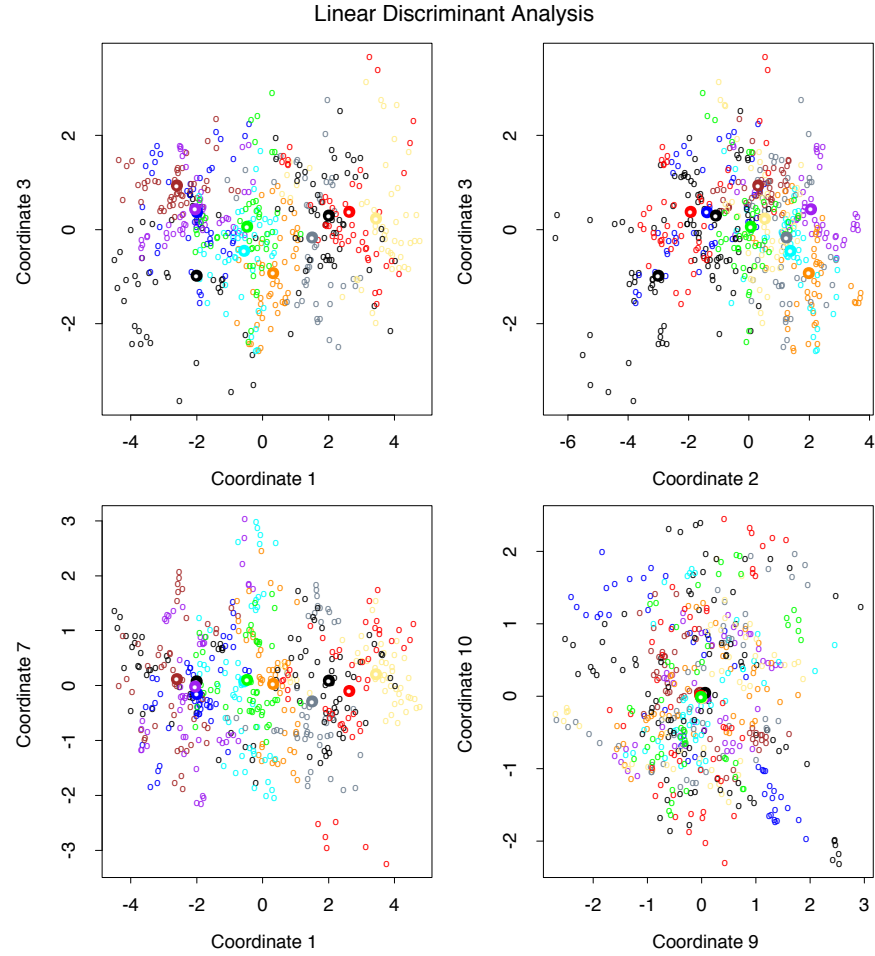


FIGURE 4.8. Four projections onto pairs of canonical variates. Notice that as the rank of the canonical variates increases, the centroids become less spread out. In the lower right panel they appear to be superimposed, and the classes most confused.

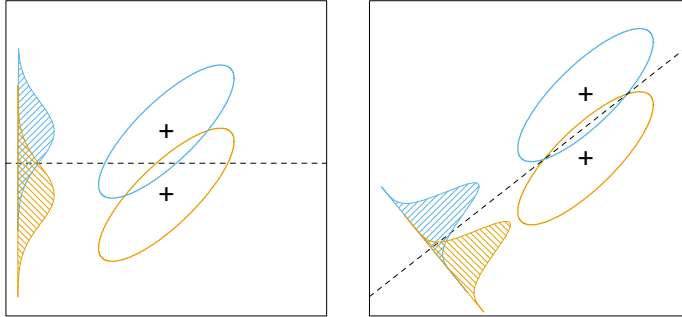


FIGURE 4.9. Although the line joining the centroids defines the direction of greatest centroid spread, the projected data overlap because of the covariance (left panel). The discriminant direction minimizes this overlap for Gaussian data (right panel).

Fisher's problem therefore amounts to maximizing the *Rayleigh quotient*,

$$\max_a \frac{a^T \mathbf{B} a}{a^T \mathbf{W} a}, \quad (4.15)$$

or equivalently

$$\max_a a^T \mathbf{B} a \text{ subject to } a^T \mathbf{W} a = 1. \quad (4.16)$$

This is a generalized eigenvalue problem, with a given by the largest eigenvalue of $\mathbf{W}^{-1}\mathbf{B}$. It is not hard to show (Exercise 4.1) that the optimal a_1 is identical to v_1 defined above. Similarly one can find the next direction a_2 , orthogonal in \mathbf{W} to a_1 , such that $a_2^T \mathbf{B} a_2 / a_2^T \mathbf{W} a_2$ is maximized; the solution is $a_2 = v_2$, and so on. The a_ℓ are referred to as *discriminant coordinates*, not to be confused with discriminant functions. They are also referred to as *canonical variates*, since an alternative derivation of these results is through a canonical correlation analysis of the indicator response matrix \mathbf{Y} on the predictor matrix \mathbf{X} . This line is pursued in Section 12.5.

To summarize the developments so far:

- Gaussian classification with common covariances leads to linear decision boundaries. Classification can be achieved by spherling the data with respect to \mathbf{W} , and classifying to the closest centroid (modulo $\log \pi_k$) in the sphered space.
- Since only the relative distances to the centroids count, one can confine the data to the subspace spanned by the centroids in the sphered space.
- This subspace can be further decomposed into successively optimal subspaces in term of centroid separation. This decomposition is identical to the decomposition due to Fisher.

LDA and Dimension Reduction on the Vowel Data

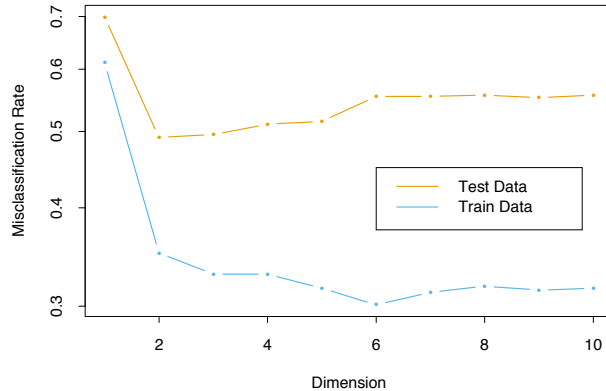


FIGURE 4.10. Training and test error rates for the vowel data, as a function of the dimension of the discriminant subspace. In this case the best error rate is for dimension 2. Figure 4.11 shows the decision boundaries in this space.

The reduced subspaces have been motivated as a data reduction (for viewing) tool. Can they also be used for classification, and what is the rationale? Clearly they can, as in our original derivation; we simply limit the distance-to-centroid calculations to the chosen subspace. One can show that this is a Gaussian classification rule with the additional restriction that the centroids of the Gaussians lie in a L -dimensional subspace of \mathbb{R}^p . Fitting such a model by maximum likelihood, and then constructing the posterior probabilities using Bayes' theorem amounts to the classification rule described above (Exercise 4.8).

Gaussian classification dictates the $\log \pi_k$ correction factor in the distance calculation. The reason for this correction can be seen in Figure 4.9. The misclassification rate is based on the area of overlap between the two densities. If the π_k are equal (implicit in that figure), then the optimal cut-point is midway between the projected means. If the π_k are not equal, moving the cut-point toward the *smaller* class will improve the error rate. As mentioned earlier for two classes, one can derive the linear rule using LDA (or any other method), and then choose the cut-point to minimize misclassification error over the training data.

As an example of the benefit of the reduced-rank restriction, we return to the vowel data. There are 11 classes and 10 variables, and hence 10 possible dimensions for the classifier. We can compute the training and test error in each of these hierarchical subspaces; Figure 4.10 shows the results. Figure 4.11 shows the decision boundaries for the classifier based on the two-dimensional LDA solution.

There is a close connection between Fisher's reduced rank discriminant analysis and regression of an indicator response matrix. It turns out that

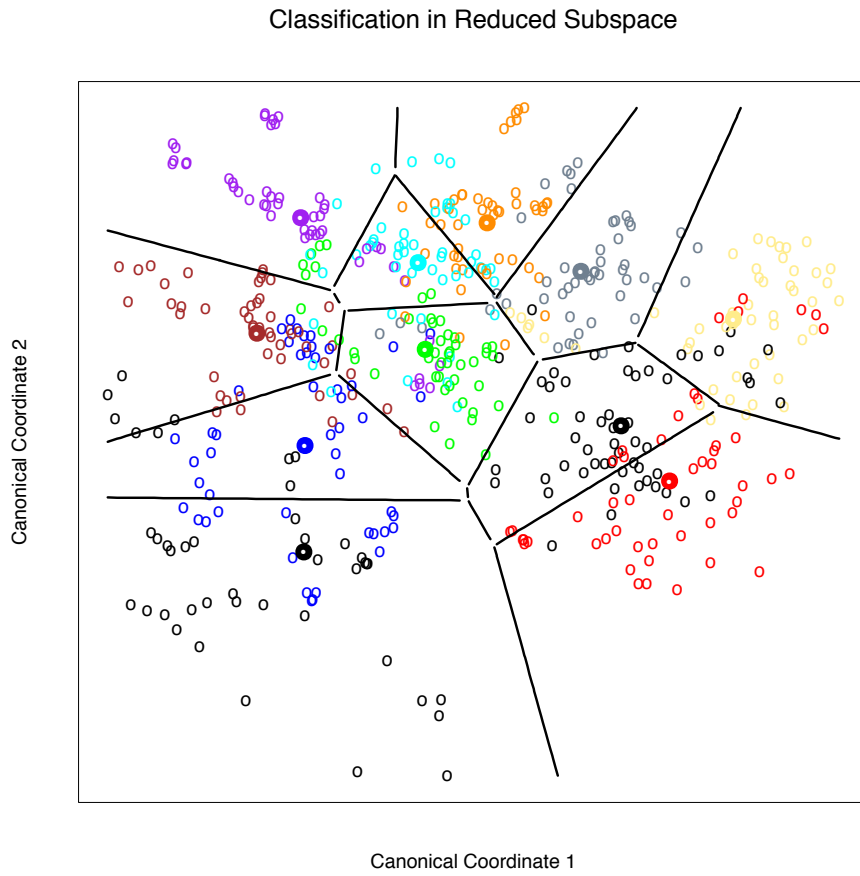


FIGURE 4.11. Decision boundaries for the vowel training data, in the two-dimensional subspace spanned by the first two canonical variates. Note that in any higher-dimensional subspace, the decision boundaries are higher-dimensional affine planes, and could not be represented as lines.

LDA amounts to the regression followed by an eigen-decomposition of $\hat{\mathbf{Y}}^T \hat{\mathbf{Y}}$. In the case of two classes, there is a single discriminant variable that is identical up to a scalar multiplication to either of the columns of $\hat{\mathbf{Y}}$. These connections are developed in Chapter 12. A related fact is that if one transforms the original predictors \mathbf{X} to $\hat{\mathbf{Y}}$, then LDA using $\hat{\mathbf{Y}}$ is identical to LDA in the original space (Exercise 4.3).

4.4 Logistic Regression

The logistic regression model arises from the desire to model the posterior probabilities of the K classes via linear functions in x , while at the same time ensuring that they sum to one and remain in $[0, 1]$. The model has the form

$$\begin{aligned} \log \frac{\Pr(G = 1|X = x)}{\Pr(G = K|X = x)} &= \beta_{10} + \beta_1^T x \\ \log \frac{\Pr(G = 2|X = x)}{\Pr(G = K|X = x)} &= \beta_{20} + \beta_2^T x \\ &\vdots \\ \log \frac{\Pr(G = K - 1|X = x)}{\Pr(G = K|X = x)} &= \beta_{(K-1)0} + \beta_{K-1}^T x. \end{aligned} \tag{4.17}$$

The model is specified in terms of $K - 1$ log-odds or logit transformations (reflecting the constraint that the probabilities sum to one). Although the model uses the last class as the denominator in the odds-ratios, the choice of denominator is arbitrary in that the estimates are equivariant under this choice. A simple calculation shows that

$$\begin{aligned} \Pr(G = k|X = x) &= \frac{\exp(\beta_{k0} + \beta_k^T x)}{1 + \sum_{\ell=1}^{K-1} \exp(\beta_{\ell0} + \beta_\ell^T x)}, \quad k = 1, \dots, K - 1, \\ \Pr(G = K|X = x) &= \frac{1}{1 + \sum_{\ell=1}^{K-1} \exp(\beta_{\ell0} + \beta_\ell^T x)}, \end{aligned} \tag{4.18}$$

and they clearly sum to one. To emphasize the dependence on the entire parameter set $\theta = \{\beta_{10}, \beta_1^T, \dots, \beta_{(K-1)0}, \beta_{K-1}^T\}$, we denote the probabilities $\Pr(G = k|X = x) = p_k(x; \theta)$.

When $K = 2$, this model is especially simple, since there is only a single linear function. It is widely used in biostatistical applications where binary responses (two classes) occur quite frequently. For example, patients survive or die, have heart disease or not, or a condition is present or absent.

4.4.1 Fitting Logistic Regression Models

Logistic regression models are usually fit by maximum likelihood, using the conditional likelihood of G given X . Since $\Pr(G|X)$ completely specifies the conditional distribution, the *multinomial* distribution is appropriate. The log-likelihood for N observations is

$$\ell(\theta) = \sum_{i=1}^N \log p_{g_i}(x_i; \theta), \quad (4.19)$$

where $p_k(x_i; \theta) = \Pr(G = k|X = x_i; \theta)$.

We discuss in detail the two-class case, since the algorithms simplify considerably. It is convenient to code the two-class g_i via a 0/1 response y_i , where $y_i = 1$ when $g_i = 1$, and $y_i = 0$ when $g_i = 2$. Let $p_1(x; \theta) = p(x; \theta)$, and $p_2(x; \theta) = 1 - p(x; \theta)$. The log-likelihood can be written

$$\begin{aligned} \ell(\beta) &= \sum_{i=1}^N \left\{ y_i \log p(x_i; \beta) + (1 - y_i) \log(1 - p(x_i; \beta)) \right\} \\ &= \sum_{i=1}^N \left\{ y_i \beta^T x_i - \log(1 + e^{\beta^T x_i}) \right\}. \end{aligned} \quad (4.20)$$

Here $\beta = \{\beta_{10}, \beta_1\}$, and we assume that the vector of inputs x_i includes the constant term 1 to accommodate the intercept.

To maximize the log-likelihood, we set its derivatives to zero. These *score* equations are

$$\frac{\partial \ell(\beta)}{\partial \beta} = \sum_{i=1}^N x_i(y_i - p(x_i; \beta)) = 0, \quad (4.21)$$

which are $p+1$ equations *nonlinear* in β . Notice that since the first component of x_i is 1, the first score equation specifies that $\sum_{i=1}^N y_i = \sum_{i=1}^N p(x_i; \beta)$; the *expected* number of class ones matches the observed number (and hence also class twos.)

To solve the score equations (4.21), we use the Newton–Raphson algorithm, which requires the second-derivative or Hessian matrix

$$\frac{\partial^2 \ell(\beta)}{\partial \beta \partial \beta^T} = - \sum_{i=1}^N x_i x_i^T p(x_i; \beta)(1 - p(x_i; \beta)). \quad (4.22)$$

Starting with β^{old} , a single Newton update is

$$\beta^{\text{new}} = \beta^{\text{old}} - \left(\frac{\partial^2 \ell(\beta)}{\partial \beta \partial \beta^T} \right)^{-1} \frac{\partial \ell(\beta)}{\partial \beta}, \quad (4.23)$$

where the derivatives are evaluated at β^{old} .

It is convenient to write the score and Hessian in matrix notation. Let \mathbf{y} denote the vector of y_i values, \mathbf{X} the $N \times (p + 1)$ matrix of x_i values, \mathbf{p} the vector of fitted probabilities with i th element $p(x_i; \beta^{\text{old}})$ and \mathbf{W} a $N \times N$ diagonal matrix of weights with i th diagonal element $p(x_i; \beta^{\text{old}})(1 - p(x_i; \beta^{\text{old}}))$. Then we have

$$\frac{\partial \ell(\beta)}{\partial \beta} = \mathbf{X}^T(\mathbf{y} - \mathbf{p}) \quad (4.24)$$

$$\frac{\partial^2 \ell(\beta)}{\partial \beta \partial \beta^T} = -\mathbf{X}^T \mathbf{W} \mathbf{X} \quad (4.25)$$

The Newton step is thus

$$\begin{aligned} \beta^{\text{new}} &= \beta^{\text{old}} + (\mathbf{X}^T \mathbf{W} \mathbf{X})^{-1} \mathbf{X}^T(\mathbf{y} - \mathbf{p}) \\ &= (\mathbf{X}^T \mathbf{W} \mathbf{X})^{-1} \mathbf{X}^T \mathbf{W} (\mathbf{X} \beta^{\text{old}} + \mathbf{W}^{-1}(\mathbf{y} - \mathbf{p})) \\ &= (\mathbf{X}^T \mathbf{W} \mathbf{X})^{-1} \mathbf{X}^T \mathbf{W} \mathbf{z}. \end{aligned} \quad (4.26)$$

In the second and third line we have re-expressed the Newton step as a weighted least squares step, with the response

$$\mathbf{z} = \mathbf{X} \beta^{\text{old}} + \mathbf{W}^{-1}(\mathbf{y} - \mathbf{p}), \quad (4.27)$$

sometimes known as the *adjusted response*. These equations get solved repeatedly, since at each iteration \mathbf{p} changes, and hence so does \mathbf{W} and \mathbf{z} . This algorithm is referred to as *iteratively reweighted least squares* or IRLS, since each iteration solves the weighted least squares problem:

$$\beta^{\text{new}} \leftarrow \arg \min_{\beta} (\mathbf{z} - \mathbf{X} \beta)^T \mathbf{W} (\mathbf{z} - \mathbf{X} \beta). \quad (4.28)$$

It seems that $\beta = 0$ is a good starting value for the iterative procedure, although convergence is never guaranteed. Typically the algorithm does converge, since the log-likelihood is concave, but overshooting can occur. In the rare cases that the log-likelihood decreases, step size halving will guarantee convergence.

For the multiclass case ($K \geq 3$) the Newton algorithm can also be expressed as an iteratively reweighted least squares algorithm, but with a *vector* of $K - 1$ responses and a nondiagonal weight matrix per observation. The latter precludes any simplified algorithms, and in this case it is numerically more convenient to work with the expanded vector θ directly (Exercise 4.4). Alternatively coordinate-descent methods (Section 3.8.6) can be used to maximize the log-likelihood efficiently. The R package `glmnet` (Friedman et al., 2010) can fit very large logistic regression problems efficiently, both in N and p . Although designed to fit regularized models, options allow for unregularized fits.

Logistic regression models are used mostly as a data analysis and inference tool, where the goal is to understand the role of the input variables

TABLE 4.2. Results from a logistic regression fit to the South African heart disease data.

	Coefficient	Std. Error	Z Score
(Intercept)	-4.130	0.964	-4.285
sbp	0.006	0.006	1.023
tobacco	0.080	0.026	3.034
ldl	0.185	0.057	3.219
famhist	0.939	0.225	4.178
obesity	-0.035	0.029	-1.187
alcohol	0.001	0.004	0.136
age	0.043	0.010	4.184

in *explaining* the outcome. Typically many models are fit in a search for a parsimonious model involving a subset of the variables, possibly with some interactions terms. The following example illustrates some of the issues involved.

4.4.2 Example: South African Heart Disease

Here we present an analysis of binary data to illustrate the traditional statistical use of the logistic regression model. The data in Figure 4.12 are a subset of the Coronary Risk-Factor Study (CORIS) baseline survey, carried out in three rural areas of the Western Cape, South Africa (Rousseauw et al., 1983). The aim of the study was to establish the intensity of ischemic heart disease risk factors in that high-incidence region. The data represent white males between 15 and 64, and the response variable is the presence or absence of myocardial infarction (MI) at the time of the survey (the overall prevalence of MI was 5.1% in this region). There are 160 cases in our data set, and a sample of 302 controls. These data are described in more detail in Hastie and Tibshirani (1987).

We fit a logistic-regression model by maximum likelihood, giving the results shown in Table 4.2. This summary includes Z scores for each of the coefficients in the model (coefficients divided by their standard errors); a nonsignificant Z score suggests a coefficient can be dropped from the model. Each of these correspond formally to a test of the null hypothesis that the coefficient in question is zero, while all the others are not (also known as the Wald test). A Z score greater than approximately 2 in absolute value is significant at the 5% level.

There are some surprises in this table of coefficients, which must be interpreted with caution. Systolic blood pressure (`sbp`) is not significant! Nor is `obesity`, and its sign is negative. This confusion is a result of the correlation between the set of predictors. On their own, both `sbp` and `obesity` are significant, and with positive sign. However, in the presence of many

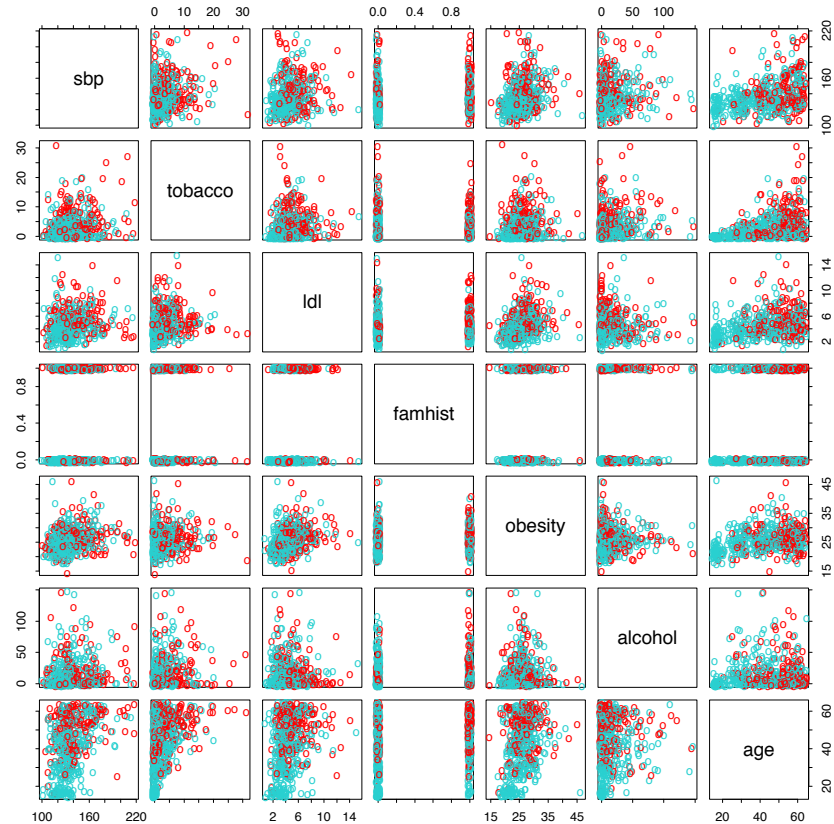


FIGURE 4.12. A scatterplot matrix of the South African heart disease data. Each plot shows a pair of risk factors, and the cases and controls are color coded (red is a case). The variable family history of heart disease (famhist) is binary (yes or no).

TABLE 4.3. Results from stepwise logistic regression fit to South African heart disease data.

	Coefficient	Std. Error	Z score
(Intercept)	-4.204	0.498	-8.45
tobacco	0.081	0.026	3.16
ldl	0.168	0.054	3.09
famhist	0.924	0.223	4.14
age	0.044	0.010	4.52

other correlated variables, they are no longer needed (and can even get a negative sign).

At this stage the analyst might do some model selection; find a subset of the variables that are sufficient for explaining their joint effect on the prevalence of `chd`. One way to proceed by is to drop the least significant coefficient, and refit the model. This is done repeatedly until no further terms can be dropped from the model. This gave the model shown in Table 4.3.

A better but more time-consuming strategy is to refit each of the models with one variable removed, and then perform an *analysis of deviance* to decide which variable to exclude. The residual deviance of a fitted model is minus twice its log-likelihood, and the deviance between two models is the difference of their individual residual deviances (in analogy to sums-of-squares). This strategy gave the same final model as above.

How does one interpret a coefficient of 0.081 (Std. Error = 0.026) for `tobacco`, for example? Tobacco is measured in total lifetime usage in kilograms, with a median of 1.0kg for the controls and 4.1kg for the cases. Thus an increase of 1kg in lifetime tobacco usage accounts for an increase in the odds of coronary heart disease of $\exp(0.081) = 1.084$ or 8.4%. Incorporating the standard error we get an approximate 95% confidence interval of $\exp(0.081 \pm 2 \times 0.026) = (1.03, 1.14)$.

We return to these data in Chapter 5, where we see that some of the variables have nonlinear effects, and when modeled appropriately, are not excluded from the model.

4.4.3 Quadratic Approximations and Inference

The maximum-likelihood parameter estimates $\hat{\beta}$ satisfy a self-consistency relationship: they are the coefficients of a weighted least squares fit, where the responses are

$$z_i = x_i^T \hat{\beta} + \frac{(y_i - \hat{p}_i)}{\hat{p}_i(1 - \hat{p}_i)}, \quad (4.29)$$

and the weights are $w_i = \hat{p}_i(1 - \hat{p}_i)$, both depending on $\hat{\beta}$ itself. Apart from providing a convenient algorithm, this connection with least squares has more to offer:

- The weighted residual sum-of-squares is the familiar Pearson chi-square statistic

$$\sum_{i=1}^N \frac{(y_i - \hat{p}_i)^2}{\hat{p}_i(1 - \hat{p}_i)}, \quad (4.30)$$

a quadratic approximation to the deviance.

- Asymptotic likelihood theory says that if the model is correct, then $\hat{\beta}$ is consistent (i.e., converges to the *true* β).
- A central limit theorem then shows that the distribution of $\hat{\beta}$ converges to $N(\beta, (\mathbf{X}^T \mathbf{W} \mathbf{X})^{-1})$. This and other asymptotics can be derived directly from the weighted least squares fit by mimicking normal theory inference.
- Model building can be costly for logistic regression models, because each model fitted requires iteration. Popular shortcuts are the *Rao score test* which tests for inclusion of a term, and the *Wald test* which can be used to test for exclusion of a term. Neither of these require iterative fitting, and are based on the maximum-likelihood fit of the current model. It turns out that both of these amount to adding or dropping a term from the weighted least squares fit, using the *same* weights. Such computations can be done efficiently, without recomputing the entire weighted least squares fit.

Software implementations can take advantage of these connections. For example, the generalized linear modeling software in R (which includes logistic regression as part of the binomial family of models) exploits them fully. GLM (generalized linear model) objects can be treated as linear model objects, and all the tools available for linear models can be applied automatically.

4.4.4 L_1 Regularized Logistic Regression

The L_1 penalty used in the lasso (Section 3.4.2) can be used for variable selection and shrinkage with any linear regression model. For logistic regression, we would maximize a penalized version of (4.20):

$$\max_{\beta_0, \beta} \left\{ \sum_{i=1}^N \left[y_i(\beta_0 + \beta^T x_i) - \log(1 + e^{\beta_0 + \beta^T x_i}) \right] - \lambda \sum_{j=1}^p |\beta_j| \right\}. \quad (4.31)$$

As with the lasso, we typically do not penalize the intercept term, and standardize the predictors for the penalty to be meaningful. Criterion (4.31) is

concave, and a solution can be found using nonlinear programming methods (Koh et al., 2007, for example). Alternatively, using the same quadratic approximations that were used in the Newton algorithm in Section 4.4.1, we can solve (4.31) by repeated application of a weighted lasso algorithm. Interestingly, the score equations [see (4.24)] for the variables with non-zero coefficients have the form

$$\mathbf{x}_j^T(\mathbf{y} - \mathbf{p}) = \lambda \cdot \text{sign}(\beta_j), \quad (4.32)$$

which generalizes (3.58) in Section 3.4.4; the active variables are tied in their *generalized* correlation with the residuals.

Path algorithms such as LAR for lasso are more difficult, because the coefficient profiles are piecewise smooth rather than linear. Nevertheless, progress can be made using quadratic approximations.

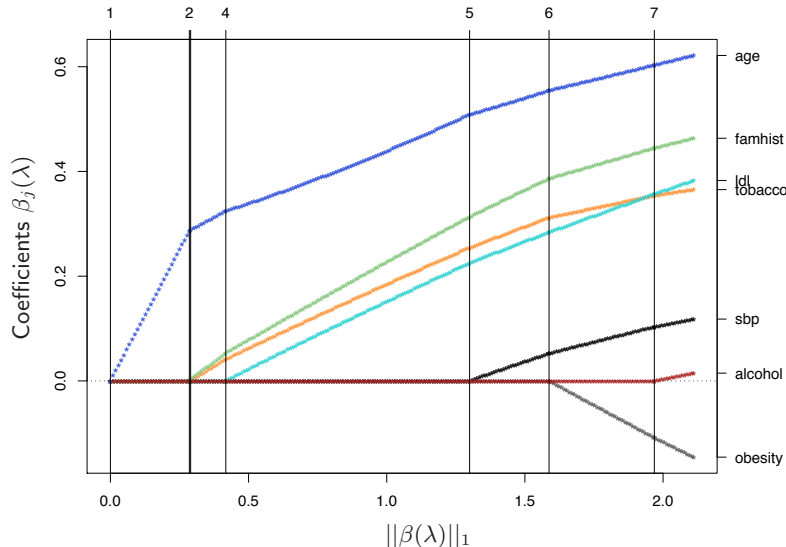


FIGURE 4.13. L_1 regularized logistic regression coefficients for the South African heart disease data, plotted as a function of the L_1 norm. The variables were all standardized to have unit variance. The profiles are computed exactly at each of the plotted points.

Figure 4.13 shows the L_1 regularization path for the South African heart disease data of Section 4.4.2. This was produced using the R package `glmmpath` (Park and Hastie, 2007), which uses *predictor–corrector* methods of convex optimization to identify the exact values of λ at which the active set of non-zero coefficients changes (vertical lines in the figure). Here the profiles look almost linear; in other examples the curvature will be more visible.

Coordinate descent methods (Section 3.8.6) are very efficient for computing the coefficient profiles on a grid of values for λ . The R package `glmnet`

(Friedman et al., 2010) can fit coefficient paths for very large logistic regression problems efficiently (large in N or p). Their algorithms can exploit sparsity in the predictor matrix \mathbf{X} , which allows for even larger problems. See Section 18.4 for more details, and a discussion of L_1 -regularized multinomial models.

4.4.5 Logistic Regression or LDA?

In Section 4.3 we find that the log-posterior odds between class k and K are linear functions of x (4.9):

$$\begin{aligned} \log \frac{\Pr(G = k|X = x)}{\Pr(G = K|X = x)} &= \log \frac{\pi_k}{\pi_K} - \frac{1}{2}(\mu_k + \mu_K)^T \Sigma^{-1}(\mu_k - \mu_K) \\ &\quad + x^T \Sigma^{-1}(\mu_k - \mu_K) \\ &= \alpha_{k0} + \alpha_k^T x. \end{aligned} \quad (4.33)$$

This linearity is a consequence of the Gaussian assumption for the class densities, as well as the assumption of a common covariance matrix. The linear logistic model (4.17) by construction has linear logits:

$$\log \frac{\Pr(G = k|X = x)}{\Pr(G = K|X = x)} = \beta_{k0} + \beta_k^T x. \quad (4.34)$$

It seems that the models are the same. Although they have exactly the same form, the difference lies in the way the linear coefficients are estimated. The logistic regression model is more general, in that it makes less assumptions. We can write the *joint density* of X and G as

$$\Pr(X, G = k) = \Pr(X)\Pr(G = k|X), \quad (4.35)$$

where $\Pr(X)$ denotes the marginal density of the inputs X . For both LDA and logistic regression, the second term on the right has the logit-linear form

$$\Pr(G = k|X = x) = \frac{e^{\beta_{k0} + \beta_k^T x}}{1 + \sum_{\ell=1}^{K-1} e^{\beta_{\ell0} + \beta_\ell^T x}}, \quad (4.36)$$

where we have again arbitrarily chosen the last class as the reference.

The logistic regression model leaves the marginal density of X as an arbitrary density function $\Pr(X)$, and fits the parameters of $\Pr(G|X)$ by maximizing the *conditional likelihood*—the multinomial likelihood with probabilities the $\Pr(G = k|X)$. Although $\Pr(X)$ is totally ignored, we can think of this marginal density as being estimated in a fully nonparametric and unrestricted fashion, using the empirical distribution function which places mass $1/N$ at each observation.

With LDA we fit the parameters by maximizing the full log-likelihood, based on the joint density

$$\Pr(X, G = k) = \phi(X; \mu_k, \Sigma)\pi_k, \quad (4.37)$$

where ϕ is the Gaussian density function. Standard normal theory leads easily to the estimates $\hat{\mu}_k$, $\hat{\Sigma}$, and $\hat{\pi}_k$ given in Section 4.3. Since the linear parameters of the logistic form (4.33) are functions of the Gaussian parameters, we get their maximum-likelihood estimates by plugging in the corresponding estimates. However, unlike in the conditional case, the marginal density $\Pr(X)$ does play a role here. It is a mixture density

$$\Pr(X) = \sum_{k=1}^K \pi_k \phi(X; \mu_k, \Sigma), \quad (4.38)$$

which also involves the parameters.

What role can this additional component/restriction play? By relying on the additional model assumptions, we have more information about the parameters, and hence can estimate them more efficiently (lower variance). If in fact the true $f_k(x)$ are Gaussian, then in the worst case ignoring this marginal part of the likelihood constitutes a loss of efficiency of about 30% asymptotically in the error rate (Efron, 1975). Paraphrasing: with 30% more data, the conditional likelihood will do as well.

For example, observations far from the decision boundary (which are down-weighted by logistic regression) play a role in estimating the common covariance matrix. This is not all good news, because it also means that LDA is not robust to gross outliers.

From the mixture formulation, it is clear that even observations without class labels have information about the parameters. Often it is expensive to generate class labels, but unclassified observations come cheaply. By relying on strong model assumptions, such as here, we can use both types of information.

The marginal likelihood can be thought of as a regularizer, requiring in some sense that class densities be *visible* from this marginal view. For example, if the data in a two-class logistic regression model can be perfectly separated by a hyperplane, the maximum likelihood estimates of the parameters are undefined (i.e., infinite; see Exercise 4.5). The LDA coefficients for the same data will be well defined, since the marginal likelihood will not permit these degeneracies.

In practice these assumptions are never correct, and often some of the components of X are qualitative variables. It is generally felt that logistic regression is a safer, more robust bet than the LDA model, relying on fewer assumptions. It is our experience that the models give very similar results, even when LDA is used inappropriately, such as with qualitative predictors.

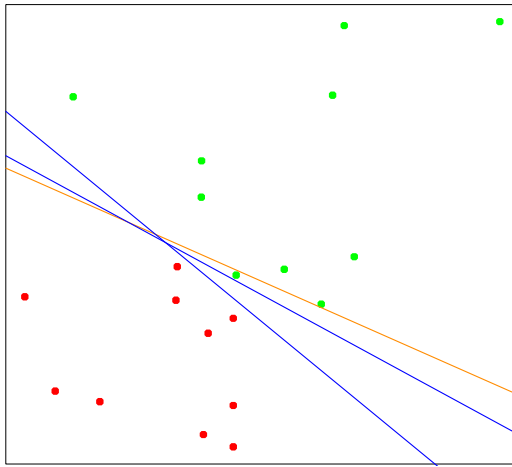


FIGURE 4.14. A toy example with two classes separable by a hyperplane. The orange line is the least squares solution, which misclassifies one of the training points. Also shown are two blue separating hyperplanes found by the perceptron learning algorithm with different random starts.

4.5 Separating Hyperplanes

We have seen that linear discriminant analysis and logistic regression both estimate linear decision boundaries in similar but slightly different ways. For the rest of this chapter we describe separating hyperplane classifiers. These procedures construct linear decision boundaries that explicitly try to separate the data into different classes as well as possible. They provide the basis for support vector classifiers, discussed in Chapter 12. The mathematical level of this section is somewhat higher than that of the previous sections.

Figure 4.14 shows 20 data points in two classes in \mathbb{R}^2 . These data can be separated by a linear boundary. Included in the figure (blue lines) are two of the infinitely many possible *separating hyperplanes*. The orange line is the least squares solution to the problem, obtained by regressing the $-1/1$ response Y on X (with intercept); the line is given by

$$\{x : \hat{\beta}_0 + \hat{\beta}_1 x_1 + \hat{\beta}_2 x_2 = 0\}. \quad (4.39)$$

This least squares solution does not do a perfect job in separating the points, and makes one error. This is the same boundary found by LDA, in light of its equivalence with linear regression in the two-class case (Section 4.3 and Exercise 4.2).

Classifiers such as (4.39), that compute a linear combination of the input features and return the sign, were called *perceptrons* in the engineering liter-

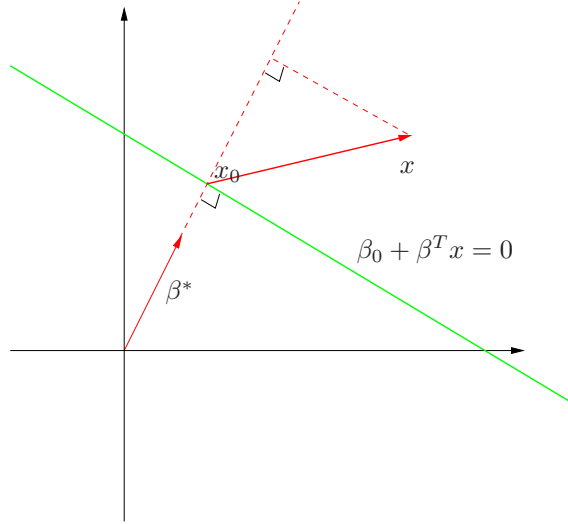


FIGURE 4.15. The linear algebra of a hyperplane (affine set).

ature in the late 1950s (Rosenblatt, 1958). Perceptrons set the foundations for the neural network models of the 1980s and 1990s.

Before we continue, let us digress slightly and review some vector algebra. Figure 4.15 depicts a hyperplane or *affine set* L defined by the equation $f(x) = \beta_0 + \beta^T x = 0$; since we are in \mathbb{R}^2 this is a line.

Here we list some properties:

1. For any two points x_1 and x_2 lying in L , $\beta^T(x_1 - x_2) = 0$, and hence $\beta^* = \beta/\|\beta\|$ is the vector normal to the surface of L .
2. For any point x_0 in L , $\beta^T x_0 = -\beta_0$.
3. The signed distance of any point x to L is given by

$$\begin{aligned}\beta^{*T}(x - x_0) &= \frac{1}{\|\beta\|}(\beta^T x + \beta_0) \\ &= \frac{1}{\|f'(x)\|}f(x).\end{aligned}\tag{4.40}$$

Hence $f(x)$ is proportional to the signed distance from x to the hyperplane defined by $f(x) = 0$.

4.5.1 Rosenblatt's Perceptron Learning Algorithm

The *perceptron learning algorithm* tries to find a separating hyperplane by minimizing the distance of misclassified points to the decision boundary. If

a response $y_i = 1$ is misclassified, then $x_i^T \beta + \beta_0 < 0$, and the opposite for a misclassified response with $y_i = -1$. The goal is to minimize

$$D(\beta, \beta_0) = - \sum_{i \in \mathcal{M}} y_i (x_i^T \beta + \beta_0), \quad (4.41)$$

where \mathcal{M} indexes the set of misclassified points. The quantity is non-negative and proportional to the distance of the misclassified points to the decision boundary defined by $\beta^T x + \beta_0 = 0$. The gradient (assuming \mathcal{M} is fixed) is given by

$$\partial \frac{D(\beta, \beta_0)}{\partial \beta} = - \sum_{i \in \mathcal{M}} y_i x_i, \quad (4.42)$$

$$\partial \frac{D(\beta, \beta_0)}{\partial \beta_0} = - \sum_{i \in \mathcal{M}} y_i. \quad (4.43)$$

The algorithm in fact uses *stochastic gradient descent* to minimize this piecewise linear criterion. This means that rather than computing the sum of the gradient contributions of each observation followed by a step in the negative gradient direction, a step is taken after each observation is visited. Hence the misclassified observations are visited in some sequence, and the parameters β are updated via

$$\begin{pmatrix} \beta \\ \beta_0 \end{pmatrix} \leftarrow \begin{pmatrix} \beta \\ \beta_0 \end{pmatrix} + \rho \begin{pmatrix} y_i x_i \\ y_i \end{pmatrix}. \quad (4.44)$$

Here ρ is the learning rate, which in this case can be taken to be 1 without loss in generality. If the classes are linearly separable, it can be shown that the algorithm converges to a separating hyperplane in a finite number of steps (Exercise 4.6). Figure 4.14 shows two solutions to a toy problem, each started at a different random guess.

There are a number of problems with this algorithm, summarized in Ripley (1996):

- When the data are separable, there are many solutions, and which one is found depends on the starting values.
- The “finite” number of steps can be very large. The smaller the gap, the longer the time to find it.
- When the data are not separable, the algorithm will not converge, and cycles develop. The cycles can be long and therefore hard to detect.

The second problem can often be eliminated by seeking a hyperplane not in the original space, but in a much enlarged space obtained by creating

many basis-function transformations of the original variables. This is analogous to driving the residuals in a polynomial regression problem down to zero by making the degree sufficiently large. Perfect separation cannot always be achieved: for example, if observations from two different classes share the same input. It may not be desirable either, since the resulting model is likely to be overfit and will not generalize well. We return to this point at the end of the next section.

A rather elegant solution to the first problem is to add additional constraints to the separating hyperplane.

4.5.2 Optimal Separating Hyperplanes



The *optimal separating hyperplane* separates the two classes and maximizes the distance to the closest point from either class (Vapnik, 1996). Not only does this provide a unique solution to the separating hyperplane problem, but by maximizing the margin between the two classes on the training data, this leads to better classification performance on test data.

We need to generalize criterion (4.41). Consider the optimization problem

$$\begin{aligned} & \max_{\beta, \beta_0, \|\beta\|=1} M \\ & \text{subject to } y_i(x_i^T \beta + \beta_0) \geq M, \quad i = 1, \dots, N. \end{aligned} \tag{4.45}$$

The set of conditions ensure that all the points are at least a signed distance M from the decision boundary defined by β and β_0 , and we seek the largest such M and associated parameters. We can get rid of the $\|\beta\| = 1$ constraint by replacing the conditions with

$$\frac{1}{\|\beta\|} y_i(x_i^T \beta + \beta_0) \geq M, \tag{4.46}$$

(which redefines β_0) or equivalently

$$y_i(x_i^T \beta + \beta_0) \geq M \|\beta\|. \tag{4.47}$$

Since for any β and β_0 satisfying these inequalities, any positively scaled multiple satisfies them too, we can arbitrarily set $\|\beta\| = 1/M$. Thus (4.45) is equivalent to

$$\begin{aligned} & \min_{\beta, \beta_0} \frac{1}{2} \|\beta\|^2 \\ & \text{subject to } y_i(x_i^T \beta + \beta_0) \geq 1, \quad i = 1, \dots, N. \end{aligned} \tag{4.48}$$

In light of (4.40), the constraints define an empty slab or margin around the linear decision boundary of thickness $1/\|\beta\|$. Hence we choose β and β_0 to maximize its thickness. This is a convex optimization problem (quadratic

criterion with linear inequality constraints). The Lagrange (primal) function, to be minimized w.r.t. β and β_0 , is

$$L_P = \frac{1}{2} \|\beta\|^2 - \sum_{i=1}^N \alpha_i [y_i(x_i^T \beta + \beta_0) - 1]. \quad (4.49)$$

Setting the derivatives to zero, we obtain:

$$\beta = \sum_{i=1}^N \alpha_i y_i x_i, \quad (4.50)$$

$$0 = \sum_{i=1}^N \alpha_i y_i, \quad (4.51)$$

and substituting these in (4.49) we obtain the so-called Wolfe dual

$$L_D = \sum_{i=1}^N \alpha_i - \frac{1}{2} \sum_{i=1}^N \sum_{k=1}^N \alpha_i \alpha_k y_i y_k x_i^T x_k$$

subject to $\alpha_i \geq 0$ and $\sum_{i=1}^N \alpha_i y_i = 0$. (4.52)

The solution is obtained by maximizing L_D in the positive orthant, a simpler convex optimization problem, for which standard software can be used. In addition the solution must satisfy the Karush–Kuhn–Tucker conditions, which include (4.50), (4.51), (4.52) and

$$\alpha_i [y_i(x_i^T \beta + \beta_0) - 1] = 0 \quad \forall i. \quad (4.53)$$

From these we can see that

- if $\alpha_i > 0$, then $y_i(x_i^T \beta + \beta_0) = 1$, or in other words, x_i is on the boundary of the slab;
- if $y_i(x_i^T \beta + \beta_0) > 1$, x_i is not on the boundary of the slab, and $\alpha_i = 0$.

From (4.50) we see that the solution vector β is defined in terms of a linear combination of the *support points* x_i —those points defined to be on the boundary of the slab via $\alpha_i > 0$. Figure 4.16 shows the optimal separating hyperplane for our toy example; there are three support points. Likewise, β_0 is obtained by solving (4.53) for any of the support points.

The optimal separating hyperplane produces a function $\hat{f}(x) = x^T \hat{\beta} + \hat{\beta}_0$ for classifying new observations:

$$\hat{G}(x) = \text{sign}(\hat{f}(x)). \quad (4.54)$$

Although none of the training observations fall in the margin (by construction), this will not necessarily be the case for test observations. The

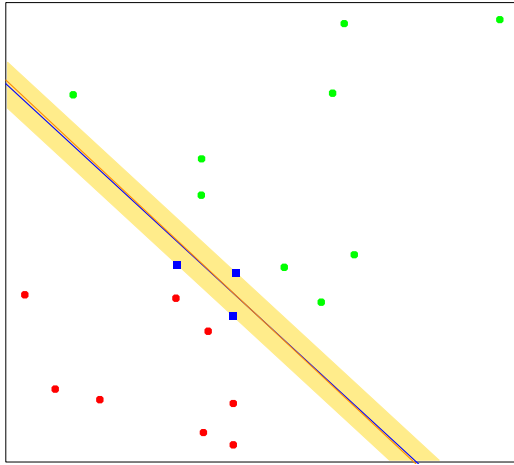


FIGURE 4.16. The same data as in Figure 4.14. The shaded region delineates the maximum margin separating the two classes. There are three support points indicated, which lie on the boundary of the margin, and the optimal separating hyperplane (blue line) bisects the slab. Included in the figure is the boundary found using logistic regression (red line), which is very close to the optimal separating hyperplane (see Section 12.3.3).

intuition is that a large margin on the training data will lead to good separation on the test data.

The description of the solution in terms of support points seems to suggest that the optimal hyperplane focuses more on the points that count, and is more robust to model misspecification. The LDA solution, on the other hand, depends on all of the data, even points far away from the decision boundary. Note, however, that the identification of these support points required the use of all the data. Of course, if the classes are really Gaussian, then LDA is optimal, and separating hyperplanes will pay a price for focusing on the (noisier) data at the boundaries of the classes.

Included in Figure 4.16 is the logistic regression solution to this problem, fit by maximum likelihood. Both solutions are similar in this case. When a separating hyperplane exists, logistic regression will always find it, since the log-likelihood can be driven to 0 in this case (Exercise 4.5). The logistic regression solution shares some other qualitative features with the separating hyperplane solution. The coefficient vector is defined by a weighted least squares fit of a zero-mean linearized response on the input features, and the weights are larger for points near the decision boundary than for those further away.

When the data are not separable, there will be no feasible solution to this problem, and an alternative formulation is needed. Again one can enlarge the space using basis transformations, but this can lead to artificial

separation through over-fitting. In Chapter 12 we discuss a more attractive alternative known as the *support vector machine*, which allows for overlap, but minimizes a measure of the extent of this overlap.

Bibliographic Notes

Good general texts on classification include Duda et al. (2000), Hand (1981), McLachlan (1992) and Ripley (1996). Mardia et al. (1979) have a concise discussion of linear discriminant analysis. Michie et al. (1994) compare a large number of popular classifiers on benchmark datasets. Linear separating hyperplanes are discussed in Vapnik (1996). Our account of the perceptron learning algorithm follows Ripley (1996).

Exercises

Ex. 4.1 Show how to solve the generalized eigenvalue problem $\max a^T \mathbf{B}a$ subject to $a^T \mathbf{W}a = 1$ by transforming to a standard eigenvalue problem.

Ex. 4.2 Suppose we have features $x \in \mathbb{R}^p$, a two-class response, with class sizes N_1, N_2 , and the target coded as $-N/N_1, N/N_2$.

(a) Show that the LDA rule classifies to class 2 if

$$x^T \hat{\Sigma}^{-1} (\hat{\mu}_2 - \hat{\mu}_1) > \frac{1}{2} (\hat{\mu}_2 + \hat{\mu}_1)^T \hat{\Sigma}^{-1} (\hat{\mu}_2 - \hat{\mu}_1) - \log(N_2/N_1),$$

and class 1 otherwise.

(b) Consider minimization of the least squares criterion

$$\sum_{i=1}^N (y_i - \beta_0 - x_i^T \beta)^2. \quad (4.55)$$

Show that the solution $\hat{\beta}$ satisfies

$$[(N-2)\hat{\Sigma} + N\hat{\Sigma}_B] \beta = N(\hat{\mu}_2 - \hat{\mu}_1) \quad (4.56)$$

(after simplification), where $\hat{\Sigma}_B = \frac{N_1 N_2}{N^2} (\hat{\mu}_2 - \hat{\mu}_1)(\hat{\mu}_2 - \hat{\mu}_1)^T$.

(c) Hence show that $\hat{\Sigma}_B \beta$ is in the direction $(\hat{\mu}_2 - \hat{\mu}_1)$ and thus

$$\hat{\beta} \propto \hat{\Sigma}^{-1} (\hat{\mu}_2 - \hat{\mu}_1). \quad (4.57)$$

Therefore the least-squares regression coefficient is identical to the LDA coefficient, up to a scalar multiple.

- (d) Show that this result holds for any (distinct) coding of the two classes.
- (e) Find the solution $\hat{\beta}_0$ (up to the same scalar multiple as in (c), and hence the predicted value $\hat{f}(x) = \hat{\beta}_0 + x^T \hat{\beta}$). Consider the following rule: classify to class 2 if $\hat{f}(x) > 0$ and class 1 otherwise. Show this is not the same as the LDA rule unless the classes have equal numbers of observations.

(Fisher, 1936; Ripley, 1996)

Ex. 4.3 Suppose we transform the original predictors \mathbf{X} to $\hat{\mathbf{Y}}$ via linear regression. In detail, let $\hat{\mathbf{Y}} = \mathbf{X}(\mathbf{X}^T \mathbf{X})^{-1} \mathbf{X}^T \mathbf{Y} = \mathbf{X}\hat{\mathbf{B}}$, where \mathbf{Y} is the indicator response matrix. Similarly for any input $x \in \mathbb{R}^p$, we get a transformed vector $\hat{y} = \hat{\mathbf{B}}^T x \in \mathbb{R}^K$. Show that LDA using $\hat{\mathbf{Y}}$ is identical to LDA in the original space.

Ex. 4.4 Consider the multilogit model with K classes (4.17). Let β be the $(p+1)(K-1)$ -vector consisting of all the coefficients. Define a suitably enlarged version of the input vector x to accommodate this vectorized coefficient matrix. Derive the Newton-Raphson algorithm for maximizing the multinomial log-likelihood, and describe how you would implement this algorithm.

Ex. 4.5 Consider a two-class logistic regression problem with $x \in \mathbb{R}$. Characterize the maximum-likelihood estimates of the slope and intercept parameter if the sample x_i for the two classes are separated by a point $x_0 \in \mathbb{R}$. Generalize this result to (a) $x \in \mathbb{R}^p$ (see Figure 4.16), and (b) more than two classes.

Ex. 4.6 Suppose we have N points x_i in \mathbb{R}^p in general position, with class labels $y_i \in \{-1, 1\}$. Prove that the perceptron learning algorithm converges to a separating hyperplane in a finite number of steps:

- (a) Denote a hyperplane by $f(x) = \beta_1^T x + \beta_0 = 0$, or in more compact notation $\beta^T x^* = 0$, where $x^* = (x, 1)$ and $\beta = (\beta_1, \beta_0)$. Let $z_i = x_i^*/\|x_i^*\|$. Show that separability implies the existence of a β_{sep} such that $y_i \beta_{\text{sep}}^T z_i \geq 1 \forall i$
- (b) Given a current β_{old} , the perceptron algorithm identifies a point z_i that is misclassified, and produces the update $\beta_{\text{new}} \leftarrow \beta_{\text{old}} + y_i z_i$. Show that $\|\beta_{\text{new}} - \beta_{\text{sep}}\|^2 \leq \|\beta_{\text{old}} - \beta_{\text{sep}}\|^2 - 1$, and hence that the algorithm converges to a separating hyperplane in no more than $\|\beta_{\text{start}} - \beta_{\text{sep}}\|^2$ steps (Ripley, 1996).

Ex. 4.7 Consider the criterion

$$D^*(\beta, \beta_0) = - \sum_{i=1}^N y_i (x_i^T \beta + \beta_0), \quad (4.58)$$

a generalization of (4.41) where we sum over all the observations. Consider minimizing D^* subject to $\|\beta\| = 1$. Describe this criterion in words. Does it solve the optimal separating hyperplane problem?

Ex. 4.8 Consider the multivariate Gaussian model $X|G = k \sim N(\mu_k, \Sigma)$, with the additional restriction that $\text{rank}\{\mu_k\}_1^K = L < \max(K - 1, p)$. Derive the constrained MLEs for the μ_k and Σ . Show that the Bayes classification rule is equivalent to classifying in the reduced subspace computed by LDA (Hastie and Tibshirani, 1996b).

Ex. 4.9 Write a computer program to perform a quadratic discriminant analysis by fitting a separate Gaussian model per class. Try it out on the vowel data, and compute the misclassification error for the test data. The data can be found in the book website www-stat.stanford.edu/ElemStatLearn.

5

Basis Expansions and Regularization

5.1 Introduction

We have already made use of models linear in the input features, both for regression and classification. Linear regression, linear discriminant analysis, logistic regression and separating hyperplanes all rely on a linear model. It is extremely unlikely that the true function $f(X)$ is actually linear in X . In regression problems, $f(X) = E(Y|X)$ will typically be nonlinear and nonadditive in X , and representing $f(X)$ by a linear model is usually a convenient, and sometimes a necessary, approximation. Convenient because a linear model is easy to interpret, and is the first-order Taylor approximation to $f(X)$. Sometimes necessary, because with N small and/or p large, a linear model might be all we are able to fit to the data without overfitting. Likewise in classification, a linear, Bayes-optimal decision boundary implies that some monotone transformation of $\Pr(Y = 1|X)$ is linear in X . This is inevitably an approximation.

In this chapter and the next we discuss popular methods for moving beyond linearity. The core idea in this chapter is to augment/replace the vector of inputs X with additional variables, which are transformations of X , and then use linear models in this new space of derived input features.

Denote by $h_m(X) : \mathbb{R}^p \mapsto \mathbb{R}$ the m th transformation of X , $m = 1, \dots, M$. We then model

$$f(X) = \sum_{m=1}^M \beta_m h_m(X), \quad (5.1)$$

a *linear basis expansion* in X . The beauty of this approach is that once the basis functions h_m have been determined, the models are linear in these new variables, and the fitting proceeds as before.

Some simple and widely used examples of the h_m are the following:

- $h_m(X) = X_m$, $m = 1, \dots, p$ recovers the original linear model.
- $h_m(X) = X_j^2$ or $h_m(X) = X_j X_k$ allows us to augment the inputs with polynomial terms to achieve higher-order Taylor expansions. Note, however, that the number of variables grows exponentially in the degree of the polynomial. A full quadratic model in p variables requires $O(p^2)$ square and cross-product terms, or more generally $O(p^d)$ for a degree- d polynomial.
- $h_m(X) = \log(X_j)$, $\sqrt{X_j}, \dots$ permits other nonlinear transformations of single inputs. More generally one can use similar functions involving several inputs, such as $h_m(X) = \|X\|$.
- $h_m(X) = I(L_m \leq X_k < U_m)$, an indicator for a region of X_k . By breaking the range of X_k up into M_k such nonoverlapping regions results in a model with a piecewise constant contribution for X_k .

Sometimes the problem at hand will call for particular basis functions h_m , such as logarithms or power functions. More often, however, we use the basis expansions as a device to achieve more flexible representations for $f(X)$. Polynomials are an example of the latter, although they are limited by their global nature—tweaking the coefficients to achieve a functional form in one region can cause the function to flap about madly in remote regions. In this chapter we consider more useful families of *piecewise-polynomials* and *splines* that allow for local polynomial representations. We also discuss the *wavelet* bases, especially useful for modeling signals and images. These methods produce a *dictionary* \mathcal{D} consisting of typically a very large number $|\mathcal{D}|$ of basis functions, far more than we can afford to fit to our data. Along with the dictionary we require a method for controlling the complexity of our model, using basis functions from the dictionary. There are three common approaches:

- Restriction methods, where we decide before-hand to limit the class of functions. Additivity is an example, where we assume that our model has the form

$$\begin{aligned} f(X) &= \sum_{j=1}^p f_j(X_j) \\ &= \sum_{j=1}^p \sum_{m=1}^{M_j} \beta_{jm} h_{jm}(X_j). \end{aligned} \tag{5.2}$$

The size of the model is limited by the number of basis functions M_j used for each component function f_j .

- Selection methods, which adaptively scan the dictionary and include only those basis functions h_m that contribute significantly to the fit of the model. Here the variable selection techniques discussed in Chapter 3 are useful. The stagewise greedy approaches such as CART, MARS and boosting fall into this category as well.
- Regularization methods where we use the entire dictionary but restrict the coefficients. Ridge regression is a simple example of a regularization approach, while the lasso is both a regularization and selection method. Here we discuss these and more sophisticated methods for regularization.

5.2 Piecewise Polynomials and Splines

We assume until Section 5.7 that X is one-dimensional. A piecewise polynomial function $f(X)$ is obtained by dividing the domain of X into contiguous intervals, and representing f by a separate polynomial in each interval. Figure 5.1 shows two simple piecewise polynomials. The first is piecewise constant, with three basis functions:

$$h_1(X) = I(X < \xi_1), \quad h_2(X) = I(\xi_1 \leq X < \xi_2), \quad h_3(X) = I(\xi_2 \leq X).$$

Since these are positive over disjoint regions, the least squares estimate of the model $f(X) = \sum_{m=1}^3 \beta_m h_m(X)$ amounts to $\hat{\beta}_m = \bar{Y}_m$, the mean of Y in the m th region.

The top right panel shows a piecewise linear fit. Three additional basis functions are needed: $h_{m+3} = h_m(X)X$, $m = 1, \dots, 3$. Except in special cases, we would typically prefer the third panel, which is also piecewise linear, but restricted to be continuous at the two knots. These continuity restrictions lead to linear constraints on the parameters; for example, $f(\xi_1^-) = f(\xi_1^+)$ implies that $\beta_1 + \xi_1\beta_4 = \beta_2 + \xi_1\beta_5$. In this case, since there are two restrictions, we expect to *get back* two parameters, leaving four free parameters.

A more direct way to proceed in this case is to use a basis that incorporates the constraints:

$$h_1(X) = 1, \quad h_2(X) = X, \quad h_3(X) = (X - \xi_1)_+, \quad h_4(X) = (X - \xi_2)_+,$$

where t_+ denotes the positive part. The function h_3 is shown in the lower right panel of Figure 5.1. We often prefer smoother functions, and these can be achieved by increasing the order of the local polynomial. Figure 5.2 shows a series of piecewise-cubic polynomials fit to the same data, with

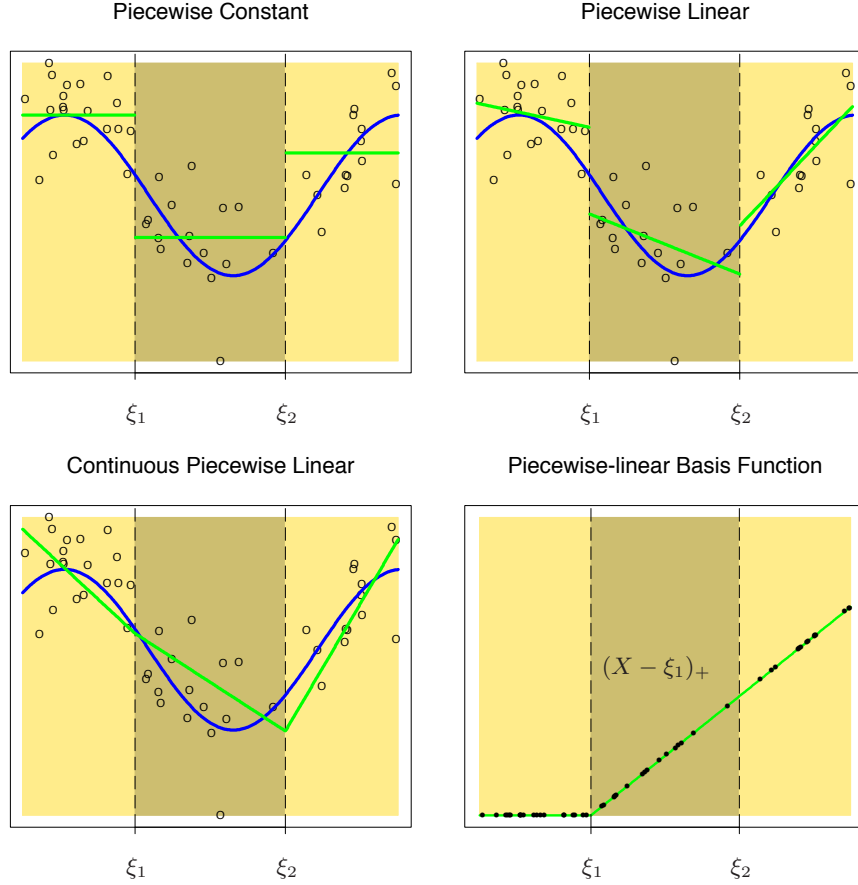


FIGURE 5.1. The top left panel shows a piecewise constant function fit to some artificial data. The broken vertical lines indicate the positions of the two knots ξ_1 and ξ_2 . The blue curve represents the true function, from which the data were generated with Gaussian noise. The remaining two panels show piecewise linear functions fit to the same data—the top right unrestricted, and the lower left restricted to be continuous at the knots. The lower right panel shows a piecewise-linear basis function, $h_3(X) = (X - \xi_1)_+$, continuous at ξ_1 . The black points indicate the sample evaluations $h_3(x_i)$, $i = 1, \dots, N$.

Piecewise Cubic Polynomials

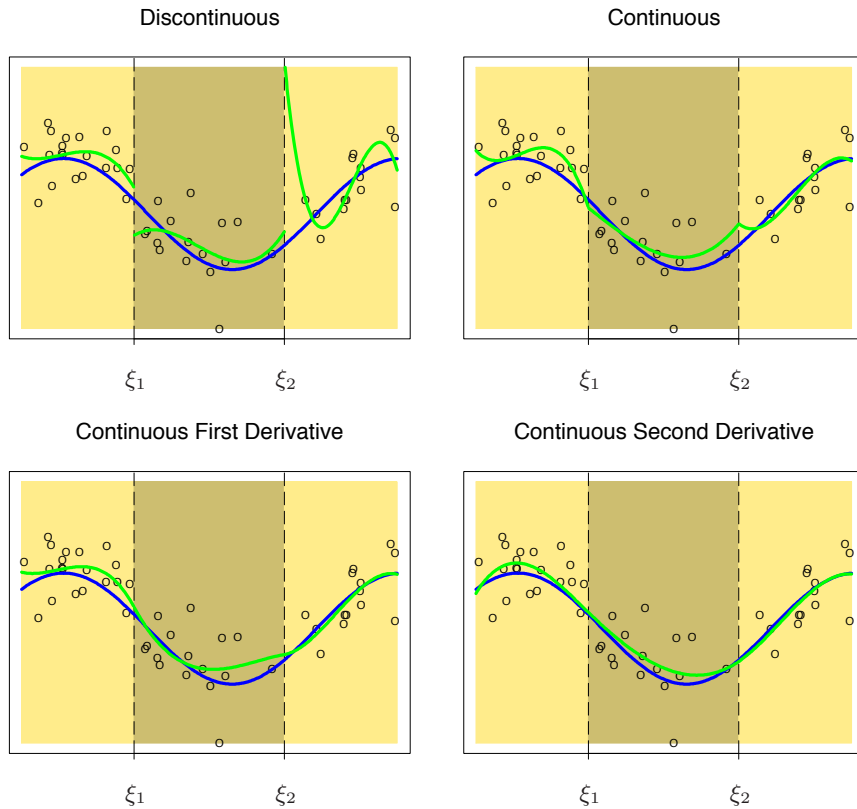


FIGURE 5.2. A series of piecewise-cubic polynomials, with increasing orders of continuity.

increasing orders of continuity at the knots. The function in the lower right panel is continuous, and has continuous first and second derivatives at the knots. It is known as a *cubic spline*. Enforcing one more order of continuity would lead to a global cubic polynomial. It is not hard to show (Exercise 5.1) that the following basis represents a cubic spline with knots at ξ_1 and ξ_2 :

$$\begin{aligned} h_1(X) &= 1, & h_3(X) &= X^2, & h_5(X) &= (X - \xi_1)_+^3, \\ h_2(X) &= X, & h_4(X) &= X^3, & h_6(X) &= (X - \xi_2)_+^3. \end{aligned} \quad (5.3)$$

There are six basis functions corresponding to a six-dimensional linear space of functions. A quick check confirms the parameter count: $(3 \text{ regions}) \times (4 \text{ parameters per region}) - (2 \text{ knots}) \times (3 \text{ constraints per knot}) = 6$.

More generally, an order- M spline with knots ξ_j , $j = 1, \dots, K$ is a piecewise-polynomial of order M , and has continuous derivatives up to order $M - 2$. A cubic spline has $M = 4$. In fact the piecewise-constant function in Figure 5.1 is an order-1 spline, while the continuous piecewise linear function is an order-2 spline. Likewise the general form for the truncated-power basis set would be

$$\begin{aligned} h_j(X) &= X^{j-1}, \quad j = 1, \dots, M, \\ h_{M+\ell}(X) &= (X - \xi_\ell)_+^{M-1}, \quad \ell = 1, \dots, K. \end{aligned}$$

It is claimed that cubic splines are the lowest-order spline for which the knot-discontinuity is not visible to the human eye. There is seldom any good reason to go beyond cubic-splines, unless one is interested in smooth derivatives. In practice the most widely used orders are $M = 1, 2$ and 4 .

These fixed-knot splines are also known as *regression splines*. One needs to select the order of the spline, the number of knots and their placement. One simple approach is to parameterize a family of splines by the number of basis functions or degrees of freedom, and have the observations x_i determine the positions of the knots. For example, the expression `bs(x, df=7)` in R generates a basis matrix of cubic-spline functions evaluated at the N observations in `x`, with the $7 - 3 = 4^1$ interior knots at the appropriate percentiles of `x` (20, 40, 60 and 80th.) One can be more explicit, however; `bs(x, degree=1, knots = c(0.2, 0.4, 0.6))` generates a basis for linear splines, with three interior knots, and returns an $N \times 4$ matrix.

Since the space of spline functions of a particular order and knot sequence is a vector space, there are many equivalent bases for representing them (just as there are for ordinary polynomials.) While the truncated power basis is conceptually simple, it is not too attractive numerically: powers of large numbers can lead to severe rounding problems. The *B-spline* basis, described in the Appendix to this chapter, allows for efficient computations even when the number of knots K is large.

5.2.1 Natural Cubic Splines

We know that the behavior of polynomials fit to data tends to be erratic near the boundaries, and extrapolation can be dangerous. These problems are exacerbated with splines. The polynomials fit beyond the boundary knots behave even more wildly than the corresponding global polynomials in that region. This can be conveniently summarized in terms of the pointwise variance of spline functions fit by least squares (see the example in the next section for details on these variance calculations). Figure 5.3 compares

¹A cubic spline with four knots is eight-dimensional. The `bs()` function omits by default the constant term in the basis, since terms like this are typically included with other terms in the model.

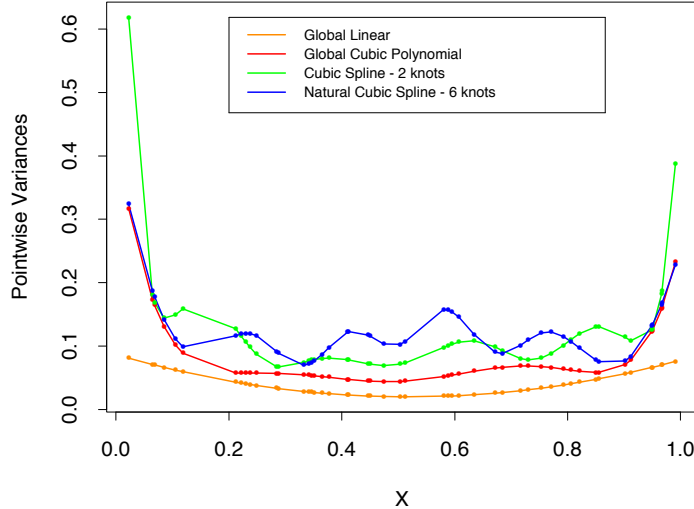


FIGURE 5.3. Pointwise variance curves for four different models, with X consisting of 50 points drawn at random from $U[0, 1]$, and an assumed error model with constant variance. The linear and cubic polynomial fits have two and four degrees of freedom, respectively, while the cubic spline and natural cubic spline each have six degrees of freedom. The cubic spline has two knots at 0.33 and 0.66, while the natural spline has boundary knots at 0.1 and 0.9, and four interior knots uniformly spaced between them.

the pointwise variances for a variety of different models. The explosion of the variance near the boundaries is clear, and inevitably is worst for cubic splines.

A *natural cubic spline* adds additional constraints, namely that the function is linear beyond the boundary knots. This frees up four degrees of freedom (two constraints each in both boundary regions), which can be spent more profitably by sprinkling more knots in the interior region. This tradeoff is illustrated in terms of variance in Figure 5.3. There will be a price paid in bias near the boundaries, but assuming the function is linear near the boundaries (where we have less information anyway) is often considered reasonable.

A natural cubic spline with K knots is represented by K basis functions. One can start from a basis for cubic splines, and derive the reduced basis by imposing the boundary constraints. For example, starting from the truncated power series basis described in Section 5.2, we arrive at (Exercise 5.4):

$$N_1(X) = 1, \quad N_2(X) = X, \quad N_{k+2}(X) = d_k(X) - d_{K-1}(X), \quad (5.4)$$

where

$$d_k(X) = \frac{(X - \xi_k)_+^3 - (X - \xi_K)_+^3}{\xi_K - \xi_k}. \quad (5.5)$$

Each of these basis functions can be seen to have zero second and third derivative for $X \geq \xi_K$.

5.2.2 Example: South African Heart Disease (Continued)

In Section 4.4.2 we fit linear logistic regression models to the South African heart disease data. Here we explore nonlinearities in the functions using natural splines. The functional form of the model is

$$\text{logit}[\Pr(\text{chd}|X)] = \theta_0 + h_1(X_1)^T \theta_1 + h_2(X_2)^T \theta_2 + \cdots + h_p(X_p)^T \theta_p, \quad (5.6)$$

where each of the θ_j are vectors of coefficients multiplying their associated vector of natural spline basis functions h_j .

We use four natural spline bases for each term in the model. For example, with X_1 representing `sbp`, $h_1(X_1)$ is a basis consisting of four basis functions. This actually implies three rather than two interior knots (chosen at uniform quantiles of `sbp`), plus two boundary knots at the extremes of the data, since we exclude the constant term from each of the h_j .

Since `famhist` is a two-level factor, it is coded by a simple binary or dummy variable, and is associated with a single coefficient in the fit of the model.

More compactly we can combine all p vectors of basis functions (and the constant term) into one big vector $h(X)$, and then the model is simply $h(X)^T \theta$, with total number of parameters $\text{df} = 1 + \sum_{j=1}^p \text{df}_j$, the sum of the parameters in each component term. Each basis function is evaluated at each of the N samples, resulting in a $N \times \text{df}$ basis matrix \mathbf{H} . At this point the model is like any other linear logistic model, and the algorithms described in Section 4.4.1 apply.

We carried out a backward stepwise deletion process, dropping terms from this model while preserving the group structure of each term, rather than dropping one coefficient at a time. The AIC statistic (Section 7.5) was used to drop terms, and all the terms remaining in the final model would cause AIC to increase if deleted from the model (see Table 5.1). Figure 5.4 shows a plot of the final model selected by the stepwise regression. The functions displayed are $\hat{f}_j(X_j) = h_j(X_j)^T \hat{\theta}_j$ for each variable X_j . The covariance matrix $\text{Cov}(\hat{\theta}) = \Sigma$ is estimated by $\hat{\Sigma} = (\mathbf{H}^T \mathbf{W} \mathbf{H})^{-1}$, where \mathbf{W} is the diagonal weight matrix from the logistic regression. Hence $v_j(X_j) = \text{Var}[\hat{f}_j(X_j)] = h_j(X_j)^T \hat{\Sigma}_{jj} h_j(X_j)$ is the pointwise variance function of \hat{f}_j , where $\text{Cov}(\hat{\theta}_j) = \hat{\Sigma}_{jj}$ is the appropriate sub-matrix of $\hat{\Sigma}$. The shaded region in each panel is defined by $\hat{f}_j(X_j) \pm 2\sqrt{v_j(X_j)}$.

The AIC statistic is slightly more generous than the likelihood-ratio test (deviance test). Both `sbp` and `obesity` are included in this model, while

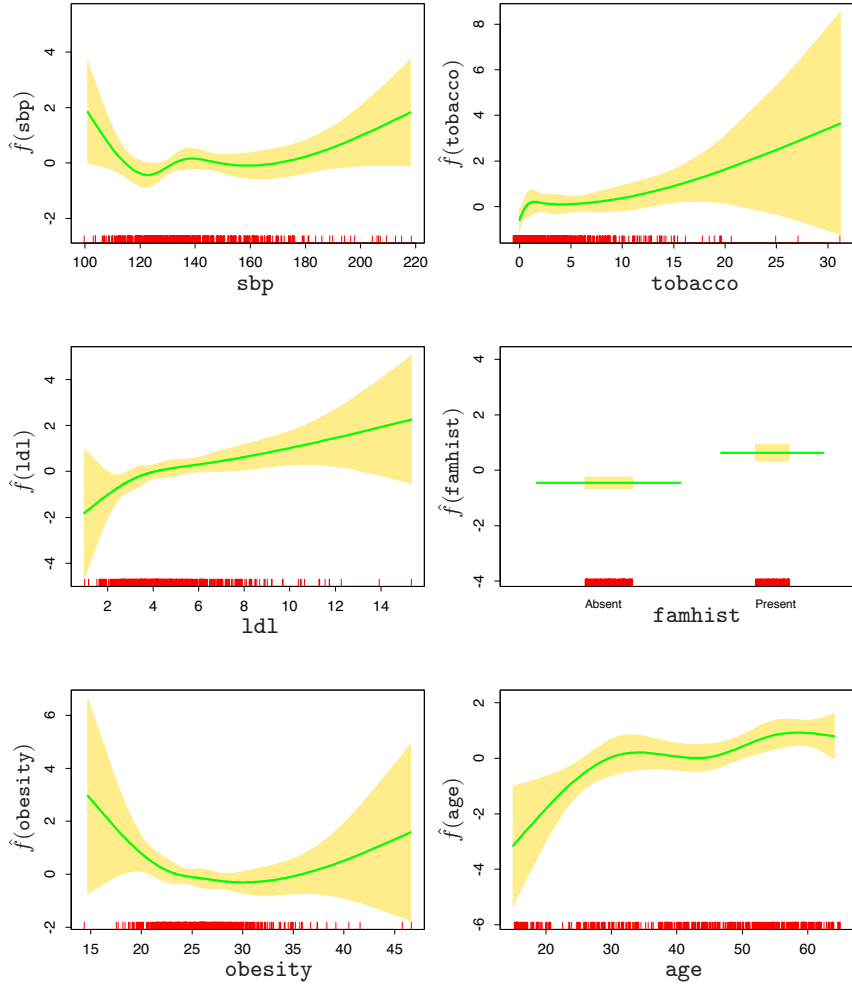


FIGURE 5.4. Fitted natural-spline functions for each of the terms in the final model selected by the stepwise procedure. Included are pointwise standard-error bands. The rug plot at the base of each figure indicates the location of each of the sample values for that variable (jittered to break ties).

TABLE 5.1. Final logistic regression model, after stepwise deletion of natural splines terms. The column labeled “LRT” is the likelihood-ratio test statistic when that term is deleted from the model, and is the change in deviance from the full model (labeled “none”).

Terms	Df	Deviance	AIC	LRT	P-value
none		458.09	502.09		
sbp	4	467.16	503.16	9.076	0.059
tobacco	4	470.48	506.48	12.387	0.015
ldl	4	472.39	508.39	14.307	0.006
famhist	1	479.44	521.44	21.356	0.000
obesity	4	466.24	502.24	8.147	0.086
age	4	481.86	517.86	23.768	0.000

they were not in the linear model. The figure explains why, since their contributions are inherently nonlinear. These effects at first may come as a surprise, but an explanation lies in the nature of the retrospective data. These measurements were made sometime after the patients suffered a heart attack, and in many cases they had already benefited from a healthier diet and lifestyle, hence the apparent *increase* in risk at low values for `obesity` and `sbp`. Table 5.1 shows a summary of the selected model.

5.2.3 Example: Phoneme Recognition

In this example we use splines to reduce flexibility rather than increase it; the application comes under the general heading of *functional* modeling. In the top panel of Figure 5.5 are displayed a sample of 15 log-periodograms for each of the two phonemes “aa” and “ao” measured at 256 frequencies. The goal is to use such data to classify a spoken phoneme. These two phonemes were chosen because they are difficult to separate.

The input feature is a vector x of length 256, which we can think of as a vector of evaluations of a function $X(f)$ over a grid of frequencies f . In reality there is a continuous analog signal which is a function of frequency, and we have a sampled version of it.

The gray lines in the lower panel of Figure 5.5 show the coefficients of a linear logistic regression model fit by maximum likelihood to a training sample of 1000 drawn from the total of 695 “aa”s and 1022 “ao”s. The coefficients are also plotted as a function of frequency, and in fact we can think of the model in terms of its continuous counterpart

$$\log \frac{\Pr(\text{aa}|X)}{\Pr(\text{ao}|X)} = \int X(f)\beta(f)df, \quad (5.7)$$

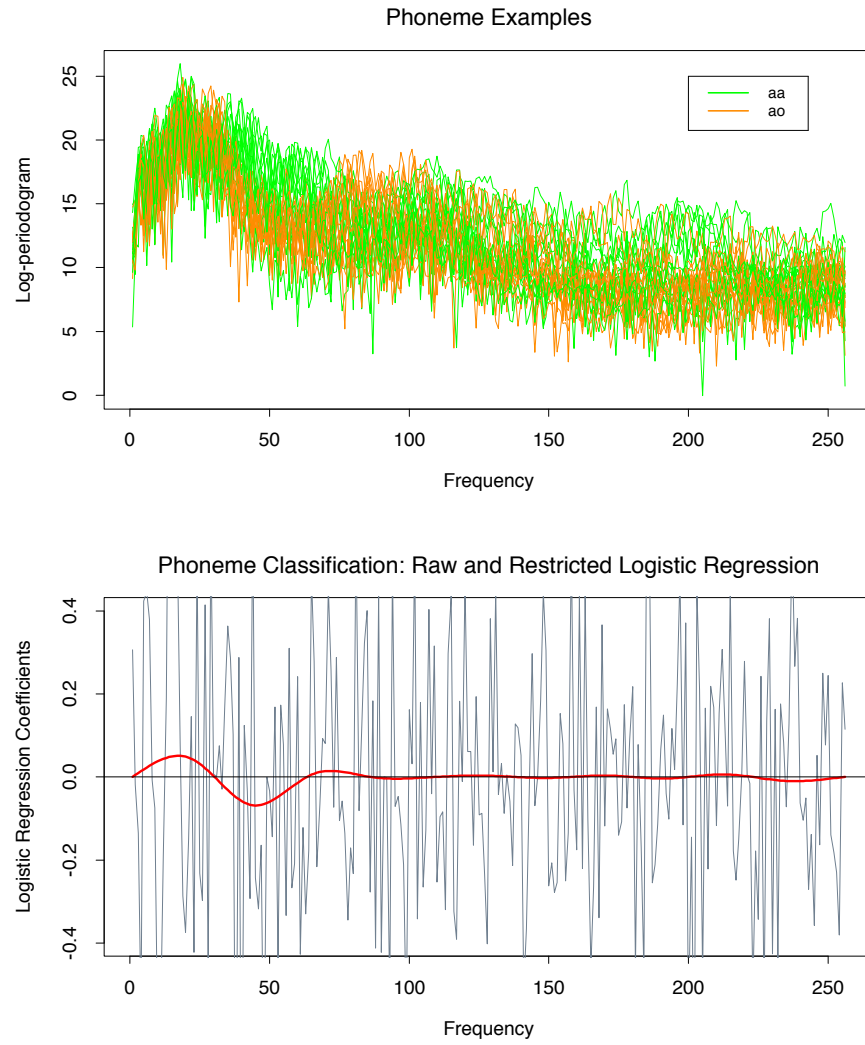


FIGURE 5.5. The top panel displays the log-periodogram as a function of frequency for 15 examples each of the phonemes “aa” and “ao” sampled from a total of 695 “aa”s and 1022 “ao”s. Each log-periodogram is measured at 256 uniformly spaced frequencies. The lower panel shows the coefficients (as a function of frequency) of a logistic regression fit to the data by maximum likelihood, using the 256 log-periodogram values as inputs. The coefficients are restricted to be smooth in the red curve, and are unrestricted in the jagged gray curve.

which we approximate by

$$\sum_{j=1}^{256} X(f_j) \beta(f_j) = \sum_{j=1}^{256} x_j \beta_j. \quad (5.8)$$

The coefficients compute a contrast functional, and will have appreciable values in regions of frequency where the log-periodograms differ between the two classes.

The gray curves are very rough. Since the input signals have fairly strong positive autocorrelation, this results in negative autocorrelation in the coefficients. In addition the sample size effectively provides only four observations per coefficient.

Applications such as this permit a natural regularization. We force the coefficients to vary smoothly as a function of frequency. The red curve in the lower panel of Figure 5.5 shows such a smooth coefficient curve fit to these data. We see that the lower frequencies offer the most discriminatory power. Not only does the smoothing allow easier interpretation of the contrast, it also produces a more accurate classifier:

	Raw	Regularized
Training error	0.080	0.185
Test error	0.255	0.158

The smooth red curve was obtained through a very simple use of natural cubic splines. We can represent the coefficient function as an expansion of splines $\beta(f) = \sum_{m=1}^M h_m(f)\theta_m$. In practice this means that $\beta = \mathbf{H}\theta$ where, \mathbf{H} is a $p \times M$ basis matrix of natural cubic splines, defined on the set of frequencies. Here we used $M = 12$ basis functions, with knots uniformly placed over the integers $1, 2, \dots, 256$ representing the frequencies. Since $x^T\beta = x^T\mathbf{H}\theta$, we can simply replace the input features x by their *filtered* versions $x^* = \mathbf{H}^Tx$, and fit θ by linear logistic regression on the x^* . The red curve is thus $\hat{\beta}(f) = h(f)^T\hat{\theta}$.

5.3 Filtering and Feature Extraction

In the previous example, we constructed a $p \times M$ basis matrix \mathbf{H} , and then transformed our features x into new features $x^* = \mathbf{H}^Tx$. These filtered versions of the features were then used as inputs into a learning procedure: in the previous example, this was linear logistic regression.

Preprocessing of high-dimensional features is a very general and powerful method for improving the performance of a learning algorithm. The preprocessing need not be linear as it was above, but can be a general

(nonlinear) function of the form $x^* = g(x)$. The derived features x^* can then be used as inputs into any (linear or nonlinear) learning procedure.

For example, for signal or image recognition a popular approach is to first transform the raw features via a wavelet transform $x^* = \mathbf{H}^T x$ (Section 5.9) and then use the features x^* as inputs into a neural network (Chapter 11). Wavelets are effective in capturing discrete jumps or edges, and the neural network is a powerful tool for constructing nonlinear functions of these features for predicting the target variable. By using domain knowledge to construct appropriate features, one can often improve upon a learning method that has only the raw features x at its disposal.

5.4 Smoothing Splines

Here we discuss a spline basis method that avoids the knot selection problem completely by using a maximal set of knots. The complexity of the fit is controlled by regularization. Consider the following problem: among all functions $f(x)$ with two continuous derivatives, find one that minimizes the penalized residual sum of squares

$$\text{RSS}(f, \lambda) = \sum_{i=1}^N \{y_i - f(x_i)\}^2 + \lambda \int \{f''(t)\}^2 dt, \quad (5.9)$$

where λ is a fixed *smoothing parameter*. The first term measures closeness to the data, while the second term penalizes curvature in the function, and λ establishes a tradeoff between the two. Two special cases are:

$\lambda = 0$: f can be any function that interpolates the data.

$\lambda = \infty$: the simple least squares line fit, since no second derivative can be tolerated.

These vary from very rough to very smooth, and the hope is that $\lambda \in (0, \infty)$ indexes an interesting class of functions in between.

The criterion (5.9) is defined on an infinite-dimensional function space—in fact, a Sobolev space of functions for which the second term is defined. Remarkably, it can be shown that (5.9) has an explicit, finite-dimensional, unique minimizer which is a natural cubic spline with knots at the unique values of the x_i , $i = 1, \dots, N$ (Exercise 5.7). At face value it seems that the family is still over-parametrized, since there are as many as N knots, which implies N degrees of freedom. However, the penalty term translates to a penalty on the spline coefficients, which are shrunk some of the way toward the linear fit.

Since the solution is a natural spline, we can write it as

$$f(x) = \sum_{j=1}^N N_j(x) \theta_j, \quad (5.10)$$

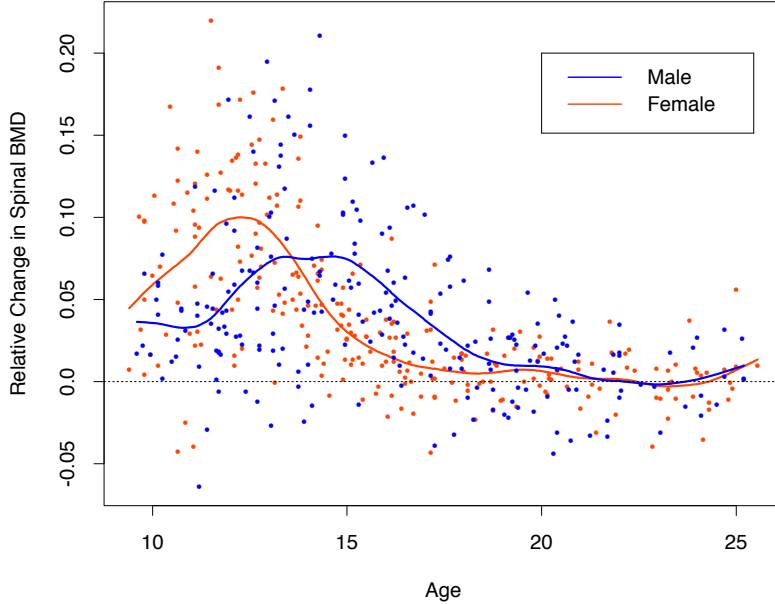


FIGURE 5.6. The response is the relative change in bone mineral density measured at the spine in adolescents, as a function of age. A separate smoothing spline was fit to the males and females, with $\lambda \approx 0.00022$. This choice corresponds to about 12 degrees of freedom.

where the $N_j(x)$ are an N -dimensional set of basis functions for representing this family of natural splines (Section 5.2.1 and Exercise 5.4). The criterion thus reduces to

$$\text{RSS}(\theta, \lambda) = (\mathbf{y} - \mathbf{N}\theta)^T(\mathbf{y} - \mathbf{N}\theta) + \lambda\theta^T\Omega_N\theta, \quad (5.11)$$

where $\{\mathbf{N}\}_{ij} = N_j(x_i)$ and $\{\Omega_N\}_{jk} = \int N_j''(t)N_k''(t)dt$. The solution is easily seen to be

$$\hat{\theta} = (\mathbf{N}^T\mathbf{N} + \lambda\Omega_N)^{-1}\mathbf{N}^T\mathbf{y}, \quad (5.12)$$

a generalized ridge regression. The fitted smoothing spline is given by

$$\hat{f}(x) = \sum_{j=1}^N N_j(x)\hat{\theta}_j. \quad (5.13)$$

Efficient computational techniques for smoothing splines are discussed in the Appendix to this chapter.

Figure 5.6 shows a smoothing spline fit to some data on bone mineral density (BMD) in adolescents. The response is relative change in spinal BMD over two consecutive visits, typically about one year apart. The data are color coded by gender, and two separate curves were fit. This simple

summary reinforces the evidence in the data that the growth spurt for females precedes that for males by about two years. In both cases the smoothing parameter λ was approximately 0.00022; this choice is discussed in the next section.

5.4.1 Degrees of Freedom and Smoother Matrices

We have not yet indicated how λ is chosen for the smoothing spline. Later in this chapter we describe automatic methods using techniques such as cross-validation. In this section we discuss intuitive ways of prespecifying the amount of smoothing.

A smoothing spline with prechosen λ is an example of a *linear smoother* (as in linear operator). This is because the estimated parameters in (5.12) are a linear combination of the y_i . Denote by $\hat{\mathbf{f}}$ the N -vector of fitted values $\hat{f}(x_i)$ at the training predictors x_i . Then

$$\begin{aligned}\hat{\mathbf{f}} &= \mathbf{N}(\mathbf{N}^T \mathbf{N} + \lambda \boldsymbol{\Omega}_N)^{-1} \mathbf{N}^T \mathbf{y} \\ &= \mathbf{S}_\lambda \mathbf{y}.\end{aligned}\tag{5.14}$$

Again the fit is linear in \mathbf{y} , and the finite linear operator \mathbf{S}_λ is known as the *smoother matrix*. One consequence of this linearity is that the recipe for producing $\hat{\mathbf{f}}$ from \mathbf{y} does not depend on \mathbf{y} itself; \mathbf{S}_λ depends only on the x_i and λ .

Linear operators are familiar in more traditional least squares fitting as well. Suppose \mathbf{B}_ξ is a $N \times M$ matrix of M cubic-spline basis functions evaluated at the N training points x_i , with knot sequence ξ , and $M \ll N$. Then the vector of fitted spline values is given by

$$\begin{aligned}\hat{\mathbf{f}} &= \mathbf{B}_\xi (\mathbf{B}_\xi^T \mathbf{B}_\xi)^{-1} \mathbf{B}_\xi^T \mathbf{y} \\ &= \mathbf{H}_\xi \mathbf{y}.\end{aligned}\tag{5.15}$$

Here the linear operator \mathbf{H}_ξ is a projection operator, also known as the *hat matrix* in statistics. There are some important similarities and differences between \mathbf{H}_ξ and \mathbf{S}_λ :

- Both are symmetric, positive semidefinite matrices.
- $\mathbf{H}_\xi \mathbf{H}_\xi = \mathbf{H}_\xi$ (idempotent), while $\mathbf{S}_\lambda \mathbf{S}_\lambda \preceq \mathbf{S}_\lambda$, meaning that the right-hand side exceeds the left-hand side by a positive semidefinite matrix. This is a consequence of the *shrinking* nature of \mathbf{S}_λ , which we discuss further below.
- \mathbf{H}_ξ has rank M , while \mathbf{S}_λ has rank N .

The expression $M = \text{trace}(\mathbf{H}_\xi)$ gives the dimension of the projection space, which is also the number of basis functions, and hence the number of parameters involved in the fit. By analogy we define the *effective degrees of*

freedom of a smoothing spline to be

$$df_\lambda = \text{trace}(\mathbf{S}_\lambda), \quad (5.16)$$

the sum of the diagonal elements of \mathbf{S}_λ . This very useful definition allows us a more intuitive way to parameterize the smoothing spline, and indeed many other smoothers as well, in a consistent fashion. For example, in Figure 5.6 we specified $df_\lambda = 12$ for each of the curves, and the corresponding $\lambda \approx 0.00022$ was derived numerically by solving $\text{trace}(\mathbf{S}_\lambda) = 12$. There are many arguments supporting this definition of degrees of freedom, and we cover some of them here.

Since \mathbf{S}_λ is symmetric (and positive semidefinite), it has a real eigen-decomposition. Before we proceed, it is convenient to rewrite \mathbf{S}_λ in the *Reinsch* form

$$\mathbf{S}_\lambda = (\mathbf{I} + \lambda \mathbf{K})^{-1}, \quad (5.17)$$

where \mathbf{K} does not depend on λ (Exercise 5.9). Since $\hat{\mathbf{f}} = \mathbf{S}_\lambda \mathbf{y}$ solves

$$\min_{\mathbf{f}} \mathbf{y}^T (\mathbf{y} - \mathbf{f})^T (\mathbf{y} - \mathbf{f}) + \lambda \mathbf{f}^T \mathbf{K} \mathbf{f}, \quad (5.18)$$

\mathbf{K} is known as the *penalty matrix*, and indeed a quadratic form in \mathbf{K} has a representation in terms of a weighted sum of squared (divided) second differences. The eigen-decomposition of \mathbf{S}_λ is

$$\mathbf{S}_\lambda = \sum_{k=1}^N \rho_k(\lambda) \mathbf{u}_k \mathbf{u}_k^T \quad (5.19)$$

with

$$\rho_k(\lambda) = \frac{1}{1 + \lambda d_k}, \quad (5.20)$$

and d_k the corresponding eigenvalue of \mathbf{K} . Figure 5.7 (top) shows the results of applying a cubic smoothing spline to some air pollution data (128 observations). Two fits are given: a *smoother* fit corresponding to a larger penalty λ and a *rougher* fit for a smaller penalty. The lower panels represent the eigenvalues (lower left) and some eigenvectors (lower right) of the corresponding smoother matrices. Some of the highlights of the eigenrepresentation are the following:

- The eigenvectors are not affected by changes in λ , and hence the whole family of smoothing splines (for a particular sequence \mathbf{x}) indexed by λ have the same eigenvectors.
- $\mathbf{S}_\lambda \mathbf{y} = \sum_{k=1}^N \mathbf{u}_k \rho_k(\lambda) \langle \mathbf{u}_k, \mathbf{y} \rangle$, and hence the smoothing spline operates by decomposing \mathbf{y} w.r.t. the (complete) basis $\{\mathbf{u}_k\}$, and differentially shrinking the contributions using $\rho_k(\lambda)$. This is to be contrasted with a basis-regression method, where the components are

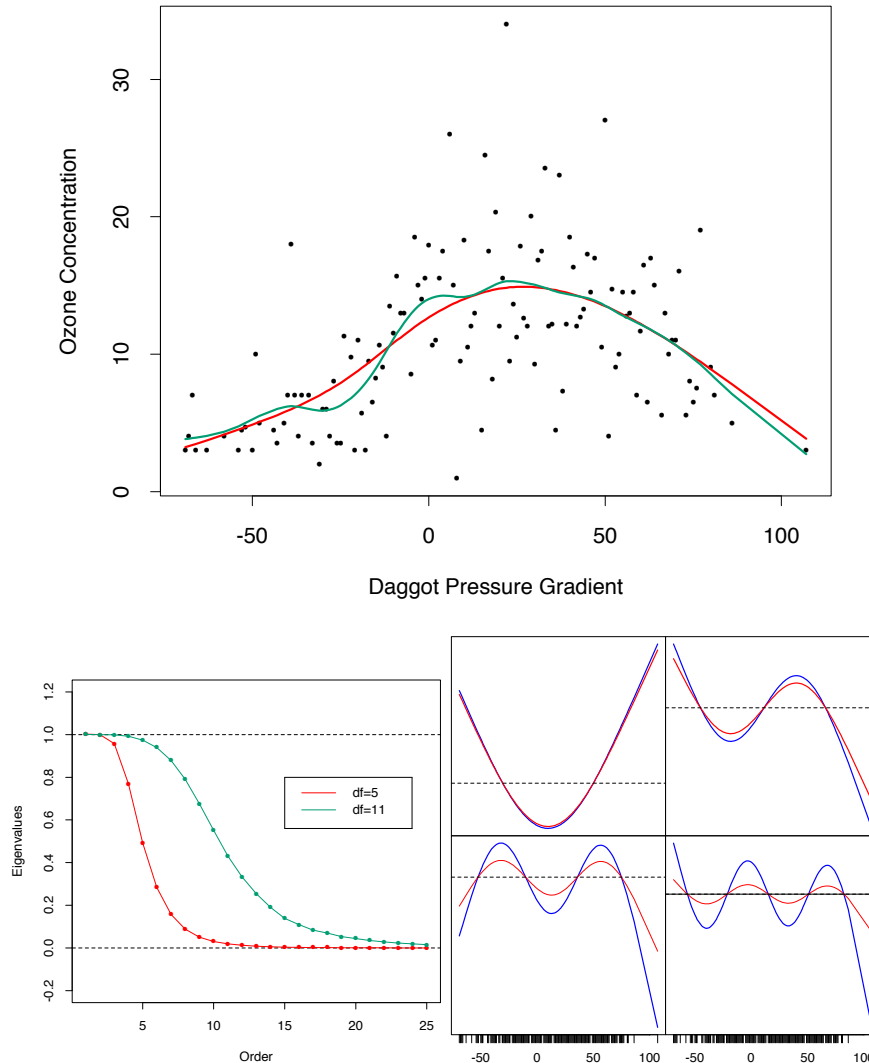


FIGURE 5.7. (Top:) Smoothing spline fit of ozone concentration versus Daggot pressure gradient. The two fits correspond to different values of the smoothing parameter, chosen to achieve five and eleven effective degrees of freedom, defined by $df_\lambda = \text{trace}(\mathbf{S}_\lambda)$. (Lower left:) First 25 eigenvalues for the two smoothing-spline matrices. The first two are exactly 1, and all are ≥ 0 . (Lower right:) Third to sixth eigenvectors of the spline smoother matrices. In each case, \mathbf{u}_k is plotted against \mathbf{x} , and as such is viewed as a function of x . The rug at the base of the plots indicate the occurrence of data points. The damped functions represent the smoothed versions of these functions (using the 5 df smoother).

either left alone, or shrunk to zero—that is, a projection matrix such as \mathbf{H}_ξ above has M eigenvalues equal to 1, and the rest are 0. For this reason smoothing splines are referred to as *shrinking* smoothers, while regression splines are *projection* smoothers (see Figure 3.17 on page 80).

- The sequence of \mathbf{u}_k , ordered by decreasing $\rho_k(\lambda)$, appear to increase in complexity. Indeed, they have the zero-crossing behavior of polynomials of increasing degree. Since $\mathbf{S}_\lambda \mathbf{u}_k = \rho_k(\lambda) \mathbf{u}_k$, we see how each of the eigenvectors themselves are shrunk by the smoothing spline: the higher the complexity, the more they are shrunk. If the domain of X is periodic, then the \mathbf{u}_k are sines and cosines at different frequencies.
- The first two eigenvalues are *always* one, and they correspond to the two-dimensional eigenspace of functions linear in x (Exercise 5.11), which are never shrunk.
- The eigenvalues $\rho_k(\lambda) = 1/(1 + \lambda d_k)$ are an inverse function of the eigenvalues d_k of the penalty matrix \mathbf{K} , moderated by λ ; λ controls the rate at which the $\rho_k(\lambda)$ decrease to zero. $d_1 = d_2 = 0$ and again linear functions are not penalized.
- One can reparametrize the smoothing spline using the basis vectors \mathbf{u}_k (the *Demmler–Reinsch* basis). In this case the smoothing spline solves

$$\min_{\boldsymbol{\theta}} \|\mathbf{y} - \mathbf{U}\boldsymbol{\theta}\|^2 + \lambda \boldsymbol{\theta}^T \mathbf{D} \boldsymbol{\theta}, \quad (5.21)$$

where \mathbf{U} has columns \mathbf{u}_k and \mathbf{D} is a diagonal matrix with elements d_k .

- $\text{df}_\lambda = \text{trace}(\mathbf{S}_\lambda) = \sum_{k=1}^N \rho_k(\lambda)$. For projection smoothers, all the eigenvalues are 1, each one corresponding to a dimension of the projection subspace.

Figure 5.8 depicts a smoothing spline matrix, with the rows ordered with x . The banded nature of this representation suggests that a smoothing spline is a local fitting method, much like the locally weighted regression procedures in Chapter 6. The right panel shows in detail selected rows of \mathbf{S} , which we call the *equivalent kernels*. As $\lambda \rightarrow 0$, $\text{df}_\lambda \rightarrow N$, and $\mathbf{S}_\lambda \rightarrow \mathbf{I}$, the N -dimensional identity matrix. As $\lambda \rightarrow \infty$, $\text{df}_\lambda \rightarrow 2$, and $\mathbf{S}_\lambda \rightarrow \mathbf{H}$, the hat matrix for linear regression on \mathbf{x} .

5.5 Automatic Selection of the Smoothing Parameters

The smoothing parameters for regression splines encompass the degree of the splines, and the number and placement of the knots. For smoothing

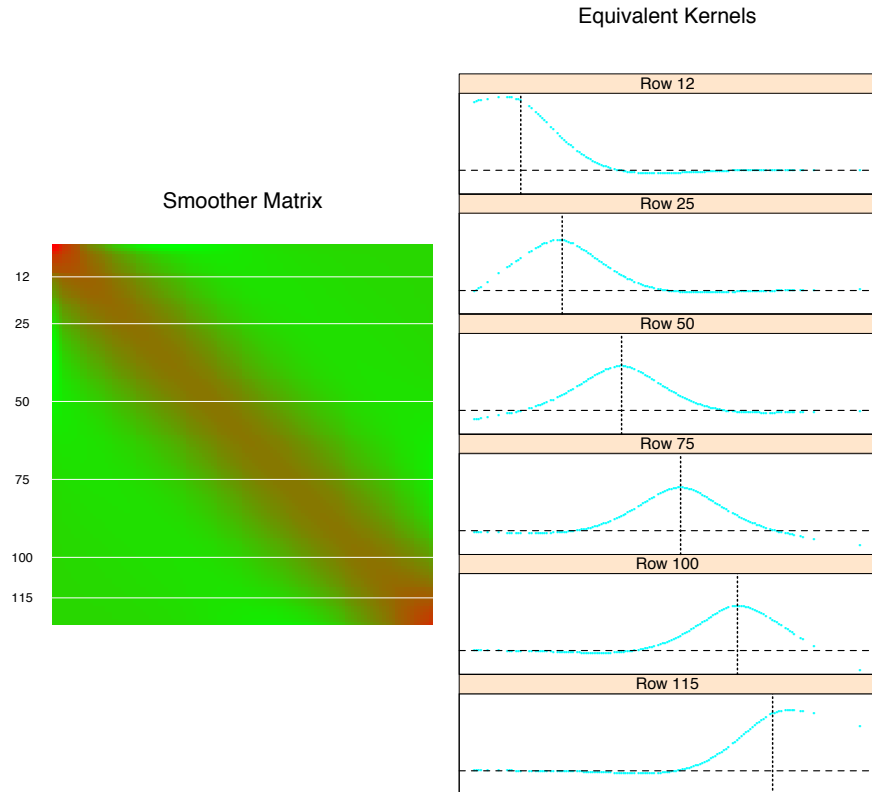


FIGURE 5.8. The smoother matrix for a smoothing spline is nearly banded, indicating an equivalent kernel with local support. The left panel represents the elements of \mathbf{S} as an image. The right panel shows the equivalent kernel or weighting function in detail for the indicated rows.

splines, we have only the penalty parameter λ to select, since the knots are at all the unique training X 's, and cubic degree is almost always used in practice.

Selecting the placement and number of knots for regression splines can be a combinatorially complex task, unless some simplifications are enforced. The MARS procedure in Chapter 9 uses a greedy algorithm with some additional approximations to achieve a practical compromise. We will not discuss this further here.

5.5.1 Fixing the Degrees of Freedom

Since $df_\lambda = \text{trace}(\mathbf{S}_\lambda)$ is monotone in λ for smoothing splines, we can invert the relationship and specify λ by fixing df . In practice this can be achieved by simple numerical methods. So, for example, in R one can use `smooth.spline(x,y,df=6)` to specify the amount of smoothing. This encourages a more traditional mode of model selection, where we might try a couple of different values of df , and select one based on approximate F -tests, residual plots and other more subjective criteria. Using df in this way provides a uniform approach to compare many different smoothing methods. It is particularly useful in *generalized additive models* (Chapter 9), where several smoothing methods can be simultaneously used in one model.

5.5.2 The Bias–Variance Tradeoff

Figure 5.9 shows the effect of the choice of df_λ when using a smoothing spline on a simple example:

$$\begin{aligned} Y &= f(X) + \varepsilon, \\ f(X) &= \frac{\sin(12(X + 0.2))}{X + 0.2}, \end{aligned} \tag{5.22}$$

with $X \sim U[0, 1]$ and $\varepsilon \sim N(0, 1)$. Our training sample consists of $N = 100$ pairs x_i, y_i drawn independently from this model.

The fitted splines for three different values of df_λ are shown. The yellow shaded region in the figure represents the pointwise standard error of \hat{f}_λ , that is, we have shaded the region between $\hat{f}_\lambda(x) \pm 2 \cdot \text{se}(\hat{f}_\lambda(x))$. Since $\hat{\mathbf{f}} = \mathbf{S}_\lambda \mathbf{y}$,

$$\begin{aligned} \text{Cov}(\hat{\mathbf{f}}) &= \mathbf{S}_\lambda \text{Cov}(\mathbf{y}) \mathbf{S}_\lambda^T \\ &= \mathbf{S}_\lambda \mathbf{S}_\lambda^T. \end{aligned} \tag{5.23}$$

The diagonal contains the pointwise variances at the training x_i . The bias is given by

$$\begin{aligned} \text{Bias}(\hat{\mathbf{f}}) &= \mathbf{f} - E(\hat{\mathbf{f}}) \\ &= \mathbf{f} - \mathbf{S}_\lambda \mathbf{f}, \end{aligned} \tag{5.24}$$

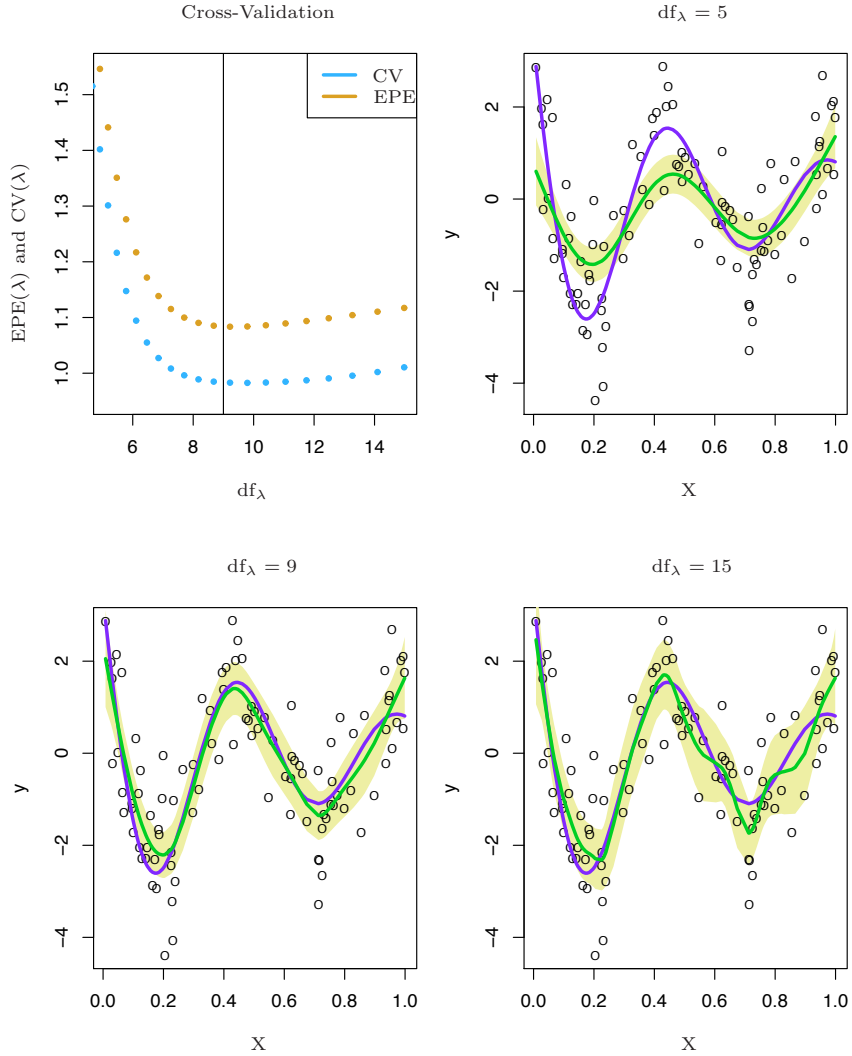


FIGURE 5.9. The top left panel shows the $EPE(\lambda)$ and $CV(\lambda)$ curves for a realization from a nonlinear additive error model (5.22). The remaining panels show the data, the true functions (in purple), and the fitted curves (in green) with yellow shaded $\pm 2 \times$ standard error bands, for three different values of df_λ .

where \mathbf{f} is the (unknown) vector of evaluations of the true f at the training X 's. The expectations and variances are with respect to repeated draws of samples of size $N = 100$ from the model (5.22). In a similar fashion $\text{Var}(\hat{f}_\lambda(x_0))$ and $\text{Bias}(\hat{f}_\lambda(x_0))$ can be computed at any point x_0 (Exercise 5.10). The three fits displayed in the figure give a visual demonstration of the bias-variance tradeoff associated with selecting the smoothing parameter.

$\text{df}_\lambda = 5$: The spline under fits, and clearly *trims down the hills and fills in the valleys*. This leads to a bias that is most dramatic in regions of high curvature. The standard error band is very narrow, so we estimate a badly biased version of the true function with great reliability!

$\text{df}_\lambda = 9$: Here the fitted function is close to the true function, although a slight amount of bias seems evident. The variance has not increased appreciably.

$\text{df}_\lambda = 15$: The fitted function is somewhat wiggly, but close to the true function. The wigginess also accounts for the increased width of the standard error bands—the curve is starting to follow some individual points too closely.

Note that in these figures we are seeing a single realization of data and hence fitted spline \hat{f} in each case, while the bias involves an expectation $E(\hat{f})$. We leave it as an exercise (5.10) to compute similar figures where the bias is shown as well. The middle curve seems “just right,” in that it has achieved a good compromise between bias and variance.

The integrated squared prediction error (EPE) combines both bias and variance in a single summary:

$$\begin{aligned}\text{EPE}(\hat{f}_\lambda) &= E(Y - \hat{f}_\lambda(X))^2 \\ &= \text{Var}(Y) + E \left[\text{Bias}^2(\hat{f}_\lambda(X)) + \text{Var}(\hat{f}_\lambda(X)) \right] \\ &= \sigma^2 + \text{MSE}(\hat{f}_\lambda).\end{aligned}\tag{5.25}$$

Note that this is averaged both over the training sample (giving rise to \hat{f}_λ), and the values of the (independently chosen) prediction points (X, Y) . EPE is a natural quantity of interest, and does create a tradeoff between bias and variance. The blue points in the top left panel of Figure 5.9 suggest that $\text{df}_\lambda = 9$ is spot on!

Since we don't know the true function, we do not have access to EPE, and need an estimate. This topic is discussed in some detail in Chapter 7, and techniques such as K-fold cross-validation, GCV and C_p are all in common use. In Figure 5.9 we include the N -fold (leave-one-out) cross-validation curve:

$$\text{CV}(\hat{f}_\lambda) = \frac{1}{N} \sum_{i=1}^N (y_i - \hat{f}_\lambda^{(-i)}(x_i))^2 \quad (5.26)$$

$$= \frac{1}{N} \sum_{i=1}^N \left(\frac{y_i - \hat{f}_\lambda(x_i)}{1 - S_\lambda(i, i)} \right)^2, \quad (5.27)$$

which can (remarkably) be computed for each value of λ from the original fitted values and the diagonal elements $S_\lambda(i, i)$ of \mathbf{S}_λ (Exercise 5.13).

The EPE and CV curves have a similar shape, but the entire CV curve is above the EPE curve. For some realizations this is reversed, and overall the CV curve is approximately unbiased as an estimate of the EPE curve.

5.6 Nonparametric Logistic Regression

The smoothing spline problem (5.9) in Section 5.4 is posed in a regression setting. It is typically straightforward to transfer this technology to other domains. Here we consider logistic regression with a single quantitative input X . The model is

$$\log \frac{\Pr(Y = 1|X = x)}{\Pr(Y = 0|X = x)} = f(x), \quad (5.28)$$

which implies

$$\Pr(Y = 1|X = x) = \frac{e^{f(x)}}{1 + e^{f(x)}}. \quad (5.29)$$

Fitting $f(x)$ in a smooth fashion leads to a smooth estimate of the conditional probability $\Pr(Y = 1|x)$, which can be used for classification or risk scoring.

We construct the penalized log-likelihood criterion

$$\begin{aligned} \ell(f; \lambda) &= \sum_{i=1}^N [y_i \log p(x_i) + (1 - y_i) \log(1 - p(x_i))] - \frac{1}{2}\lambda \int \{f''(t)\}^2 dt \\ &= \sum_{i=1}^N \left[y_i f(x_i) - \log(1 + e^{f(x_i)}) \right] - \frac{1}{2}\lambda \int \{f''(t)\}^2 dt, \end{aligned} \quad (5.30)$$

where we have abbreviated $p(x) = \Pr(Y = 1|x)$. The first term in this expression is the log-likelihood based on the binomial distribution (c.f. Chapter 4, page 120). Arguments similar to those used in Section 5.4 show that the optimal f is a finite-dimensional natural spline with knots at the unique

values of x . This means that we can represent $f(x) = \sum_{j=1}^N N_j(x)\theta_j$. We compute the first and second derivatives

$$\frac{\partial \ell(\theta)}{\partial \theta} = \mathbf{N}^T(\mathbf{y} - \mathbf{p}) - \lambda \Omega \theta, \quad (5.31)$$

$$\frac{\partial^2 \ell(\theta)}{\partial \theta \partial \theta^T} = -\mathbf{N}^T \mathbf{W} \mathbf{N} - \lambda \Omega, \quad (5.32)$$

where \mathbf{p} is the N -vector with elements $p(x_i)$, and \mathbf{W} is a diagonal matrix of weights $p(x_i)(1 - p(x_i))$. The first derivative (5.31) is nonlinear in θ , so we need to use an iterative algorithm as in Section 4.4.1. Using Newton–Raphson as in (4.23) and (4.26) for linear logistic regression, the update equation can be written

$$\begin{aligned} \theta^{\text{new}} &= (\mathbf{N}^T \mathbf{W} \mathbf{N} + \lambda \Omega)^{-1} \mathbf{N}^T \mathbf{W} (\mathbf{N} \theta^{\text{old}} + \mathbf{W}^{-1}(\mathbf{y} - \mathbf{p})) \\ &= (\mathbf{N}^T \mathbf{W} \mathbf{N} + \lambda \Omega)^{-1} \mathbf{N}^T \mathbf{W} \mathbf{z}. \end{aligned} \quad (5.33)$$

We can also express this update in terms of the fitted values

$$\begin{aligned} \mathbf{f}^{\text{new}} &= \mathbf{N}(\mathbf{N}^T \mathbf{W} \mathbf{N} + \lambda \Omega)^{-1} \mathbf{N}^T \mathbf{W} (\mathbf{f}^{\text{old}} + \mathbf{W}^{-1}(\mathbf{y} - \mathbf{p})) \\ &= \mathbf{S}_{\lambda, w} \mathbf{z}. \end{aligned} \quad (5.34)$$

Referring back to (5.12) and (5.14), we see that the update fits a weighted smoothing spline to the working response \mathbf{z} (Exercise 5.12).

The form of (5.34) is suggestive. It is tempting to replace $\mathbf{S}_{\lambda, w}$ by any nonparametric (weighted) regression operator, and obtain general families of nonparametric logistic regression models. Although here x is one-dimensional, this procedure generalizes naturally to higher-dimensional x . These extensions are at the heart of *generalized additive models*, which we pursue in Chapter 9.

5.7 Multidimensional Splines

So far we have focused on one-dimensional spline models. Each of the approaches have multidimensional analogs. Suppose $X \in \mathbb{R}^2$, and we have a basis of functions $h_{1k}(X_1)$, $k = 1, \dots, M_1$ for representing functions of coordinate X_1 , and likewise a set of M_2 functions $h_{2k}(X_2)$ for coordinate X_2 . Then the $M_1 \times M_2$ dimensional *tensor product basis* defined by

$$g_{jk}(X) = h_{1j}(X_1)h_{2k}(X_2), \quad j = 1, \dots, M_1, \quad k = 1, \dots, M_2 \quad (5.35)$$

can be used for representing a two-dimensional function:

$$g(X) = \sum_{j=1}^{M_1} \sum_{k=1}^{M_2} \theta_{jk} g_{jk}(X). \quad (5.36)$$

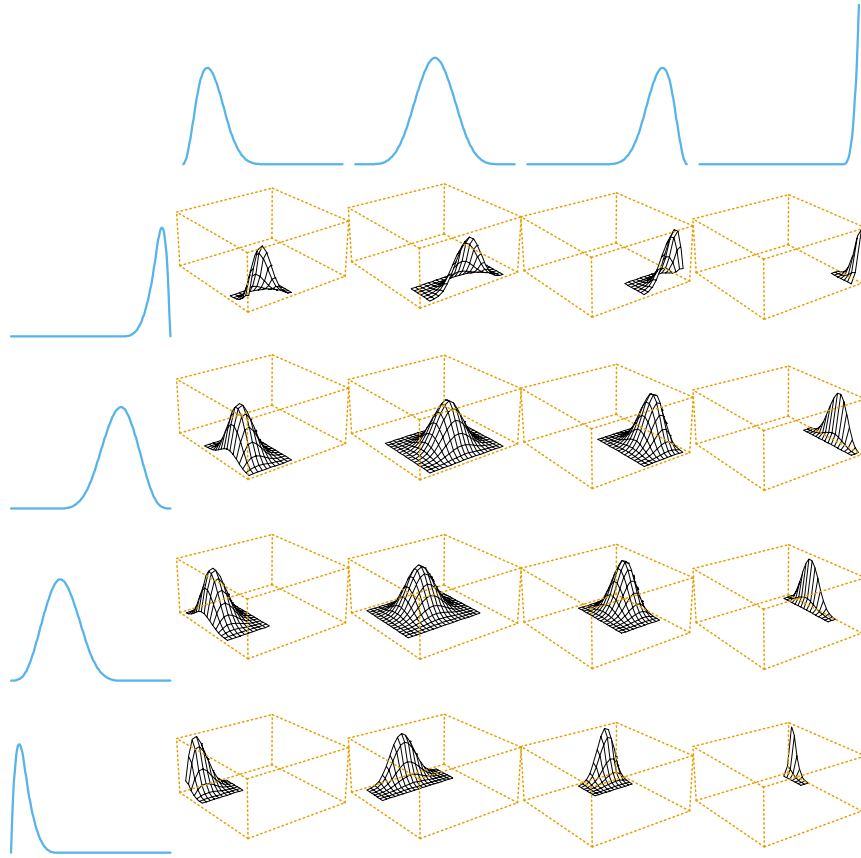


FIGURE 5.10. A tensor product basis of B-splines, showing some selected pairs. Each two-dimensional function is the tensor product of the corresponding one dimensional marginals.

Figure 5.10 illustrates a tensor product basis using B-splines. The coefficients can be fit by least squares, as before. This can be generalized to d dimensions, but note that the dimension of the basis grows exponentially fast—yet another manifestation of the curse of dimensionality. The MARS procedure discussed in Chapter 9 is a greedy forward algorithm for including only those tensor products that are deemed necessary by least squares.

Figure 5.11 illustrates the difference between additive and tensor product (natural) splines on the simulated classification example from Chapter 2. A logistic regression model $\text{logit}[\Pr(T|x)] = h(x)^T \theta$ is fit to the binary response, and the estimated decision boundary is the contour $h(x)^T \hat{\theta} = 0$. The tensor product basis can achieve more flexibility at the decision boundary, but introduces some spurious structure along the way.

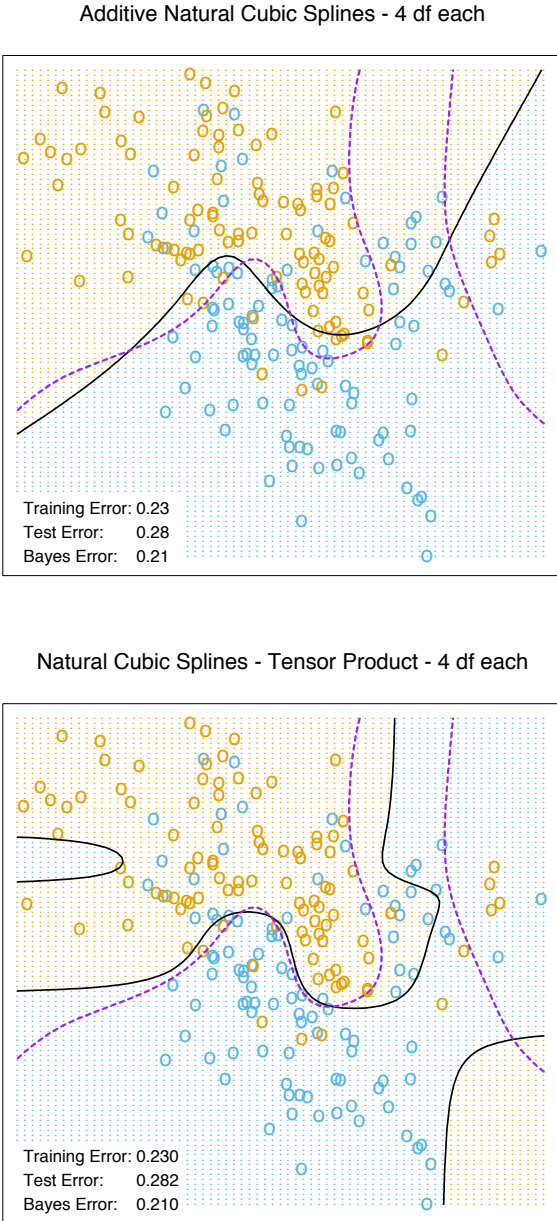


FIGURE 5.11. The simulation example of Figure 2.1. The upper panel shows the decision boundary of an additive logistic regression model, using natural splines in each of the two coordinates (total $df = 1 + (4 - 1) + (4 - 1) = 7$). The lower panel shows the results of using a tensor product of natural spline bases in each coordinate ($total\ df = 4 \times 4 = 16$). The broken purple boundary is the Bayes decision boundary for this problem.

One-dimensional smoothing splines (via regularization) generalize to higher dimensions as well. Suppose we have pairs y_i, x_i with $x_i \in \mathbb{R}^d$, and we seek a d -dimensional regression function $f(x)$. The idea is to set up the problem

$$\min_f \sum_{i=1}^N \{y_i - f(x_i)\}^2 + \lambda J[f], \quad (5.37)$$

where J is an appropriate penalty functional for stabilizing a function f in \mathbb{R}^d . For example, a natural generalization of the one-dimensional roughness penalty (5.9) for functions on \mathbb{R}^2 is

$$J[f] = \int \int_{\mathbb{R}^2} \left[\left(\frac{\partial^2 f(x)}{\partial x_1^2} \right)^2 + 2 \left(\frac{\partial^2 f(x)}{\partial x_1 \partial x_2} \right)^2 + \left(\frac{\partial^2 f(x)}{\partial x_2^2} \right)^2 \right] dx_1 dx_2. \quad (5.38)$$

Optimizing (5.37) with this penalty leads to a smooth two-dimensional surface, known as a thin-plate spline. It shares many properties with the one-dimensional cubic smoothing spline:

- as $\lambda \rightarrow 0$, the solution approaches an interpolating function [the one with smallest penalty (5.38)];
- as $\lambda \rightarrow \infty$, the solution approaches the least squares plane;
- for intermediate values of λ , the solution can be represented as a linear expansion of basis functions, whose coefficients are obtained by a form of generalized ridge regression.

The solution has the form

$$f(x) = \beta_0 + \beta^T x + \sum_{j=1}^N \alpha_j h_j(x), \quad (5.39)$$

where $h_j(x) = \|x - x_j\|^2 \log \|x - x_j\|$. These h_j are examples of *radial basis functions*, which are discussed in more detail in the next section. The coefficients are found by plugging (5.39) into (5.37), which reduces to a finite-dimensional penalized least squares problem. For the penalty to be finite, the coefficients α_j have to satisfy a set of linear constraints; see Exercise 5.14.

Thin-plate splines are defined more generally for arbitrary dimension d , for which an appropriately more general J is used.

There are a number of hybrid approaches that are popular in practice, both for computational and conceptual simplicity. Unlike one-dimensional smoothing splines, the computational complexity for thin-plate splines is $O(N^3)$, since there is not in general any sparse structure that can be exploited. However, as with univariate smoothing splines, we can get away with substantially less than the N knots prescribed by the solution (5.39).

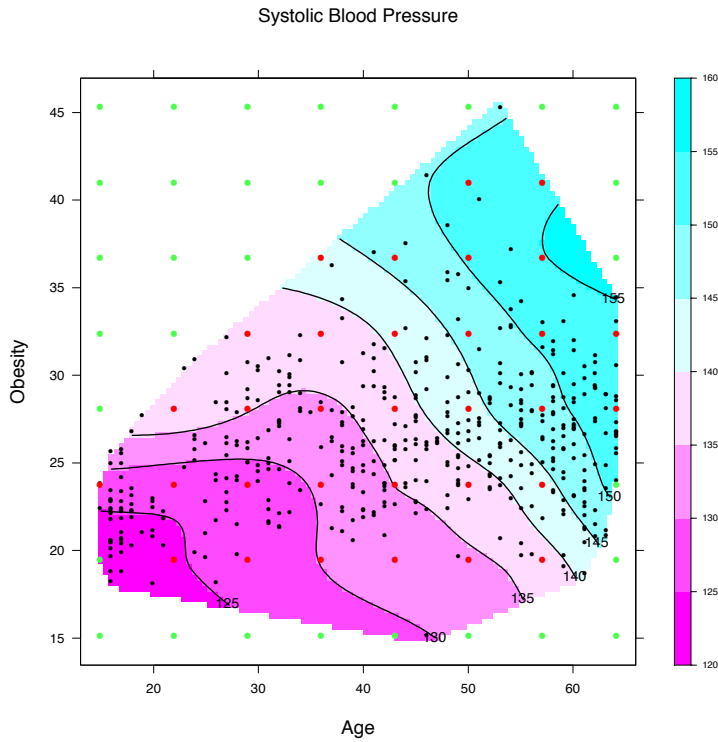


FIGURE 5.12. A thin-plate spline fit to the heart disease data, displayed as a contour plot. The response is systolic blood pressure, modeled as a function of age and obesity. The data points are indicated, as well as the lattice of points used as knots. Care should be taken to use knots from the lattice inside the convex hull of the data (red), and ignore those outside (green).

In practice, it is usually sufficient to work with a lattice of knots covering the domain. The penalty is computed for the reduced expansion just as before. Using K knots reduces the computations to $O(NK^2 + K^3)$. Figure 5.12 shows the result of fitting a thin-plate spline to some heart disease risk factors, representing the surface as a contour plot. Indicated are the location of the input features, as well as the knots used in the fit. Note that λ was specified via $\text{df}_\lambda = \text{trace}(S_\lambda) = 15$.

More generally one can represent $f \in \mathbb{IR}^d$ as an expansion in any arbitrarily large collection of basis functions, and control the complexity by applying a regularizer such as (5.38). For example, we could construct a basis by forming the tensor products of all pairs of univariate smoothing-spline basis functions as in (5.35), using, for example, the univariate B -splines recommended in Section 5.9.2 as ingredients. This leads to an exponential

growth in basis functions as the dimension increases, and typically we have to reduce the number of functions per coordinate accordingly.

The additive spline models discussed in Chapter 9 are a restricted class of multidimensional splines. They can be represented in this general formulation as well; that is, there exists a penalty $J[f]$ that guarantees that the solution has the form $f(X) = \alpha + f_1(X_1) + \cdots + f_d(X_d)$ and that each of the functions f_j are univariate splines. In this case the penalty is somewhat degenerate, and it is more natural to *assume* that f is additive, and then simply impose an additional penalty on each of the component functions:

$$\begin{aligned} J[f] &= J(f_1 + f_2 + \cdots + f_d) \\ &= \sum_{j=1}^d \int f_j''(t_j)^2 dt_j. \end{aligned} \quad (5.40)$$

These are naturally extended to ANOVA spline decompositions,

$$f(X) = \alpha + \sum_j f_j(X_j) + \sum_{j < k} f_{jk}(X_j, X_k) + \cdots, \quad (5.41)$$

where each of the components are splines of the required dimension. There are many choices to be made:

- The maximum order of interaction—we have shown up to order 2 above.
- Which terms to include—not all main effects and interactions are necessarily needed.
- What representation to use—some choices are:
 - regression splines with a relatively small number of basis functions per coordinate, and their tensor products for interactions;
 - a complete basis as in smoothing splines, and include appropriate regularizers for each term in the expansion.

In many cases when the number of potential dimensions (features) is large, automatic methods are more desirable. The MARS and MART procedures (Chapters 9 and 10, respectively), both fall into this category.

5.8 Regularization and Reproducing Kernel Hilbert Spaces



In this section we cast splines into the larger context of regularization methods and reproducing kernel Hilbert spaces. This section is quite technical and can be skipped by the disinterested or intimidated reader.

A general class of regularization problems has the form

$$\min_{f \in \mathcal{H}} \left[\sum_{i=1}^N L(y_i, f(x_i)) + \lambda J(f) \right] \quad (5.42)$$

where $L(y, f(x))$ is a loss function, $J(f)$ is a penalty functional, and \mathcal{H} is a space of functions on which $J(f)$ is defined. Girosi et al. (1995) describe quite general penalty functionals of the form

$$J(f) = \int_{\mathbb{R}^d} \frac{|\tilde{f}(s)|^2}{\tilde{G}(s)} ds, \quad (5.43)$$

where \tilde{f} denotes the Fourier transform of f , and \tilde{G} is some positive function that falls off to zero as $\|s\| \rightarrow \infty$. The idea is that $1/\tilde{G}$ increases the penalty for high-frequency components of f . Under some additional assumptions they show that the solutions have the form

$$f(X) = \sum_{k=1}^K \alpha_k \phi_k(X) + \sum_{i=1}^N \theta_i G(X - x_i), \quad (5.44)$$

where the ϕ_k span the null space of the penalty functional J , and G is the inverse Fourier transform of \tilde{G} . Smoothing splines and thin-plate splines fall into this framework. The remarkable feature of this solution is that while the criterion (5.42) is defined over an infinite-dimensional space, the solution is finite-dimensional. In the next sections we look at some specific examples.

5.8.1 Spaces of Functions Generated by Kernels

An important subclass of problems of the form (5.42) are generated by a positive definite kernel $K(x, y)$, and the corresponding space of functions \mathcal{H}_K is called a *reproducing kernel Hilbert space* (RKHS). The penalty functional J is defined in terms of the kernel as well. We give a brief and simplified introduction to this class of models, adapted from Wahba (1990) and Girosi et al. (1995), and nicely summarized in Evgeniou et al. (2000).

Let $x, y \in \mathbb{R}^p$. We consider the space of functions generated by the linear span of $\{K(\cdot, y), y \in \mathbb{R}^p\}$; i.e arbitrary linear combinations of the form $f(x) = \sum_m \alpha_m K(x, y_m)$, where each kernel term is viewed as a function of the first argument, and indexed by the second. Suppose that K has an eigen-expansion

$$K(x, y) = \sum_{i=1}^{\infty} \gamma_i \phi_i(x) \phi_i(y) \quad (5.45)$$

with $\gamma_i \geq 0$, $\sum_{i=1}^{\infty} \gamma_i^2 < \infty$. Elements of \mathcal{H}_K have an expansion in terms of these eigen-functions,

$$f(x) = \sum_{i=1}^{\infty} c_i \phi_i(x), \quad (5.46)$$

with the constraint that

$$\|f\|_{\mathcal{H}_K}^2 \stackrel{\text{def}}{=} \sum_{i=1}^{\infty} c_i^2 / \gamma_i < \infty, \quad (5.47)$$

where $\|f\|_{\mathcal{H}_K}$ is the norm induced by K . The penalty functional in (5.42) for the space \mathcal{H}_K is defined to be the squared norm $J(f) = \|f\|_{\mathcal{H}_K}^2$. The quantity $J(f)$ can be interpreted as a generalized ridge penalty, where functions with large eigenvalues in the expansion (5.45) get penalized less, and vice versa.

Rewriting (5.42) we have

$$\min_{f \in \mathcal{H}_K} \left[\sum_{i=1}^N L(y_i, f(x_i)) + \lambda \|f\|_{\mathcal{H}_K}^2 \right] \quad (5.48)$$

or equivalently

$$\min_{\{c_j\}_{j=1}^{\infty}} \left[\sum_{i=1}^N L(y_i, \sum_{j=1}^{\infty} c_j \phi_j(x_i)) + \lambda \sum_{j=1}^{\infty} c_j^2 / \gamma_j \right]. \quad (5.49)$$

It can be shown (Wahba, 1990, see also Exercise 5.15) that the solution to (5.48) is finite-dimensional, and has the form

$$f(x) = \sum_{i=1}^N \alpha_i K(x, x_i). \quad (5.50)$$

The basis function $h_i(x) = K(x, x_i)$ (as a function of the first argument) is known as the *representer of evaluation* at x_i in \mathcal{H}_K , since for $f \in \mathcal{H}_K$, it is easily seen that $\langle K(\cdot, x_i), f \rangle_{\mathcal{H}_K} = f(x_i)$. Similarly $\langle K(\cdot, x_i), K(\cdot, x_j) \rangle_{\mathcal{H}_K} = K(x_i, x_j)$ (the *reproducing* property of \mathcal{H}_K), and hence

$$J(f) = \sum_{i=1}^N \sum_{j=1}^N K(x_i, x_j) \alpha_i \alpha_j \quad (5.51)$$

for $f(x) = \sum_{i=1}^N \alpha_i K(x, x_i)$.

In light of (5.50) and (5.51), (5.48) reduces to a finite-dimensional criterion

$$\min_{\boldsymbol{\alpha}} L(\mathbf{y}, \mathbf{K}\boldsymbol{\alpha}) + \lambda \boldsymbol{\alpha}^T \mathbf{K} \boldsymbol{\alpha}. \quad (5.52)$$

We are using a vector notation, in which \mathbf{K} is the $N \times N$ matrix with ij th entry $K(x_i, x_j)$ and so on. Simple numerical algorithms can be used to optimize (5.52). This phenomenon, whereby the infinite-dimensional problem (5.48) or (5.49) reduces to a finite dimensional optimization problem, has been dubbed the *kernel property* in the literature on support-vector machines (see Chapter 12).

There is a Bayesian interpretation of this class of models, in which f is interpreted as a realization of a zero-mean stationary Gaussian process, with prior covariance function K . The eigen-decomposition produces a series of orthogonal eigen-functions $\phi_j(x)$ with associated variances γ_j . The typical scenario is that “smooth” functions ϕ_j have large prior variance, while “rough” ϕ_j have small prior variances. The penalty in (5.48) is the contribution of the prior to the joint likelihood, and penalizes more those components with smaller prior variance (compare with (5.43)).

For simplicity we have dealt with the case here where all members of \mathcal{H} are penalized, as in (5.48). More generally, there may be some components in \mathcal{H} that we wish to leave alone, such as the linear functions for cubic smoothing splines in Section 5.4. The multidimensional thin-plate splines of Section 5.7 and tensor product splines fall into this category as well. In these cases there is a more convenient representation $\mathcal{H} = \mathcal{H}_0 \oplus \mathcal{H}_1$, with the *null space* \mathcal{H}_0 consisting of, for example, low degree polynomials in x that do not get penalized. The penalty becomes $J(f) = \|P_1 f\|$, where P_1 is the orthogonal projection of f onto \mathcal{H}_1 . The solution has the form $f(x) = \sum_{j=1}^M \beta_j h_j(x) + \sum_{i=1}^N \alpha_i K(x, x_i)$, where the first term represents an expansion in \mathcal{H}_0 . From a Bayesian perspective, the coefficients of components in \mathcal{H}_0 have improper priors, with infinite variance.

5.8.2 Examples of RKHS

The machinery above is driven by the choice of the kernel K and the loss function L . We consider first regression using squared-error loss. In this case (5.48) specializes to penalized least squares, and the solution can be characterized in two equivalent ways corresponding to (5.49) or (5.52):

$$\min_{\{c_j\}_{1}^{\infty}} \sum_{i=1}^N \left(y_i - \sum_{j=1}^{\infty} c_j \phi_j(x_i) \right)^2 + \lambda \sum_{j=1}^{\infty} \frac{c_j^2}{\gamma_j} \quad (5.53)$$

an infinite-dimensional, generalized ridge regression problem, or

$$\min_{\boldsymbol{\alpha}} (\mathbf{y} - \mathbf{K}\boldsymbol{\alpha})^T (\mathbf{y} - \mathbf{K}\boldsymbol{\alpha}) + \lambda \boldsymbol{\alpha}^T \mathbf{K} \boldsymbol{\alpha}. \quad (5.54)$$

The solution for $\boldsymbol{\alpha}$ is obtained simply as

$$\hat{\boldsymbol{\alpha}} = (\mathbf{K} + \lambda \mathbf{I})^{-1} \mathbf{y}, \quad (5.55)$$

and

$$\hat{f}(x) = \sum_{j=1}^N \hat{\alpha}_j K(x, x_j). \quad (5.56)$$

The vector of N fitted values is given by

$$\hat{\mathbf{f}} = \mathbf{K}\hat{\boldsymbol{\alpha}} \quad (5.57)$$

$$= \mathbf{K}(\mathbf{K} + \lambda\mathbf{I})^{-1}\mathbf{y} \quad (5.58)$$

The estimate (5.57) also arises as the *kriging* estimate of a Gaussian random field in spatial statistics (Cressie, 1993). Compare also (5.58) with the smoothing spline fit (5.17) on page 154.

Penalized Polynomial Regression

The kernel $K(x, y) = (\langle x, y \rangle + 1)^d$ (Vapnik, 1996), for $x, y \in \mathbb{R}^p$, has $M = \binom{p+d}{d}$ eigen-functions that span the space of polynomials in \mathbb{R}^p of total degree d . For example, with $p = 2$ and $d = 2$, $M = 6$ and

$$K(x, y) = 1 + 2x_1y_1 + 2x_2y_2 + x_1^2y_1^2 + x_2^2y_2^2 + 2x_1x_2y_1y_2 \quad (5.59)$$

$$= \sum_{m=1}^M h_m(x)h_m(y) \quad (5.60)$$

with

$$h(x)^T = (1, \sqrt{2}x_1, \sqrt{2}x_2, x_1^2, x_2^2, \sqrt{2}x_1x_2). \quad (5.61)$$

One can represent h in terms of the M orthogonal eigen-functions and eigenvalues of K ,

$$h(x) = \mathbf{V}\mathbf{D}_\gamma^{\frac{1}{2}}\phi(x), \quad (5.62)$$

where $\mathbf{D}_\gamma = \text{diag}(\gamma_1, \gamma_2, \dots, \gamma_M)$, and \mathbf{V} is $M \times M$ and orthogonal.

Suppose we wish to solve the penalized polynomial regression problem

$$\min_{\{\beta_m\}_{1}^M} \sum_{i=1}^N \left(y_i - \sum_{m=1}^M \beta_m h_m(x_i) \right)^2 + \lambda \sum_{m=1}^M \beta_m^2. \quad (5.63)$$

Substituting (5.62) into (5.63), we get an expression of the form (5.53) to optimize (Exercise 5.16).

The number of basis functions $M = \binom{p+d}{d}$ can be very large, often much larger than N . Equation (5.55) tells us that if we use the kernel representation for the solution function, we have only to evaluate the kernel N^2 times, and can compute the solution in $O(N^3)$ operations.

This simplicity is not without implications. Each of the polynomials h_m in (5.61) inherits a scaling factor from the particular form of K , which has a bearing on the impact of the penalty in (5.63). We elaborate on this in the next section.

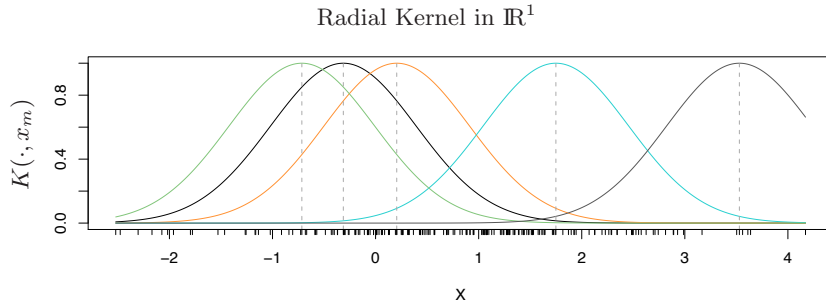


FIGURE 5.13. Radial kernels $k_k(x)$ for the mixture data, with scale parameter $\nu = 1$. The kernels are centered at five points x_m chosen at random from the 200.

Gaussian Radial Basis Functions

In the preceding example, the kernel is chosen because it represents an expansion of polynomials and can conveniently compute high-dimensional inner products. In this example the kernel is chosen because of its functional form in the representation (5.50).

The Gaussian kernel $K(x, y) = e^{-\nu||x-y||^2}$ along with squared-error loss, for example, leads to a regression model that is an expansion in Gaussian radial basis functions,

$$k_m(x) = e^{-\nu||x-x_m||^2}, \quad m = 1, \dots, N, \quad (5.64)$$

each one centered at one of the training feature vectors x_m . The coefficients are estimated using (5.54).

Figure 5.13 illustrates radial kernels in \mathbb{R}^1 using the first coordinate of the mixture example from Chapter 2. We show five of the 200 kernel basis functions $k_m(x) = K(x, x_m)$.

Figure 5.14 illustrates the implicit feature space for the radial kernel with $x \in \mathbb{R}^1$. We computed the 200×200 kernel matrix \mathbf{K} , and its eigen-decomposition $\Phi \mathbf{D}_\gamma \Phi^T$. We can think of the columns of Φ and the corresponding eigenvalues in \mathbf{D}_γ as empirical estimates of the eigen expansion (5.45)². Although the eigenvectors are discrete, we can represent them as functions on \mathbb{R}^1 (Exercise 5.17). Figure 5.15 shows the largest 50 eigenvalues of \mathbf{K} . The leading eigenfunctions are smooth, and they are successively more wiggly as the order increases. This brings to life the penalty in (5.49), where we see the coefficients of higher-order functions get penalized more than lower-order ones. The right panel in Figure 5.14 shows the correspond-

²The ℓ th column of Φ is an estimate of ϕ_ℓ , evaluated at each of the N observations. Alternatively, the i th row of Φ is the estimated vector of basis functions $\phi(x_i)$, evaluated at the point x_i . Although in principle, there can be infinitely many elements in ϕ , our estimate has at most N elements.

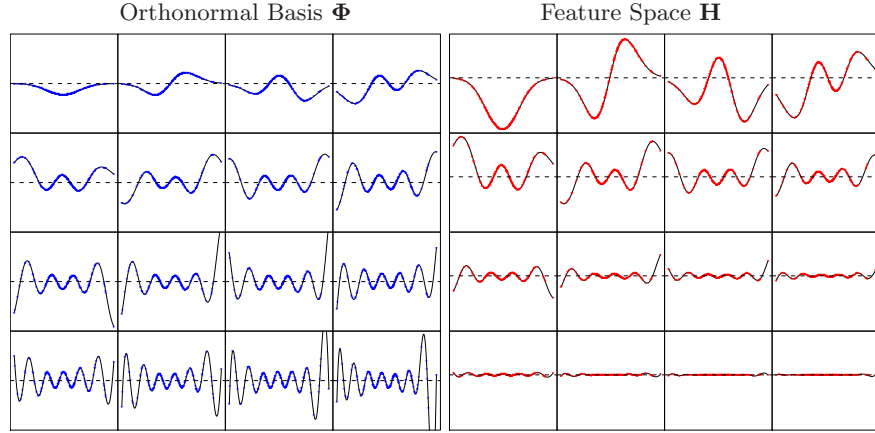


FIGURE 5.14. (Left panel) The first 16 normalized eigenvectors of \mathbf{K} , the 200×200 kernel matrix for the first coordinate of the mixture data. These are viewed as estimates $\hat{\phi}_\ell$ of the eigenfunctions in (5.45), and are represented as functions in \mathbb{R}^1 with the observed values superimposed in color. They are arranged in rows, starting at the top left. (Right panel) Rescaled versions $h_\ell = \sqrt{\gamma_\ell} \hat{\phi}_\ell$ of the functions in the left panel, for which the kernel computes the “inner product.”

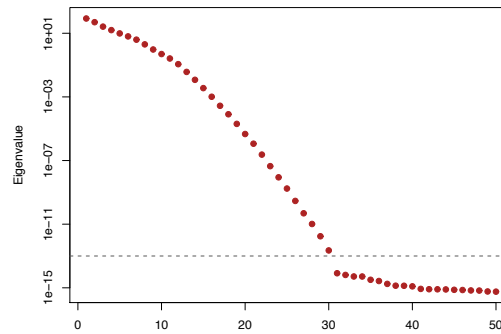


FIGURE 5.15. The largest 50 eigenvalues of \mathbf{K} ; all those beyond the 30th are effectively zero.

ing *feature space* representation of the eigenfunctions

$$h_\ell(x) = \sqrt{\hat{\gamma}_\ell} \hat{\phi}_\ell(x), \quad \ell = 1, \dots, N. \quad (5.65)$$

Note that $\langle h(x_i), h(x_{i'}) \rangle = K(x_i, x_{i'})$. The scaling by the eigenvalues quickly shrinks most of the functions down to zero, leaving an effective dimension of about 12 in this case. The corresponding optimization problem is a standard ridge regression, as in (5.63). So although in principle the implicit feature space is infinite dimensional, the effective dimension is dramatically lower because of the relative amounts of shrinkage applied to each basis function. The kernel scale parameter ν plays a role here as well; larger ν implies more local k_m functions, and increases the effective dimension of the feature space. See Hastie and Zhu (2006) for more details.

It is also known (Girosi et al., 1995) that a thin-plate spline (Section 5.7) is an expansion in radial basis functions, generated by the kernel

$$K(x, y) = \|x - y\|^2 \log(\|x - y\|). \quad (5.66)$$

Radial basis functions are discussed in more detail in Section 6.7.

Support Vector Classifiers

The support vector machines of Chapter 12 for a two-class classification problem have the form $f(x) = \alpha_0 + \sum_{i=1}^N \alpha_i K(x, x_i)$, where the parameters are chosen to minimize

$$\min_{\alpha_0, \alpha} \left\{ \sum_{i=1}^N [1 - y_i f(x_i)]_+ + \frac{\lambda}{2} \alpha^T \mathbf{K} \alpha \right\}, \quad (5.67)$$

where $y_i \in \{-1, 1\}$, and $[z]_+$ denotes the positive part of z . This can be viewed as a quadratic optimization problem with linear constraints, and requires a quadratic programming algorithm for its solution. The name *support vector* arises from the fact that typically many of the $\hat{\alpha}_i = 0$ [due to the piecewise-zero nature of the loss function in (5.67)], and so \hat{f} is an expansion in a subset of the $K(\cdot, x_i)$. See Section 12.3.3 for more details.

5.9 Wavelet Smoothing

We have seen two different modes of operation with dictionaries of basis functions. With regression splines, we select a subset of the bases, using either subject-matter knowledge, or else automatically. The more adaptive procedures such as MARS (Chapter 9) can capture both smooth and non-smooth behavior. With smoothing splines, we use a complete basis, but then shrink the coefficients toward smoothness.

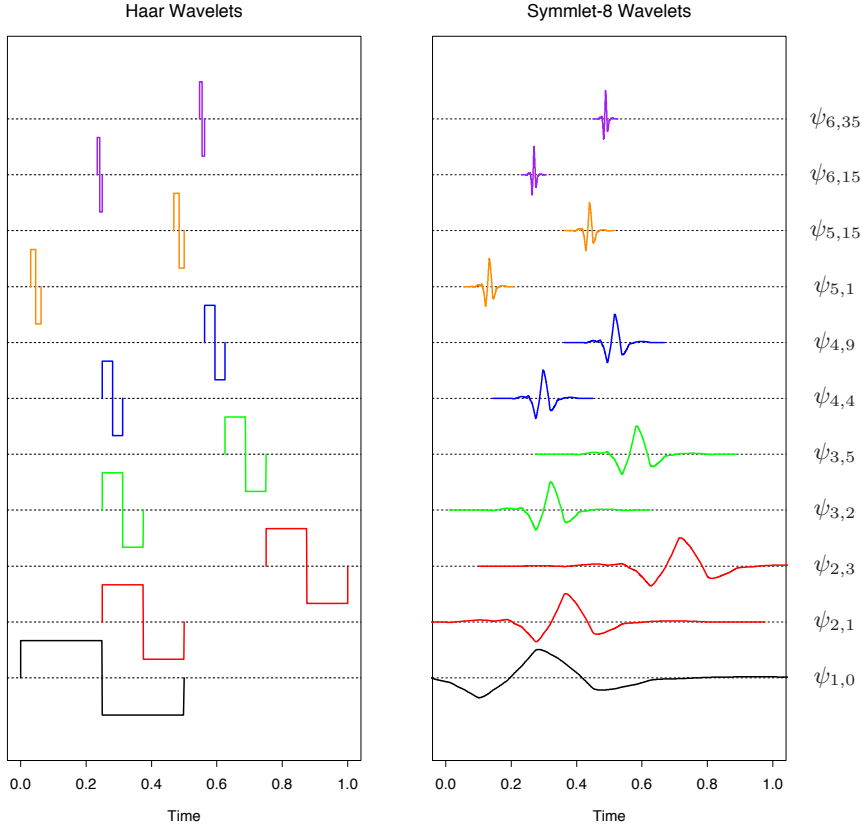


FIGURE 5.16. Some selected wavelets at different translations and dilations for the Haar and symmlet families. The functions have been scaled to suit the display.

Wavelets typically use a complete orthonormal basis to represent functions, but then shrink and select the coefficients toward a *sparse* representation. Just as a smooth function can be represented by a few spline basis functions, a mostly flat function with a few isolated bumps can be represented with a few (bumpy) basis functions. Wavelets bases are very popular in signal processing and compression, since they are able to represent both smooth and/or locally bumpy functions in an efficient way—a phenomenon dubbed *time and frequency localization*. In contrast, the traditional Fourier basis allows only frequency localization.

Before we give details, let's look at the Haar wavelets in the left panel of Figure 5.16 to get an intuitive idea of how wavelet smoothing works. The vertical axis indicates the scale (frequency) of the wavelets, from low scale at the bottom to high scale at the top. At each scale the wavelets are “packed in” side-by-side to completely fill the time axis: we have only shown

a selected subset. Wavelet smoothing fits the coefficients for this basis by least squares, and then thresholds (discards, filters) the smaller coefficients. Since there are many basis functions at each scale, it can use bases where it needs them and discard the ones it does not need, to achieve time and frequency localization. The Haar wavelets are simple to understand, but not smooth enough for most purposes. The *symmlet* wavelets in the right panel of Figure 5.16 have the same orthonormal properties, but are smoother.

Figure 5.17 displays an NMR (nuclear magnetic resonance) signal, which appears to be composed of smooth components and isolated spikes, plus some noise. The wavelet transform, using a symmlet basis, is shown in the lower left panel. The wavelet coefficients are arranged in rows, from lowest scale at the bottom, to highest scale at the top. The length of each line segment indicates the size of the coefficient. The bottom right panel shows the wavelet coefficients after they have been thresholded. The threshold procedure, given below in equation (5.69), is the same soft-thresholding rule that arises in the lasso procedure for linear regression (Section 3.4.2). Notice that many of the smaller coefficients have been set to zero. The green curve in the top panel shows the back-transform of the thresholded coefficients: this is the smoothed version of the original signal. In the next section we give the details of this process, including the construction of wavelets and the thresholding rule.

5.9.1 Wavelet Bases and the Wavelet Transform



In this section we give details on the construction and filtering of wavelets. Wavelet bases are generated by translations and dilations of a single scaling function $\phi(x)$ (also known as the *father*). The red curves in Figure 5.18 are the *Haar* and *symmlet-8* scaling functions. The Haar basis is particularly easy to understand, especially for anyone with experience in analysis of variance or trees, since it produces a piecewise-constant representation. Thus if $\phi(x) = I(x \in [0, 1])$, then $\phi_{0,k}(x) = \phi(x - k)$, k an integer, generates an orthonormal basis for functions with jumps at the integers. Call this *reference* space V_0 . The dilations $\phi_{1,k}(x) = \sqrt{2}\phi(2x - k)$ form an orthonormal basis for a space $V_1 \supset V_0$ of functions piecewise constant on intervals of length $\frac{1}{2}$. In fact, more generally we have $\cdots \supset V_1 \supset V_0 \supset V_{-1} \supset \cdots$ where each V_j is spanned by $\phi_{j,k} = 2^{j/2}\phi(2^j x - k)$.

Now to the definition of wavelets. In analysis of variance, we often represent a pair of means μ_1 and μ_2 by their grand mean $\mu = \frac{1}{2}(\mu_1 + \mu_2)$, and then a contrast $\alpha = \frac{1}{2}(\mu_1 - \mu_2)$. A simplification occurs if the contrast α is very small, because then we can set it to zero. In a similar manner we might represent a function in V_{j+1} by a component in V_j plus the component in the orthogonal complement W_j of V_j to V_{j+1} , written as $V_{j+1} = V_j \oplus W_j$. The component in W_j represents *detail*, and we might wish to set some elements of this component to zero. It is easy to see that the functions $\psi(x - k)$

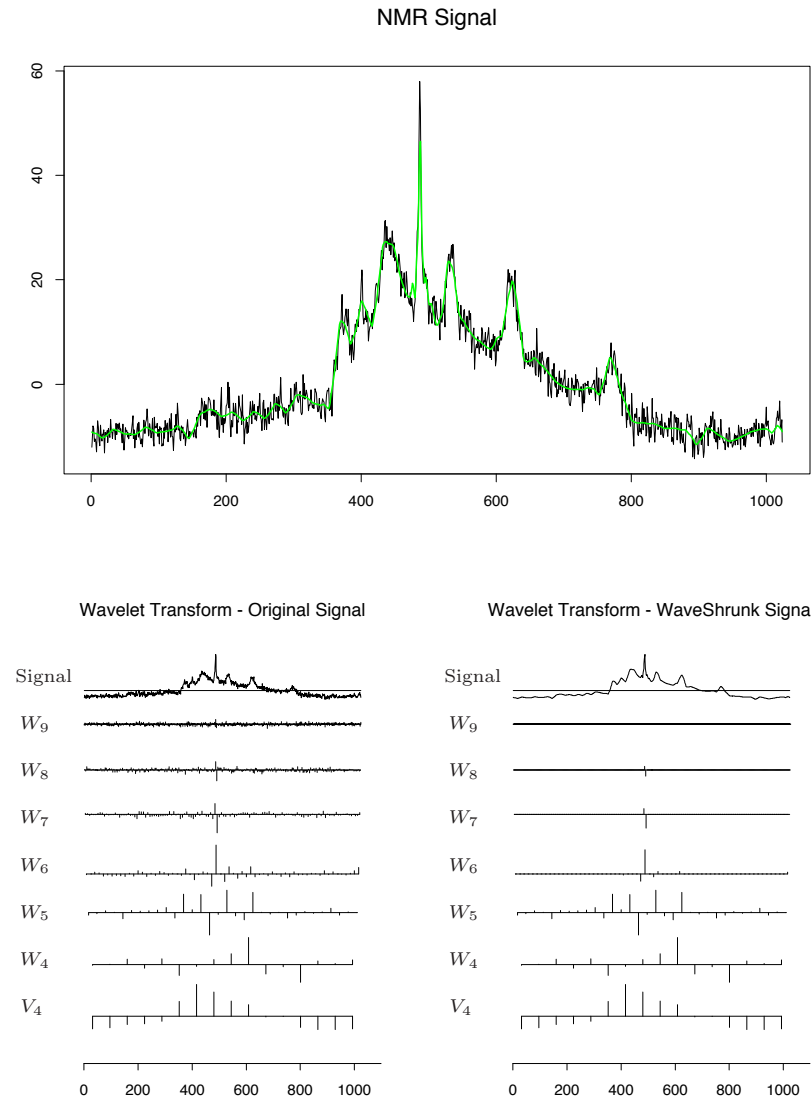


FIGURE 5.17. The top panel shows an NMR signal, with the wavelet-shrunk version superimposed in green. The lower left panel represents the wavelet transform of the original signal, down to V_4 , using the symmlet-8 basis. Each coefficient is represented by the height (positive or negative) of the vertical bar. The lower right panel represents the wavelet coefficients after being shrunk using the `wavelets` function in S-PLUS, which implements the SureShrink method of wavelet adaptation of Donoho and Johnstone.

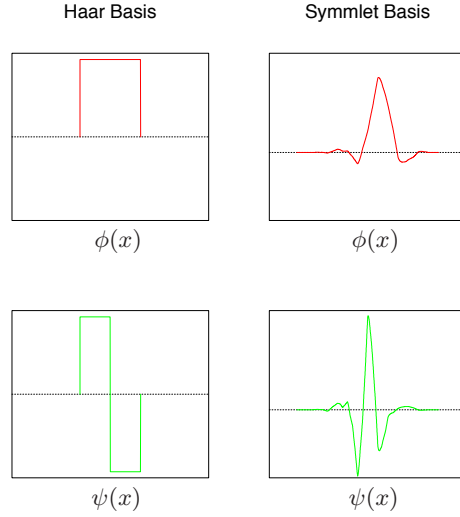


FIGURE 5.18. The Haar and symmlet father (scaling) wavelet $\phi(x)$ and mother wavelet $\psi(x)$.

generated by the *mother wavelet* $\psi(x) = \phi(2x) - \phi(2x-1)$ form an orthonormal basis for W_0 for the Haar family. Likewise $\psi_{j,k} = 2^{j/2}\psi(2^j x - k)$ form a basis for W_j .

Now $V_{j+1} = V_j \oplus W_j = V_{j-1} \oplus W_{j-1} \oplus W_j$, so besides representing a function by its level- j detail and level- j rough components, the latter can be broken down to level- $(j-1)$ detail and rough, and so on. Finally we get a representation of the form $V_J = V_0 \oplus W_0 \oplus W_1 \cdots \oplus W_{J-1}$. Figure 5.16 on page 175 shows particular wavelets $\psi_{j,k}(x)$.

Notice that since these spaces are orthogonal, all the basis functions are orthonormal. In fact, if the domain is discrete with $N = 2^J$ (time) points, this is as far as we can go. There are 2^j basis elements at level j , and adding up, we have a total of $2^J - 1$ elements in the W_j , and one in V_0 . This structured orthonormal basis allows for a *multiresolution analysis*, which we illustrate in the next section.

While helpful for understanding the construction above, the Haar basis is often too coarse for practical purposes. Fortunately, many clever wavelet bases have been invented. Figures 5.16 and 5.18 include the *Daubechies symmlet-8* basis. This basis has smoother elements than the corresponding Haar basis, but there is a tradeoff:

- Each wavelet has a support covering 15 consecutive time intervals, rather than one for the Haar basis. More generally, the symmlet- p family has a support of $2p - 1$ consecutive intervals. The wider the support, the more time the wavelet has to die to zero, and so it can

achieve this more smoothly. Note that the effective support seems to be much narrower.

- The symmlet- p wavelet $\psi(x)$ has p vanishing moments; that is,

$$\int \psi(x)x^j dx = 0, \quad j = 0, \dots, p-1.$$

One implication is that any order- p polynomial over the $N = 2^J$ times points is reproduced exactly in V_0 (Exercise 5.18). In this sense V_0 is equivalent to the null space of the smoothing-spline penalty. The Haar wavelets have one vanishing moment, and V_0 can reproduce any constant function.

The symmlet- p scaling functions are one of many families of wavelet generators. The operations are similar to those for the Haar basis:

- If V_0 is spanned by $\phi(x - k)$, then $V_1 \supset V_0$ is spanned by $\phi_{1,k}(x) = \sqrt{2}\phi(2x - k)$ and $\phi(x) = \sum_{k \in \mathcal{Z}} h(k)\phi_{1,k}(x)$, for some filter coefficients $h(k)$.
- V_0 is spanned by $\psi(x) = \sum_{k \in \mathcal{Z}} g(k)\phi_{1,k}(x)$, with filter coefficients $g(k) = (-1)^{1-k}h(1-k)$.

5.9.2 Adaptive Wavelet Filtering



Wavelets are particularly useful when the data are measured on a uniform lattice, such as a discretized signal, image, or a time series. We will focus on the one-dimensional case, and having $N = 2^J$ lattice-points is convenient. Suppose \mathbf{y} is the response vector, and \mathbf{W} is the $N \times N$ orthonormal wavelet basis matrix evaluated at the N uniformly spaced observations. Then $\mathbf{y}^* = \mathbf{W}^T \mathbf{y}$ is called the *wavelet transform* of \mathbf{y} (and is the full least squares regression coefficient). A popular method for adaptive wavelet fitting is known as *SURE shrinkage* (Stein Unbiased Risk Estimation, Donoho and Johnstone (1994)). We start with the criterion

$$\min_{\boldsymbol{\theta}} \|\mathbf{y} - \mathbf{W}\boldsymbol{\theta}\|_2^2 + 2\lambda\|\boldsymbol{\theta}\|_1, \quad (5.68)$$

which is the same as the lasso criterion in Chapter 3. Because \mathbf{W} is orthonormal, this leads to the simple solution:

$$\hat{\theta}_j = \text{sign}(y_j^*)(|y_j^*| - \lambda)_+. \quad (5.69)$$

The least squares coefficients are translated toward zero, and truncated at zero. The fitted function (vector) is then given by the *inverse wavelet transform* $\hat{\mathbf{f}} = \mathbf{W}\hat{\boldsymbol{\theta}}$.

A simple choice for λ is $\lambda = \sigma\sqrt{2\log N}$, where σ is an estimate of the standard deviation of the noise. We can give some motivation for this choice. Since \mathbf{W} is an orthonormal transformation, if the elements of \mathbf{y} are white noise (independent Gaussian variates with mean 0 and variance σ^2), then so are \mathbf{y}^* . Furthermore if random variables Z_1, Z_2, \dots, Z_N are white noise, the expected maximum of $|Z_j|, j = 1, \dots, N$ is approximately $\sigma\sqrt{2\log N}$. Hence all coefficients below $\sigma\sqrt{2\log N}$ are likely to be noise and are set to zero.

The space \mathbf{W} could be any basis of orthonormal functions: polynomials, natural splines or cosinusoids. What makes wavelets special is the particular form of basis functions used, which allows for a representation *localized in time and in frequency*.

Let's look again at the NMR signal of Figure 5.17. The wavelet transform was computed using a *symmlet-8* basis. Notice that the coefficients do not descend all the way to V_0 , but stop at V_4 which has 16 basis functions. As we ascend to each level of detail, the coefficients get smaller, except in locations where spiky behavior is present. The wavelet coefficients represent characteristics of the signal localized in time (the basis functions at each level are translations of each other) and localized in frequency. Each dilation increases the detail by a factor of two, and in this sense corresponds to doubling the frequency in a traditional Fourier representation. In fact, a more mathematical understanding of wavelets reveals that the wavelets at a particular scale have a Fourier transform that is restricted to a limited range or octave of frequencies.

The shrinking/truncation in the right panel was achieved using the SURE approach described in the introduction to this section. The orthonormal $N \times N$ basis matrix \mathbf{W} has columns which are the wavelet basis functions evaluated at the N time points. In particular, in this case there will be 16 columns corresponding to the $\phi_{4,k}(x)$, and the remainder devoted to the $\psi_{j,k}(x)$, $j = 4, \dots, 11$. In practice λ depends on the noise variance, and has to be estimated from the data (such as the variance of the coefficients at the highest level).

Notice the similarity between the SURE criterion (5.68) on page 179, and the smoothing spline criterion (5.21) on page 156:

- Both are hierarchically structured from coarse to fine detail, although wavelets are also localized in time within each resolution level.
- The splines build in a bias toward smooth functions by imposing differential shrinking constants d_k . Early versions of SURE shrinkage treated all scales equally. The **S+wavelets** function **waveshrink()** has many options, some of which allow for differential shrinkage.
- The spline L_2 penalty cause pure shrinkage, while the SURE L_1 penalty does shrinkage and selection.

More generally smoothing splines achieve compression of the original signal by imposing smoothness, while wavelets impose sparsity. Figure 5.19 compares a wavelet fit (using SURE shrinkage) to a smoothing spline fit (using cross-validation) on two examples different in nature. For the NMR data in the upper panel, the smoothing spline introduces detail everywhere in order to capture the detail in the isolated spikes; the wavelet fit nicely localizes the spikes. In the lower panel, the true function is smooth, and the noise is relatively high. The wavelet fit has let in some additional and unnecessary wiggles—a price it pays in variance for the additional adaptivity.

The wavelet transform is not performed by matrix multiplication as in $\mathbf{y}^* = \mathbf{W}^T \mathbf{y}$. In fact, using clever pyramidal schemes \mathbf{y}^* can be obtained in $O(N)$ computations, which is even faster than the $N \log(N)$ of the fast Fourier transform (FFT). While the general construction is beyond the scope of this book, it is easy to see for the Haar basis (Exercise 5.19). Likewise, the inverse wavelet transform $\mathbf{W}\hat{\theta}$ is also $O(N)$.

This has been a very brief glimpse of this vast and growing field. There is a very large mathematical and computational base built on wavelets. Modern image compression is often performed using two-dimensional wavelet representations.

Bibliographic Notes

Splines and B -splines are discussed in detail in de Boor (1978). Green and Silverman (1994) and Wahba (1990) give a thorough treatment of smoothing splines and thin-plate splines; the latter also covers reproducing kernel Hilbert spaces. See also Girosi et al. (1995) and Evgeniou et al. (2000) for connections between many nonparametric regression techniques using RKHS approaches. Modeling functional data, as in Section 5.2.3, is covered in detail in Ramsay and Silverman (1997).

Daubechies (1992) is a classic and mathematical treatment of wavelets. Other useful sources are Chui (1992) and Wickerhauser (1994). Donoho and Johnstone (1994) developed the SURE shrinkage and selection technology from a statistical estimation framework; see also Vidakovic (1999). Bruce and Gao (1996) is a useful applied introduction, which also describes the wavelet software in S-PLUS.

Exercises

Ex. 5.1 Show that the truncated power basis functions in (5.3) represent a basis for a cubic spline with the two knots as indicated.

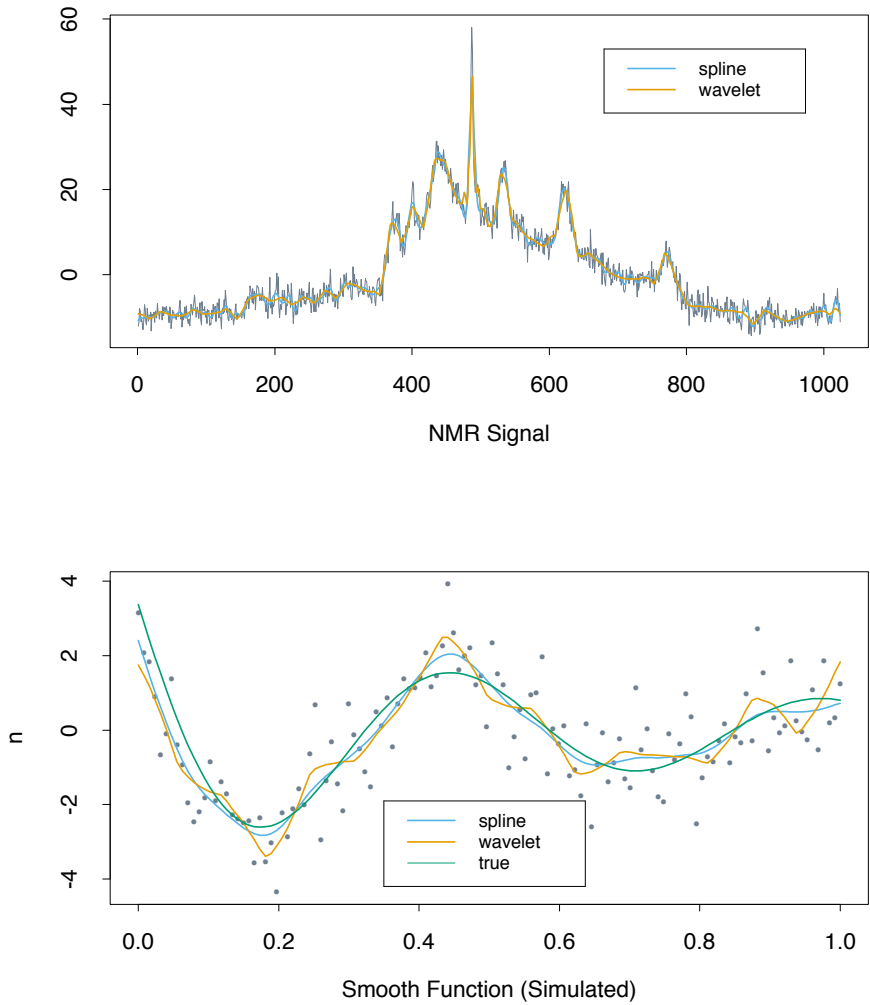


FIGURE 5.19. Wavelet smoothing compared with smoothing splines on two examples. Each panel compares the SURE-shrunk wavelet fit to the cross-validated smoothing spline fit.

Ex. 5.2 Suppose that $B_{i,M}(x)$ is an order- M B -spline defined in the Appendix on page 186 through the sequence (5.77)–(5.78).

- (a) Show by induction that $B_{i,M}(x) = 0$ for $x \notin [\tau_i, \tau_{i+M}]$. This shows, for example, that the support of cubic B -splines is at most 5 knots.
- (b) Show by induction that $B_{i,M}(x) > 0$ for $x \in (\tau_i, \tau_{i+M})$. The B -splines are positive in the interior of their support.
- (c) Show by induction that $\sum_{i=1}^{K+M} B_{i,M}(x) = 1 \forall x \in [\xi_0, \xi_{K+1}]$.
- (d) Show that $B_{i,M}$ is a piecewise polynomial of order M (degree $M-1$) on $[\xi_0, \xi_{K+1}]$, with breaks only at the knots ξ_1, \dots, ξ_K .
- (e) Show that an order- M B -spline basis function is the density function of a convolution of M uniform random variables.

Ex. 5.3 Write a program to reproduce Figure 5.3 on page 145.

Ex. 5.4 Consider the truncated power series representation for cubic splines with K interior knots. Let

$$f(X) = \sum_{j=0}^3 \beta_j X^j + \sum_{k=1}^K \theta_k (X - \xi_k)_+^3. \quad (5.70)$$

Prove that the natural boundary conditions for natural cubic splines (Section 5.2.1) imply the following linear constraints on the coefficients:

$$\begin{aligned} \beta_2 &= 0, & \sum_{k=1}^K \theta_k &= 0, \\ \beta_3 &= 0, & \sum_{k=1}^K \xi_k \theta_k &= 0. \end{aligned} \quad (5.71)$$

Hence derive the basis (5.4) and (5.5).

Ex. 5.5 Write a program to classify the `phoneme` data using a quadratic discriminant analysis (Section 4.3). Since there are many correlated features, you should filter them using a smooth basis of natural cubic splines (Section 5.2.3). Decide beforehand on a series of five different choices for the number and position of the knots, and use tenfold cross-validation to make the final selection. The `phoneme` data are available from the book website www-stat.stanford.edu/ElemStatLearn.

Ex. 5.6 Suppose you wish to fit a periodic function, with a known period T . Describe how you could modify the truncated power series basis to achieve this goal.

Ex. 5.7 *Derivation of smoothing splines* (Green and Silverman, 1994). Suppose that $N \geq 2$, and that g is the natural cubic spline interpolant to the pairs $\{x_i, z_i\}_1^N$, with $a < x_1 < \dots < x_N < b$. This is a natural spline

with a knot at every x_i ; being an N -dimensional space of functions, we can determine the coefficients such that it interpolates the sequence z_i exactly. Let \tilde{g} be any other differentiable function on $[a, b]$ that interpolates the N pairs.

- (a) Let $h(x) = \tilde{g}(x) - g(x)$. Use integration by parts and the fact that g is a natural cubic spline to show that

$$\begin{aligned} \int_a^b g''(x)h''(x)dx &= -\sum_{j=1}^{N-1} g'''(x_j^+) \{h(x_{j+1}) - h(x_j)\} \\ &= 0. \end{aligned} \quad (5.72)$$

- (b) Hence show that

$$\int_a^b \tilde{g}''(t)^2 dt \geq \int_a^b g''(t)^2 dt,$$

and that equality can only hold if h is identically zero in $[a, b]$.

- (c) Consider the penalized least squares problem

$$\min_f \left[\sum_{i=1}^N (y_i - f(x_i))^2 + \lambda \int_a^b f''(t)^2 dt \right].$$

Use (b) to argue that the minimizer must be a cubic spline with knots at each of the x_i .

Ex. 5.8 In the appendix to this chapter we show how the smoothing spline computations could be more efficiently carried out using a $(N + 4)$ dimensional basis of B -splines. Describe a slightly simpler scheme using a $(N + 2)$ dimensional B -spline basis defined on the $N - 2$ interior knots.

Ex. 5.9 Derive the Reinsch form $\mathbf{S}_\lambda = (\mathbf{I} + \lambda \mathbf{K})^{-1}$ for the smoothing spline.

Ex. 5.10 Derive an expression for $\text{Var}(\hat{f}_\lambda(x_0))$ and $\text{bias}(\hat{f}_\lambda(x_0))$. Using the example (5.22), create a version of Figure 5.9 where the mean and several (pointwise) quantiles of $\hat{f}_\lambda(x)$ are shown.

Ex. 5.11 Prove that for a smoothing spline the null space of \mathbf{K} is spanned by functions linear in X .

Ex. 5.12 Characterize the solution to the following problem,

$$\min_f \text{RSS}(f, \lambda) = \sum_{i=1}^N w_i \{y_i - f(x_i)\}^2 + \lambda \int \{f''(t)\}^2 dt, \quad (5.73)$$

where the $w_i \geq 0$ are observation weights.

Characterize the solution to the smoothing spline problem (5.9) when the training data have ties in X .

Ex. 5.13 You have fitted a smoothing spline \hat{f}_λ to a sample of N pairs (x_i, y_i) . Suppose you augment your original sample with the pair $x_0, \hat{f}_\lambda(x_0)$, and refit; describe the result. Use this to derive the N -fold cross-validation formula (5.26).

Ex. 5.14 Derive the constraints on the α_j in the thin-plate spline expansion (5.39) to guarantee that the penalty $J(f)$ is finite. How else could one ensure that the penalty was finite?

Ex. 5.15 This exercise derives some of the results quoted in Section 5.8.1. Suppose $K(x, y)$ satisfying the conditions (5.45) and let $f(x) \in \mathcal{H}_K$. Show that

- (a) $\langle K(\cdot, x_i), f \rangle_{\mathcal{H}_K} = f(x_i)$.
- (b) $\langle K(\cdot, x_i), K(\cdot, x_j) \rangle_{\mathcal{H}_K} = K(x_i, x_j)$.
- (c) If $g(x) = \sum_{i=1}^N \alpha_i K(x, x_i)$, then

$$J(g) = \sum_{i=1}^N \sum_{j=1}^N K(x_i, x_j) \alpha_i \alpha_j.$$

Suppose that $\tilde{g}(x) = g(x) + \rho(x)$, with $\rho(x) \in \mathcal{H}_K$, and orthogonal in \mathcal{H}_K to each of $K(x, x_i)$, $i = 1, \dots, N$. Show that

$$(d) \quad \sum_{i=1}^N L(y_i, \tilde{g}(x_i)) + \lambda J(\tilde{g}) \geq \sum_{i=1}^N L(y_i, g(x_i)) + \lambda J(g) \quad (5.74)$$

with equality iff $\rho(x) = 0$.

Ex. 5.16 Consider the ridge regression problem (5.53), and assume $M \geq N$. Assume you have a kernel K that computes the inner product $K(x, y) = \sum_{m=1}^M h_m(x)h_m(y)$.

- (a) Derive (5.62) on page 171 in the text. How would you compute the matrices \mathbf{V} and \mathbf{D}_γ , given K ? Hence show that (5.63) is equivalent to (5.53).
- (b) Show that

$$\begin{aligned} \hat{\mathbf{f}} &= \mathbf{H}\hat{\boldsymbol{\beta}} \\ &= \mathbf{K}(\mathbf{K} + \lambda\mathbf{I})^{-1}\mathbf{y}, \end{aligned} \quad (5.75)$$

where \mathbf{H} is the $N \times M$ matrix of evaluations $h_m(x_i)$, and $\mathbf{K} = \mathbf{H}\mathbf{H}^T$ the $N \times N$ matrix of inner-products $h(x_i)^T h(x_j)$.

(c) Show that

$$\begin{aligned}\hat{f}(x) &= h(x)^T \hat{\beta} \\ &= \sum_{i=1}^N K(x, x_i) \hat{\alpha}_i\end{aligned}\quad (5.76)$$

and $\hat{\alpha} = (\mathbf{K} + \lambda \mathbf{I})^{-1} \mathbf{y}$.

(d) How would you modify your solution if $M < N$?

Ex. 5.17 Show how to convert the discrete eigen-decomposition of \mathbf{K} in Section 5.8.2 to estimates of the eigenfunctions of K .

Ex. 5.18 The wavelet function $\psi(x)$ of the symmlet- p wavelet basis has vanishing moments up to order p . Show that this implies that polynomials of order p are represented exactly in V_0 , defined on page 176.

Ex. 5.19 Show that the Haar wavelet transform of a signal of length $N = 2^J$ can be computed in $O(N)$ computations.

Appendix: Computations for Splines



In this Appendix, we describe the B -spline basis for representing polynomial splines. We also discuss their use in the computations of smoothing splines.

B-splines

Before we can get started, we need to augment the knot sequence defined in Section 5.2. Let $\xi_0 < \xi_1$ and $\xi_K < \xi_{K+1}$ be two *boundary* knots, which typically define the domain over which we wish to evaluate our spline. We now define the augmented knot sequence τ such that

- $\tau_1 \leq \tau_2 \leq \cdots \leq \tau_M \leq \xi_0$;
- $\tau_{j+M} = \xi_j$, $j = 1, \dots, K$;
- $\xi_{K+1} \leq \tau_{K+M+1} \leq \tau_{K+M+2} \leq \cdots \leq \tau_{K+2M}$.

The actual values of these additional knots beyond the boundary are arbitrary, and it is customary to make them all the same and equal to ξ_0 and ξ_{K+1} , respectively.

Denote by $B_{i,m}(x)$ the i th B -spline basis function of order m for the knot-sequence τ , $m \leq M$. They are defined recursively in terms of divided

differences as follows:

$$B_{i,1}(x) = \begin{cases} 1 & \text{if } \tau_i \leq x < \tau_{i+1} \\ 0 & \text{otherwise} \end{cases} \quad (5.77)$$

for $i = 1, \dots, K + 2M - 1$. These are also known as Haar basis functions.

$$B_{i,m}(x) = \frac{x - \tau_i}{\tau_{i+m-1} - \tau_i} B_{i,m-1}(x) + \frac{\tau_{i+m} - x}{\tau_{i+m} - \tau_{i+1}} B_{i+1,m-1}(x)$$

for $i = 1, \dots, K + 2M - m$. (5.78)

Thus with $M = 4$, $B_{i,4}$, $i = 1, \dots, K + 4$ are the $K + 4$ cubic B -spline basis functions for the knot sequence ξ . This recursion can be continued and will generate the B -spline basis for any order spline. Figure 5.20 shows the sequence of B -splines up to order four with knots at the points $0.0, 0.1, \dots, 1.0$. Since we have created some duplicate knots, some care has to be taken to avoid division by zero. If we adopt the convention that $B_{i,1} = 0$ if $\tau_i = \tau_{i+1}$, then by induction $B_{i,m} = 0$ if $\tau_i = \tau_{i+1} = \dots = \tau_{i+m}$. Note also that in the construction above, only the subset $B_{i,m}$, $i = M - m + 1, \dots, M + K$ are required for the B -spline basis of order $m < M$ with knots ξ .

To fully understand the properties of these functions, and to show that they do indeed span the space of cubic splines for the knot sequence, requires additional mathematical machinery, including the properties of divided differences. Exercise 5.2 explores these issues.

The scope of B -splines is in fact bigger than advertised here, and has to do with knot duplication. If we duplicate an interior knot in the construction of the τ sequence above, and then generate the B -spline sequence as before, the resulting basis spans the space of piecewise polynomials with one less continuous derivative at the duplicated knot. In general, if in addition to the repeated boundary knots, we include the interior knot ξ_j $1 \leq r_j \leq M$ times, then the lowest-order derivative to be discontinuous at $x = \xi_j$ will be order $M - r_j$. Thus for cubic splines with no repeats, $r_j = 1$, $j = 1, \dots, K$, and at each interior knot the third derivatives ($4 - 1$) are discontinuous. Repeating the j th knot three times leads to a discontinuous 1st derivative; repeating it four times leads to a discontinuous zeroth derivative, i.e., the function is discontinuous at $x = \xi_j$. This is exactly what happens at the boundary knots; we repeat the knots M times, so the spline becomes discontinuous at the boundary knots (i.e., undefined beyond the boundary).

The local support of B -splines has important computational implications, especially when the number of knots K is large. Least squares computations with N observations and $K + M$ variables (basis functions) take $O(N(K + M)^2 + (K + M)^3)$ flops (floating point operations.) If K is some appreciable fraction of N , this leads to $O(N^3)$ algorithms which becomes

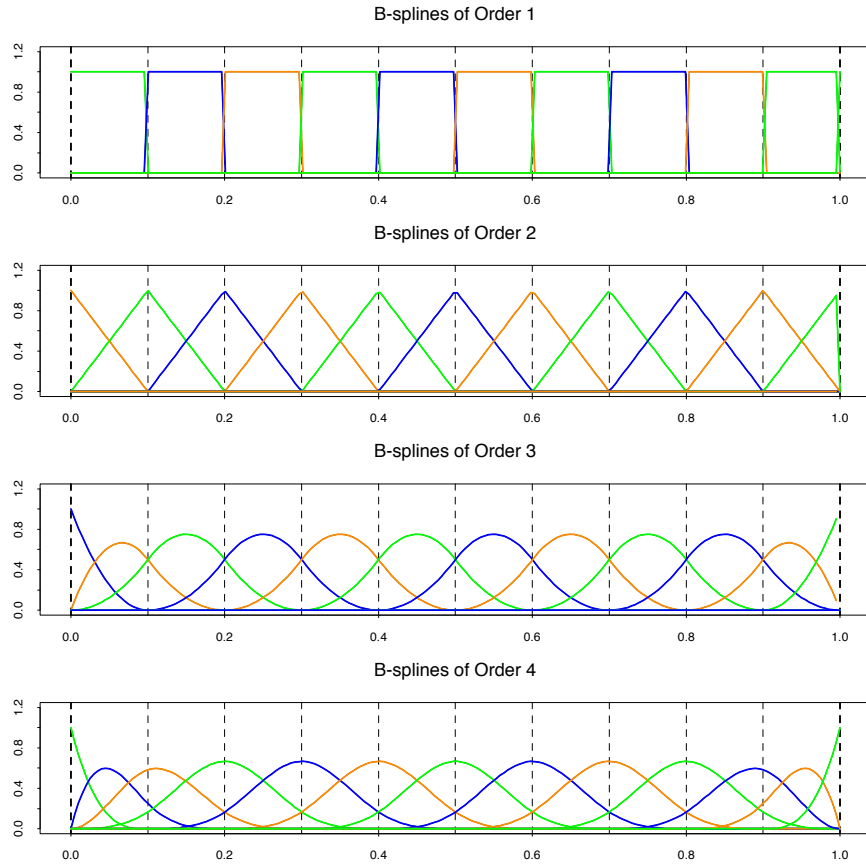


FIGURE 5.20. The sequence of B-splines up to order four with ten knots evenly spaced from 0 to 1. The B-splines have local support; they are nonzero on an interval spanned by $M + 1$ knots.

unacceptable for large N . If the N observations are sorted, the $N \times (K+M)$ regression matrix consisting of the $K + M$ B -spline basis functions evaluated at the N points has many zeros, which can be exploited to reduce the computational complexity back to $O(N)$. We take this up further in the next section.

Computations for Smoothing Splines

Although natural splines (Section 5.2.1) provide a basis for smoothing splines, it is computationally more convenient to operate in the larger space of unconstrained B -splines. We write $f(x) = \sum_1^{N+4} \gamma_j B_j(x)$, where γ_j are coefficients and the B_j are the cubic B -spline basis functions. The solution looks the same as before,

$$\hat{\boldsymbol{\gamma}} = (\mathbf{B}^T \mathbf{B} + \lambda \boldsymbol{\Omega}_B)^{-1} \mathbf{B}^T \mathbf{y}, \quad (5.79)$$

except now the $N \times N$ matrix \mathbf{N} is replaced by the $N \times (N + 4)$ matrix \mathbf{B} , and similarly the $(N + 4) \times (N + 4)$ penalty matrix $\boldsymbol{\Omega}_B$ replaces the $N \times N$ dimensional $\boldsymbol{\Omega}_N$. Although at face value it seems that there are no boundary derivative constraints, it turns out that the penalty term automatically imposes them by giving effectively infinite weight to any non zero derivative beyond the boundary. In practice, $\hat{\boldsymbol{\gamma}}$ is restricted to a linear subspace for which the penalty is always finite.

Since the columns of \mathbf{B} are the evaluated B -splines, in order from left to right and evaluated at the *sorted* values of X , and the cubic B -splines have local support, \mathbf{B} is lower 4-banded. Consequently the matrix $\mathbf{M} = (\mathbf{B}^T \mathbf{B} + \lambda \boldsymbol{\Omega})$ is 4-banded and hence its Cholesky decomposition $\mathbf{M} = \mathbf{L} \mathbf{L}^T$ can be computed easily. One then solves $\mathbf{L} \mathbf{L}^T \boldsymbol{\gamma} = \mathbf{B}^T \mathbf{y}$ by back-substitution to give $\boldsymbol{\gamma}$ and hence the solution \hat{f} in $O(N)$ operations.

In practice, when N is large, it is unnecessary to use all N interior knots, and any reasonable *thinning* strategy will save in computations and have negligible effect on the fit. For example, the `smooth.spline` function in S-PLUS uses an approximately logarithmic strategy: if $N < 50$ all knots are included, but even at $N = 5,000$ only 204 knots are used.

